The University Of Sheffield.

Adult generation of dopaminergic neurons in a genetic model of Parkinson's disease

Sarah J. Brown

A thesis submitted in partial fulfilment of the requirements for the degree of Doctor of Philosophy

The University of Sheffield
Faculty of Science
Department of Biomedical Science

April 2018

Acknowledgements

I would first like to express my appreciation and gratitude to my supervisors, Marysia Placzek and Oliver Bandmann, whose support over the course of my PhD has been invaluable. Marysia, you have been an outstanding mentor to me from when I first joined your lab during my MSc. and throughout my PhD. Your enthusiasm and work ethic is inspirational and your trust in me helped me believe in what I could achieve both in and outside the lab. Oliver, having observed one of your clinics, I have seen the huge impact you have on your patients and that deserves immense respect. You always had great confidence in me, and your encouragement and passion for science was motivating. It has been a pleasure to work with you both, and I appreciate the support you have both given me during my time at Sheffield.

I would also like to thank to Iain Stewart. Iain, you took me under your wing when I first joined the lab and taught me everything I needed to know to stand on my own. Your patience and attention to detail showed me how to approach scientific questions in a logical and organised manner. I am extremely grateful to have had you as a role model.

I must say thanks to all past and present members of both D18 and the Bandmann lab, who have helped me with my work and have given advice. In particular, Marcus and Lisa, who taught me everything I needed to know about working with zebrafish and who provided a supportive and friendly environment to work in.

I want to dedicate special thanks to my partner, Harry. You were always there to support me and your genuine interest in my research helped me see things from a different perspective. I am forever in awe of your selflessness, tolerance and positivity and I truly believe that I would not be the person I am without you.

I owe much gratitude to my family. To my parents, who brought me up to enquire and explore. You taught me to work hard, encouraged me and gave me confidence to push myself. To my sister, Jennie, who has always been excited and proud of my research, and to my grandparents, whose pride in me was never ending.

I would finally like to show my appreciation to the humble zebrafish, without which, this work would not have been possible.

Tables

Figures

Abstract

In the central nervous system, neuronal population size is a function of the number of neurons generated and the number lost through apoptosis or degeneration. Postnatal neurogenesis has been observed in several areas of the vertebrate brain and a reduced generation of neurons through life could contribute to neurodegenerative disease. Parkinson's disease (PD) is underlain by a reduced number of dopaminergic (DA) neurons, in particular, ascending neurons of the substantia nigra pars compacta. The degeneration of DA neurons is a known contributory factor, but may not account fully for disease pathogenesis. Here I examine the character and generation of DA neurons in the adult zebrafish posterior tuberculum (PT) in wild type and in a model of genetic PD, the *pink1* knockout zebrafish.

I first characterise embryonic and adult DA neuronal populations in the zebrafish PT and show that throughout life, DA neuronal populations reside close to populations of stem and progenitor cells that are themselves maintained in the PT in adulthood. I show that ascending DA neurons of the PT, functionally-equivalent to those of the substantia nigra, express the transcription factor, OTPb, and that local-projecting DA neurons of the paraventricular organ (PVO) in the ventral PT/dorsal hypothalamus express *rx3*. Using EdU analyses and lineage-tracing studies, I demonstrate that a subset of ascending DA neurons (those of the periventricular nucleus of the posterior tuberculum (TPp) and the local-projecting DA neurons of the paraventricular organ (PVO)) are generated in adulthood in wild type animals at a rate that decreases with age. Using a robust model of PD, the *pink1-/-* zebrafish, I show that Pink1-deficiency impedes DA neurogenesis in early adult life. Analysis of population size shows that zebrafish lacking functional Pink1 fail to expand DA neuronal populations in adulthood and display reduced numbers of OTPb-expressing progenitors.

Together this work reveals that subsets of ascending DA neurons of the PT and local-projecting DA neurons of PVO in the ventral PT/dorsal hypothalamus are generated throughout life, demonstrates a novel role for Pink1 in adult DA neurogenesis and suggests potential future applications of stimulation of de novo neurogenesis in PD.

Abbreviations

Aa, amino acid; ARC, arcuate nucleus; ATN, anterior tuberal nucleus; ATP, Adenosine Triphosphate; BDNF, brain derived neurotrophic factor; BMP, bone morphogenic protein; BrdU, bromodeoxyurine; Cb/Ce, cerebellum; CC, cerebellar crest; CNS, central nervous system; CNTF, ciliary neurotrophic factor; COR, C-terminal domain; CRISPR, Clustered Regularly Interspaced Short Palindromic Repeats; CSF, cerebrospinal fluid; DA, dopaminergic; Dcx, doublecortin; DiV, diencephalic ventricle; DON, descending octaval nucleus; Dpf, days post fertilization; Drp1, dynamin-related protein-1; DT, dorsal thalamus; E, Epiphysis; EdU, 5-Ethynyl-2´-deoxyuridine; EGF, epidermal growth factor; EOPD, early onset Parkinson's disease; FGF, fibroblastic growth factor; FISH, fluorescent in situ hybridisation; FLo, facial lobe; GCL, granule cell layer; GFAP, glial fibrillary acidic protein; gRNA, guide RNA; Ha, Habenula; Hc, caudal hypothalamus; Hd, dorsal hypothalamus; Hpf, hours post fertilization; HmNPC, human midbrain-derived neural progenitor cell; Hv, ventral hypothalamus; Hyp, hypothalamus; IGF, insulin-like growth factor; Lc, locus coeruleus; L-DOPA, Levodopa; LH, lateral hypothalamus; LOPD, late onset Parkinson's disease; Lrrk2, leucine rich repeat kinase-2; ME, median eminence; Mfn-1, mitofusin-1; MO, medulla oblongata; MPTP, 1-methyl-4-phenyl-1,2,3,6-tetrahydropyridine; mRNA, messenger RNA; MTOR, mammalian target of rapamycin complex 2; NC, horizontal commissure, NMLF, nucleus of the medial longitudinal fascicle; OB, olfactory bulb; OTP; Orthopedia; P, pallium; PAM, protospacer adjacent motif; PARL, presenilin associated rhomboid like protein; Pc, posterior commissure; PD, Parkinson's disease; Pink1, PTEN-induced putative kinase-1; Po, preoptic area; Pr; pretectum; PSA-NCAM, polysialylated-neural cell adhesion molecule; PT, posterior tuberculum; PVO, paraventricular organ; RG, radial glia; Roc, RAS-like GTPase domain; SGZ, subgranular zone; Shh, sonic hedgehog; SiRNA, small interfering RNA; SNCA, alpha-synuclein; SN, substantia nigra; SNpc, substantia nigra pars compacta; SP, subpallium; SVZ, subventricular zone; T, tegmentum; Tel, telencephalon; TeO, optic tectum; Th1, tyrosine hydroxylase-1; Th, thalamus; TigarB, TP53-induced glycolysis and apoptosis regulator; TILLING, targeting induced local lesions in genomes; TL, longitudinal torus; TPp, periventricular nucleus of the posterior tuberculum; UPS, ubiquitin proteasome system; Vd, dorsal nucleus of the ventral telencephalic area; VLo, vagal lobe; vDC, ventral diencephalon; VM, ventral midbrain, VMN, ventromedial nucleus; Vs, supracommissural nucleus of the ventral telencephalic area; VT, ventral thalamus; Vv, ventral nucleus of the ventral telencephalic area; VZ, ventricular zone; Zf, zebrafish.

Chapter 1

Introduction

1.0: Introduction

My thesis focuses on the de novo generation of ascending dopaminergic neurons in the adult zebrafish brain and the effects of a Parkinson's disease (PD) gene mutation*, pink1-/-,* on dopaminergic neurogenesis. This introduction first describes PD, from incidence, symptoms and treatment to causes and genetic models of the disease. Next, I describe adult neurogenesis, including the methods used to investigate adult neurogenesis, the evidence for de novo neurogenesis in adulthood and the mechanisms that regulate it. I then discuss the evidence for altered adult neurogenesis in PD. Finally, I outline the aims and hypothesis of my study.

1.1: PD; incidence, symptoms and treatment

1.1.1: Overall introduction to PD

PD is classically defined as a neurodegenerative condition and is the second most common form of neurodegeneration after Alzheimer's disease. Increased average life-span in the human population means that PD is expected to impose an increasing social and economic burden. There is therefore a pressing need to fully understand the disease (de Lau & Breteler, 2006; Kowal *et al.*, 2013). PD is pathologically characterised by degeneration of dopaminergic (DA) neurons in a region of the midbrain termed the substantia nigra pars compacta: the reduced DA signalling results in several cardinal motor symptoms, including tremor, bradykinesia and rigidity. PD patients also often experience wider, non-motor symptoms, including depression, anosmia and sleep disturbances (Jankovic, 2008), though the cause of these symptoms is less well understood. Currently, there is no cure for this condition. Existing treatments centre on dopamine replacement. Although these treatments initially alleviate motor symptoms, efficacy reduces with disease progression and often leave patients with unpleasant side effects such as dyskinesia and behavioural problems (Connolly & Lang, 2014). This highlights a need for greater understanding of the disease, and development of more effective treatments. Despite huge efforts in the Parkinson's field, the aetiology of PD is not fully understood, and around 90% of cases appear to be sporadic or environmental. Only around 10% of PD patients develop the

disease due to monogenic gene mutations. However studying these Mendelian inherited forms of PD provides insight into disease pathogenesis (Lesage & Brice, 2009). In the following sections, the incidence, symptoms, treatment, known pathological mechanisms and models of PD will be discussed in detail.

1.1.2: Prevalence and incidence of PD

PD affects approximately 1% of individuals over the age of 60, increasing to 4-6% in those over 85 (Van Den Eeden *et al.*, 2003; de Lau & Breteler, 2006; Kowal *et al.*, 2013). As well as the increasing incidence rate of PD with age, gender and ethnicity are also risk factors: incidence of PD is twice as high for men compared to women, and incidence rates are highest among those of Hispanic race (Van Den Eeden *et al.*, 2003). The average age of diagnosis of PD is at around 70 years of age (Van Den Eeden *et al.*, 2003; Hawkes, 2008), however it is thought that there is a reduction of as many as 50% of DA neurons before patients become symptomatic, and this may precede diagnosis by several years (Marsden, 1990; Ross *et al.*, 2004). Patients who exhibit PD symptoms before the age of 40-50 are defined as early-onset (EOPD) or young-onset (YOPD) cases: these are a minority, making up around 5-10% of cases (Golbe, 1991). Early-onset PD patients carry Monogenically-inherited mutations in genes such as *PARKIN,* or *PINK1 (*discussed in detail in section 1.2.1) more commonly than late onset cases. For example, in one study examining known mutations in patients with EOPD, 6.7% carried mutations in *PARKIN* and 3.6% in *LRRK2* (Alcalay *et al.*, 2010), with a separate study observing a 3.7% incidence rate of mutations in *PINK1* (Tan *et al.*, 2006). Around 90% of patients (mostly late-onset cases) have no known cause of the disease, and these cases are deemed to be sporadic (de Lau & Breteler, 2006). Because of this, the biggest predictive risk factor for developing PD is ageing (Van Den Eeden *et al.*, 2003; de Lau & Breteler, 2006). As the average life expectancy of the population rises, so will incidence of PD. Indeed, one study predicts a two-fold increase in the number of PD cases by 2030 (Bach *et al.*, 2011). Together, this illustrates that PD is a highly prevalent disorder and highlights the need for greater understanding of the disease.

1.1.3: Symptoms of PD

Tremor, bradykinesia (slow movement) and rigidity are the cardinal motor features of PD, all of which are related to loss of dopaminergic signalling in the nigrostriatal system. Tremor at rest is often the first symptom noticed by the patient, which may be worse in stressful or exciting situations. In some individuals, bradykinesia manifests first, resulting in difficulties initiating and executing movement. Consequently, the patient may experience a reduced ability to perform tasks requiring fine motor control such as writing, or using utensils. Decreased leg stride, arm swing and vocal amplitude may also manifest. As the disease progresses, existing symptoms gradually worsen and new motor symptoms appear, such as freezing and decreased postural reflex resulting in postural instability. Freezing episodes cause patients to suddenly be unable to move, whereas postural instability frequently results in falls (Fahn, 2003; Jankovic, 2008).

Non-motor symptoms also manifest in patients with PD and are often underappreciated. The cause of many of these symptoms is not fully understood. Non-motor symptoms in PD include autonomic dysfunction, mood disorders, cognitive decline, sleep disturbances and changes in sense of smell (Poewe, 2008). Autonomic dysfunction in PD presents as orthostatic hypotension, sweating dysfunction, sphincter dysfunction and erectile dysfunction (Jankovic, 2008). Mood disorders are common in PD: one study reported 58% of patients experienced depression, 54% experienced apathy and 49% reported anxiety (Aarsland *et al.*, 2007). Sleep disorders, such as insomnia, are reported in around 55-60% of patients (Gjerstad *et al.*, 2007), and around a third of patients experience rapid eye movement sleep disorder, resulting in aggressive dream content (Borek *et al.*, 2007). Interestingly, disturbances in sleep/wake regulation are thought to be caused by a loss of orexin neurons in the hypothalamus (Fronczek *et al.*, 2007), suggesting PD affects neuronal populations other than DA neurons and in regions other than the midbrain. Changes in sense of smell, or olfactory dysfunction, affect around 90% of patients with PD (Ross *et al.*, 2008), and are thought to be caused by neuropathies in the olfactory bulb (Pearce *et al.*, 1995). Non-motor symptoms often precede motor symptoms by decades, with olfactory dysfunction, constipation and depression indicating increased risk of PD development (Abbott *et al.*, 2001; Schuurman *et al.*, 2002; Ross *et al.*, 2008). From the wide range of

motor and non-motor symptoms experienced in patients with PD, it is evident that PD is a multi-system disorder, disabling patients and hugely reducing quality of life.

1.1.3: Treatment of PD

There is no cure for PD and most commonly prescribed treatments focus on addressing motor symptoms. Levodopa (L-DOPA), the precursor to catecholamine neurotransmitters such as dopamine, revolutionised PD management and has remained the most efficient form of treatment (Jankovic & Aguilar, 2008). Although L-DOPA initially reverses motor symptoms in patients, the drug has many limitations. These include reduced drug efficacy with disease progression and additional motor complications such as involuntary movements (dyskinesia). In patients who received L-DOPA treatment for 5 years, 50% developed these complications, rising to 80% of patients treated for 10 years (Fahn, 2000). Additionally, EOPD patients appear to be particularly sensitive to decreased L-DOPA efficacy and dyskinesia (Golbe, 1991). Alternatives to L-DOPA include DA agonists: these are associated with fewer motor complications but in some patients, can worsen non-motor symptoms. DA agonists can also result in compulsive behaviours and difficulties with impulse control, which can lead to behaviours such as pathological gambling, compulsive shopping or hypersexuality (Voon *et al.*, 2011; Santangelo *et al.*, 2013; Atmaca, 2014). Deep brain stimulation has also been established as an effective therapy, but carries risk of surgery-related complications, infection and neuropsychiatric conditions such as those observed with DA agonist treatment (Groiss *et al.*, 2009). Although current treatments may be effective at alleviating motor symptoms, they do not halt progression of the disease and are not neuroprotective. This highlights the need for a better understanding of PD, and the need to generate better treatments that prevent or slow PD progression.

1.2: Causes and pathogenesis of PD

1.2.1: Monogenically-inherited forms of PD and genetic risk factors

For a long time, PD was considered a non-genetic disorder. However, it is now known that around 5-10% of patients have mutations in a single gene, so-termed monogenic forms of the disease. These genes include, but are not limited to, dominant PD genes such as *SNCA*, *LRRK2*, and recessive PD genes such as *PARKIN* and *PINK1* (Lesage & Brice, 2009; Puschmann, 2013). The first PD-causing mutation to be discovered was a point mutation in the *SNCA* gene, encoding alpha-synuclein. It was named the A53T mutation and was found in individuals from a kindred originating from Contursi, Italy and in three Greek families (Golbe *et al.*, 1996; Polymeropoulos *et al.*, 1997). The mutation in *SNCA* caused earlier onset of the disease than in typical cases with similar clinical phenotypes between all individuals (Polymeropoulos *et al.*, 1997). The A53T mutation has since been observed in several other families and individuals (Papadimitriou *et al.*, 1999; Papapetropoulos *et al.*, 2001; Bostantjopoulou *et al.*, 2001; Michell *et al.*, 2005; Ki *et al.*, 2007; Choi *et al.*, 2008; Puschmann *et al.*, 2009). A second point mutation in the *SNCA* gene, the A30P mutation, was identified in a German family (Krüger *et al.*, 1998), and a third, termed the E46K mutation, was found in a family originating from Spain (Zarranz *et al.*, 2004). Duplication and triplication *SNCA* mutations have been more frequently reported in families with PD, where duplication results in late-onset PD and triplication results in early-onset PD, suggesting a toxic gain of function mechanism (Singleton *et al.*, 2003; Ibáñez *et al.*, 2004). The pathogenic mechanism of *SNCA* mutations is still not clear, but is thought to be, in part, related to inappropriate alpha-synuclein protein aggregation (pathological mechanisms are discussed in detail in section 1.2.3).

Several mutations in the leucine-rich repeat kinase 2 (*LRRK2*) gene were discovered simultaneously in eight families: a family originating from Germany, Denmark and Canada (Y1699C mutation), a family from Nebraska (R1441C mutation), 4 families from the Basque region of Spain (R1441G mutation, where this mutation has since been found in 8% of patients with familial PD in the Basque region (González-Fernández *et al.*, 2007), one family from the UK (Y1699C mutation) and one family from Japan (I2020T mutation) (Paisán-Ruíz

et al., 2004; Zimprich *et al.*, 2004). Since then, a R1441H mutation was found in several families worldwide (Zabetian *et al.*, 2005; Mata *et al.*, 2005; Spanaki *et al.*, 2006), and a N1237H mutation was found in two families from Norway and one patient from Sweden (Puschmann *et al.*, 2009; Aasly *et al.*, 2010). Apart from the R1441G mutation, these *LRRK2* point mutations are relatively rare. One *LRRK2* mutation on the other hand, the G2019S mutation, is the most commonly found PD-associated mutation worldwide, and is particularly prevalent among the North African Arab population and the Ashkenazi Jewish population. The G2019S mutation has been found in 41% of sporadic PD cases and 37% of cases with a family history of PD from the North African Arab population (Lesage *et al.*, 2006), and in 18.3% of Ashkenazi Jewish patients exhibiting PD symptoms (Ozelius *et al.*, 2006). In other populations, the G2019S mutation is less common but the frequency of patients carrying this mutation is still relatively high (around 1-2% of PD patients) (Correia Guedes *et al.*, 2010). The pathology observed in *LRRK2* mutation-induced PD is highly variable, seemingly dependent upon the specific point mutation harboured by the individual. The biological role, and the role of LRRK2 in PD, remains largely unknown (Poulopoulos *et al.*, 2012). *LRRK2* is a focus of this thesis, so recent advances in the understanding of its role in PD will be discussed in section 1.2.5.

Recessive PD genes, such as *PARKIN* and *PINK1*, are frequently found in families where several individuals in one generation display PD. This is particularly common in consanguineous families (Yamamura *et al.*, 1973; Kitada *et al.*, 1998; Chishti *et al.*, 2006). Mutations in the *PARKIN* gene, encoding Parkinson protein 2 E3 ubiquitin protein ligase, were originally discovered in siblings displaying EOPD in two separate consanguineous families in Japan and Turkey (Yamamura *et al.*, 1973; Kitada *et al.*, 1998). Since then *PARKIN* mutations have been linked to (very) early-onset PD; in one study, 77% of patients who displayed PD before the age of 20 carried at least one *PARKIN* mutation (Lücking *et al.*, 2000). *PARKIN* mutations are highly variable, with over 100 different mutations reported in PD patients to date. These include deletions, insertions, multiplications, missense and truncating mutations, resulting in loss of function of Parkin (Lesage & Brice, 2009). The underlying pathological mechanisms of loss of function mutations in *PARKIN* are not well understood, though it is generally thought that this results in decreased catalytic activity, aberrant ubiquitination and impaired proteosomal degradation (Dawson & Dawson, 2010). Pathological mechanisms in PD will be discussed in greater detail in section 1.2.3.

Loss of function mutations in the phosphatase and tensin homolog (PTEN)-induced putative kinase 1 (*PINK1*) are associated with EOPD, though *PINK1* mutations are less common, detected in 1-4% of EOPD patients depending on the population (Tan *et al.*, 2006; Brooks *et al.*, 2009). More than 40 different point mutations have been detected, though large deletions are rarely detected (Lesage & Brice, 2009). *PINK1* is another focus of this study, so will be discussed in more detail later in this thesis (see section 1.2.4). Mutations in the genes *DJ-1*, *VPS35* and *EIF4G1* have also been described, though these are extremely rare, accounting for around 0-0.4% of PD cases. Monogenic mutations described in this section are summarised in table 1.1.

Recently, genome wide association studies (GWAS) using large numbers of subjects have facilitated the discovery of genetic risk factors for PD. These studies have identified genetic variants that confer small or medium increased risk for PD development. The most common are variants in *LRRK2* and *SNCA*, which confer a high risk of PD (Satake *et al.*, 2009). However, over 40 different genetic risk loci have now been identified (Nalls *et al.*, 2014; Chang *et al.*, 2017).

Gene	Disease onset	Clinical phenotype	Inheritance	Known expression
SNCA	Early	Parkinsonism, cognitive, behavioural and autonomic symptoms, muscle spasms, Lewy body pathology.	Autosomal dominant	Brain (pre-synapses). Lewy bodies.
LRRK2	Late	Parkinsonism, highly variable additional symptoms depending on mutation type.	Autosomal dominant	Brain, liver, kidney and heart. Lewy bodies.
PARKIN	Early	Parkinsonism, low risk of cognitive symptoms, cell loss in brain stem.	Autosomal recessive	Weakly expressed throughout the brain. Strong expression in brainstem.
PINK1	Early	Parkinsonism, cognitive and psychiatric symptoms, cell loss in brain stem.	Autosomal recessive	Widely expressed throughout the brain at mitochondrial membranes.
DJ-1	Early	Parkinsonism, low risk of cognitive symptoms.	Autosomal recessive	Astrocytes in brain tissue.
VPS35	Late	Parkinsonism, cognitive and behavioural changes, no Lewy body pathology.	Autosomal dominant	Gastrointestinal system, heart, liver, kidney, white blood cells.
EIF4G1	Late	Parkinsonism, mild disease, cognition preserved, Lewy body pathology.	Autosomal dominant	Brain, gastro-intestinal system, heart, white blood cells.

Table 1.1: List of genes containing mutations that are robustly associated with PD.

Onset of disease, type of inheritance and known expression profiles are also shown (Puschmann, 2013).

1.2.2: Environmental causes of PD

In cases where no clear genetic cause is discovered, environmental influences are thought to play a role in disease aetiology (Warner & Schapira, 2003). Several studies have identified rural living and exposure to pesticides as a risk factor for development of PD (Barbeau *et al.*, 1987; Semchuk *et al.*, 1992; Seidler *et al.*, 1996; Gorrell *et al.*, 1996; Fall *et al.*, 1999). Indeed one study found the pesticide Dieldrin in DA neurons in 6 of 20 PD patient brains and none in control brains (Fleming *et al.*, 1994). Furthermore, exposure to dithiocarbamate-containing fungicides has been shown to increase the toxicity of 1-methyl-4-phenyl-1,2,3,6-tetrahydropyridine (MPTP), a chemical known to cause selective destruction of nigrostriatal DA neurons (Tipton & Singer, 1993). This suggests exposure to environmental pesticides may increase susceptibility to DA neuronal decline. Exposure to widely available mitochondrial inhibitors has also been implicated with increased PD risk. Rotenone is a commonly used pesticide and is an inhibitor of mitochondrial complex I. In mice, exposure to Rotenone has been shown to cause selective destruction of nigrostriatal DA neurons resulting in a PD-like motor defect (Betarbet *et al.*, 2000). Together this data suggests that environmental agents may contribute to the risk of PD.

1.2.3: Known pathogenic mechanisms in PD

In this section, an overview of current understanding of pathological mechanisms implicated in PD will be briefly discussed, although it should be noted that many of these mechanisms are still widely debated and the overall pathogenesis of the disease is still not fully clear.

One of the cardinal features of PD is the presence of abnormal aggregates of protein in nigral DA neurons, first described by Friedrich Heinrich Lewy in 1912 and therefore termed Lewy bodies or Lewy neurites. Lewy bodies are large spherical or kidney-shaped inclusions in neuronal cell bodies, whereas Lewy neurites are aggregated strands of protein found in the neuronal processes. Both Lewy bodies and Lewy neurites are primarily formed of alpha-synuclein, and are found in DA neurons of the substantia nigra in PD patients, but have also found in other brain regions such as the hypothalamus, brain stem and the spinal cord (Jager & Bethlem, 1960; Ohama & Ikuta, 1976; Oyanagi *et al.*, 1990; Wakabayashi *et*

al., 2007). Recent reports propose that alpha-synuclein aggregates could be a protective mechanism, facilitating segregation and degradation of mutated or damaged proteins (Olanow *et al.*, 2004), suggesting altered proteasome function may play a role in PD pathogenesis. It remains possible however, that Lewy bodies expand with continued production of toxic proteins, leading to excessive protein aggregates and consequently cell death (Wakabayashi *et al.*, 2007).

Numerous studies provide evidence of altered proteasome function in PD. The ubiquitin proteasome system (UPS) is a protein degradation system, responsible for protein turnover. Briefly, proteins are targeted for degradation by ubiquitin ligation, requiring sequential action by ubiquitin activating (E1), conjugating (E2) and ligating (E3) enzymes. The protein is then degraded by a large protease complex (Hershko & Ciechanover, 1998; Lim & Tan, 2007). Discovery of a role for altered UPS function came from the discovery of *PARKIN* mutations (Parkin encodes the Parkinson protein 2 E3 ubiquitin protein ligase) in EOPD. Altered UPS function may result in toxic accumulation of intracellular proteins, such as alpha-synuclein, and subsequently neuronal cell death. However, the UPS system is not specific to DA neurons in the substantia nigra, and it remains unclear as to why DA neurons appear to be selectively vulnerable (Lim & Tan, 2007).

Mitochondrial dysfunction has also been implicated in the pathogenesis of PD. This originated from observations of mitochondrial complex I deficiency in the substantia nigra of PD patients (Schapira *et al.*, 1990). The cause and result of complex I deficiency in PD is not well understood. Some studies suggest that complex I inhibition results in increased oxidative damage in MPTP treated mice (Przedborski *et al.*, 1996; Perier *et al.*, 2005) and consequently damage to intracellular components and cell death. Other studies suggest complex I inhibition also results in reduced ATP production, adding an energy failure hypothesis (Fabre *et al.*, 1999). Both environmental and genetic factors affect mitochondrial function (Moon & Paek, 2015), and the role of mitochondrial dysfunction in PD pathogenesis has been supported by several PD gene knockout models, including those with mutation in *PINK1*, which display mitochondrial defects. PINK1 is of relevance to this study, therefore, the role of *PINK1* in mitochondrial function will be discussed in detail below (see section 1.2.4). Another gene that is of interest to this study is *LRRK2*. Therefore, the pathological mechanisms of *LRRK2* will also be further discussed (see section 1.2.5).

1.2.4: PINK1

The PTEN-induced putative kinase PINK1 is a 581 amino acid protein with a serine kinase domain and an N-terminal mitochondrial targeting sequence (Mills *et al.*, 2008). *PINK1* is expressed throughout the human and mouse brain, and is thought to localise to the mitochondrial membrane (Gandhi *et al.*, 2006; Taymans *et al.*, 2006; Blackinton *et al.*, 2007; Weihofen *et al.*, 2009; Jin *et al.*, 2010). Interestingly, *PINK1* is also expressed in the heart and muscle, which together with the brain, are all high-energy demand organs (Blackinton *et al.*, 2007). This supports the requirement for PINK1 in mitochondrial function.

Mutations in *PINK1* are the second most common cause of autosomal recessive EOPD after *PARKIN* mutations (Valente *et al.*, 2004); the majority are missense mutations in the kinase domain of the gene (Mills *et al.*, 2008). The kinase domain of *PINK1* is essential for cell survival: cell lines expressing pathogenic *PINK1* mutations display increased susceptibility to apoptotic cell death, which can be rescued by overexpression of wild type *PINK1* (Petit *et al.*, 2005; Deng *et al.*, 2005). One way PINK1 has been shown to function is through phosphorylation of the mitochondrial heat shock protein, TRAP1, preventing release of the apoptosis initiator cytochrome c and increasing neuronal survival (Pridgeon *et al.*, 2007).

Studies have shown that PINK1 may also function in the same pathway as Parkin to initiate mitophagy. In healthy mitochondria, PINK1 is rapidly degraded by the mitochondrial protease, presenilin associated rhomboid like protein (PARL), and finally fully-degraded by the proteasome (Lin & Kang, 2008). Cleavage of PINK1 by PARL is dependent on mitochondrial membrane potential, where decreased mitochondrial membrane potential (such as following damage or stress) results in no cleavage, and PINK1 accumulates on the mitochondrial membrane where it recruits Parkin. Parkin then ubiquitinates mitochondrial targets, labelling the mitochondrion for mitophagic recycling (Deas *et al.*, 2011; Okatsu *et al.*, 2012). (figure 1.1). Functional mitophagic recycling means damaged mitochondria do not accumulate, an effect that is pivotal to cell survival (Zhang *et al.*, 2017). Loss of functional PINK1 results in failed mitophagic mechanisms and mitochondrial dysfunction,

therefore could contribute to PD progression. However the relation of these factors to PD is still widely debated (Winklhofer & Haass, 2010; Matsuda *et al.*, 2013).

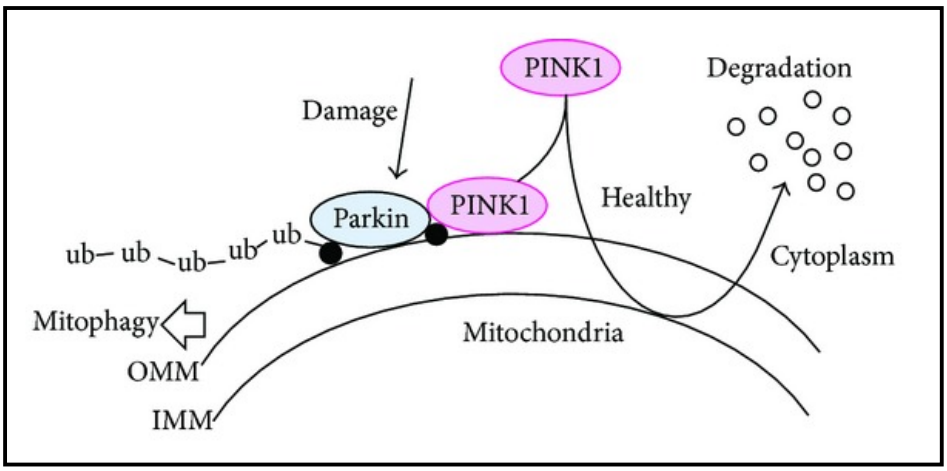

Figure 1.1: Illustration summarising the PINK1/Parkin regulatory pathway for mitophagy.

In healthy mitochondria, PINK1 is degraded. Upon mitochondrial damaged PINK1 and Parkin accumulate on the mitochondrial membrane and ubiquitination targets the mitochondrion for recycling by mitophagy. Figure reproduced from Matsuda et al., 2013.

1.2.5: LRRK2

Leucine-rich repeat kinase 2 (LRRK2) is a large protein, consisting of around 2527 amino acids, with several leucine-rich repeats, a RAS-like GTPase domain (ROC), a C-terminal domain (COR), a WD40 motif and a kinase domain. The majority of PD-casing mutations in *LRRK2* are found in the ROC, COR and kinase domains, all of which form the enzymatic core of the protein (Paisán-Ruiz *et al.*, 2013). Although it is clear that *LRRK2* dysfunction is highly important to PD pathology (as described above, mutations in *LRRK2* are the most commonly found PD-mutation worldwide), there are large gaps in the knowledge of the biological function and pathological mechanisms of *LRRK2*. This may be in part due to LRRK2 possessing a complex domain structure and two active enzymatic domains, obfuscating interpretation of its biological role and its dysfunction in PD.

The biological function of LRRK2 is a widely debated subject, and LRRK2 has been implicated in several core biological functions (Paisán-Ruiz *et al.*, 2013). Some studies have suggested a role for LRRK2 in regulation of synaptic vesicle endocytosis via interaction with endophillins (Piccoli *et al.*, 2011; Matta *et al.*, 2012) and others have shown a role in autophagy (Tong *et al.*, 2010*a*; Herzig *et al.*, 2011; Bravo-San Pedro *et al.*, 2013). LRRK2 has been implicated in protein sorting mechanisms by interaction with Rab71L, suggesting a role in the regulation of protein disposal (MacLeod *et al.*, 2013). Furthermore, LRRK2 has also been linked to regulation of micro-RNAs (miRNAs) to regulate protein translation (Gehrke *et al.*, 2010; Cho *et al.*, 2013) and has been shown to interact with cytoskeletal proteins, implicating LRRK2 in cytoskeletal remodelling such as during neurite branching (Parisiadou *et al.*, 2009). LRRK2 has additionally been shown to be expressed in circulating immune cells (Hakimi *et al.*, 2011) and has been shown to be crucial for microglial function in the brain (Moehle *et al.*, 2012). Interestingly, a recent study showed that LRRK2 could interact with Wnt signalling proteins, bridging cytosolic and membrane components (Berwick & Harvey, 2012). LRRK2 has also been shown to directly interact with the mitochondrial fission regulator, dynamin-related protein-1 (Drp1) and the mitochondrial fusion regulators, mitofusin 1/2 (Mfn 1/2) and OPA1 (Wang *et al.*, 2012; Stafa *et al.*, 2014). This suggests that LRRK2 may also play a role in mitochondrial dynamics, including fusion and fission. It is not yet clear whether the roles of LRRK2 are converging, or whether the complex structure of LRRK2 allows for multiple divergent biological functions.

The role of mutated forms of LRRK2 in PD appears to be even more complex. Clearly the enzymatic core of LRRK2 is crucial to the role of mutated forms in PD, as most pathogenic mutations are within enzymatic domains, however different mutations within the *LRRK2* gene appear to lead to different effects on enzyme activity (figure 1.2). For example, the G2019S mutation results in increased kinase activity, whereas the I2020T mutation has no effect on kinase activity (Paisán-Ruiz *et al.*, 2013). Furthermore, the R1441C, R1441G, Y1699C and G2019S mutations all result in decrease GTPase activity. The overall theme of these studies is that any type of disruption of LRRK2 enzymatic activity is deleterious and could instigate PD. The role of LRRK2 in PD requires much further investigation.

a)

Mutation	Domain	Enzymatic impact
p.N1437H	ROC	Unknown
p.R1441C	ROC	GTPase↓
p.R1441G	ROC	GTPase↓
p.Y1699C	COR	GTPase↓
p.S1761R	COR	Unknown
p.I2012T	Kinase	None
p.G2019S	Kinase	Kinase ↑ GTPase↓
p.I2020T	Kinase	None
p.G2385R	WD40	Kinase↓

b)

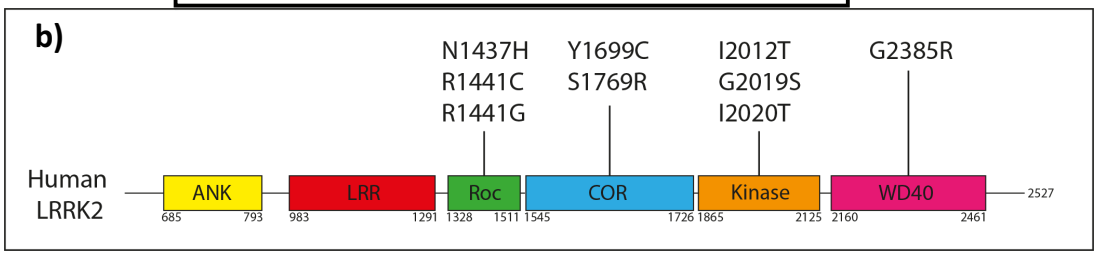

Figure 1.2: Summary of the impact of *LRRK2* mutations on biochemical readouts of enzymatic function.

a) The enzymatic impact varies depending on the position of the mutation in the *LRRK2* gene. Figure reproduced from Paisán-Ruiz *et al.*, 2013.
b) Schematic demonstrating the position of known mutations in the human LRRK2 protein.

1.3: Genetic models of PD

Over the last two decades, many animal models of PD have been created that have been pivotal to improving our understanding of the disease. Despite this, many of these models fall short of replicating many of the pathophysiological aspects of PD (Potashkin *et al.*, 2011). Some success has come from toxin-based models of PD, such as the commonly used MPTP treatment that is selectively taken in by midbrain DA neurons, causing DA neuron death via inhibition of mitochondrial complex I (Mizuno *et al.*, 1987). However, toxin-based models of PD are of limited usefulness, in that DA neuronal death is extremely acute, and so does not mimic the progressive nature of PD. Toxin-based models also do not allow for analysis of multiple converging mechanisms that are most likely present in genetic forms of the disease (see sections 1.2.3, 1.2.4, 1.2.5). Genetic models of PD can be more informative, allowing insight into gradual disease progression. Recently, many genetic models of PD have been created in different vertebrate and invertebrate species. In this section, the recent advances and limitations in genetic PD models will be briefly discussed, focusing on *PINK1* and *LRRK2* mutant models.

1.3.1: Rodent models of PD

The most widely used genetic model of PD are rodents, which has provided some insight into pathogenic mechanisms. However, rodent models of PD are limited and many do not fully model all aspects of PD. Several mouse lines have been created that model *SNCA* mutations. In these, a mixed level of nigrostriatal degeneration has been observed (Chesselet, 2008; Nuber *et al.*, 2008; Lam Hoa A. *et al.*, 2011). Various *PARKIN* knockout mice lines have been created, but none have shown substantia nigra dopaminergic loss or behavioural abnormalities. Some show impaired DA release and mild mitochondrial dysfunction (Goldberg *et al.*, 2003; Palacino *et al.*, 2004; Perez & Palmiter, 2005; Zhu *et al.*, 2007).

The success of developing rodent models of Pink1 and Lrrk2 deficiency has been much more limited. Mouse lines with loss of function *Pink1* mutations develop very mild

phenotypes. *Pink1* knockout mice have reduced striatal DA levels and exhibit a decrease in spontaneous movement by one and a half years of age, but do not show abnormalities in DA neuron number and showed no other behavioural changes such as anxiety or startle response (Gispert *et al.*, 2009). Although *Pink1* knockout mice do not display DA neuron reduction, mice lacking functional Pink1 do however display mitochondrial dysfunction, with decreased ATP production and reduced activity of mitochondrial complexes (Gautier *et al.*, 2008).

Mouse lines with loss of function mutations in *Lrrk2* show no functional abnormalities in DA neuron system (Andres-Mateos *et al.*, 2009; Tong *et al.*, 2010*b*; Hinkle *et al.*, 2012). Furthermore, *Lrrk2* knockout mice show no increased susceptibility to MPTP treatment compared to wild type mice (Andres-Mateos *et al.*, 2009). Interestingly, mice lacking functional Lrrk2 display alpha-synuclein aggregates and accumulation of ubiquitinated proteins in the kidney (Tong *et al.*, 2010*b*), and in another study displayed abnormal exploratory and motor coordination behaviour (Hinkle *et al.*, 2012). Overexpression of G2019S mutated *Lrrk2* results in reduced DA content in the striatum, and mice expressing the R1441G mutant form of *Lrrk2* showed a motor phenotype but neither displayed DA neuronal loss (Li *et al.*, 2009, 2010). Furthermore, G2019S and R1441C knock-in mice show no alterations in DA neuron number in the substantia nigra (Tong *et al.*, 2009; Herzig *et al.*, 2011). Two *Lrrk2* knockout rats have been reported, which showed alterations in kidney morphology and function, however the consequences of Lrrk2 deficiency in the brain are unknown (Baptista *et al.*, 2013; Ness *et al.*, 2013).

1.3.2: Drosophila models of PD

The limitations observed in mouse models of PD prompted the development of alternative, non-mammalian models. These models bring benefits of reduced genetic complexity, ease of manipulation and low cost. The fruit fly (*Drosophila melanogaster*) has emerged as a non-vertebrate, non-mammalian model for PD. Flies with loss of function mutations in *pink1* show a robust phenotype, displaying DA neuron degeneration, flying deficits and reduced climbing speed. Furthermore, analysis of mitochondria in *pink1* knockout flies showed decreased ATP production and swollen mitochondria. Phenotypes appeared to be

progressive, becomes worse with age and resulting in decreased lifespan (Clark *et al.*, 2006).

Flies with *LRRK2* mutations however, have shown inconsistent phenotypes. One study showed that flies with transgenic overexpression of pathogenic mutated human *LRRK2* or wild type human *LRRK2* showed no overall defects. Whereas loss of function mutations in *LRRK2* resulted in severely impaired locomotive activity, reduced tyrosine hydroxylase staining of DA neurons and DA neurons with shrunken morphology (Lee *et al.*, 2007). However, another study showed that flies overexpressing either wild type human *LRRK2* or pathogenic mutated *LRRK2* resulted in adult onset loss of DA neurons, locomotor dysfunction and reduced lifespan (Liu *et al.*, 2008)

1.3.3: The zebrafish as a model for PD

The zebrafish (*Danio rerio)* has now also been established as a unique and valuable vertebrate tool for studying neurodegenerative conditions, including PD. There are several reasons for its popularity, including external development allowing easy visualisation and manipulation, high fecundity, relatively short generation time and the fact that the zebrafish genome has been fully sequenced. Together these features allow easy genetic manipulation and high throughput studies (Xi *et al.*, 2011). Additional benefits include closer genetic homology to humans compared to invertebrate models and the similar functional organisation of the DA neuron system. The DA neuron system in zebrafish has been extensively characterised and this will be discussed below, after which I will describe recent advances in generating zebrafish models of PD.

1.3.3.1: The zebrafish ascending dopaminergic system

In humans, DA neurons that form the nigrostriatal pathway originate in the midbrain, specifically the substantia nigra (pars compacta), and send ascending projections rostrally to the dorsal striatum, specifically the basal ganglial caudate nucleus and putamen. This dopaminergic system modulates motor control and characteristically degenerates in PD (Ayano, 2016). In zebrafish, DA neurons do not develop in the mesencephalon, which is attributed to a positional shift of DA activity during evolution of fish to mammals and is a major difference between zebrafish and mammals (Ryu *et al.*, 2006). However, specific regions of the zebrafish brain do show striking similarities to mammalian brain regions. A region of the ventral telencephalon in zebrafish, named the subpallium (SP), is homologous to the mammalian striatum (Ganz *et al.*, 2010*a*). Furthermore, retrograde dye tracing studies have shown that populations of DA neurons in a region of the ventral diencephalon called the posterior tuberculum (PT) project to the subpallium (Fig.1.3) (Rink & Wullimann, 2001*a*). These ascending neurons are confined to the rostral portion of the PT. It is therefore generally considered that populations of DA neurons in the rostral PT are analogous to the mammalian substantia nigra, and these populations have been comprehensively characterised (Rink & Wullimann, 2001*a*, 2002*a*, 2004).

The PT comprises six discrete populations of DA neurons that show distinct morphology, that can therefore be grouped into three different cell types: small (parvocellular) neurons (type 1), large (magnocellular) pear-shaped neurons (type 2) and parvocellular bipolar cerebrospinal-fluid (CSF) contacting neurons (type 3). The DA neurons can be further grouped into subpopulations, dependent on position along the rostro-caudal axis. The first population is a population of type 1 DA neurons that occupy the periventricular nucleus of the PT (TPp). DA neurons in this population ascend to the subpallium. Second, is a population of type 2 DA neurons that do not belong to any distinct nucleus, but also project to the subpallium. Third, is a population of locally projecting type 3 DA neurons in the paraventricular organ (PVO). Fourth, a second more caudal population of type 2 DA neurons that ascend to the subpallium, and do not belong to any nucleus. Fifth, a population of type 1 DA neurons, immediately dorsal to the posterior tuberal nucleus (PTN), and finally another population of type 1 DA neurons located within the PTN (Rink & Wullimann, 2001*a*). The rostral portion of the PT contains the only three populations of DA neurons that are ascending: the TPp and the two populations of type 2 magnocellular DA

neurons (figure 1.3)(Rink & Wullimann, 2002*a*, 2004). Therefore, the rostral portion of the PT will be the focus of this study, and will be further described as part of results chapter 3.

Aside from the PT, the adult zebrafish brain also contains DA neurons in the telencephalon that are widely dispersed throughout the olfactory bulb, the ventral telencephalon (subpallium) and the preoptic nucleus. In the remaining diencephalon, DA populations are more discrete, and are found in the pretectum, the thalamus, the dorsal and caudal zones of the periventricular hypothalamus, the lateral hypothalamus, the posterior recess of the diencephalic ventricle (caudal hypothalamus) and the locus coeruleus (Fig1.4) (Rink & Wullimann, 2001*a*). Indeed, the overlap between the ventral part of the rostral PT and the hypothalamus is ill-defined, and it remains possible that neurons of the PVO are hypothalamic.

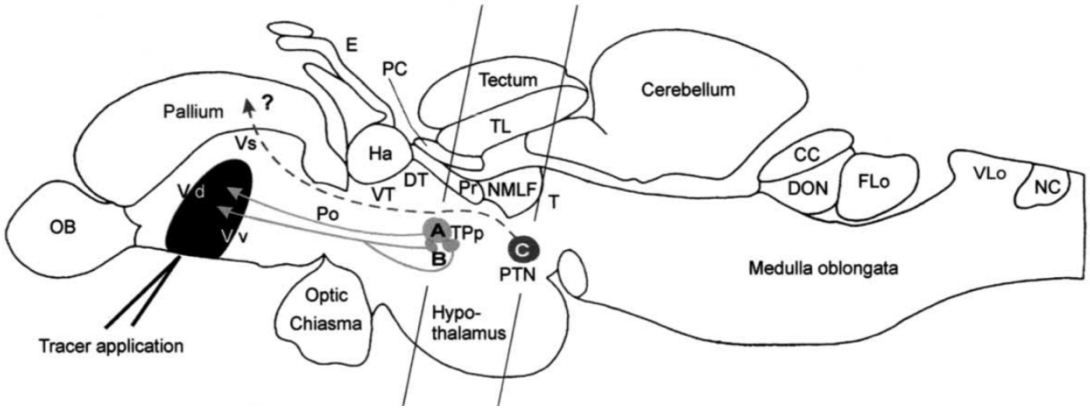

Figure 1.3: Lateral view of the adult zebrafish brain showing tracer injections (black) in the ventral telencephalon.

Three populations of DA neurons in the PT can be identified to be retrogradely tracer-labelled: the periventricular nucleus of the PT (TPp) and two populations of type-2 magnocellular DA neurons adjacent to the TPp (grey). DA neurons in the PTN are thought to project to the dorsal pallium, though this has not been confirmed. Reproduced from Rink and Wullimann, 2002a.

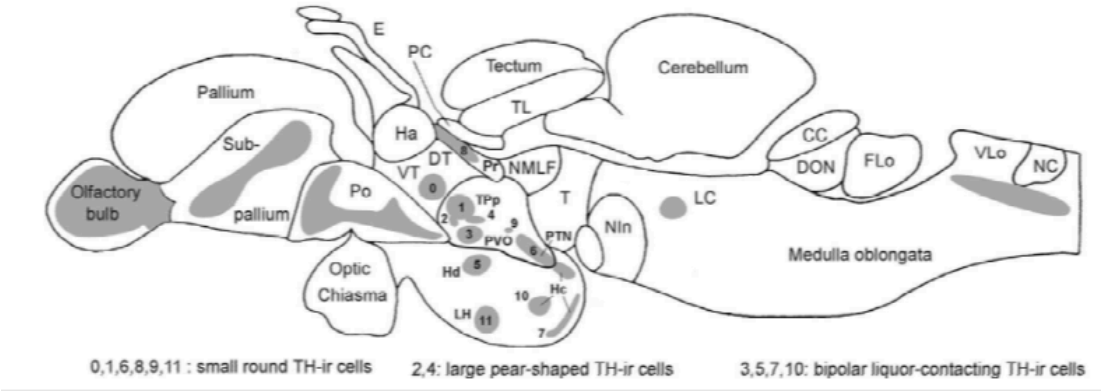

Figure 1.4: Lateral view of the adult zebrafish brain showing all dopaminergic populations.

DA neurons are found in the olfactory bulb, the ventral telencephalon (subpallium), the preoptic region (PO), the ventral and dorsal thalamus (VT,DT), the pretectum (Pr), the PT, the hypothalamus and the locus coeruleus. Reproduced from Rink and Wullimann, 2002b.

Dopaminergic populations in the embryonic and larval zebrafish, and the developmental time course of generation of these populations, have also previously been characterised (Rink & Wullimann, 2002*b*; Mahler *et al.*, 2010). These studies have shown that DA neuron populations in the embryo are observed in positions that correspond to adult populations and have comparable morphology to these corresponding adult populations. It is therefore thought that dopaminergic clusters in the embryo originate in their final adult topological position, although importantly, this has not been directly lineage traced (Rink & Wullimann, 2002*b*). When describing embryonic or larval diencephalic DA populations, previous studies have used numbered format. In the rest of this thesis, I have applied this nomenclature to describe embryonic DA neuron populations. This numbering system is shown in Table 1.2 and shown in Fig.1.4.

In the embryonic zebrafish, several DA neuron populations found in the adult zebrafish are also discernible at 2dpf, in particular those in the olfactory bulb, the ventral telencephalon, the preoptic area and diencephalic populations 1-6 and the locus coeruleus. Diencephalic DA neurons in the pretectum (8), the lateral hypothalamus (11), the periventricular hypothalamus (5), two populations in the caudal hypothalamus (10, 7) and one small population next to the posterior tuberal nucleus (9) are not discernible at 2dpf (Fig.1.5). In

larval zebrafish (5dpf), DA neurons in the pretectum (8) and one of the populations in the caudal hypothalamus (7) are now also present, but those in the lateral hypothalamus (11), the small population adjacent to the posterior tuberal nucleus (9) and one of the populations in the caudal hypothalamus (10) are not (Fig.1.6) (Rink & Wullimann, 2002*b*).

It should be noted that at both 2dpf and 5dpf, DA neurons in the periventricular nucleus of the PT and the ventral thalamus form a contiguous population and cannot be distinguished from one another (Rink & Wullimann, 2002*b*). Here, and for the remainder of this thesis, this population is termed population 1 (figure 1.5, 1.6, table 1.2).

Notably, all DA neuron populations in the rostral PT are present by 2dpf, including ascending DA neuron populations. The developmental time course of some of these populations has also previously been described (Mahler *et al.*, 2010) and is summarised in Table 1.2.

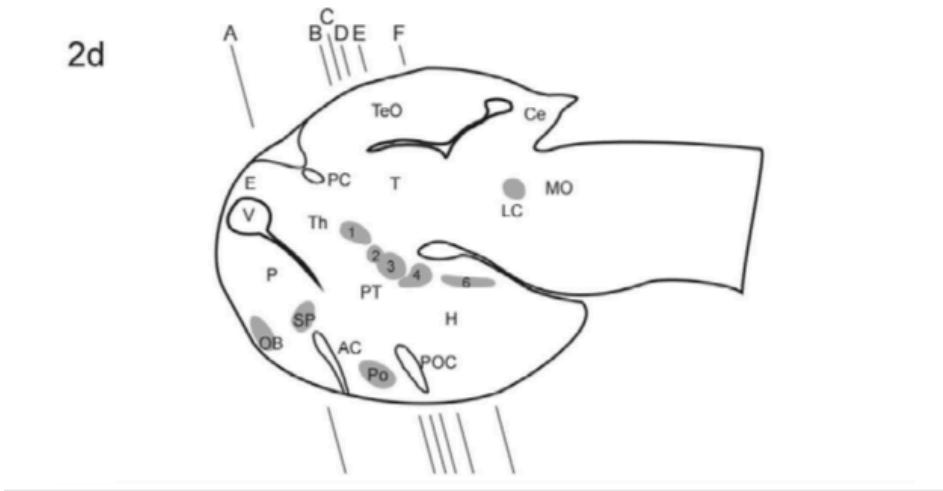

Figure 1.5: Illustration showing DA neuron populations in the 2-day old zebrafish embryo.

Telencephalic populations are present, as well as diencephalic populations 1-6. Reproduced from Rink and Wullimann, 2002b.

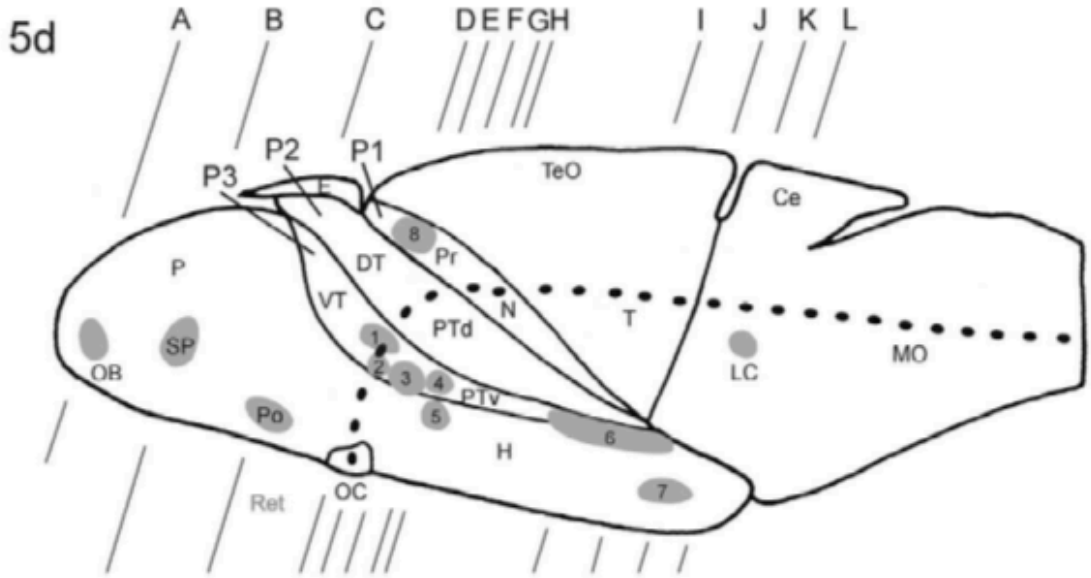

Figure 1.6: Illustration showing DA neuron populations in the 5-day old zebrafish embryo.

Telencephalic populations are present, as well as diencephalic populations 1-8. Reproduced from Rink and Wullimann, 2002b.

Adult population name	Group number (0-11)	Order of appearance (A-F)
Olfactory bulb	-	?
Ventral telencephalon (SP)	-	E (42hpf)
Preoptic area	-	E (42hpf)
Ventral thalamus	1	E (42hpf)
Periventricular nucleus of the posterior tuberculum	**1**	**E (42hpf)**
Large pear shaped neurons of the posterior tuberculum (rostral population)	**2**	**A (18hpf)**
Paraventricular organ	3	D (30hpf)
Large pear shaped neurons of the posterior tuberculum (caudal population)	**4**	**C (24hpf)**
Periventricular hypothalamus	5	E (42hpf)
Posterior tuberal nucleus	6	E (42hpf)
Posterior recess of the diencephalic ventricle (caudal hypothalamus)	7	F (54hpf)
Pretectum	8	?
Small round DA neurons adjacent to the posterior tuberal nucleus	9	?
Caudal hypothalamus	10	?
Lateral hypothalamus	11	?
Locus coeruleus	-	B (20hpf)

Table 1.2: Adult DA neuron populations in the zebrafish and the corresponding group number, used for embryonic and larval terminology, and the order that these populations appear during development.

Populations in the telencephalon and the locus coeruleus are named as adult populations (labelled with a dash). Ascending DA neuron populations are shown in red. Greyed boxes show the populations investigated in this study (i.e. the rostral posterior tuberculum). Question marks are shown for populations where no data showing order of appearance is available. Group numbers are taken from Rink and Wullimann, 2002b, order of appearance data is taken from Mahler et al., 2010.

1.3.3.2: Zebrafish models of PD

Treatment of zebrafish embryos with MPTP results in reduced numbers of DA neurons in the diencephalon and movement deficits, giving a robust PD phenotype (Bretaud *et al.*, 2004; Sallinen *et al.*, 2009). Several studies have also treated zebrafish embryos with morpholinos, allowing knockdown of PD-genes including *parkin, pink1* and *lrrk2* (Anichtchik *et al.*, 2008; Sallinen *et al.*, 2009; Flinn *et al.*, 2009; Xi *et al.*, 2010; Sheng *et al.*, 2010; Ren *et al.*, 2011). However, this data has provided conflicting results, with varied levels of reduction in DA neuron number and movement phenotype, where some studies show no reduction at all. This could be explained by the fact that morpholinos can give many off-target effects and phenotypic outcome also depends on the knockdown efficiency. Furthermore, morpholinos lose their effect by 3-5dpf, preventing investigation of the effects of gene dysfunction in adulthood.

Our group has created a *pink1* knockout zebrafish line using the targeting induced local lesions in genomes (TILLING) approach. TILLING involves chemical mutagenesis using a mutagen such as ethyl methanesulfonate (EMS), followed by a sensitive DNA screening technique to identify single base mutations in the target gene. Identification of mutations relies on the formation of DNA heteroduplexes, formed by genetic recombination of complementary strands after amplification by PCR, where one strand includes a slightly different sequence caused by the mutagenesis. This forms a "bubble" at the mismatch of the DNA strands, which is cleaved by a DNA nuclease, resulting in the separation of the different sized PCR products in gel electrophoresis (Kurowska *et al.*, 2011). TILLING mutagenesis by Flinn et al. (2013) resulted in the generation of a zebrafish line that carries a point mutation in the kinase domain of *pink1*, resulting in the introduction of a premature stop codon, reduced catalytic activity of Pink1 and decreased mRNA stability. Furthermore, it was demonstrated that this *pink1* knockout line displays loss of dopaminergic neurons in the embryo and in the adult, along with mitochondrial impairment. Flinn et al. showed that the TP53-induced glycolysis and apoptosis regulator, TigarB, was upregulated; furthermore, knockdown of *TigarB* resulted in the rescue of DA neuronal number and mitochondrial function (Flinn *et al.*, 2013). This provides an extremely robust model of monogenic-inherited PD, and a marked improvement on previous mouse models that have failed to fully recapitulate *pink1*-mediated PD.

In this thesis, the *pink1* mutant zebrafish line will be used to study the effect of Pink1 deficiency on neurogenesis. In addition, a *lrrk2* mutant line was made to allow future investigations of *lrrk2* in a novel model organism.

1.4: PD and neurogenesis

Recent evidence has suggested that one pathogenic mechanism, contributing to PD onset or progression may be dysregulated neurogenesis. Neurogenesis is defined as the process of generating functional neurons from neural stem and progenitor cells. Until the 1990s, it was believed that neurogenesis in most of the CNS was restricted to embryonic/foetal life, but in the last three decades, evidence has mounted to suggest that neurogenesis may continue in adulthood in distinct regions of the brain (Ming & Song, 2011). Evidence for the hypothesis that neurogenesis may become dysregulated in PD arises from studies showing that PD-genes can regulate neural stem and progenitor cells. However, although some studies have begun to show dysregulated neurogenesis in PD models, none has investigated the generation of DA neurons themselves. Furthermore, ageing is the biggest risk factor for developing PD, and ageing also negatively regulates neurogenesis.

In this section, I briefly summarise our current understanding of the neurogenesis of dopaminergic neurons in prenatal life in mammals and zebrafish, then summarise our current understanding of adult neurogenesis in mammals and zebrafish. I will also discuss the role of ageing in regulation of adult neurogenesis, and finally, I will discuss the current evidence for PD-gene regulation of neural stem and progenitor cells.

1.4.1: DA neurogenesis in embryonic life

The transcriptional control of developmental specification of ventral midbrain (VM) DA neurons in mammals is complex, though key signalling pathways have been shown to be crucial to DA neurogenesis. FGF8, Sonic Hedgehog (Shh) and Wnt1 are required for induction of VM patterning, Lmx1a, Lmx1b and FoxA2 expression is essential to induce VM DA progenitors, and Nurr1 and Pitx3 are crucial for the transition of VM DA progenitors to DA neurons (Hegarty *et al.*, 2013). However, in zebrafish the roles of these factors do not appear to comparatively regulate ventral diencephalic (vDC) DA neuron populations (summarised in table 1.3).

One transcription factor that has been shown to be crucial to zebrafish ascending DA populations is OTP: loss of OTP results in the absence of the ascending populations DC2 and DC4 (Ryu *et al.*, 2007*a*). The role of OTP in development of mammalian ascending neurons is not clear, though one study has shown OTP expression in the nigrostriatal bundle in the postnatal mouse ventral midbrain (Wang & Lufkin, 2000). Another transcription factor that is crucial to the development of ventral diencephalic DA neurons in zebrafish is the Rax orthologue, *rx3*: DA neurons in the rostral posterior tuberculum are missing in *rx3* knockout zebrafish embryos (Muthu *et al.*, 2016). However, the role of Rax in the development of mammalian ascending populations is not clear.

Gene	Effect of knockout in mouse on VM development	Effect of knockdown/ knockout in zebrafish on vDC development
FGF	Loss of FGFR: absent VM DA neurons (Lahti *et al.*, 2012). Loss of FGF2: Post-natal increase in VM DA neurons (Ratzka *et al.*, 2012)	Loss of FGF8: absent DC1 DA neurons. No other groups affected (Holzschuh *et al.*, 2003)
Gli1/2 (Shh effector) /Shh	Deficient VM neurogenesis (Park *et al.*, 2000)	No defects in vDC initiation Reduced proliferation and survival of DA progenitors (Holzschuh *et al.*, 2003)
Wnt	Severe reduction of VM neurogenesis and of DA neurons (Prakash *et al.*, 2006)	Wnt antagonist causes an increase in DA cell number (Russek-Blum *et al.*, 2008)
Lmx1a	Reduction of VM DA neurons (Deng *et al.*, 2011)	Unknown
Lmx1b	Reduction of VM DA neurons (Deng *et al.*, 2011)	Reduction of DA neurons in DC1 population (Filippi *et al.*, 2007)
FoxA2	Increase in $Nurr1^{+}Th^{-}$ neurons in VM (Ferri *et al.*, 2007)	Unknown
Nurr1	No Th, VMAT2, DAT expression in VM DA neurons, DA neurons are subsequently lost (Smits *et al.*, 2003)	Altered spatial organisation of vDC groups, no apparent reduction in number (Filippi *et al.*, 2007)
Pitx3	No SNpc DA neurons VTA unaffected (Hwang *et al.*, 2003)	No effect on DA neurons (Filippi *et al.*, 2007)
OTP	Absent A11 neurons (hypothalamus) (Ryu *et al.*, 2007)	Absent DC2, DC4, DC5 and DC6 DA neurons DC1 and DC3 unaffected (Ryu *et al.*, 2007)
Rax/*rx3*	Unknown	Absent DC1, DC2, DC3 (potentially DC4) neurons (Muthu *et al.*, 2016)

Table 1.3: Summary of the effects of knocking out genes involved in ventral midbrain (VM) or ventral diencephalon (vDC) formation in mouse and zebrafish.

1.4.2: Common methods used for investigating adult neurogenesis: nucleotide analogues and conditional genetic lineage tracing

In the 1950s a new method allowed labelling of dividing cells using [H^3]-thymidine, a radioactive nucleoside that is incorporated into replicating DNA during the S-phase of proliferation, which can be detected by autoradiography. Using this technique, several studies were published that showed [H^3]-thymidine incorporation in various regions of the adult rat brain (Altman & Das, 1965, 1966; Altman, 1969). Subsequently, studies of adult neurogenesis in songbirds began to provide evidence for a functional role of neurogenesis in song learning (Nottebohm, 1980; Brenowitz & Larson, 2015) and later, neural stem cells were isolated from the adult mammalian brain (Reynolds & Weiss, 1992). The field of adult neurogenesis was transformed by the introduction of novel techniques, such as labelling with the S-phase marker, bromodeoxyurine (BrdU) and conditional lineage tracing methods, allowing the tracing of neurons from resident stem and progenitor cells. These techniques will be briefly discussed.

Nucleotide analogues, such as [H^3]-thymidine and BrdU, are incorporated into replicating DNA during the S-phase of proliferation, labelling the cell that is proliferating, but also all progeny from that cell. Variations of both pulse frequency (i.e. frequency of injection of analogues) and chase time (the time after injection and before culling) allows analysis of proliferation and differentiation of newborn cells. In recent years, BrdU labelling has become more common for analysing neurogenesis than [H^3]-thymidine, as BrdU can be detected by immunohistochemistry, whereas [H^3]-thymidine requires autoradiographic detection. However, there are several limitations to BrdU labelling. Firstly, DNA denaturation is required to expose BrdU for detection, which can reduce tissue quality and hinder labelling with other markers. Recently the thymidine analogue 5-ethynyl-2´-deoxyuridine (EdU) has been introduced to combat this problem, requiring no denaturation.

However, with both these techniques, cells that undergo multiple rounds of proliferation can gradually dilute the label and may become undetectable. In addition to this, as nucleotide analogues indicate DNA synthesis, they may also be incorporated into cells undergoing repair, though incorporation through repair tends to be on a much smaller scale (Ming & Song, 2005).

To combat these limitations, many studies combine nucleoside analogue studies with lineage tracing. One way to lineage trace dividing cells is through retroviral labelling. In this technique, retroviruses carrying reporter genes are injected into model animals. The retroviral DNA is incorporated into the host genome during the M-phase of cell cycle, and so are only infectious to dividing cells (Imayoshi *et al.*, 2009). However, this technique is also limited: retroviruses have to be directly injected into the brain, and generally this causes injury, and only allowing infection of small populations. Another method is genetic lineage tracing. In this technique, a recombinase enzyme is expressed in a cell specific manner, and activates the expression of a reporter gene. This permanently labels the cell of interest, and all progeny derived from that cell. One example of this system is the Cre-loxP recombination system. Cre is a recombinase, originally isolated from bacteriophage, that recognises and excises a specific DNA sequence termed loxP. LoxP sites are absent from vertebrate genomes so can be synthetically introduced to allow Cre-mediated recombination. In this system, Cre recombinase is expressed under the control of a specific promotor. In a variation of this method that allows for temporal conditional lineage tracing, Cre can also be fused to the human estrogen receptor (ER^{T2}), so that Cre is only activated by the tamoxifen ligand. This results in specific Cre expression only in cells expressing the gene of interest and only upon addition of tamoxifen. This line is then crossed to another line in which a reporter gene (for example GFP) is preceded by a stop sequence, flanked by loxP sites (loxP-STOP-loxP). In double transgenic animals, conditional expression of Cre results in excision of loxP sites along with the stop sequence, and subsequent expression of the reporter gene. Progeny can then be robustly traced back to the original stem or progenitor cell expressing the gene of interest (Fig.1.7) (Kretzschmar & Watt, 2012).

These methods have revolutionised the field of neurogenesis, allowing robust labelling and lineage tracing of newly generated neurons in the adult brain.

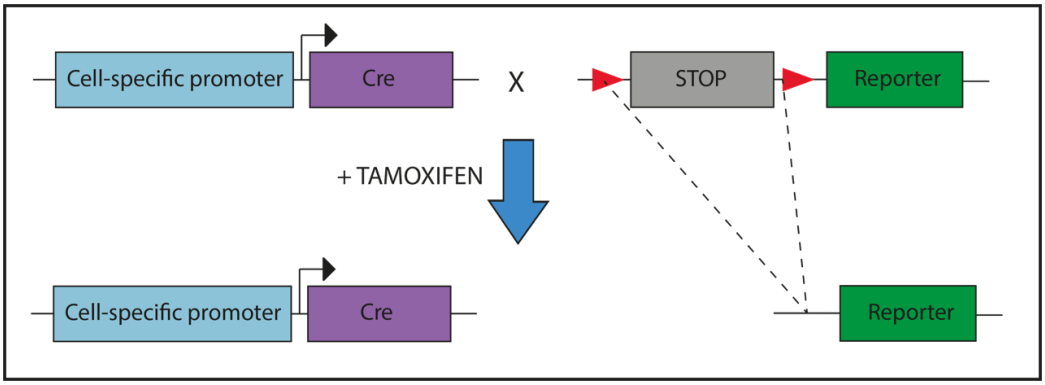

Figure 1.7: Illustration showing the mechanism of conditional lineage tracing using the Cre-loxP recombination system.

Cre recombinase (purple), bound to an estrogen receptor, is driven by a cell-specific promotor (blue). This line is crossed to a reporter line, that has a stop sequence (grey) flanked by loxP sites (red triangles) upstream of a genetic reporter (green). Upon addition of tamoxifen, Cre recombinase excises the stop codon, allowing permanent expression of the reporter gene in the desired cell and its progeny.

1.4.3: Evidence for neurogenesis in the adult mammalian brain

The renewed interest in adult neurogenesis was initially sparked by the demonstration of new neuron production in the dentate gyrus of adult humans (Eriksson *et al.*, 1998). In this study, patients with cancer were injected with BrdU to examine proliferating cells in their tumours. This revealed numerous BrdU-positive neurons in the hippocampus. Since then, numerous studies have demonstrated neurogenesis in the SGZ of the hippocampus (Cameron & McKay, 2001; van Praag *et al.*, 2002; Zhao *et al.*, 2006; Ramirez-Amaya *et al.*, 2006) and have revealed the different cell subtypes associated with de novo neurogenesis. Type B-cells have long radial processes that project through the granule cell layer and express glial fibrillary acidic protein (GFAP) and type D-cells have short processes, and are GFAP-negative. Both type B-cells and type D-cells express Nestin and both are progenitor populations for new granule neurons (termed G cells) (Seri *et al.*, 2001), that migrate a short distance to the granule cell layer GCL (Imayoshi *et al.*, 2009) (Fig.1.8A). Previous studies have shown that very few neurons die in the dentate gyrus, and that the number of granule cells increases during adulthood, suggesting adult neurogenesis contributes to expanding populations in the hippocampus (Bayer *et al.*, 1982; Crespo *et al.*, 1986; Kempermann *et al.*, 2003). Furthermore, conditional lineage tracing of Nestin-expressing

progenitors showed an expansion of labelled granule neurons in early life, and blockade of neurogenesis prevented this expansion. Blockade of neurogenesis was performed using a NSE-DTA mouse line, which carry a loxP-STOP-loxP-IRES-diptheria toxin fragment (DTA) gene cassette in a neuron specific gene. When crossed to Nestin:CreER^{T2} mice, and upon administration of tamoxifen, the STOP region was deleted. This results in expression of DTA in developing neurons, and subsequently cell death. Interestingly, blockade of neurogenesis in this manner resulted in impaired contextual and spatial memory, suggesting neurogenesis in the adult dentate gyrus is required for functional hippocampus-dependent memory (Imayoshi *et al.*, 2008).

Another region generally accepted to harbour cells with neurogenic potential in the adult brain is the SVZ of the lateral ventricles. The SVZ is a layer of cells that extends along the wall of the lateral ventricles, and contains many proliferating cells. Cell subtypes within the SVZ are identified by morphological features and expression of distinct markers, and are termed A, B, C and E cells. A-cells are defined as migrating neuroblasts (migrating immature neurons, committed to a neuronal fate but not terminally differentiated), expressing doublecortin (DCX) and polysialylated-neural cell adhesion molecule (PSA-NCAM). B-cells express GFAP, and can be split into two distinct populations – radial glial-like cells that contact the ventricle (B1) and cells that have stellate morphology and do not contact the ventricle (B2). C-cells express Nestin and are highly proliferative and are also termed transit amplifying cells. E-cells are ependymal cells, lining the ventricular wall (Fig1.8B). Previous studies using retroviral lineage tracing techniques have shown that B1-cells function as neural stem cells in the adult SVZ, giving rise to C-cells (transit amplifying cells), which subsequently give rise to type A-cells (neuroblasts) (Doetsch *et al.*, 1999). Neuroblasts generated from the SVZ migrate through the rostral migratory stream to the olfactory bulb and differentiate into interneurons (Imayoshi *et al.*, 2009). In contrast to the dentate gyrus, studies show that in the olfactory bulb old neurons are replaced by new neurons, as evidenced by unchanged neuron number and high levels of apoptosis (Kaplan *et al.*, 1985; Biebl *et al.*, 2000; Petreanu & Alvarez-Buylla, 2002). This suggests that olfactory bulb population numbers are tightly regulated through the rate of cell death. Indeed, conditional lineage tracing of Nestin-positive progenitors in mice revealed the presence of labelled neurons in the olfactory bulb, where long-term lineage tracing showed that almost the entire population in the olfactory bulb was replaced over a 12-

month period. Furthermore, blockage of neurogenesis in the SVZ resulted in a gradual decrease in population number, suggesting death of olfactory neurons occurs independent of the generation of new neurons and that continued neurogenesis is essential for maintenance of cell number. Interestingly however, blockage of SVZ neurogenesis showed no effect on simple tests of olfactory discrimination of odours, though more complex tasks were not investigated (Imayoshi *et al.*, 2008).

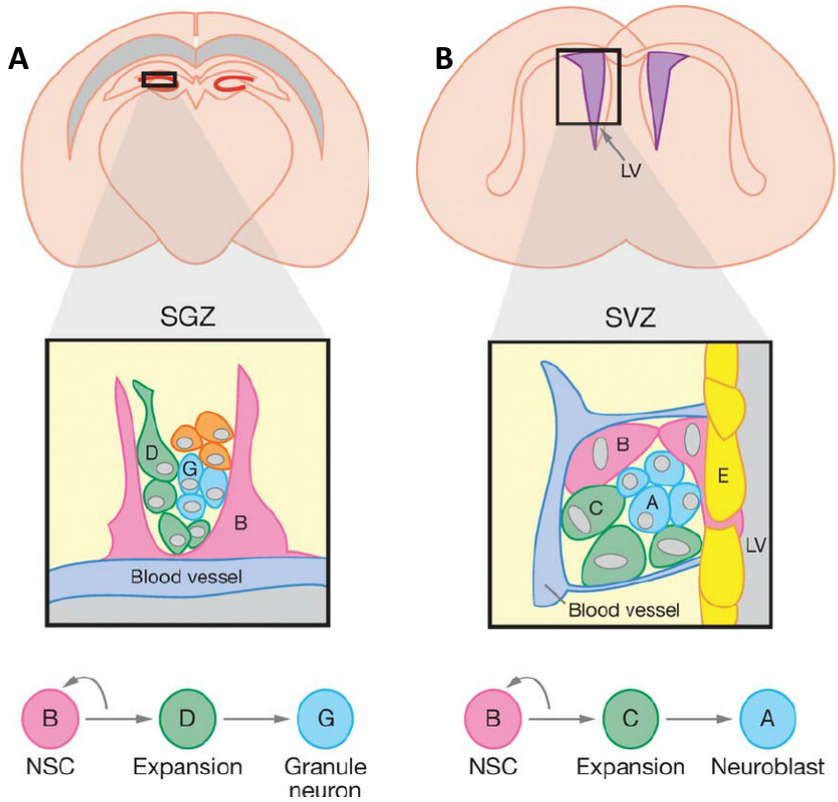

Figure 1.8: Illustration showing the organisation of the neural stem cell niche in the SGZ (A) of the lateral ventricles and the SVZ (B) of the dentate gyrus.

A: In the SGZ, type B-cells are defined as neural stem cells, type D cells as transit amplifying progenitors, and type G-cells as granule neurons.

B: In the SVZ, type B-cells are defined as neural stem cells, type C cells as transit amplifying progenitors, type A-cells as neuroblasts and type E-cells as ependymal cells. Figure reproduced from Li and Xie, 2005.

More recent studies have shown the hypothalamus to be a neurogenic region in the adult mammalian brain. The hypothalamus acts as a homeostatic regulator of many core bodily functions, including energy balance, stress regulation and reproduction. The hypothalamus is centred around the third ventricle, which is lined by radial-glial like cells named tanycytes. Tanycytes are specialised ependymal cells, thought to bridge the gap between the central nervous system and the cerebrospinal fluid, allowing transfer of neuroendocrine signals. To achieve this, tanycytes project a basal extension to surrounding nuclei, and apically, contact the cerebrospinal fluid (CSF). Tanycytes are classed into subgroups, dependent on their position along the ventricle and their expression of distinct markers. These groups are: α1-, α2- and β-tanycytes (Fig.1.9).

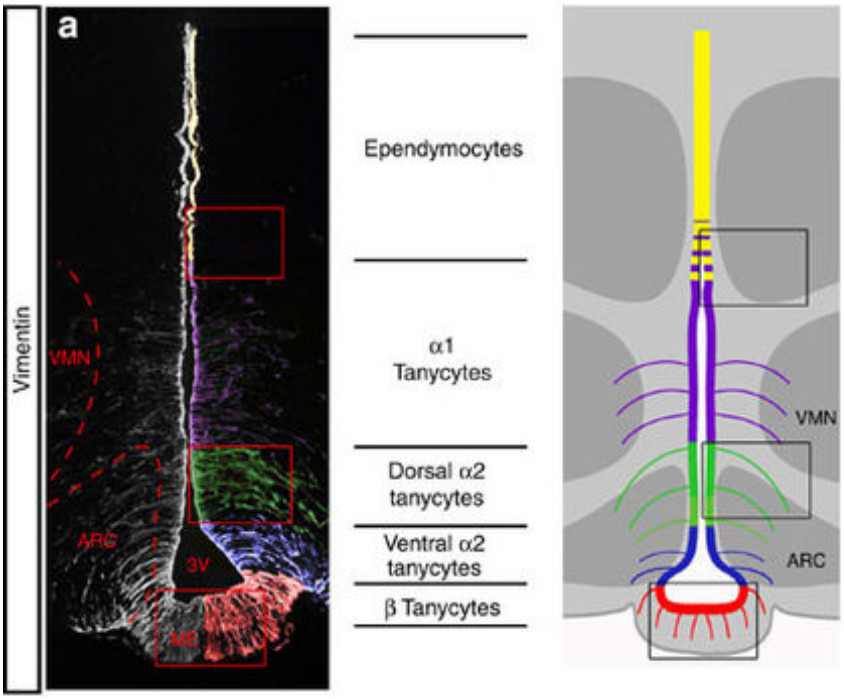

Figure 1.9: Tanycyte subgroups in the hypothalamus.

Tanycytes lining the third ventricle in the hypothalamus can be grouped into different classes depending on their position in the ventricle.

Tanycytes of the hypothalamic third ventricle have been suggested to be potential stem and progenitor cells, due to shared similarities with stem/progenitor cells of the SVZ and SGZ, including similarities in morphology and in gene expression, for instance, a radial glial-like morphology and expression of GFAP and Nestin (Recabal *et al.*, 2017). Indeed, several studies using conditional lineage tracing techniques have shown that subsets of tanycytes give rise to other tanycytes and neurons in the surrounding parenchyma (Robins *et al.*, 2013; Haan *et al.*, 2013). These studies, together with neurospherogenic assays ex vivo confirm their role as neural stem and progenitor cells in the adult brain. The basal rate of neurogenesis in the adult hypothalamus is lower than in the SVZ and the SGZ (Migaud *et al.*, 2010), however this niche appears to be extremely responsive to a number of growth factors, including insulin-like growth factor (IGF), brain-derived neurotrophic factor (BDNF), ciliary neurotrophic factor (CNTF) and fibroblastic growth factor (FGF) (Pencea *et al.*, 2001; Kokoeva *et al.*, 2005; Pérez-Martín *et al.*, 2010 p.1; Robins *et al.*, 2013), all of which markedly enhance proliferation of resident cells in the ventricular and subventricular zone of the third ventricle. Interestingly, changes in metabolic conditions can also modify hypothalamic progenitor proliferation, including high temperature, exercise and a high fat diet (Kokoeva *et al.*, 2005; Matsuzaki *et al.*, 2009; Nascimento *et al.*, 2016; Niwa *et al.*, 2016). This suggests that progenitors in the adult mammalian hypothalamus are part of an environmentally responsive niche. Although the precise functional relationships between different cell types in the adult SGZ, SVZ and hypothalamus is still not fully understood, the studies described above support the idea that cells with radial glial morphology give rise to transit amplifying progenitors and neurons, suggesting their role as neural stem cells in the adult brain.

Aside from the SVZ, the SGZ and the hypothalamus, several other adult mammalian brain regions have been shown to show some level of neurogenic potential, though it should be noted that these studies are controversial and highly disputed. In the adult neocortex, several studies have combined BrdU labelling with antibodies that detect neuronal markers, such as NeuN, in mammalian species. These studies have shown evidence for newly generated neurons in the adult neocortex in rats and primates (Gould *et al.*, 1999, 2001, 2001; Bernier *et al.*, 2002). However, other studies have failed to replicate this finding in mice and in primates (Kornack & Rakic, 2001; Ehninger & Kempermann, 2003). Several studies have also reported adult neurogenesis in the striatum (Dayer *et al.*, 2005;

Luzzati *et al.*, 2006; Bédard *et al.*, 2006), however others have only found such evidence after stimulation with growth factors or pharmacological manipulations (Gould, 2007).

Most pertinent to this study are investigations into neurogenesis of dopaminergic neurons in the mammalian substantia nigra. One study by Zhao et al. (2003) demonstrated the addition of new DA neurons to the substantia nigra in adult mice. In this study, the number of DA neurons in the substantia nigra was quantified: there was no change in numbers of DA neurons between 2- and 20-months of age. However, analysis of cell death showed that a proportion of DA neurons were dying. This provided initial evidence that DA neurons were generated in adulthood. Analysis with BrdU labelling then showed the presence of a small number of newly generated DA neurons in the 16-week-old mouse. Furthermore, dye labelling of cells lining the lateral ventricles resulted in dye labelled DA neurons in the substantia nigra (Zhao *et al.*, 2003). This study suggests the possibility of de novo DA neurogenesis in the substantia nigra. However it has been disputed by a study using similar experimental procedures that could not replicate this data (Frielingsdorf *et al.*, 2004). Furthermore, other studies have shown no evidence for DA neurogenesis using BrdU analyses (Kay & Blum, 2000; Lie *et al.*, 2002). On the other hand, two studies have provided evidence that DA neurogenesis can be stimulated under specific conditions: first, rat midbrain progenitors can give rise to DA neurons in vitro (Lie *et al.*, 2002); second, lesioning the substantia nigra with MPTP stimulates DA neurogenesis in mice (Shan *et al.*, 2006). Finally, rodent, primate and human substantia nigra contain DA neurons with polysialic-like immunoreactivity, indicative of newly differentiated neurons (Yoshimi *et al.*, 2005).

There could be numerous reasons for such discrepancies. Firstly, it is possible that any neurogenesis in the substantia nigra occurs at an extremely low rate, raising the question of whether negative results result from a lack of sensitivity in technique: Lie et al. used sections sampled infrequently: every 6th section was examined, therefore may not have detected new-born DA neurons. Secondly, small differences in analytical technique could explain some discrepancies. For example, Zhao et al. analysed male mice at 16 weeks of age, whereas Frielingsdorf et al. analysed male mice at 9-10 weeks of age. It is possible that there are differences in the rate of generation at different ages. Additionally,

Frielingsdorf et al. used a lower concentration of BrdU in their experiments. Thirdly, differences in housing conditions could result in discrepancies: as discussed above in other neurogenic regions such as the hypothalamus, environmental conditions can influence neurogenesis. Finally, none of these studies utilise a conditional genetic lineage tracing approach, which would definitively determine whether new DA neurons are generated from resident stem and progenitor cells. In summary, then, from these studies, it is not clear whether DA neurons can be generated in the adult mammalian substantia nigra. Together with other studies showing that murine models do not effectively recapitulate all aspects of PD, particularly DA neurodegeneration (see section 1.3.1), this suggests that murine models may not be the best animal to model the ascending dopaminergic neuron system. It is unknown whether adult DA neurogenesis of ascending populations occurs in non-mammalian models, such as zebrafish, and this was one of the aims of my study.

1.4.4: Regulation of vertebrate neurogenesis

Homeostatic regulation of neurogenesis requires the balance of maintaining a stem cell pool whilst also generating neurons. Both intrinsic and extrinsic mechanisms regulate adult neurogenesis. Many of these mechanisms have been characterised, and extensively studied, through analyses of embryonic development. Such studies have elucidated the signalling pathways that regulate proliferation and differentiation of neural stem and progenitor cells. in both embryonic and adult life.

Several secreted ligands have been shown to act as regulators of stem and progenitor cells in the central nervous system, including Notch, Sonic hedgehog (Shh), Wnts and bone-morphogenetic proteins (BMPs)(Ming & Song, 2011). These ligands regulate stem/progenitor cell maintenance, proliferation and differentiation. For example, studies showed that in the embryonic CNS, Notch signalling plays a crucial role in the maintenance of stem and progenitor populations (Lasky & Wu, 2005). Notch signalling has also been shown to be required for maintenance of stem and progenitor populations in the adult SVZ. Conditional deletion of a downstream mediator of the Notch receptor, RBPj, results in premature differentiation of neural stem/progenitor cells and depletion of the stem/progenitor cell pool in both embryonic and adult mice (Imayoshi *et al.*, 2010).

Another study also implicated Notch in the maintenance of ependymal cell fate. Upon injury of the SVZ, ependymal cells give rise to astrocytes, and vice versa. Blockage of another downstream mediator of Notch, Ephrin, resulted in the differentiation of ependymal cells to astrocytes (Nomura *et al.*, 2010). Shh, well-known for its ability to govern progenitor patterning, proliferation and even neurogenesis in the embryo (Ingham & Placzek, 2006) has also been shown to play a role in regulation of adult neurogenesis: Shh signalling in the SVZ and the SGZ is required for the formation and maintenance of neural stem cells. In the SGZ, mutant mice that lack primary cilia (which is required for Shh signalling) in a subset of embryonic stem cells, results in reduced numbers of type D-cells in the postnatal SGZ and an absence of type B-cells, the stem-like radial glial population in the SGZ. This suggests that functional cilia and Shh signalling are required for establishment of neural stem cells and neurogenesis in postnatal life (Han *et al.*, 2008). In another study, conditional knockout of the Shh mediator Smoothened (Smo) in the postnatal mouse SVZ resulted in the depletion of the stem cell population, suggesting Shh is required for maintaining neural stem cells in a quiescent state. In addition, the authors observed a reduction in proliferation of transit amplifying cells and failed migration of neuroblasts. This suggests Shh signalling mediates diverse functions in different cell types in the SVZ (Balordi & Fishell, 2007). Wnt signalling, originally characterised in the embryo and shown to be required for early embryonic patterning events and cell fate determination in the embryo (Bielen & Houart, 2014; Noelanders & Vleminckx, 2017) has also been shown to promote proliferation and specification of progenitors to a neuronal fate in adult mice: overexpression of Wnt3 increases proliferation and neurogenesis (Lie *et al.*, 2005). BMPs, described to promote non-neuronal ectoderm in the developing embryo, where inhibition of BMPs is required to establish neuroectoderm (Bond *et al.*, 2012), have been shown to promote gliogenesis and block neuronal differentiation in the adult SVZ. Overexpression of BMP4 increases the number of astrocytes but depletes astrocyte progenitor pools. Furthermore, inhibition of BMP4 results in expansion of the astrocyte progenitor pool and decreases the number of astrocytes (Bonaguidi *et al.*, 2005).

Several growth factors have also been implicated in the regulation of adult neurogenesis. Epidermal growth factor (EGF) and fibroblast growth factor 2 (FGF2) both promote proliferation in the SVZ; FGF2 increases the number of newly generated neurons in the olfactory bulb, and EGF increases the number of astrocytes in the olfactory bulb (Kuhn *et*

al., 1997). In the hypothalamus, FGF2 has also been shown to increase tanycyte proliferation (Robins *et al.*, 2013). Furthermore, BDNF is also a key regulator of adult neurogenesis: adult mice lacking the BDNF receptor, p75, display deceased neurogenesis in the SVZ and BDNF enhances survival of newborn neurons in the hippocampus (Zhao *et al.*, 2008).

Several external stimuli also influence neurogenesis. For example, physical exercise increases cell proliferation in the adult mouse SGZ (van Praag *et al.*, 1999) and high temperature, exercise or a high fat diet can influence progenitor behaviour in the adult hypothalamus (Kokoeva *et al.*, 2005; Matsuzaki *et al.*, 2009; Nascimento *et al.*, 2016; Niwa *et al.*, 2016). Ageing has also been previously shown to negatively regulate adult neurogenesis in several studies (Smith *et al.*, 2017). As ageing remains the biggest risk factor for developing PD, the role of ageing in the regulation of neurogenesis is particularly relevant to this study and will be discussed below.

In the rodent, the rate of proliferation and neurogenesis decreases with age in both the SGZ and the SVZ (Seki & Arai, 1995; Kuhn *et al.*, 1996; Kempermann *et al.*, 2002; Jin *et al.*, 2003; Luo *et al.*, 2006). The major decrease in neurogenesis occurs between 3- and 12-months of age (Kuhn *et al.*, 1996). Interestingly, age-related decline in neurogenesis in the SVZ has been linked to functional decline in olfaction in adult mice (Enwere *et al.*, 2004). In humans, one study measured the level of nuclear bomb test-derived ^{14}C in the nuclear DNA of neurons. By comparing neuronal ^{14}C levels to yearly atmospheric measurements, neurons could effectively be birth-dated. Not only did this study show evidence for addition of SVZ-derived neurons to the striatum in adulthood, the authors also demonstrated an age-related decrease in neurogenesis (Spalding *et al.*, 2013). By contrast, one recent study showed that young neurons could not be detected in the dentate gyrus of adults aged 18-77, with numbers of proliferating cells (measured by expression of the transient proliferation marker, Ki67) declining sharply during infancy (Sorrells *et al.*, 2018). However, the patient tissue analysed in this study was obtained either 48-hours after patient death or from patients with epilepsy undergoing brain surgery. It is not clear how neurogenesis is affected by subsequent death or by diseases such as epilepsy, though epileptic seizures have been shown to induce proliferation of neural stem cells, suggesting

repeated seizures may cause depletion of the stem cell pool (Lugert *et al.*, 2010). If true, this study suggests that neurogenic potential falls rapidly in the first year after birth. Due to the difficulty in obtaining enough tissue from human patients that are healthy, the implications of these studies are not yet clear, though understanding the limitations of adult human neurogenesis is pivotal to the interpretation of findings from other animal models.

The cause of an age-related decline in neurogenesis is not yet understood, though several studies have proposed various mechanisms to explain the decrease (Riddle & Lichtenwalner, 2007). One theory is that neural stem and progenitor cells in the adult brain may stop cycling, or cycle less frequently, due to a decrease in environmental cues or the accumulation of inhibitory factors. Indeed, the addition of growth factors such as IGF, EGF or FGF can negate the effects of age on proliferation in mice (Lichtenwalner *et al.*, 2001; Jin *et al.*, 2003). This suggests that responsive neural stem and progenitor cells are still present in the aged brain. Furthermore, reduction of corticosteroid levels by adrenalectomy also results in increased proliferation in aged mice (Cameron & McKay, 1999), suggesting increased corticosteroid levels with age may contribute to neurogenic decline. Another theory is that the decline is due to a reduction in the number and proliferation rate of more committed progenitor cells. Decreases in BrdU labelling in aged animals most likely reflect a decrease in the proliferation of rapidly dividing progenitor cells, i.e. transit amplifying cells, and in theory, could reflect smaller populations of progenitor cells or a slower progenitor cell cycle. Studies have shown that cell cycle length increases with age in the SVZ (Luo *et al.*, 2006), though this occurs later in life than does the decline in proliferation. This suggests that the decrease in proliferation is more likely due to smaller populations of rapidly proliferating progenitors. In addition to this, neuronal commitment and differentiation also appear to be affected by age. For example, middle-age rats show approximately a 60% decrease in the percentage of newborn cells in the SGZ that express neuronal markers compared to young rats (Lichtenwalner *et al.*, 2001). The number of newborn cells expressing the neuroblast marker DCX does not change with age, implying that alterations arise in late stages of differentiation or maturation (Rao *et al.*, 2005).

Interestingly, studies show that levels of gliogenesis are not reduced with ageing in mice, with no age related decrease in the number of newly generated oligodendrocytes in the olfactory bulb (Capilla-Gonzalez *et al.*, 2015). Together this suggests that an age-related

decline in neurogenesis may be caused by several factors, including alterations to environmental cues, reduced progenitor populations, impeded differentiation of late-stage neurons and an alteration in the balance of neurogenesis and gliogenesis.

In summary, this data shows that multiple signalling pathways and environmental cues act on adult neural stem and progenitor cells to allow tight regulation of the number of quiescent stem cells and the number of new neurons and astrocytes generated, and shows that, in general, there is an age-related decline in de novo adult neurogenesis.

1.4.5: Using zebrafish to investigate adult neurogenesis

In my PhD thesis, I used the zebrafish to analyse the generation of dopaminergic neurons in the posterior tuberculum (PT) in both wild type and a genetic model of PD (see chapters 5 and 6). Zebrafish have recently emerged as a useful tool for analysing adult neurogenesis, as they harbour many similarities to mammals. Firstly, zebrafish and mammals share many molecular and cellular regulatory mechanisms of neurogenesis. Secondly, neurogenesis in zebrafish is confined to distinct regions in the adult brain, suggesting the presence of defined neurogenic niches comparable to the adult mammalian brain. Although there are some differences, including more widespread proliferation zones in zebrafish, understanding the mechanisms that allow increased generation could result in the development of treatments to stimulate endogenous neurogenesis in humans (Alunni & Bally-Cuif, 2016), or to direct the differentiation of pluripotent cells towards defined adult neuronal populations. In this section, the similarities and differences between zebrafish and mammalian neurogenesis will be described.

One of the most well studied neurogenic regions in the adult zebrafish is the dorsal telencephalon, also called the pallium, which contains regions that bear similarity to the mammalian SVZ, SGZ and neocortex. In the zebrafish pallium, populations of cells with radial glial morphology line the ventricle, covering a large majority of the ventricular zone (VZ). Radial glia organise into a monolayer, contacting the CSF and projecting long processes into the surrounding parenchyma of the pallium (Than-Trong & Bally-Cuif, 2015). Radial glial cells form a heterogeneous population, and are derived from distinct

embryonic progenitor populations (Dirian *et al.*, 2014). Adult telencephalic radial glia show differences in the expression of glial markers such as Nestin, GFAP, S100B, BLBP and Vimentin; the functional significance of pallial VZ heterogeneity remain poorly-understood. Analysis of BrdU and proliferative markers such as PCNA, have shown that dividing cells along the ventricle include pallial radial glia. After longer chase times, neurons in the pallium also express BrdU, indicating they are newly generated (Adolf *et al.*, 2006). Furthermore, conditional lineage tracing studies have shown that pallial radial glial cells can self-renew and generate multipotent progenitors which subsequently give rise to new neurons in the pallium and the olfactory bulb (Kroehne *et al.*, 2011). Lineage tracing was performed using a genetic strategy (section 5.2.3), in which Cre recombinase was driven by the Her4 gene. Her4 (the zebrafish orthologue of Hes5) is a transcription factor of the Hairy/Enhancer-of-split family. Expression of Hes genes is induced by Notch signalling (Fig.10), and Hes5/Her4 act to promote self-renewal and maintenance of neural stem cells (Kageyama *et al.*, 2008; Chapouton *et al.*, 2010, 2011). The extent of the neuronal subtypes that are generated in the pallium, and their function, are not yet fully understood. However, the finding that neurogenesis is driven from radial glial stem and progenitor cells suggests a similarity to mammalian neurogenesis.

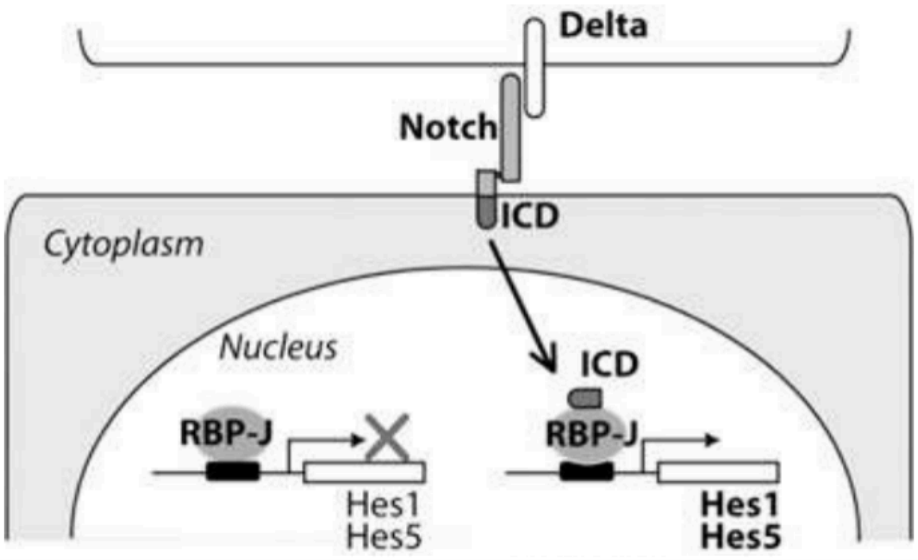

Figure 1.10: Notch induced Hes1/Hes5 signalling.

Upon activation of Notch by one of its ligands, for example Delta, the intracellular domain (ICD) is cleaved and enters the nucleus. ICD forms a complex with the DNA-binding protein RBP-J. In the absence of nuclear ICD, RBP-J represses Hes1/Hes5 by binding to their promoters. Upon Notch activation and subsequent RBP-J binding, Hes1 and Hes5 expression is induced. Figure reproduced from Kageyama et al., 2008.

In addition to similarities in stem and progenitor populations between mammals and zebrafish, many regulatory factors of neurogenesis are also conserved between species. One of the most studied is the Notch signalling pathway. Much like adult mammals, Notch is also crucial for maintaining quiescence in neural stem cells in adult zebrafish. This is evidenced by expression of Notch target genes in quiescent radial glia in the pallium (Chapouton *et al.*, 2010, 2011) and by experiments that show that blockage of Notch3 signalling by inhibition of γ-secretase results in increased proliferation of pallial radial glia and overgrowth of the pallial VZ (Alunni *et al.*, 2013). Expression of *her4* is widespread in the zebrafish brain, suggesting that the majority of radial glial cells are in a quiescent state (Chapouton *et al.*, 2011). Indeed, the average time between two divisions in the same pallial radial glial cell has been estimated to be one month (Rothenaigner *et al.*, 2011). Another similarity between zebrafish and mammalian neurogenesis is that zebrafish also display an age-related decline in telencephalic neurogenesis. One study showed that between 2 and 20 months of age, the number of BrdU-labelled cells significantly decreased in the VZ of the telencephalon, with an additional decrease in the number of newly generated neurons in the olfactory bulb. The authors also showed that restricted regions of the VZ became devoid of progenitors in aged zebrafish, with a decrease in the number of cycling progenitors (Edelmann *et al.*, 2013). This suggests that fewer radial glia enter the cell cycle in the aged brain, and therefore reduce the number of transit amplifying progenitors that are generated.

The diencephalon of the zebrafish has received much less attention, in terms of adult neurogenesis. However, it is clear that in the diencephalon, radial glial cells, including *her* expressing radial glia, similarly populate the ventricular zone, though their density varies, depending on the precise location within the diencephalon (Menuet *et al.*, 2005; Chapouton *et al.*, 2011; Than-Trong & Bally-Cuif, 2015). Furthermore, it is known that the diencephalon retains several proliferative zones, including distinct proliferative zones in the posterior tuberculum (Grandel *et al.*, 2006). One such proliferative zone is the TPp, which contains ascending DA neurons. It is not clear from these studies however, whether DA neurons are generated in this region in adulthood. Interestingly, a second proliferative zone within the posterior tuberculum, the paraventricular organ, has been described to be particularly rich in radial glial cells. Unusually, the nuclei of the radial glia in this zone are located away from the VZ, and project a short process toward the ventricle (Pérez *et al.*,

2013). Again, the extent of de novo neurogenesis in the adult paraventricular organ is not known.

Although the mammalian and zebrafish brain display many similarities, some key differences are also present. The mammalian telencephalon develops by evagination of the neural tube, whereas the zebrafish telencephalon develops by eversion (outward folding of the neural tube). Therefore the proliferative zones in zebrafish are present in the internal ventricle, but also cover the external pallial surface (Schmidt *et al.*, 2013). This means that proliferative zones in the zebrafish possess different architecture to those in mammals: in mammals, the proliferative zones are covered by an epithelium (ependymal cell layer), whereas in zebrafish, the ependymal layer is restricted to dorsal proliferative zones and more ventral zones are devoid of this layer. Perhaps the most crucial difference between zebrafish and mammalian neurogenesis is the rate of de novo cell generation: zebrafish display more widespread proliferation zones, a more constitutive form of neurogenesis and more efficient regeneration after injury (Grandel *et al.*, 2006; Chapouton *et al.*, 2011; Than-Trong & Bally-Cuif, 2015). The reasons behind this are not fully understood, though studies investigating the effect of injury in the telencephalon have shown that zebrafish possess an ability to stimulate reactive neurogenesis from quiescent radial glia, which contributes to regenerative potential in the telencephalon (Kroehne *et al.*, 2011; Schmidt *et al.*, 2013). Interestingly, this regenerative potential does not appear to negate the effects of ageing on neurogenesis (Edelmann *et al.*, 2013), suggesting common mechanisms may exist between mammals and zebrafish in regulation of neurogenesis with age. Understanding the mechanisms that underlie adult neurogenesis in zebrafish is crucial to understanding the mechanisms and limitations of human neurogenesis, and subsequently to the development of treatments that can harness an endogenous potential to repair. However currently, the shared attributes of mammalian and zebrafish neurogenesis allow insight into neural stem and progenitor cell biology in brain regions that share homology with mammalian counterparts. Furthermore, with the recent generation of a robust zebrafish model of PD, the zebrafish provides a unique opportunity to study adult neurogenesis in the context of the disease.

1.4.6: PD-genes regulate neural stem and progenitor cells

Non-motor symptoms such as anosmia, depression, anxiety and sleep disturbances are not thought to be directly associated with the degeneration of the nigrostriatal DA system. Instead, these processes rely directly on function of the olfactory system, the hippocampus and the hypothalamus: regions that display neurogenesis in adult life (Winner *et al.*, 2011*a*). It is therefore conceivable that some non-motor symptoms experienced by patients with PD may be related to altered neurogenesis in these regions. This idea is strengthened by recent studies that show that genes found to be mutated in cases of PD, including *SNCA*, *PINK1* and *LRRK2,* also play a role in regulation of neural stem and progenitor cells. This begins to suggest that dysregulated neurogenesis may be one pathological mechanism in PD, and could contribute to disease onset, progression or development of non-motor symptoms.

Alpha-synuclein, encoded by *SNCA*, has been implicated in the regulation of neural stem/progenitor cells in the adult brain. In one study, the pathogenic role of alpha-synuclein inclusions in neurogenesis was investigated by overexpressing human *SNCA* in adult mice. No overall difference in proliferation was observed in the SVZ or the SGZ, however a cell fate analysis after 1-month of BrdU injection showed around 50% fewer newly-generated cells in the olfactory bulb and the dentate gyrus in *SNCA* overexpressing mice and around 60% fewer newly-generated DA neurons in the olfactory bulb. Furthermore, around a 50% increase in the number of apoptotic cells in the dentate gyrus (but no difference in the SVZ) in mice overexpressing *SNCA* was observed. Analysis of the number of early and mature neural progenitors in the SGZ revealed no difference in the number of early progenitors, but around a 60% decrease in the number of mature progenitors. Together this study suggests that overexpression of human *SNCA* results in reduced survival of progenitors in the SGZ and the olfactory bulb (OB), and consequently reduced DA neurogenesis in the dentate gyrus and the OB (Winner *et al.*, 2004). In another study, the effect of overexpressing a mutant form of human *SNCA* (A53T) on adult neurogenesis was analysed in mice, showing that expression of mutant *SNCA* aggravates the reduced neurogenesis observed in mice overexpressing wild type human *SNCA*. Mice expressing A53T *SNCA* displayed a more pronounced reduction in the number of newly generated neurons compared to mice overexpressing human wild type *SNCA*. This was

combined with increased levels of cell death in the SVZ and an added phenotype of reduced levels of proliferation. Interestingly, cell death was observed in the SVZ and the OB in mice expressing A53T *SNCA*, but only in the OB in mice overexpressing wild type *SNCA*. This suggests that an excess of wild type alpha-synuclein diminishes survival of new neurons, but that A53T mutant alpha-synuclein decreases survival at an earlier stage, potentially in migrating neuroblasts (Winner *et al.*, 2008). It is not clear from this study whether overexpression of mutant or wild type *SNCA* results in diminished neurogenesis due to cell intrinsic toxicity, or due to changes in microenvironment. However, these studies clearly show that increased levels of both wild type and mutated forms of alpha-synuclein are deleterious to adult neurogenesis. Interestingly, investigations into the effects of the loss of alpha-synuclein show that *SNCA* knockout results in increased numbers of newly generated neurons in the SGZ (Winner *et al.*, 2012). Together, this data suggests that alpha-synuclein may negatively regulate adult neurogenesis, such that overexpression may cause reduced survival of neural progenitors. The underlying mechanisms however, are not clear.

PINK1 has also been implicated in the regulation of adult neurogenesis. *PINK1* mRNA is detected throughout the adult brain, including the substantia nigra, but is also strongly expressed in regions that have been shown to display adult neurogenesis, such as the dentate gyrus and the hypothalamus (Taymans *et al.*, 2006). One study in *Drosophila* has shown that PINK1 can interact with Notch, in a noncanonical Notch signalling pathway, to directly regulate the self-renewal and differentiation of neuroblasts (the *Drosophila* equivalent of neural stem cells)(Lee *et al.*, 2013). In this study, the authors showed that Notch gain of function resulted in increased self-renewal of neuroblasts, correlating with increased levels of phosphorylated AKT (protein kinase B), and increased activation of the kinase that is responsible for AKT phosphorylation, mammalian target of rapamycin complex 2 (mTORC2). In Notch loss of function mutants, mTORC2 was inhibited. This suggests that Notch activation of mTORC2/AKT signalling results in the increased self-renewal of neuroblasts. The authors next showed that Notch was localised at the mitochondrial membrane, suggesting that Notch exerts its effect at the mitochondrial membrane. Since PINK1 is involved in the recruitment of proteins to the mitochondrial surface, the authors next assessed the interaction of Notch with PINK1. Interestingly, Notch mitochondrial localisation was decreased in PINK1 knockout *Drosophila*, and Notch

and PINK1 were also shown to associate in co-immunoprecipitation studies. This suggests that the mitochondrial localisation of Notch, and therefore mTORC2/AKT signalling is dependent on PINK1, and that activation of this pathway results in self-renewal of neuroblasts (Lee *et al.*, 2013). More recently, PINK1 has been implicated in the regulation of neural progenitors in the mouse hippocampus. Cultured neural stem/progenitor cells from the mouse *PINK1*-/- hippocampus displayed lower mitochondrial membrane potential, suggesting mitochondrial dysfunction, and an upregulation of glycolysis. Cultured cells from *PINK1*-/- mice also showed impeded differentiation to neurons, and neurons derived from *PINK1*-/- neural stem/progenitor cells displayed fewer dendritic branches. Interestingly, oligodendrocytes were generated from *PINK1*-/- neural stem/progenitor cells, but were not observed in wild type cultures and the number of astrocytes generated was not different between genotypes. In vivo experiments showed an increase in the proportion of early neuroblasts and transit amplifying progenitors, with reduced numbers of intermediate and late stage neuroblasts in *PINK1*-/- mice. Furthermore, EdU pulse/chase analyses showed fewer newly generated neuroblasts and neurons in the hippocampus in *PINK1*-/- mice, whilst overall levels of proliferation were not changed (Agnihotri *et al.*, 2017). Together, this suggests that loss of PINK1 results in mitochondrial dysfunction in SGZ neural stem cells, increased propensity for NSCs to differentiate into oligodendrocytes and impeded differentiation of neurons in vitro and in vivo.

Another gene commonly found to be mutated in PD, *LRRK2*, has also been shown to play a role in neural stem and progenitor cell regulation. *LRRK2* mRNA is expressed throughout the adult brain, including expression in neurogenic regions such as the dentate gyrus, the SVZ and the hypothalamus (Taymans *et al.*, 2006; Winner *et al.*, 2011*b*). In one study, the role of LRRK2 in the regulation of stem and progenitor cells was investigated using human midbrain-derived neural progenitor cell (hmNPC) cultures. This showed that cultured hmNPCs that expressed Nestin also expressed LRRK2 and furthermore that knockdown of *LRRK2* using small interfering RNA (siRNA) resulted in impeded ability to differentiate into DA neurons, but not to other neuronal or glial cell types. The authors further showed that *LRRK2* knockdown results in DA neurons expressing the cell death marker, cleaved caspase-3, indicating that DA neurons are lost via apoptosis (Milosevic *et al.*, 2009). This study suggests a biological role for non-mutated LRRK2 in the differentiation and survival

of DA neurons, where knockdown of LRRK2 results in impeded differentiation and cell death. Another study has shown that adult mice expressing human *LRRK2* with the G2019S mutation also display decreased proliferation in the SGZ and the SVZ, and reduced generation of neurons in the hippocampus and OB, including DA neurons in the OB. Reduced neurogenesis was accompanied by structural defects of hippocampal neurons, including decreased neurite length and decreased number of spines (Winner *et al.*, 2011*b*). The G2019S mutation is thought to be a toxic gain of function mutation (see section 1.2.5), suggesting that overexpression of *LRRK2* results in reduced neurogenesis. Together with reduced neurogenesis observed in *LRRK2* knockdown (Milosevic *et al.*, 2009), this supports the idea that any type of disruption of LRRK2 enzymatic activity is deleterious, be it overexpression or loss of function. Recently, a *lrrk2* knockout zebrafish line was created. *Lrrk2* knockout zebrafish displayed no differences in DA neuron number in the ascending posterior tuberculum, however did show decreased levels of DA and serotonin, and increased levels of their catabolites, suggesting perturbed amine catabolism. Furthermore, *lrrk2* knockout zebrafish displayed reduced proliferation in the telencephalon at 5dpf, and in both the telencephalon and the diencephalon at 10dpf. Intriguingly, overexpression of a Lrrk2 protein fragment containing the catalytic core rescued the proliferation defect in *lrrk2* knockout zebrafish embryos, suggesting the enzymatic function of lrrk2 may play a role in proliferation regulation. In 6-month old zebrafish, levels of proliferation in the telencephalon were modestly reduced and upon telencephalic injury, 30% fewer new neurons were generated. However, constitutive neurogenesis in the uninjured telencephalon was unaltered (Suzzi *et al.*, 2017). Together this shows that lrrk2 is required both for proliferation of neural stem and progenitor cells, amine catabolism and regeneration upon injury.

Altogether, these studies demonstrate that monogenic-inherited PD-genes play divergent roles in regulating neural stem and progenitor cell proliferation and differentiation in the adult brain. Although these investigations provide insight into the regulation of neurogenesis in the context of PD, adult dopaminergic neurogenesis has not yet been examined. Thus, the extent to which production of new DA neurons contributes to existing populations that are affected in PD remains unclear. Further, the question of whether PD-genes alter DA neurogenesis in the adult brain has not been addressed.

1.5: Thesis hypotheses and aims

I hypothesise that DA neurons of the zebrafish posterior tuberculum are generated in adult life, and that generation of ascending DA neurons is impeded in a genetic model of PD.

To address these hypotheses, my aims were as follows:

1. To characterise DA neurons in the embryonic and the adult zebrafish posterior tuberculum, to define distinct DA neuronal populations and to test the previous suggestion that embryonic and adult populations are related.

2. To examine the expression of neural stem/progenitor cell markers in the posterior tuberculum at different stages through life, to provide evidence for the existence of neural stem/progenitor cells in this region.

3. To perform EdU pulse/chase analyses and conditional genetic lineage tracing to address whether new DA neurons are added to existing populations of DA neurons at different stages throughout adult life.

4. To perform EdU pulse/chase analyses to assess whether generation of DA neurons is impeded in a zebrafish model of PD, the *pink1* knockout zebrafish.

5. To create a new model of genetic PD, the *lrrk2* knockout zebrafish which at the start of this study was entirely novel.

Chapter 2

Materials and Methods

2.1 Zebrafish

2.1.1 Zebrafish husbandry

Adult and larval zebrafish were housed at The Bateson Centre, University of Sheffield; experimental procedures were in accordance with UK Home Office Animals (Scientific Procedures) Act 1986 (Project license number: PPL70/8437, held by Professor Oliver Bandmann. Personal license: PILI5B38EB05, held by Sarah Brown). Zebrafish were housed in tanks at a density of no more than four zebrafish per litre, at a constant temperature of 28°c and on a 14-hour light, 10-hour dark cycle.

2.1.2 Collection and maintenance of zebrafish embryos

To collect zebrafish embryos, a marble tank was put into the tank in the evening to stimulate mating at the beginning of the light cycle the following morning. Alternatively, zebrafish were pair mated by putting a male and a female in a divided tank overnight. The divider was removed to allow fertilization at a specific time. Zebrafish embryos/larvae were kept at 28°c in 10cm petri dishes filled with E3 media (500μM NaCl, 17μM KCL, 33μM CaCl and 33μM $MgSO_4$ and 2 drops per litre of methylene blue antifungal agent). Zebrafish embryos/larvae were kept at a density of no more than 60 zebrafish per plate.

2.1.3 Zebrafish anesthesia and culling

For procedures, adult zebrafish were briefly anaesthetized using tricane (PharmaQ Hampshire) (0.016% w/v). Once the procedure is complete, zebrafish were placed back into a clean tank in a quiet area of the aquarium to recover. For adult brain dissections, zebrafish were anaesthetized with a stronger solution of tricane (0.4% w/v) to allow immediate anesthesia, and culled by decapitation. This allowed quick dissection of the brain to give the best possible tissue quality for histological techniques.

2.1.4 Fin clipping

Adult zebrafish were genotyped by fin clipping. Zebrafish were anaesthetized using tricane and a small clip of tailfin was cut with sterilized surgical scissors. The clipped fish was put into an individual tank to allow genotyping of tissue, and the tail clip was put into the corresponding well of a 96-well plate. Once genotypes had been determined, fish were separated back into tanks by genotype.

2.1.4 Adult EdU Injections

For EdU analysis in this study, wild type zebrafish at 3 months, 6 months, 12 months and 22 months old or *pink1-/-* zebrafish at 3 months old were injected with 5µl of 10mM EdU (C10339; ThermoFisher Scientific) in HBSS (14025-092; ThermoFisher Scientific). Zebrafish were anaesthetized with tricane (0.016% w/v) and injected intraperitoneally with EdU (figure 2.1) once daily for 3 consecutive days. After an additional 5 days, zebrafish were sacrificed and brains were collected. EdU injected zebrafish were checked regularly for health problems, none were observed.

Figure 2.1: Intraperitoneal injection of EdU into adult zebrafish.

The zebrafish was anaesthetized and placed on a tricane-soaked sponge. EdU was injected into the peritoneal cavity.

2.1.5 Embryonic EdU Injections

5nl of 5mM EdU (2 volumes 10mM EdU:1 volume 0.3x HBSS:1 volume Phenol Red) was microinjected into the yolk sac of embryos 31hpf. The embryos were left to develop at 28°c until 55hpf. At this point the embryos were sacrificed and collected. EdU injected zebrafish embryos were checked regularly for health problems, none were observed.

2.1.6 Transgenic zebrafish

The Nestin:GFP transgenic line was kindly provided to The University Of Sheffield by Dr. Uwe Strahle (Karlsruhe Institute of Technology, Germany) (Lam *et al.*, 2009). The Tg(her4:ERT2CreERT2) and Tg(ubi:loxGFPloxmCherry) transgenic lines were a kind gift from Laure Bally-Cuif (Dirian *et al.*, 2014).

2.1.7 Conditional recombination

To induce recombination of the Tg(her4:ERT2CreERT2);Tg(ubi:loxGFPloxmCherry) line, 5µl of 10mM tamoxifen (T5648-1G) diluted 1:5 in sunflower oil was injected intraperitoneally once and zebrafish were replaced in tanks and chased for 32-days. A control group was injected with oil alone alongside experimental animals. After the chase period, zebrafish were sacrificed and brains were collected. Tamoxifen injected zebrafish were checked regularly for health problems. None were observed.

2.2 Molecular Biology

2.2.1 Basic local alignment search tool (BLAST)

To identify zebrafish orthologues of human genes, the human protein sequence was searched for in ENSEMBL and then searched for in the Basic Local Alignment Search Tool (BLAST) in ENSEMBL. Sensitivity was selected at no optimization. The result with the greatest homology was selected. The zebrafish and human gene were compared by genetic architecture (exon number, gene length, genomic regions). Gene synteny was calculated using the 'compare region' function in ENSEMBL.

2.2.2 DNA extraction

Genomic DNA (gDNA) was extracted from adult tail clips or whole embryos using sodium hydroxide extraction. 100μl of 50mM NaOH was added to a zebrafish tail clip in each well of a 96-well plate and heated at 98°c for 5 minutes. The solution was neutralized with 10μl of 1M Tris-HCl (pH 8), vortexed and centrifuged at 4200rpm for 10 minutes.

2.2.3 RNA extraction

RNA was extracted from either 20 whole zebrafish larvae or 1 whole adult zebrafish brain using Trizol. Tissue was placed in a microcentrifuge tube with 250μl of TRIzol® (Life Technologies) and homogenized using a 23g needle. Homogenized tissue was incubated at room temperature for 5 minutes, followed by addition of 50μl of chloroform, inversion of the tube 8 times to mix and further incubation at room temperature for 5 minutes. Samples were centrifuged at 13,000rpm for 15 minutes at 4°c. The top layer of supernatant (100μl) was removed and transferred to a fresh centrifuge tube. 100μl of isopropanol was added, the tube was mixed by inversion and incubated at room temperature for 10 minutes. Samples were centrifuged at 13,000rpm for 15 minutes at 4°c and the supernatant discarded to leave an RNA pellet. The pellet was washed with 70% EtOH, centrifuged for 5 minutes at 7,000rpm at 4°c and the supernatant was discarded. The pellet was air dried for 1 minute and resuspended in 20ul DEPC H_20 (RNase free). RNA concentration and purity was determined using a Nanodrop (Thermo Scientific).

2.2.4 Reverse transcription (cDNA synthesis)

cDNA was made using Verso cDNA Synthesis Kit (Thermo Scientific). 1μg of RNA was made in 10μl DEPC H_20. A 20ul reaction mix was composed of; 4μl 5x cDNA synthesis buffer, 2μl dNTP mix, 1μl RNA primer, 1μl Verso enzyme mix, 10μl RNA in DEPC H_20. Samples were incubated for 30 minutes at 42°c then 2 minutes at 95°c to inactivate the Verso enzyme.

2.2.5 Polymerase Chain Reaction/Reverse Transcriptase PCR

PCR or RT-PCR was used to amplify gDNA and cDNA respectively in a Biorad DNA Gradient Thermo Cycler (Biorad). A 10ul PCR reaction mix was composed of; 5μl Biomix Red™ (Bioline), 1μl forward primer (10μM), 1μl reverse primer (10μM), 2μl ddH_20 and 1μl of gDNA/cDNA. The reaction was heated to 95°c for 3 minutes, followed by 34 cycles of; 95°c for 30 seconds, 60°c for 30 seconds, 72°c for 1 minute and a final single incubation at 72°c for 5 minutes. Primers were designed using Primer3 software (http://primer3.ut.ee) and produced by Integrated DNA Technologies Ltd. For a list of primer sequences, see table 2.1.

2.2.6 DNA gel electrophoresis

To visualize PCR products, gel electrophoresis was used. A 2% agarose gel was made with 2g of agarose powder in 100ml of TAE buffer (40mM Tris, 20mM acetic acid, 1mM EDTA) and heated until dissolved. Ethidium bromide was added to the agarose solution, and the solution was poured into a gel tray and left to cool and set. The solidified gel was placed into an electrophoresis tank and covered with TAE buffer. 2μl of each sample was pipetted into gel wells alongside a single well containing 2μl of Hyper ladder IV (Bioline) for product size reference. A current was applied to the gel (150v for 10-30 minutes) and DNA was visualized and imaged by applying UV light to the gel.

2.2.7 Genotyping

PCR was used to amplify the region of the gene containing the mutation using gDNA, primers are listed in table 2.1. The *pink1* line was genotyped using sequencing at The University of Sheffield Core Genomics Facility. PCR product was sequenced using the reverse primer only, and sequencing data was analysed using FinchTV software, version 1.5.0 (Geospiza Inc.). The *pink1* sequences were reverse complemented and the lead up

sequence; GCGATCGCTTA was searched for. Wild type *pink1*: GCGATCGCTTAT, heterozygous *pink1* Y431* stop mutation: GCGATCGCTTAN, homozygous *pink1* Y431* stop mutation: GCGATCGCTTAG. The *pink1* line was maintained as a heterozygote colony. For raising adult *pink1* Y431* homozygote mutants, heterozygotes were incrossed. For generating homozygote mutant embryos, homozygote mutants were incrossed. The *lrrk2* line was genotyped by restriction digest. PCR product was digested with Bsl1 for 2 hours at 55°c to identify mutation site. Bsl1 recognises and cuts DNA with the sequence CCNNNNN▽NNGG. The *lrrk2* 5 base pair insertion interrupts the Bsl1 cut site, therefore Bsl1 does not digest lrrk2 5bp insertion homozygous DNA, partially digests *lrrk2* 5bp insertion heterozygous DNA and fully digests wild type *lrrk2* DNA (figure 2.2).

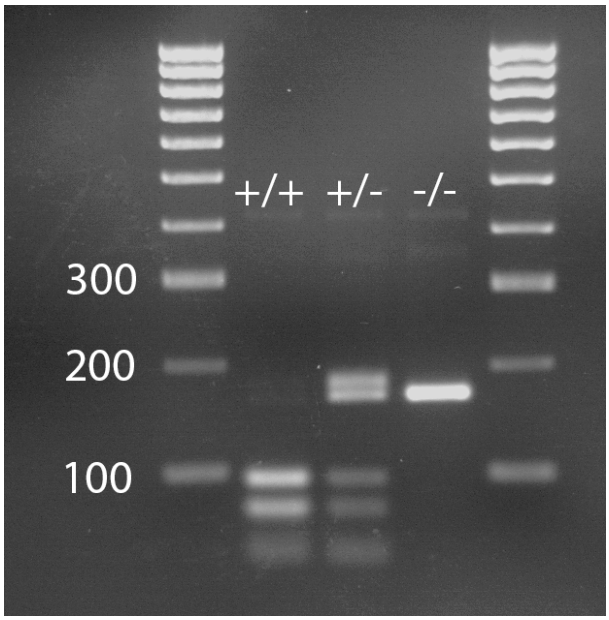

Figure 2.2: *lrrk2* 5bp insertion genotyping.

Genomic PCR illustrating Bsl1 digestion of wild type *lrrk2*, giving products of 100bp and a 92bp. In zebrafish that are heterozygous for the *lrrk2* 5bp insertion, the wild type *lrrk2* gene is digested by Bsl1 giving products of 100bp and a 92bp, and the *lrrk2* 5bp insertion gene is not digested by Bsl1, giving a product of 192bp. gDNA from zebrafish that are homozygous for the *lrrk2* 5bp insertion is not digested by Bsl1, giving a 192bp product.

2.2.8 Quantitative PCR

Quantitative PCR (qPCR) was used to measure relative quantities of mRNA transcripts. Fluorescent SYBR green dye (Agilent) incorporates into double-stranded DNA upon replication, and fluorescence intensity can be measured after each PCR cycle to measure the quantity of PCR product. This gives a Ct value, which is defined as the number of cycles required for fluorescence intensity to reach a threshold. Primers were optimized for qPCR by testing primer pairs are varying concentrations (100nM, 300nM and 500nM). A standard curve was created using cDNA standard dilutions for each primer concentration, this ensured primer efficiency was as close to 100% (±10%). A dissociation curve was also generated, ensuring there is a single peak and that only one PCR product is being produced. For qPCR reactions, a 20µl reaction mix contained 10µl SYBR green, primers and cDNA at required concentrations and made up to 20µl with nuclease free ddH_20. Reactions were put into a 96-well qPCR plate (Geneflow) and centrifuged at 1760rpm for 1 minute.

Zebrafish *ef1α* was used as housekeeper genes in primer optimisation and to calculate fold changes in quantities of mRNA transcripts. To calculate fold changes, reference gene Ct value was subtracted from gene of interest (GOI) Ct value. Delta-delta-Ct value was calculated by subtracting the dCt value from the dCt value of mutant mRNA transcripts. Fold change in mRNA transcript quantity was calculated by using the formula: $2^{(-ddCt)}$. This can be converted to percentage by multiplying the fold change value by 100.

2.2.9 CRISPR-Cas9 design

ENSEMBL was used to provide the sequence of the gene of interest (GOI) in zebrafish. CRISPR-Cas9 sites were identified by location of PAM sites (5'NGG or 3'NCC) within exons of the GOI, where Cas9 cuts the DNA 3 base pairs upstream from the PAM site. Cut sites were chosen if they disrupted a restriction site, allowing for confirmation of successful CRISPR-Cas9 cuts by restriction digest (table 2.2) (restriction site is underlined). The reverse complement of the 18bp upstream of the PAM site was placed into a guide RNA template, which allows specific binding of CRISPR-Cas9 to the region of interest, where the guide RNA template contains sequences for recruitment of Cas9 and the T7 promotor (figure 2.3) (table 2.2) (T7 promotor is shown in bold).

Primer	Sequence (5'-3')	Description
pink1 genotyping F	AAAGCAGATGTGTGGGCTGT	Pink1 line genotyping
pink1 genotyping R	AGCTTCACCACCAGCTGAAC	Pink1 line genotyping
lrrk2 genotyping F	CTTCAGGCGTTCATGAGCAG	Lrrk2 line genotyping
lrrk2 genotyping R	GAGGCCTTCATGTGTCCGAT	Lrrk2 line genotyping
ef1α qPCR F	TGGTACTTCTCAGGCTGACT	qPCR Housekeeper
ef1α qPCR R	TGACTCCAACGATCAGCTGT	qPCR Housekeeper
lrrk2 qPCR F	CCACAGGAGCGCGATATTCA	Lrrk2 NMD qPCR
lrrk2 qPCR R	TTTGTGTTTCCGCACAGAGC	Lrrk2 NMD qPCR

Table 2.1: Primers used for genotyping in this study

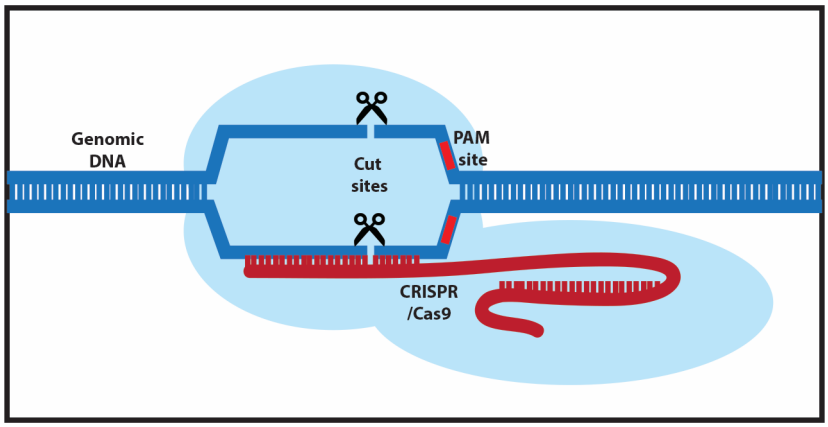

Figure 2.3: Schematic demonstrating binding and cutting of CRISPR-Cas9 constructs to the gene of interest

Primer	Sequence (5'-3')
Ultramer F	AAAGCACCGACTCGGTGCCAC
Ultramer R	GCGTAATACGACTCACTATAG
lrrk2 exon 19 Bsl1 cut site	AAAGCACCGACTCGGTGCCACTTTTTCAAGTTGATAACGGACT AGCCTTATTTTAACTTGCTATTTCTAGCTCTAAAACCCGTCTGGG ACTTGACCACC**CTATAGTGAGTCGTATTA**CGC

Table 2.2: Primers used for CRISPR-Cas9 construction in this study

2.2.10 Ultramer amplification

Upon arrival, ultramers were amplified (table 2.2) in a 100µl PCR mix containing; 50µl Biomix red™ (Bioline), 38µl ddH_20, 5µl forward primer, 5µl reverse primer and 2µl of ultramer. Reaction mix was 95°c for 3 minutes, followed by 40 cycles of; 95°c for 30 seconds, 60°c for 30 seconds, 72°c for 1 minute and a final single incubation at 72°c for 5 minutes. A successful reaction was confirmed by electrophoresis (2.2.6). PCR product was then purified.

2.2.11 PCR purification of ultramer

PCR product was purified using a QIAquick PCR purification kit (28104; Qiagen). PCR reaction was diluted by adding 5 volumes of PB buffer to 1 volume of PCR product and placed in a QIAquick column. The column was centrifuged for 1 minute and the flow-through discarded. 750µl of PE buffer was added; the column was centrifuged for 1 minute and the flow through discarded. The column was centrifuged 1 minute and the flow-through discarded. The column was put into a clean microcentrifuge tube and 20µl of elution buffer was added to the column. The column was centrifuged for 1 minute to produce the purified DNA. Purified DNA was stored at -20°c until use.

2.2.12 Transcription of purified ultramer

Purified ultramer was transcribed using the MEGAshortscript T7 kit (AM1354, Life Technologies) in a 20μl reaction mix: 2μl buffer, 2μl of each dNTP, 2μl enzyme mix, 1μl amplified and purified ultramer, 7μl nuclease-free water. Reaction was incubated at 37°c for 4 hours, followed by degradation of remaining ultramer by addition of 1μl of DNAse for 30 minutes at 37°c. A successful reaction run was confirmed by electrophoresis and volume was made up to 100μl with nuclease-free water. RNA was purified by addition of 33μl 10M NH_4Ac and 350μl ice cold EtOH, and mixture was precipitated for 2 hours at -80°c. Purified RNA was centrifuged at 13000rpm for 30 minutes at 4°c to form an RNA pellet. Supernatant was removed and the RNA pellet was washing with 70% ice cold EtOH. The supernatant was removed and the pellet briefly air dried, followed by resuspension in 10μl nuclease-free water. The concentration of RNA was measured using a Nanodrop (Thermo Scientific) and guide RNA was diluted to a concentration of 4-8μg/μl and stored at -80°c.

2.2.13 Microinjection of CRISPRs

Guide RNA and Cas9 protein (NEB) was injected into zebrafish embryos at the one-cell stage. 2.5μl Injection mixture contains; 1μl of guide RNA, 1μl of Cas9 protein (18μM stock concentration) and 0.5μl phenol red (to allow visualization of the mixture). 1nl of injection mixture was injected into the yolk sac. After injection, zebrafish embryos were incubated until 5dpf, and then transferred to aquarium tanks. A selection of embryos at 1dpf were used for determination of CRISPR-Cas9 efficiency.

2.2.14 Assessment of CRISPR-Cas9 efficiency

DNA was extracted from 8 injected and 8 uninjected embryos at 1dpf (described in 2.2.2) and DNA was amplified by PCR (described in 2.2.5) with primers specific to the region of interest (table 2.1). PCR product was digested with restriction enzymes that have cut sites within the CRISPR-Cas9 cut site. Efficient CRISPR-Cas9 results in no digestion of PCR product by relevant restriction enzyme.

2.2. Ligation independent cloning and transformation (TOPO) (cloning for sequencing)

Cloning was performed using the TOPO® TA cloning kit (K4500, Life Technologies) and allowed separation of different mutations created by the CRISPR-Cas9 to analyse types of mutations generated. PCR products from 1dpf CRISPR-Cas9 injected embryos were mixed together and product was purified using the QIAquick PCR purification kit (described in 2.2.11). 4μl of purified DNA was added to 1μl of TOPO® vector and 1μl of supplied salt solution, and the reaction was incubated at room temperate for 30 minutes. Reaction was then transformed into competent cells. Competent cells were defrosted on ice and 5μl of TOPO® mix was added to 30μl of cells, followed by incubation for 30 minutes on ice and then heatshocked at 42°c for 30 seconds. Reaction mix was incubated on ice for 5 minutes, followed by addition of 950μl SOC outgrowth medium (B9020S; NEB) and cells were incubated at 37°c for 1 hour with agitation. 100μl of cells in suspension were spread onto Ampicillin LB Agar plates (0.1% (v/v) Ampicillin). Plates were incubated overnight at 37°c. Individual colonies were picked from the plate the following morning and placed into individual PCR reaction mixes (described in 2.2.5). The PCR product was visualized using electrophoresis to show large deletions/insertions and PCR product was digested with restriction enzymes to visualize smaller deletions/insertions. Samples that contained deletions/insertions were sequenced at The University of Sheffield Core Genomics Facility and analysed using FinchTV software to determine if insertions/deletions could disrupt gene expression.

2.3 Histological techniques

2.3.1 Fixation of tissue

All tissues were fixed using ice cold 4% (w/v) paraformaldehyde (P6148; Sigma) in 0.1M phosphate buffer. Adult zebrafish brains were dissected and fixed overnight at 4°c. Whole embryonic/larval zebrafish were fixed overnight at 4°c.

2.3.2 Cryosectioning of tissue

Adult brains and zebrafish embryos/larvae were washed with phosphate buffered saline (PBS) (P4417; Sigma) and incubated in 30% (w/v) sucrose (S0389; Sigma) in 0.2M phosphate buffer overnight at 4°c. Tissue was then briefly placed in OCT (361603E; VWR International) in a petri dish, and then placed into a mold and orientated for sectioning. Tissue mounted in OCT was frozen on dry ice and stored at -20°c. Brains were sectioned using a cryostat (OFT5000; Bright) at a thickness of 15μm. Tissue was collected directly on superfrost slides (J1800AMNZ; ThermoFisher Scientific) and air dried. For immunohistochemistry, OCT was washed from slides with PBS, and for in situ hybridization, slides were frozen at -20°c.

2.3.3 Immunohistochemistry

For immunohistochemistry on sections, sections were first incubated in blocking solution (5% (w/v) heat-inactivated goat serum (HINGS) (16210-072; Gibco) and 0.5% (v/v) Triton (T8787; Sigma) in PBS for 1 hour at room temperature. Sections were then incubated in primary antibodies, diluted in blocking solution, overnight at 4°c. Primary antibody solution was removed and slides were washed 3 times in PBS. Slides were incubated in secondary antibody solution, diluted in blocking buffer, for 1 hour at room temperature and covered from light. Secondary antibody was removed and slides were washed 3 times in PBS. Slides were mounted with Fluoroshield mounting medium containing 4',6-diamidino-2-phenylindole (DAPI) (F6057; SLS) and glass coverslipped (MIC3228; SLS). Secondary antibody only controls were performed to ensure there was no non-specific binding, which was never detected. For a list of primary antibodies used, see table 2.3. For a list of secondary antibodies used, see table 2.4.

Primary antibody	Species	Dilution	Source
Cleaved Caspase-3	Rabbit polyclonal	1:400	9661; Cell Signalling
DsRed2/mCherry	Rabbit polyclonal	1:500	632496; Clontech
GFP	Rabbit polyclonal	1:200	TP401; Chemokine
OTPb	Rabbit polyclonal	1:400	A kind gift from Prof. Gil Levkowitz
Th1	Mouse IgG	1:1000	22941; Immunostar

Table 2.3: Primary antibodies used in this study

Secondary antibody	Dilution	Source
Alexa-488	1:500	Molecular Probes
Alexa-594	1:500	Molecular Probes
Alexa-647	1:500	Molecular Probes

Table 2.4: Secondary antibodies used in this study

2.3.4 EdU detection

For detection of EdU in tissue sections from EdU injected zebrafish, the Click-iT™ EdU Alexa Fluor™ 594 Imaging Kit (C10339; ThermoFisher Scientific) was used. EdU is an alternative for BrdU (5-bromo-2'-deoxyuridine), and is a thymidine analogue that incorporates into DNA during active DNA synthesis, therefore allowing labelling of newly generated cells. Detection of EdU is based on a Cu(I)-catalysed [3 + 2] cycloaddition reaction ("click" chemistry): briefly the alkyne ring in the EdU molecule reacts with an azide-containing detection reagent, forming a triazole ring and fluorescently labelling cells that have incorporated EdU. The benefits of the EdU assay over the BrdU assay are (a) no heat DNA denaturation is required to expose the label for antibody detection allowing good structural preservation and (b) the EdU Click-iT is a simple and quick protocol, allowing robust analysis of proliferation (Salic & Mitchison, 2008). After sectioning and drying of sections, slides were blocked in 3% (w/v) bovine serum albumin (BSA) (A3059; Sigma).

Block solution was removed and slides were permeabilised with Triton (0.5% (v/v) at room temperature for 20 minutes. Slides were washed in blocking solution and developed with fresh Click-iT™ reaction cocktail for 30 minutes at room temperature. Slides were washed once more with blocking solution, followed by antibody labeling as in 2.3.3.

2.3.5 Fluorescent In situ hybridization (sections)

Fluorescent in situ was achieved using the Tyramide amplification kit (B40915, ThermoFisher Scientific). Sections were post-fixed with 4% PFA for 10 minutes at room temperature, followed by PBS washes. Acetylation mix (11.2μl triethanolamine and 2.5μl acetic anhydride per 1ml of ddH_20) was added to slides and incubated for 10 minutes at room temperature, followed by PBS washes. Slides were incubated in hybridisation solution (50% formamide, 5x SSC (pH 7), 2% blocking powder (11096176001, Sigma), 0.1% Triton X-100, 0.5% CHAPS, 1mg/ml Yeast RNA, 5mM EDTA, 50μg/ml Heparin) for at least 2 hours at 68°c in a humidified chamber. Probes were diluted in hybridisation solution and 200μl was added to each slide. Slides were glass coverslipped to prevent evaporation and incubated overnight at 68°c in a humidified chamber. The following day, slides were washed in warmed solution 1 (25ml formamide, 12.5ml 5xSSC pH 4.5, 5ml 10% SDS, 7.5ml ddH_20) for 1 hour at 68°c. Slides were transferred to warmed solution 2 (25ml formamide, 5ml 5xSSC pH 4.5, 0.5ml Tween20, 19.5ml ddH_20) for 1 hour at 68°c. Slides were washed with PBS-T (PBS, 0.1% triton) twice at room temperature and rinsed with MABT (malic acid buffer, 0.1% triton). Slides were blocked in 2x/2% (w/v) blocking reagent diluted in MABT for 1 hour at room temperature. Slides were incubated in anti-DIG-POD (1:500) (11207733910, Sigma) diluted in blocking buffer overnight at 4°c. Slides were washed 6 times for 20 minutes at room temperature in PBS-T, followed by rinsing of slides in boric acid solution (100mM boric acid (pH 8.5), 0.1% triton). Tyramides were diluted (1:150) in TSA buffer (100mM boric acid (pH 8.5), 0.1% triton, 2% dextran sulphate, 0.003% H_20_2, 0.15mg/ml iodophenol) and 250μl was added to each slide with a parafilm coverslip. Slides were incubated for 25 minutes at room temperature, protected from light. Slides were rinsed in PBS-T 4 times. Slides were then processed for immunohistochemistry (described in 2.3.3).

2.3.6 Image acquisition and analyses

Immunofluorescent images were captured with an AxioImager.Z1 with Apotome (Zeiss), and Axiovision 4.8 software. For sections, z-stacks were taken and processed to give a maximum intensity projection (MIP). Chromogenic images were taken with an Olympus microscope with Q-Capture Pro 7.0 software (Q-Imaging). Images were processed in Photoshop (CC; Adobe) and brightness and contrast of whole images were adjusted to produce optimal images. Exposures were not modified in quantification experiments. Cells were quantified using the Photoshop count tool. Prism 7 was used to perform statistical analyses (unpaired t-test unless otherwise stated) and graphs were generated using Prism 7 and R (version 3.3.3). Significance values are denoted as follows; Not significant $p>0.05$, * $p<0.05$, ** $p<0.01$, *** $p<0.001$.

Chapter 3

Distinct dopaminergic populations in the posterior tuberculum increase in size from embryonic to adult stages

3.1: Introduction

As described in the main Introduction, PD is characterised by a reduced number of midbrain dopaminergic (DA) neurons, specifically within the substantia nigra pars compacta (SNpc). In mammals, SNpc DA neurons form the nigrostriatal pathway, ascending from the midbrain to the dorsal striatum in the forebrain. Functionally-equivalent DA populations are thought to exist in the zebrafish: previous studies have described distinct populations of DA neurons that ascend from the posterior tuberculum (PT) to the subpallium and are therefore thought to correspond to mesostriatal systems in the mammalian brain (Rink & Wullimann, 2001*a*, 2002*a*, 2002*b*, 2004). Thus, the zebrafish PT is a valuable system for modelling mammalian midbrain DA neurons.

DA neuronal populations in the PT have been comprehensively characterised in both the adult (Fig.3.1) and the embryonic (Fig.3.5) zebrafish. However, as yet, no study has simultaneously characterised embryonic and adult populations. In this chapter, I describe immunohistochemical analyses of the adult and the embryonic PT, using an antibody against a protein marker for DA neuronal status. I focused on the rostral portion of the PT, as this harbours the DA neurons that have been shown to ascend to the subpallium (Rink & Wullimann, 2001*b*, 2002*a*, 2004). For embryonic stages, 55hpf embryos were examined, as all DA populations have been established by this stage. For adult stages, 12-month old and 3-month old zebrafish were examined, to investigate DA populations in the adult and the young adult zebrafish.

3.2.1 Dopaminergic populations in the adult zebrafish PT

The zebrafish PT is situated in the centre of the diencephalon, bordered by the hypothalamus and the thalamus (Fig.3.1A). The distinct morphological features of the hypothalamus and thalamus mean that the PT can be accurately located after sagittal sectioning. To confirm and extend previous findings, I used an antibody against the DA neuronal marker, tyrosine hydroxylase-1 (Th1). Immunohistochemical analysis for Th1 in sagittal sections through a 12-month old zebrafish brain confirmed that distinct DA populations could be clearly identified as previously described (Fig.3.2). Small (parvocellular) round DA neurons occupy the TPp and small (parvocellular) bipolar DA neurons occupy the PVO (Fig.3.2A,B). Situated between the TPp and the PVO is the most rostral population of large (magnocellular), pear-shaped DA neurons, and adjacent/caudal to the PVO is the more caudal population of magnocellular DA neurons. In shape and position, the magnocellular neurons highly resemble embryonic populations, termed DC2 and DC4 neurons (Fig.3.5) and hereafter I therefore refer to these as $DC2^{A}$ and $DC4^{A}$ populations, where ^{A} indicates an adult population (Fig.3.2A,B).

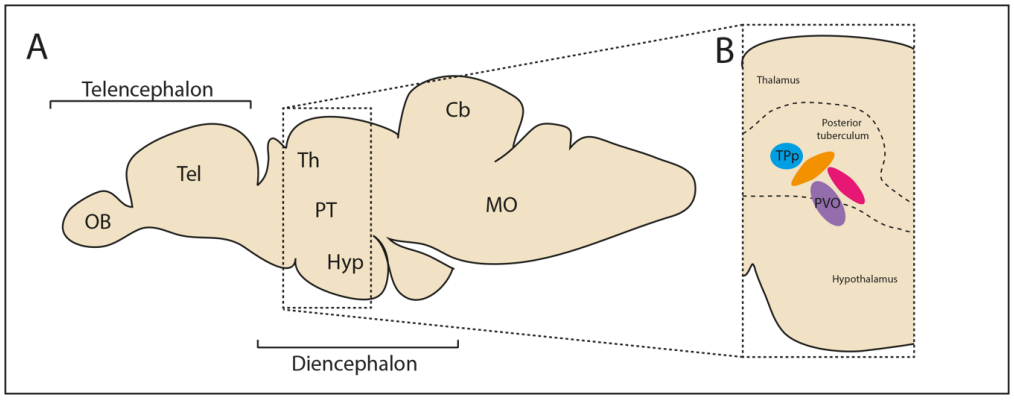

Fig. 3.1: Dopaminergic populations in the adult zebrafish rostral PT.

A. Schematic demonstrating the location of the PT in the adult zf brain.
B. Schematic showing subpopulations of DA neurons within the adult zebrafish rostral PT. Previous studies have described four populations of DA neurons in the rostral portion of the PT, three of which are ascending (Rink & Wullimann, 2001*b*, 2002*a*, 2004): the periventricular nucleus of the PT (TPp) (blue oval) and two sets of magnocellular neurons that do not belong to any defined nucleus, one rostral population (orange oval) and one caudal population (pink oval). Immediately adjacent to these ascending populations are locally-projecting DA neurons of the paraventricular organ (PVO) (purple oval). Illustration adapted from Rink and Wullimann, 2002.

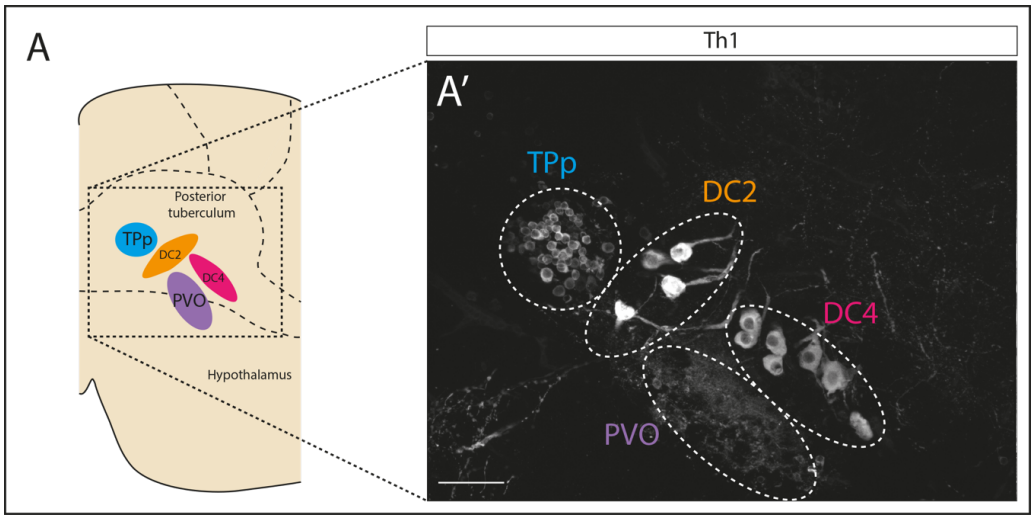

Fig.3.2: Dopaminergic populations in the adult zebrafish rostral PT – a sagittal view.

A. Schematic showing subpopulations of DA neurons within the adult zebrafish rostral PT: the TPp (blue), DC2^{A} (orange) and DC4^{A} (pink) populations and the PVO (purple). Illustration adapted from Rink and Wullimann, 2002.
B. Fluorescent MIP of a sagittal section through a 12-month old PT, labelled with the DA neuron marker, Th1. Th1 labels DA neurons in distinct subpopulations within the PT. Subpopulations are outlined and colour coding coordinates with the populations schematised in A'. Scale bar represents 50μm.

Next I performed Immunohistochemical analysis for Th1 on consecutive transverse sections through the rostral PT of a 12-month old fish, to describe the position of PT DA populations in relation to the diencephalic ventricle and the lateral ventricle (Fig.3.3). These analyses showed that the diencephalic ventricle displays characteristic changes in morphology, from rostral-most to caudal-most parts of the rostral PT (Fig.3.3 schematics). In caudal-most parts of the rostral PT, the diencephalic ventricle branches laterally to form the lateral ventricles, whereas the ventricle is central and linear in rostral-most parts of the PT. Alongside the shape of the ventricle, cell size and shape can also be used to distinguish DA neuron populations: the numerous, small, round DA neurons of the TPp and the numerous small bipolar DA neurons of the PVO lie extremely close to the ventricle (Fig.3.3A-A" and Fig.3.3C-C"); magnocellular DC2^{A} neurons reside just beyond the ventricle, and lie between the TPp and the PVO (Fig.3.2B-B") and magnocellular DC4^{A} neurons reside further away from the ventricle (Fig.3.2C-C"). Magnocellular neuronal populations (DC2^{A} and DC4^{A}) are composed of far-fewer Th1+ neurons than either of the parvocellular populations (TPp and PVO).

Together this data confirms that four DA neuronal populations in the rostral PT can be identified in the 12-month old zebrafish brain based on their number (see below), morphology, position along the rostro-caudal and dorso-ventral axes and position relative to the diencephalic and lateral ventricles (Table 3.1).

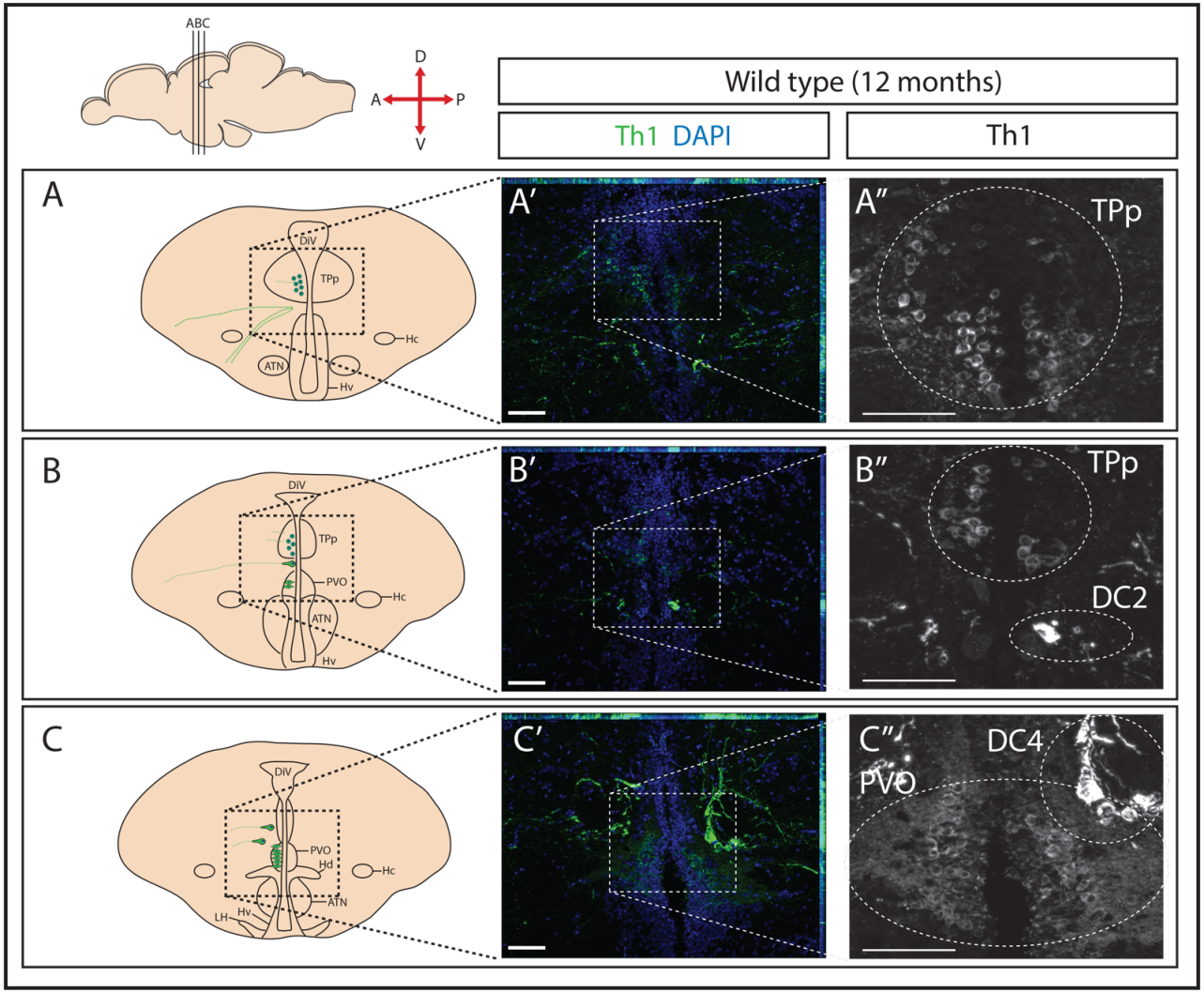
ABC
D
A
P
V
Wild type (12 months)
Th1 DAPI
Th1
A
A′
A″
TPp
DiV
TPp
Hc
ATN
Hv
B
B′
B″
TPp
DiV
TPp
PVO
Hc
ATN
Hv
DC2
C
C′
C″
DC4
PVO
DiV
PVO
Hd
Hc
ATN
LH
Hv

Fig.3.3: Dopaminergic populations in the adult zebrafish rostral PT – a transverse view.

A, B, C. Schematics showing transverse views through the rostral PT: positions and planes indicated in top schematic. The diencephalic ventricle shows distinct change in morphology from rostral to caudal. DA neurons are represented in green.

A', B', C'. Fluorescent MIP of a transverse section through a 12-month old PT, labelled with the nuclear marker, DAPI (blue) and Th1 (green). Th1 labels DA neurons in distinct subpopulations within the PT. Scale bars represent 50μm.

A", B", C". Fluorescent MIPs for Th1 are shown as magnifications of the boxed regions in A', B', C'. Subpopulations in the PT are outlined and labelled. Scale bars represent 50μm. Small round cells occupy the TPp, large pear shaped cells in DC2 and DC4 populations and small bipolar cells in the PVO.

I next asked if similar DA populations in the rostral PT can be identified in the 3-month old zebrafish brain. At 3-months of age, zebrafish have just reached sexual maturity and are classed as young adult fish. Immunohistochemical analysis for Th1 was performed in transverse sections through the 3-month old PT (Fig. 3.4). Th1+ neurons with the same morphology, similar population sizes (see below) and the same relative positions were detected as had been observed at 12 months. Thus, the TPp (Fig.3.4-A",B-B"), DC2^{A} (Fig. 3.4B-B"), DC4^{A} (Fig.3.4C-C") and PVO (Fig.3.4C,C'C") populations can be clearly identified and distinguished from one another at 3-months of age.

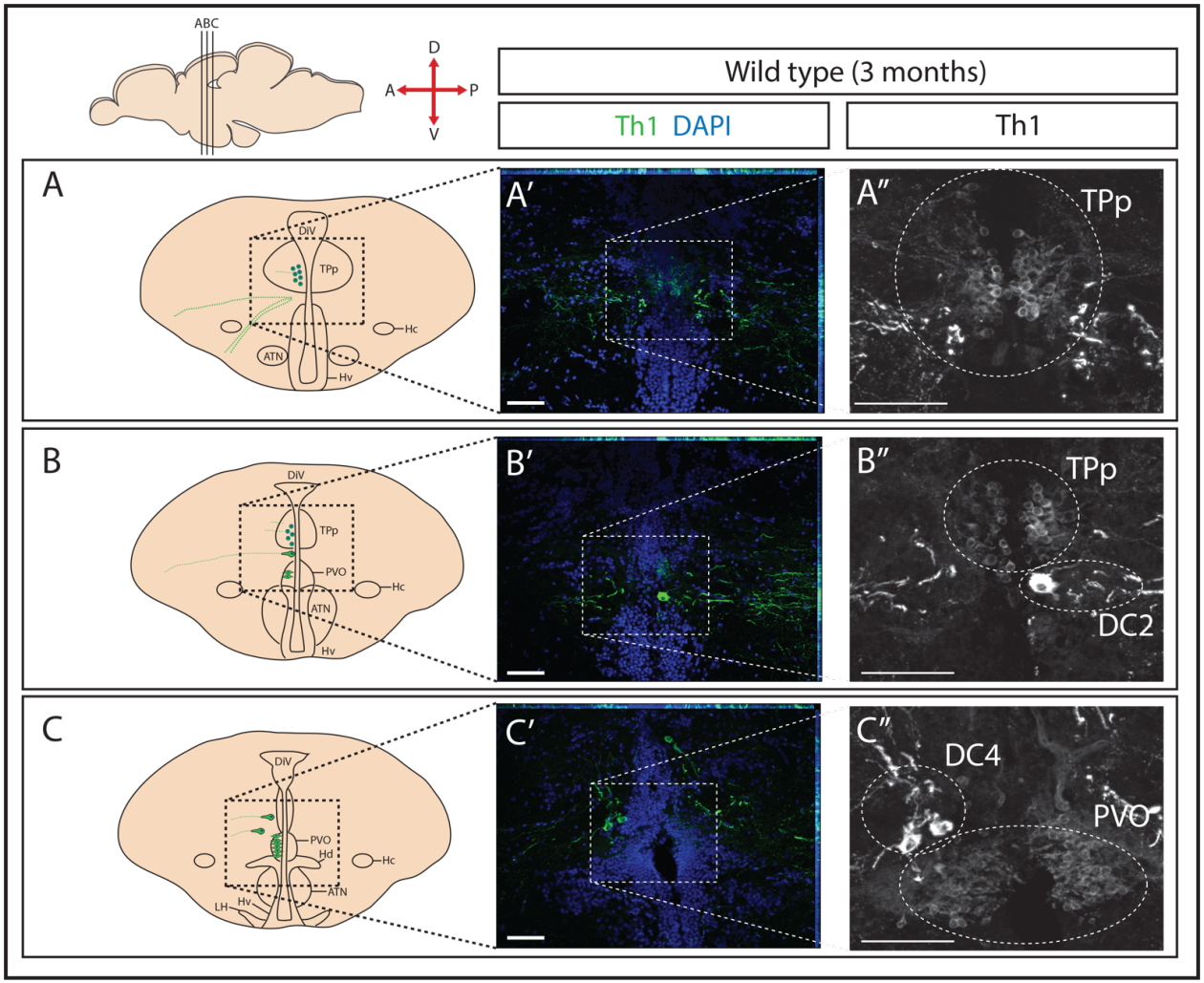
ABC
D
A
P
V
Wild type (3 months)
Th1 DAPI
Th1
A
A′
A″
TPp
DiV
TPp
Hc
ATN
Hv
B
B′
B″
TPp
DC2
DiV
TPp
PVO
Hc
ATN
Hv
C
C′
C″
DC4
PVO
DiV
PVO
Hd
Hc
ATN
LH
Hv

Fig. 3.4: Dopaminergic populations in the young adult zebrafish rostral PT – a transverse view.

A, B, C. Illustrations showing the orientation and rostral PT population location for coronal planes in A', B', C" and A", B", C". DA neurons are represented in green.

A', B', C'. Fluorescent MIP of a transverse section through a 3-month old PT, labelled with the nuclear marker, DAPI (blue) and Th1 (green). Th1 labels DA neurons in distinct subpopulations within the PT. Scale bars represent 50μM.

A", B", C". Fluorescent MIPs for Th1 are shown as magnifications of the boxed regions in A', B', C'. Subpopulations in the PT are outlined and labelled. Scale bars represent 50μM. Small round cells occupy the TPp, large pear shaped cells in DC2 and DC4 populations and small bipolar cells in the PVO.

To determine whether a mixed gender population could be used in these studies, therefore allowing a higher number of replicates in future experiments, I next quantified the number of $Th1^+$ DA neurons in each subpopulation of the rostral PT in male and female 3-month old zebrafish. Quantification revealed no significant difference between the number of DA neurons in the male TPp (346±13, n=4) and the female TPp (348±13, n=4), the number of male $DC2^A$ neurons (10±0.29, n=4) and female $DC2^A$ neurons (10±0.29, n=4), male $DC4^A$ neurons (21±0.29, n=4) and female $DC4^A$ neurons (19±0.63, n=4) or the number of male PVO (419±46, n=4) compared to female PVO (383±21, n=4) neurons (Fig.3.4). Nonetheless, these quantitative analyses confirmed that there are significant differences in DA neuronal numbers in the different populations that reside in the rostral PT. The PVO is most numerous (401±69) then the TPp (347±63). $DC2^A$ and $DC4^A$ populations are relatively small (9±0.7 and 20±1.1 respectively).

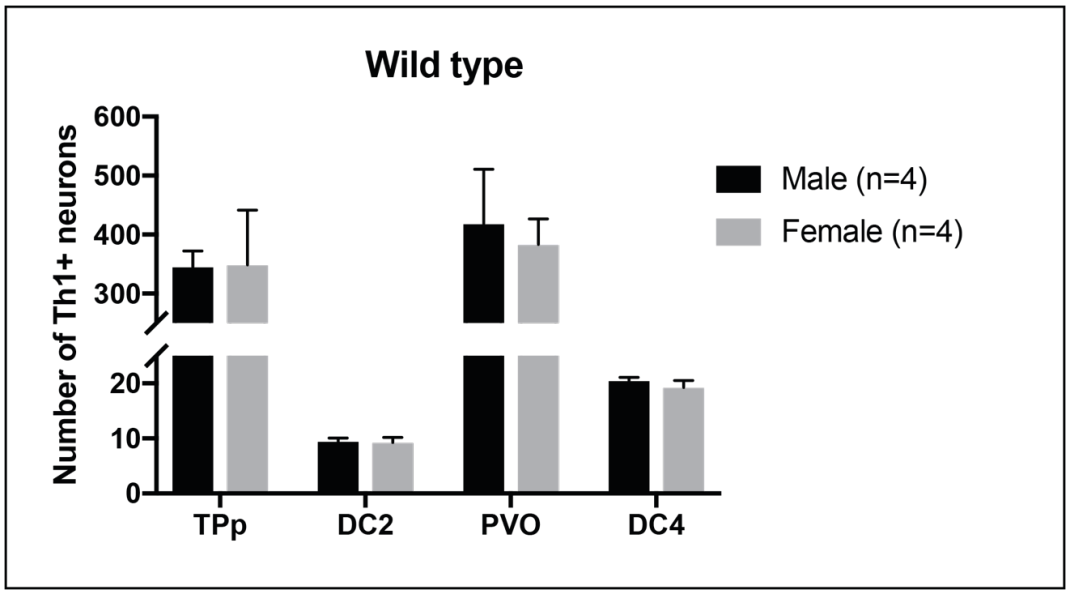

Fig.3.5: No significant difference in the number of Th1$^+$ DA neurons in any subpopulation of the rostral PT.

Quantitative analyses of the mean number of Th1+ cells in each population of the rostral PT, analysed from serial 15μm sections of 3-month old male and female zebrafish. There is no significant difference between the number of DA neurons in any population in male and female zebrafish (error bars represent standard deviation, n=4 males, n=4 females, statistically analysed by unpaired t-test).

In summary, these results confirm that distinct populations of DA neurons within the adult rostral PT can be robustly identified and categorised as described previously in the literature (Rink & Wullimann, 2001*b*). My results also provide, for the first time, an estimation of the numbers of DA neurons in each population and show that there is no significant difference in DA neuronal number in rostral PT subpopulation in male versus female zebrafish.

3.2.2 Dopaminergic populations in the embryonic zebrafish PT

Previous studies have suggested that DA neurons in the PT of the developing zebrafish embryo can be related to those of the adult, due to their position and morphology. In particular, it has been suggested that the embryonic DC1 population is equivalent to the adult TPp, and that the embryonic DC3 is equivalent to the adult PVO (Rink & Wullimann, 2002*b*). I therefore confirmed that DC1 and DC3 neurons, as well as 2 magnocellular embryonic populations (termed DC2 and DC4) could be identified as previously described. I analysed zebrafish embryos that were 55 hours post fertilization (hpf), as previous studies show that DA neurons in DC1, DC2, DC3 and DC4 populations have begun to differentiate and express Th1 by this time point (Rink & Wullimann, 2002*b*).

As in the adult, the embryonic rostral PT overlaps with, and lies dorsal to, the hypothalamus (Fig.3.6), a morphologically-distinct region of the brain. This allows accurate identification of the rostral PT in sagittal cryosections. Using the anti-Th1 antibody, I labelled DA neurons in sagittal cryosections through the 55hpf zebrafish brain, and compared these to sagittal sections through the adult PT. Direct comparison of adult and embryonic sagittal sections through the rostral PT confirms previous reports that suggest that embryonic and adult DA populations are related. Certainly, there are similarities in the morphology of DA neurons and in their relative positions along the rostro-caudal axis (Fig. 3.6). Embryonic DC1 neurons are the rostral-most population and are small and round in morphology; DC2 neurons are large and pear-shaped and reside caudal to the DC1 population; small, bipolar DC3 neurons lie caudal to these, and a population of large pear-shaped DC4 neurons lies most-caudally (Fig. 3.6B,B'). Notably, however, there appear to be far fewer numbers of Th1+ DC1 and DC3 neurons in comparison to the numerous Th1+ neurons that occupy the TPp and the PVO (Fig 3.6B').

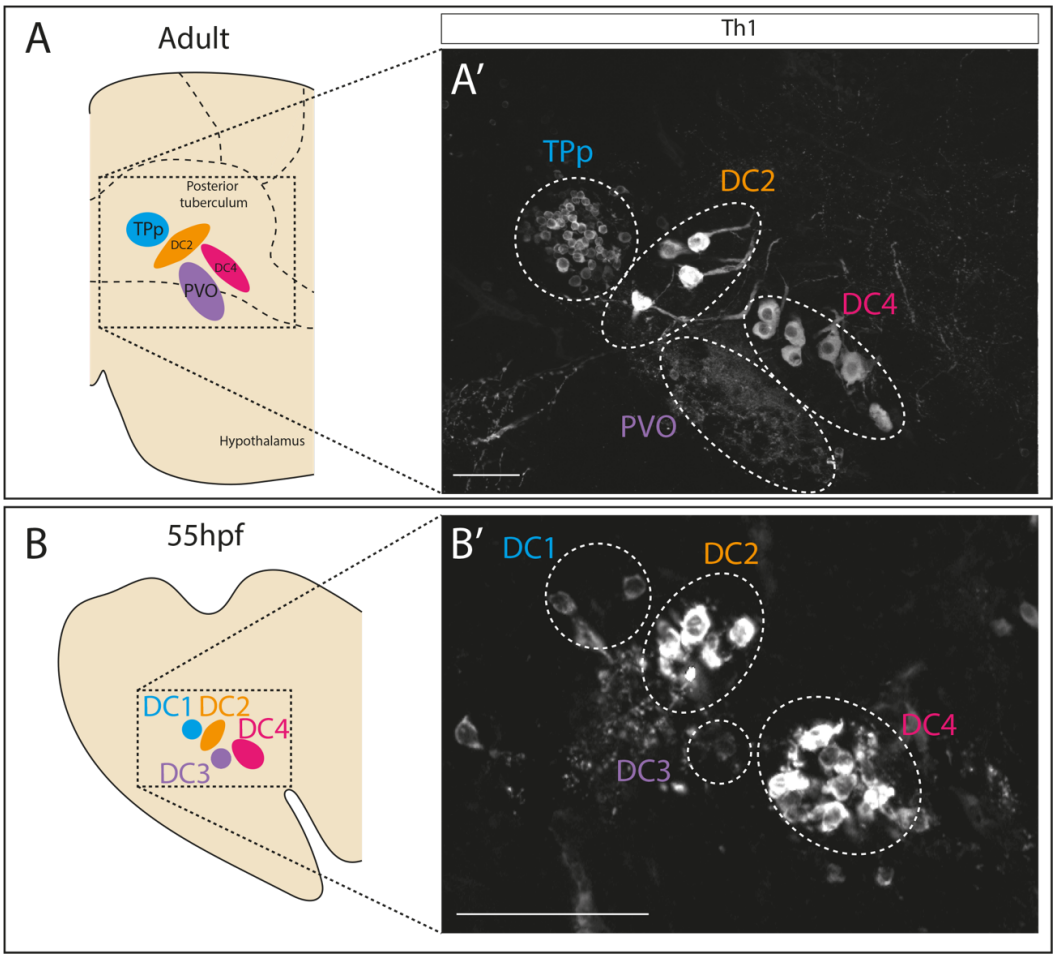

Fig. 3.6: Dopaminergic populations in the adult zebrafish rostral PT compared to the embryonic rostral PT

A-A'. As in Fig.3.2

B. Schematic showing subpopulations of DA neurons within the embryonic zebrafish rostral PT. The embryonic PT comprises 4 populations, DC1 (blue), DC2 (orange), DC3 (purple) and DC4 (pink) populations. Illustration adapted from Rink and Wullimann, 2002.

B'. Fluorescent MIP of a sagittal section through a 55hpf PT, labelled with the DA neuron marker, Th1. Th1 labels DA neurons in distinct subpopulations within the PT. Subpopulations are outlined and colour coding coordinates with the populations labelled in A. Scale bar represents 50μm.

To seek further evidence that distinct embryonic and adult DA neuronal populations are related, I examined transverse sections, to ask if embryonic DA populations occupy similar positions relative to the D-V axis and the ventricle as described for adult populations. Consecutive transverse sections through the 55hpf zebrafish brain were immunolabelled to detect Th1 (Fig.3.7). This revealed the small, round DC1 neurons (Fig. 3.7A-A"), the rostral magnocellular DC2 neurons (Fig.3.7B-B"), the small bipolar DC3 neurons (Fig.3.7C-C") and the caudal magnocellular DC4 neurons (Fig.3.7C-C"). Their relative positions along the dorso-ventral axis were similar to those of adult populations. Further, the position of DC2, DC3 and DC4 populations with respect to the ventricle was similar to those observed in adult populations: DC2 neurons were just beyond the ventricle, DC3 neurons were immediately adjacent to the ventricle and DC4 neurons were some distance from the ventricle (i.e. similar positions as $DC2^{A}$, PVO and $DC4^{A}$ respectively)(Table 3.1).

In summary, based on morphology, relative position along the DV and rostro-caudal axes, and position relative to the ventricle, my results confirm previous reports that DC1/TPp, DC2/$DC2^{A}$ populations, DC3/PVO and DC4/$DC4^{A}$ populations are likely to be related.

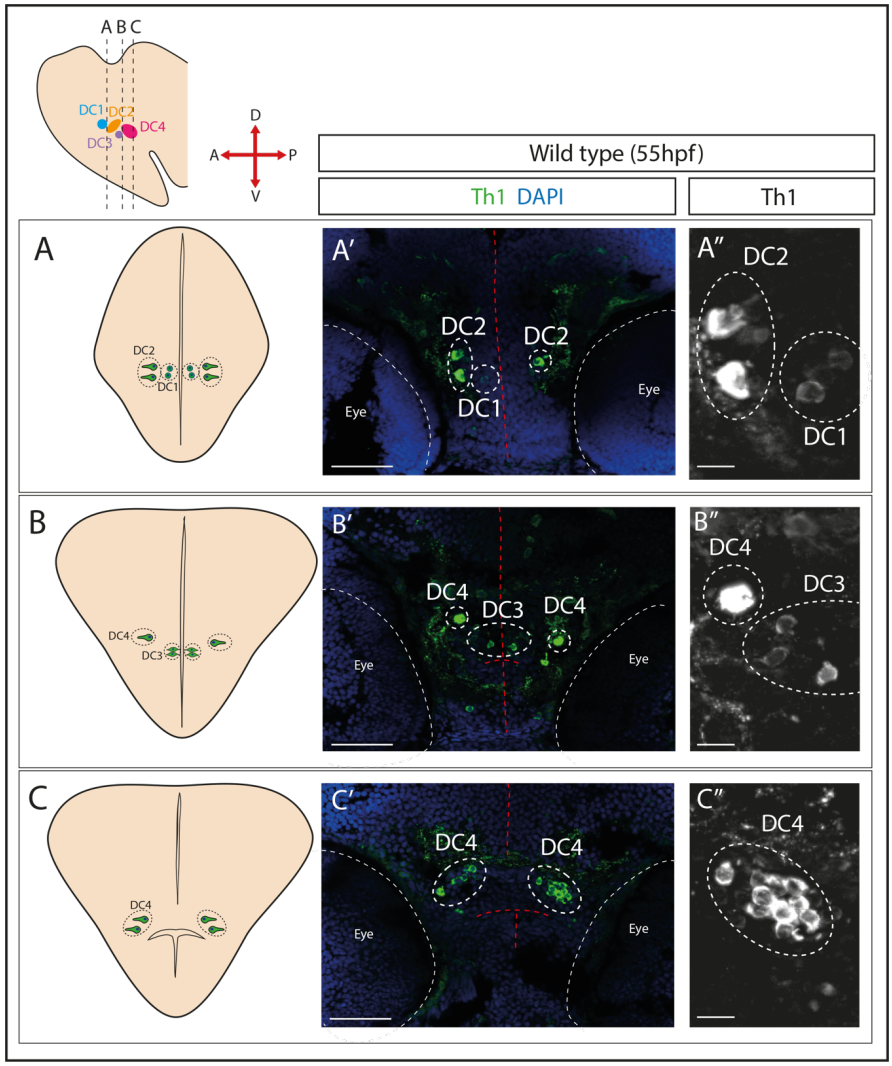

Fig.3.7: Dopaminergic populations in the embryonic zebrafish rostral PT – a transverse view.

A, B, C. Illustrations showing the orientation and rostral PT population location for transverse planes in A', B', C" and A", B", C". DA neurons are represented in green.

A', B', C'. Fluorescent MIP of a transverse section through a 55hpf PT, labelled with the nuclear marker, DAPI (blue) and Th1 (green). Different populations in the PT are outlined and labelled. Th1 labels DA neurons in distinct populations within the PT. Scale bars represent 50μm.

A", B", C". Fluorescent MIPs for Th1 are shown as magnifications of A', B', C'. Distinct populations in the PT are outlined and labelled. Scale bars represent 10μm. Small round cells occupy the TPp, large pear shaped neurons form the DC2 and DC4 populations and small bipolar cells occupy the PVO.

I next counted DA neurons in the different DA populations at 55hpf and compared these to the numbers detected in the 3-month old fish (Fig. 3.8). This analysis shows that a significant increase in the number of DC1/TPp neurons (from 2±0 to 363±9.8; Fig 3.8A), DC3/PVO neurons (18±0.89 to 356±18; Fig. 3.8C) and DC4/DC4^{A} neurons (7.3±1.5 to 18.7±0.89; Fig. 3.8D) over this period. By contrast, the numbers of DC2/DC2^{A} neurons do not increase significantly (from 7.3±0.67 to 8±0.6; Fig. 3.8B). Together this shows that two ascending populations expand in number in early stages of life: The TPp and the DC4/DC4^{A} population, together with the locally projecting DC3/PVO population, however the third ascending DC2/DC2^{A} population does not increase in size (Table 3.1).

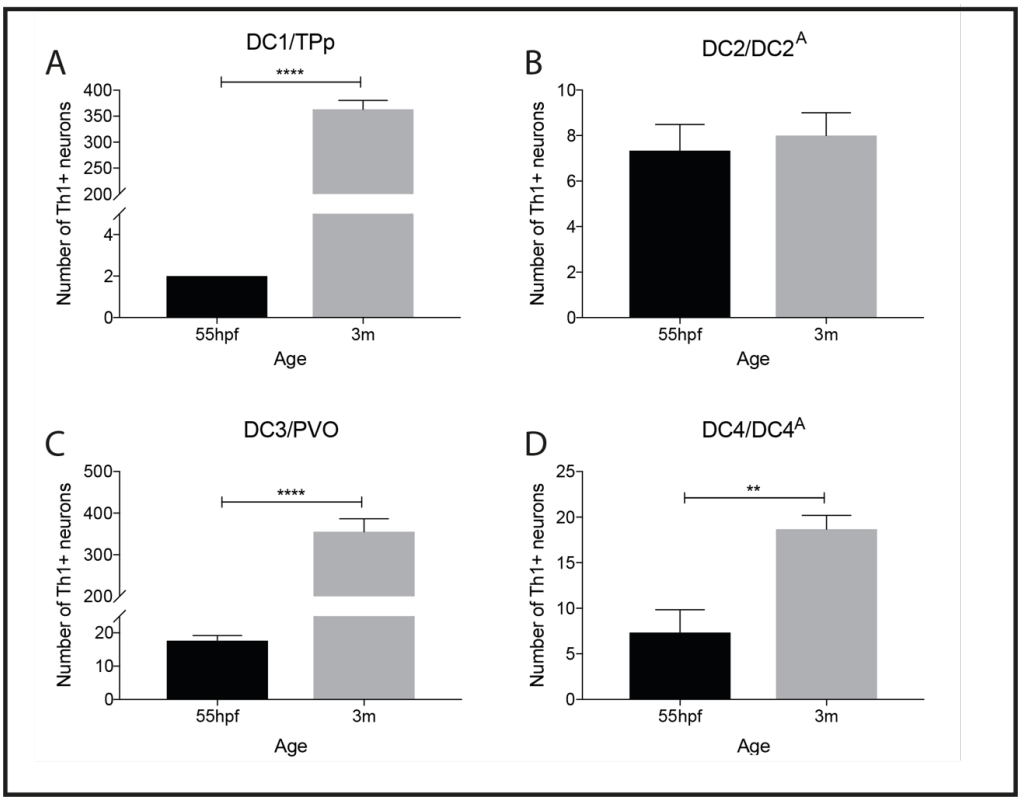

Fig.3.8: The number of Th1^{+} DA neurons increases in DC1/TPp, DC3/PVO and DC4/DC4^{A} between 55hpf and 3 months of age.

Quantitative analyses of the mean number of Th1+ cells in each population of the rostral PT, analysed from serial 15μm sections of 55hpf and 3-month old zebrafish (error bars represent standard deviation, statistically analysed by unpaired t-test).

A. The number of DA neurons significantly increases in the DC1/TPp population (p=<0.0001, n=4).
B. The number of DA neurons does not significantly increase in the DC2/DC2^{A} population (n=4).
C. The number of DA neurons significantly increases in the DC3/PVO population (p=<0.0001, n=4).
D. The number of DA neurons significantly increases in the DC4/DC4^{A} population (p=0.0026, n=4).

Population	Position			Morphology
	Antero-ventral	Dorso-ventral	Ventricle	
DC1	Anterior most	Dorsal most	At and beyond ventricle	Small (parvocellular)
DC2	Anterior	Dorsal	Beyond ventricle	Large (magnocellular)
DC3	Anterior	Ventral	At ventricle	Small, bipolar (parvocellular)
DC4	Posterior	Dorsal	Well beyond ventricle	Large (magnocellular)
TPp	Anterior most	Dorsal most	At and beyond ventricle	Small (parvocellular)
$DC2^{A}$	Anterior	Dorsal	Beyond ventricle	Large (magnocellular)
PVO	Anterior	Ventral	At ventricle	Small, bipolar (parvocellular)
$DC4^{A}$	Posterior	Dorsal	Well beyond ventricle	Large (magnocellular)

Table 3.1: Summary of the position and morphology of embryonic (DC1, DC2, DC3, DC4) and adult (TPp, $DC2^{A}$, PVO, $DC4^{A}$) rostral PT populations

3.3 Discussion

The aim of this chapter was to robustly define distinct DA neuronal populations in the adult and the embryonic rostral PT, and to test the previous suggestion (Rink & Wullimann, 2002*b*) that embryonic and adult populations are related. To achieve this, adult and embryonic zebrafish brains were sectioned in sagittal and transverse planes, and sections were analysed with the dopaminergic neuronal marker, Th1.

Rostral PT DA populations were successfully identified and characterised in the 12-month (adult) and 3-month (young adult) zebrafish brain. These consisted of the TPp, $DC2^{A}$ neurons, the PVO and $DC4^{A}$ neurons. My data adds to previous studies (Rink & Wullimann, 2001*a*, 2002*a*, 2004), providing an estimation of the numbers of DA neurons in each population and showing that there is no significant difference in DA neuronal number in rostral PT subpopulation in male versus female zebrafish.

Rostral PT DA populations were likewise successfully identified and characterised in the 55hpf embryo and, in agreement with published studies (Rink & Wullimann, 2002*b*), assigned to DC1, DC2, DC3 and DC4 populations. My studies add to previous data by directly comparing embryonic and adult populations side by side. My comparative analysis of the 55hpf and adult rostral PT shows that DA neurons in ascending populations (DC1/TPp, DC2/$DC2^{A}$ and DC4/$DC4^{A}$) and local-projecting neurons (DC3/PVO) are similar in morphology and position between embryo and adult.

My data further shows for the first time that two ascending populations (TPp/DC1 and DC4/$DC4^{A}$) increase in Th1+ neuronal number over the first 3 months of age, where the TPp is the largest ascending population. Likewise, DA neurons in the locally projecting DC3/PVO population also show a significant increase in number over the first 3 months of age.

My studies confirm the morphological and positional similarities between embryonic and adult PT populations, though future lineage tracing experiments should be performed to confirm these populations are directly related. In addition, my analyses have led me to understand overall morphology of the PT, and appreciate its growth from embryonic to adult stages. I next sought to determine whether the rostral PT contains stem/progenitor cells in embryonic and adult stages.

Chapter 4

Neural stem/progenitor cells are retained in the rostral PT in adulthood

4.1: Introduction

Adult neurogenesis has been described in most vertebrates and is a highly regulated process, driven by resident stem and progenitor cells that occupy specialised niches. In mammals, neurogenesis is restricted to discrete regions of the adult brain, in particular the SGZ of the hippocampus and the SVZ of the lateral ventricles. Low levels of neurogenesis have also been described in other regions of the CNS, including the hypothalamus (see introduction section 1.4.3). In zebrafish, neurogenesis is likewise detected in these, and other brain regions, and adult de novo neurogenesis is thought to occur at significantly greater levels than in mammals (see introduction section 1.4.5). Nonetheless, proliferation sites still appear to be restricted to distinct brain regions, suggesting the presence of distinct stem and progenitor niches. Importantly, previous studies have identified the PT as one such proliferation site (Grandel *et al.*, 2006). This, together with my observation (Chapter 3) that DA populations significantly increase in size from 55hpf to 3-months raises the possibility that the rostral PT contains neural stem and progenitor cells that are retained into adulthood. In this chapter I addressed this question by examining expression of neural stem/progenitor markers in the rostral PT, at different stages through life.

4.2.1 Expression of radial glial markers in the rostral PT

Previous studies have shown that cells with radial glial morphology act as neural stem/progenitor cells in both mammals (Alvarez-Buylla *et al.*, 2001; Kriegstein & Alvarez-Buylla, 2009) and zebrafish (Grandel *et al.*, 2006; Pellegrini *et al.*, 2007; Lam *et al.*, 2009; Ganz *et al.*, 2010*b*). However as yet, it is not known if there are radial glia-like cells in the zebrafish PT. I therefore set out to characterise the PT at different stages in life, using two markers of radial glial cells, Nestin and Her4. I aimed to determine whether radial glial cells are found in the PT, and if so, how their position relates to the distinct DA neuronal populations identified in Chapter 3.

To begin with, I examined expression of markers in the 5 dpf larva. At this time, the distinct DA neuronal populations are similar to those in the 55 hpf embryo, however at 5dpf individual radial glia are more visible as populations become more restricted with age (Rink & Wullimann, 2002*b*). Nestin is an intermediate filament protein that is expressed by radial glial cells (and is required for the self-renewal of neural stem cells) (Chen *et al.*, 2010; Park *et al.*, 2010). In the absence of an anti-Nestin antibody that labels the zebrafish, I examined a transgenic *nestin*:GFP zebrafish line that has been described previously (Lam *et al.*, 2009). In 5dpf zebrafish, Nestin is expressed by cells that line the diencephalic ventricle and that have radial glial-like morphology: a cell body at the ventricle and a basally-extending process (Fig.4A-C). Co-labelling with anti-Th1 shows that Nestin^{+} radial glial-like cells are thus adjacent to or close to DA neurons in the DC1 (Fig.4.1A), DC2 (Fig.4.1B), DC3 and DC4 (Fig.4.1C) populations.

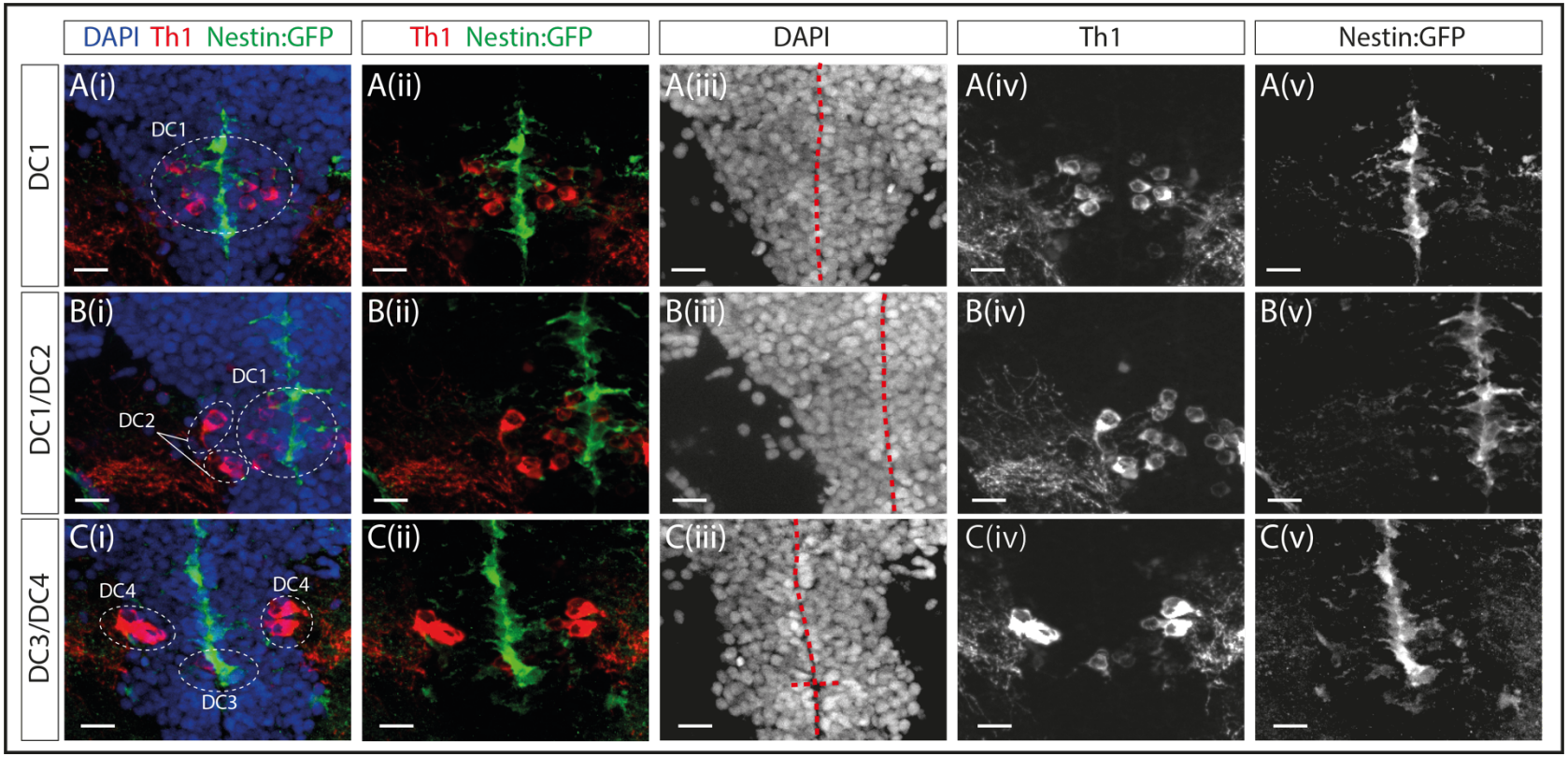
DAPI Th1 Nestin:GFP
Th1 Nestin:GFP
DAPI
Th1
Nestin:GFP
DC1
DC1/DC2
DC3/DC4
A(i)
A(ii)
A(iii)
A(iv)
A(v)
B(i)
B(ii)
B(iii)
B(iv)
B(v)
C(i)
C(ii)
C(iii)
C(iv)
C(v)
DC1
DC2
DC4
DC4
DC3

Fig.4.1: Nestin:GFP is expressed in the ventricle of the larval rostral PT

A(i-v). Fluorescent MIP of a transverse section through the DC1 population of 5dpf Nestin:GFP zebrafish larvae, labelled with DAPI (blue), Th1 (red) and Nestin:GFP (green). Th1 and Nestin:GFP are shown without DAPI (ii), DAPI is shown in (iii), Th1 is shown in (iv), Nestin:GFP is shown in (v). Scale bars represent 10 μm. DA populations are outlined in white, DiV is outlined in red in (ii).

B(i-v). Fluorescent MIP of a transverse section through the DC1/DC2 populations of 5dpf Nestin:GFP zebrafish larvae, labelled with DAPI (blue), Th1 (red) and Nestin:GFP (green). Th1 and Nestin:GFP are shown without DAPI (ii), DAPI is shown in (iii), Th1 is shown in (iv), Nestin:GFP is shown in (v). Scale bars represent 10 μm. DA populations are outlined in white, DiV is outlined in red in (ii).

C(i-v). Fluorescent MIP of a transverse section through the DC3/DC4 populations of 5dpf Nestin:GFP zebrafish larvae, labelled with DAPI (blue), Th1 (red) and Nestin:GFP (green). Th1 and Nestin:GFP are shown without DAPI (ii), DAPI is shown in (iii), Th1 is shown in (iv), Nestin:GFP is shown in (v). Scale bars represent 10 μm. DA populations are outlined in white, DiV is outlined in red in (ii).

A similar pattern of Nestin expression is observed in the adult PT. Nestin^{+} cells with radial glial morphology line the diencephalic ventricle immediately adjacent to or close to DA neurons in the TPp (Fig.4.2A), the DC2 (Fig.4.2B) and the PVO (Fig.4.2C) populations. Similarly, they line the lateral ventricles adjacent to DA neurons of the DC4 population (Fig.4.2D). In most regions of the PT, all cells at the ventricle appear to express Nestin. The exception is at the level of the PVO, where Nestin^{+} radial glial cells are extremely sparse (one to two cells) and are surrounded by Nestin^{-} cells (Fig.42C).

In summary, at both larval and adult stages, Nestin+ radial glial-like cells can be detected at the ventricular zone throughout the rostral PT, supporting the idea that a Nestin^{+} stem/progenitor population established in early life may persist into adulthood (Fig.4.9 schematic). Although Nestin^{+} radial glia lie very close to DA populations – in particular to DC1, DC3, TPp, DC2^{A} and PVO populations, no nestin^{+}Th1^{+} cells are detected, either in the embryo or the adult.

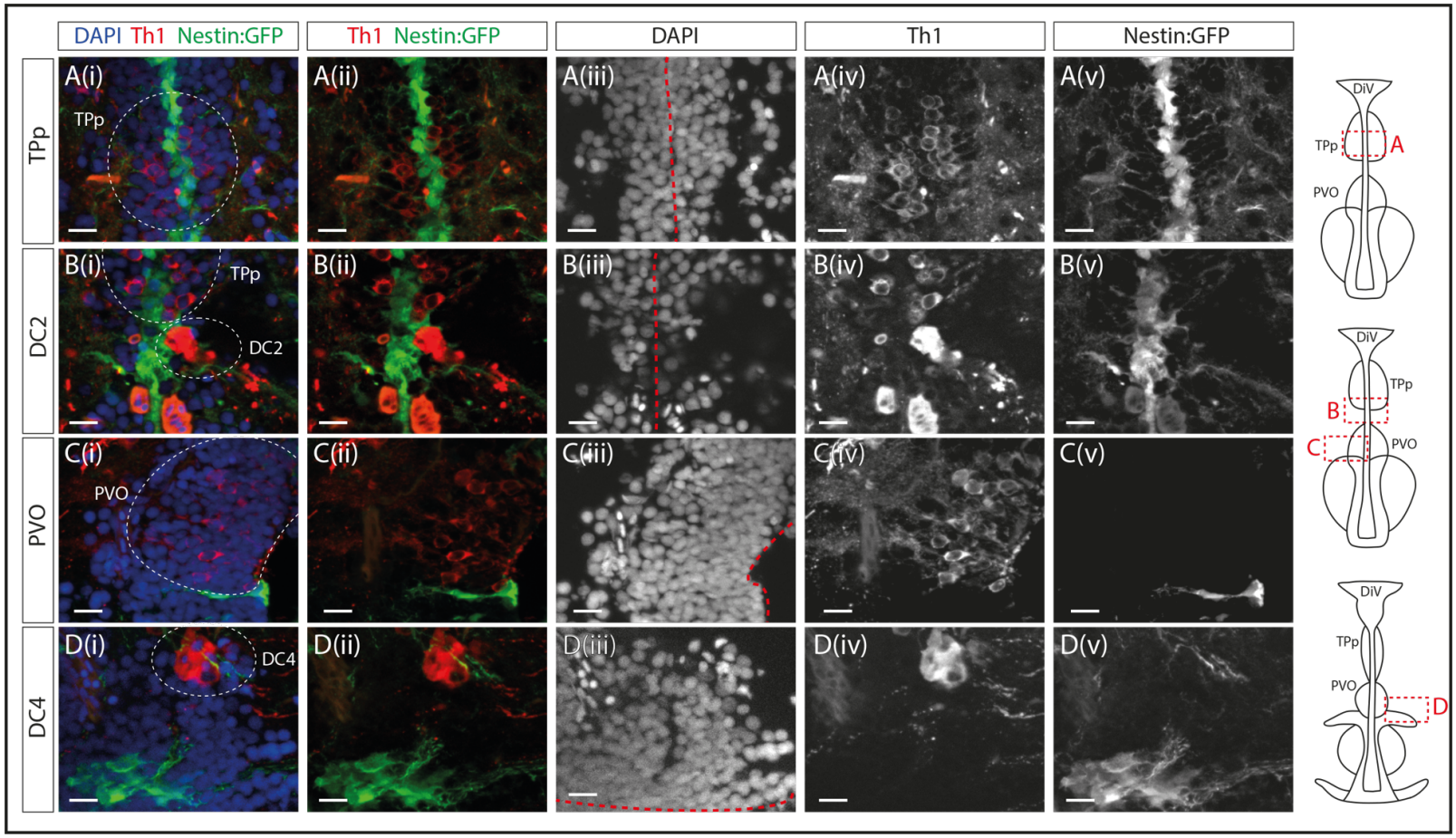
DAPI Th1 Nestin:GFP
Th1 Nestin:GFP
DAPI
Th1
Nestin:GFP
TPp
DC2
PVO
DC4
A(i)
A(ii)
A(iii)
A(iv)
A(v)
B(i)
B(ii)
B(iii)
B(iv)
B(v)
C(i)
C(ii)
C(iii)
C(iv)
C(v)
D(i)
D(ii)
D(iii)
D(iv)
D(v)
DiV
TPp
PVO
A
B
C
D

Fig. 4.2: Nestin:GFP expression persists in the ventricle of the adult rostral PT

A(i-v). Fluorescent MIP of a transverse section through the TPp of a 6-month Nestin:GFP zebrafish, labelled with DAPI (blue), Th1 (red) and Nestin:GFP (green). Th1 and Nestin:GFP are shown without DAPI (ii), DAPI is shown in (iii), Th1 is shown in (iv), Nestin:GFP is shown in (v). Scale bars represent 10 μm. DA populations are outlined, DiV is outlined in red. Schematics on right hand side indicate position of corresponding image in relation the DiV.

B(i-v). Fluorescent MIP of a transverse section through the DC2 population of a 6-month Nestin:GFP zebrafish, labelled with DAPI (blue), Th1 (red) and Nestin:GFP (green). Th1 and Nestin:GFP are shown without DAPI (ii), DAPI is shown in (iii), Th1 is shown in (iv), Nestin:GFP is shown in (v). Scale bars represent 10 μm. DA populations are outlined, DiV is outlined in red. Schematics on right hand side indicate position of corresponding image in relation the DiV.

C(i-v). Fluorescent MIP of a transverse section through PVO of a 6-month Nestin:GFP zebrafish, labelled with DAPI (blue), Th1 (red) and Nestin:GFP (green). Th1 and Nestin:GFP are shown without DAPI (ii), DAPI is shown in (iii), Th1 is shown in (iv), Nestin:GFP is shown in (v). Scale bars represent 10 μm. DA populations are outlined, DiV is outlined in red. Schematics on right hand side indicate position of corresponding image in relation the DiV.

D(i-v). Fluorescent MIP of a transverse section through the DC4 population of a 6-month Nestin:GFP zebrafish, labelled with DAPI (blue), Th1 (red) and Nestin:GFP (green). Th1 and Nestin:GFP are shown without DAPI (ii), DAPI is shown in (iii), Th1 is shown in (iv), Nestin:GFP is shown in (v). Scale bars represent 10 μm. DA populations are outlined, DiV is outlined in red. Schematics on right hand side indicate position of corresponding image in relation the DiV.

I next analysed expression of the zebrafish basic-helix-loop-helix transcription factor Her4. This protein is orthologous to mammalian Hes5, a member of the Hairy/Enhancer-of-split family. *Hes5/her4* is expressed by Notch-responsive radial glial stem/progenitor cells that can generate neurons in the adult brain (Cau *et al.*, 2000; Basak & Taylor, 2007; Chapouton *et al.*, 2010; Ganz *et al.*, 2010*a*; Kroehne *et al.*, 2011; Dirian *et al.*, 2014). Since no Her4 antibody has been described, a *her4*:mCherry line (Kroehne *et al.*, 2011) was used to investigate Her4 expression in the rostral PT. In 5 dpf zebrafish larvae, Her4 is expressed by radial glial-like cells that line the diencephalic ventricle (Fig.4.3). Co-labelling with anti-Th1 reveals that $Her4^{+}$ radial glia lie immediately adjacent to/close to DA neurons in the DC1 (Fig.4.3A), DC2 (Fig.4.3B), DC3 and DC4 (Fig.4.3C) populations. Likewise, in the adult PT, Her4 is expressed by radial glial-like cells that line the diencephalic ventricle (Fig.4.4A-C) and the lateral ventricle (Fig.4.4D). At the level of the PVO, exceptionally, a double tram-line of $Her4^{+}$ cells are detected: those located at a distance from the ventricle extend a short process towards it (Fig. 4.4C). Co-labelling with anti-Th1shows that $Her4^{+}$ radial glia lie immediately adjacent /close to DA neurons in the TPp (Fig.4.4A), DC2 (Fig.4.4B) and PVO (Fig.4.4C) populations, and line the lateral ventricles adjacent to DA neurons of the DC4 population (Fig.4.4D). Comparison with Nestin suggests that $Her4^{+}$ radial glia may be a subset of those that express Nestin (Fig.4.9 schematic).

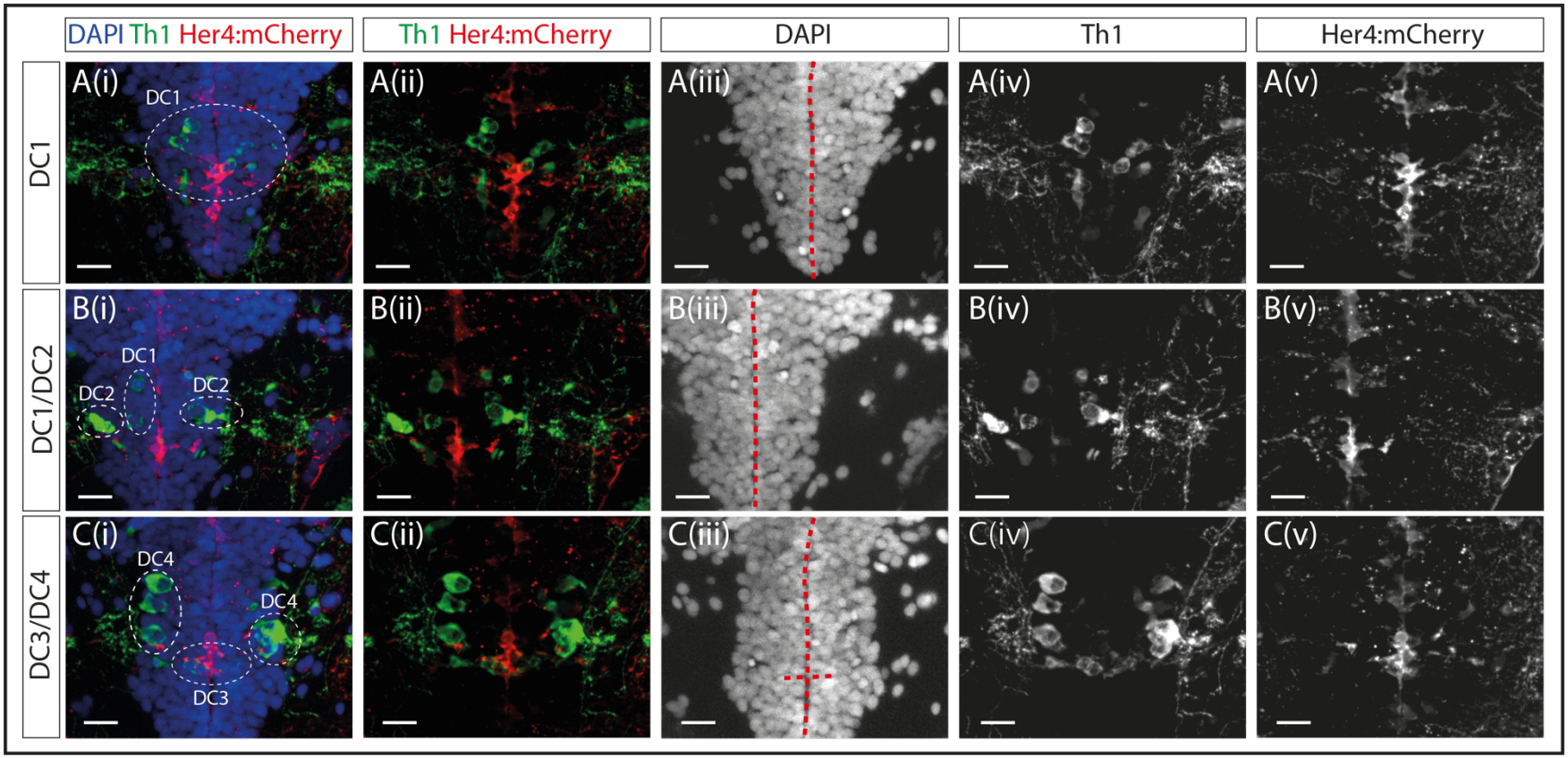
DAPI Th1 Her4:mCherry
Th1 Her4:mCherry
DAPI
Th1
Her4:mCherry
DC1
DC1/DC2
DC3/DC4
A(i)
DC1
A(ii)
A(iii)
A(iv)
A(v)
B(i)
DC1
DC2
DC2
B(ii)
B(iii)
B(iv)
B(v)
C(i)
DC4
DC4
DC3
C(ii)
C(iii)
C(iv)
C(v)

Fig. 4.3: Her4.1:mCherry is expressed in the ventricle of the larval rostral PT

A(i-v). Fluorescent MIP of a transverse section through the DC1 population of 5dpf Her4.1:mCherry zebrafish larvae, labelled with DAPI (blue), Th1 (green) and Her4.1 (red). Th1 and Her4.1 are shown without DAPI (ii), DAPI is shown in (iii), Th1 is shown in (iv), Her4.1 is shown in (v). Scale bars represent 10 μm. DA populations are outlined, DiV is outlined in red.

B(i-v). Fluorescent MIP of a transverse section through the DC1 and DC2 populations of 5dpf Her4.1:mCherry zebrafish larvae, labelled with DAPI (blue), Th1 (green) and Her4.1 (red). Th1 and Her4.1 are shown without DAPI (ii), DAPI is shown in (iii), Th1 is shown in (iv), Her4.1 is shown in (v). Scale bars represent 10 μm. DA populations are outlined, DiV is outlined in red.

C(i-v). Fluorescent MIP of a transverse section through the DC3 and DC4 populations of 5dpf Her4.1:mCherry zebrafish larvae, labelled with DAPI (blue), Th1 (green) and Her4.1 (red). Th1 and Her4.1 are shown without DAPI (ii), DAPI is shown in (iii), Th1 is shown in (iv), Her4.1 is shown in (v). Scale bars represent 10 μm. DA populations are outlined, DiV is outlined in red.

DAPI Th1 Her4:mCherry
Th1 Her4:mCherry
DAPI
Th1
Her4:mCherry
TPp
DC2
PVO
DC4
A(i)
A(ii)
A(iii)
A(iv)
A(v)
B(i)
B(ii)
B(iii)
B(iv)
B(v)
C(i)
C(ii)
C(iii)
C(iv)
C(v)
D(i)
D(ii)
D(iii)
D(iv)
D(v)
DiV
TPp
PVO
A
B
C
D

Fig. 4.4: Her4.1:mCherry expression in the ventricle is maintained in the adult rostral PT

A(i-v). Fluorescent MIP of a transverse section through the TPp of a 6-month Her4.1:mCherry zebrafish, labelled with DAPI (blue), Th1 (green) and Her4.1 (red). Th1 and Her4.1:mCherry are shown without DAPI (ii), DAPI is shown in (iii), Th1 is shown in (iv), Her4.1:mCherry is shown in (v). Scale bars represent 10 μm. DiV is outlined in red. Schematics on right hand side indicate position of corresponding image in relation the DiV.

B(i-v). Fluorescent MIP of a transverse section through the DC2 population of a 6-month Her4.1:mCherry zebrafish, labelled with DAPI (blue), Th1 (green) and Her4.1 (red). Th1 and Her4.1:mCherry are shown without DAPI (ii), DAPI is shown in (iii), Th1 is shown in (iv), Her4.1:mCherry is shown in (v). Scale bars represent 10 μm. DiV is outlined in red. Schematics on right hand side indicate position of corresponding image in relation the DiV.

C(i-v). Fluorescent MIP of a transverse section through the TPp of a 6-month Her4.1:mCherry zebrafish, labelled with DAPI (blue), Th1 (green) and Her4.1 (red). Th1 and Her4.1:mCherry are shown without DAPI (ii), DAPI is shown in (iii), Th1 is shown in (iv), Her4.1:mCherry is shown in (v). Scale bars represent 10 μm. DiV is outlined in red Schematics on right hand side indicate position of corresponding image in relation the DiV.

D(i-v). Fluorescent MIP of a transverse section through the DC4 population of a 6-month Her4.1:mCherry zebrafish, labelled with DAPI (blue), Th1 (green) and Her4.1 (red). Th1 and Her4.1:mCherry are shown without DAPI (ii), DAPI is shown in (iii), Th1 is shown in (iv), Her4.1:mCherry is shown in (v). DiV is outlined in red. Scale bars represent 10 μm. Schematics on right hand side indicate position of corresponding image in relation the DiV.

In summary, at both larval and adult stages, Her4^{+} radial glial-like cells can be observed in the rostral PT. Her4^{+} radial glia are less widespread that Nestin^{+} radial glia (Fig.4.9 schematic). Although Her4^{+} radial glia lie very close to DA populations – in particular, to DC1, DC3, TPp, and PVO populations, no Her4^{+}Th1^{+} cells are detected, either in the embryo or the adult.

4.2.2 Expression of DA-progenitor markers in the rostral PT

The paired-like homeodomain transcription factor *Rax* and the zebrafish orthologue, *rx3*, are central to the development of the retina (Mathers *et al.*, 1997; Zhang *et al.*, 2000; Loosli *et al.*, 2003; Bailey *et al.*, 2004; Kennedy *et al.*, 2004; Stigloher *et al.*, 2006; Medina-Martinez *et al.*, 2009; Muranishi *et al.*, 2012) and to the development of ventral forebrain structures, including the hypothalamus (Mathers *et al.*, 1997; Zhang *et al.*, 2000; Medina-Martinez *et al.*, 2009). Recent work from the Placzek lab, to which I have contributed, has shown that Rx3 is required to select a particular progenitor fate, directing *pea3*$^{+}$ progenitor cells to *shh*$^{+}$*pea3*$^{-}$ progenitor cells and supporting their survival and growth. In the absence of *rx3* expression, anterior/tuberal hypothalamic neurons fail to differentiate (Muthu *et al.*, 2016).

My contribution to this study was to ask whether populations of DA neurons in the PT (which lies just dorsal and rostral to the hypothalamus: Fig.3.1 and Fig.3.6) require Rx3. Analysis of Th1expression in *rx3*-null embryos showed that DC1, DC2 and DC3 populations failed to differentiate, and that the DC4 population was either missing or reduced (note, this work was performed at the beginning of my PhD studies, when I had not yet learned how to distinguish each population). This shows that progenitors expressing *rx3* are required for the generation of rostral populations of DA neurons in the zebrafish embryo.

To build on this work, which focused on *rx3* expression in the hypothalamus, I re-analysed *rx3* expression in the 55hpf embryo, but focused on the PT, and at the same time, analysed expression in the 6-month fish, to determine whether *rx3*$^{+}$ progenitors are maintained in

adulthood. To achieve this, fluorescent in situ hybridisation (FISH) of *rx3* was performed on sections through the 55hpf embryonic and 6-month adult brain (Fig. 4.5,4.6).

My studies confirm our previous analyses (Muthu et al, 2016). In regions of the PT that lie rostral to the anterior hypothalamus, *rx3* is detected at very low level (Fig.4.5Av); in regions of the PT that lie dorsal to the anterior hypothalamus, no *rx3* is detected (Fig.4.5Bv); in regions of the PT that overlap with the anterior hypothalamus, *rx3* is strongly detected within domains previously termed Zone I and Zone II (Fig.4.5Bv). Where rx3 is detected, its expression is in cells at, and adjacent to the diencephalic and the lateral ventricles (Fig 4.5Bv).

To directly compare expression of rx3 with DA neuronal populations, consecutive transverse sections were simultaneously analysed for *rx3* and Th1. This reveals that the DC1, DC2 and DC4 DA neuronal populations that reside in the dorsal PT, also lie in domains that express either low levels of *rx3* (DC1 and DC2) or that do not express *rx3* (DC4) (Fig.4.5A, B). By contrast, DA neurons of the DC3 population reside in the ventral PT/dorsal hypothalamus and lie within or adjacent to *rx3*$^{+}$ progenitor cells in Zones I and II (Fig.4.5).

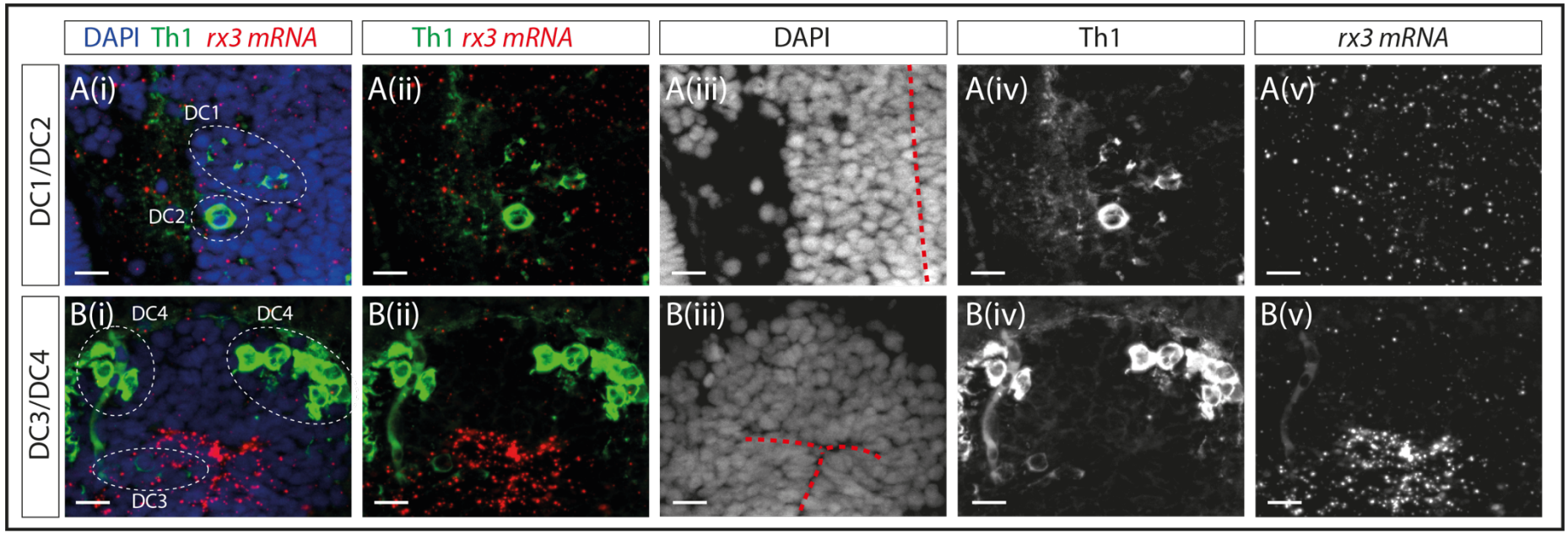
DAPI Th1 rx3 mRNA
Th1 rx3 mRNA
DAPI
Th1
rx3 mRNA
DC1/DC2
DC3/DC4
A(i)
DC1
DC2
A(ii)
A(iii)
A(iv)
A(v)
B(i)
DC4
DC4
DC3
B(ii)
B(iii)
B(iv)
B(v)

Fig. 4.5: *rx3* is expressed within the DC3 DA neuron domain at 55hpf

A(i-v). Fluorescent MIP of a transverse section through the DC1 and DC2 populations of a 55hpf zebrafish embryo, labelled with DAPI (blue), Th1 (green) and *rx3* (red). Th1 and *rx3* are shown without DAPI (ii), DAPI is shown in (iii), Th1 is shown in (iv), *rx3* is shown in (v). Scale bars represent 10 μm. DA populations are outlined, DiV is outlined in red. Low levels of *rx3* expression in DC1 and DC2 populations.

B(i-v). Fluorescent MIP of a transverse section through the DC3 and DC4 populations of a 55hpf zebrafish embryo, labelled with DAPI (blue), Th1 (green) and *rx3* (red). Th1 and *rx3* are shown without DAPI (ii), DAPI is shown in (iii), Th1 is shown in (iv), *rx3* is shown in (v). Scale bars represent 10 μm. DA populations are outlined, DiV is outlined in red. *rx3*-expressing cells are observed in the DC3 domain.

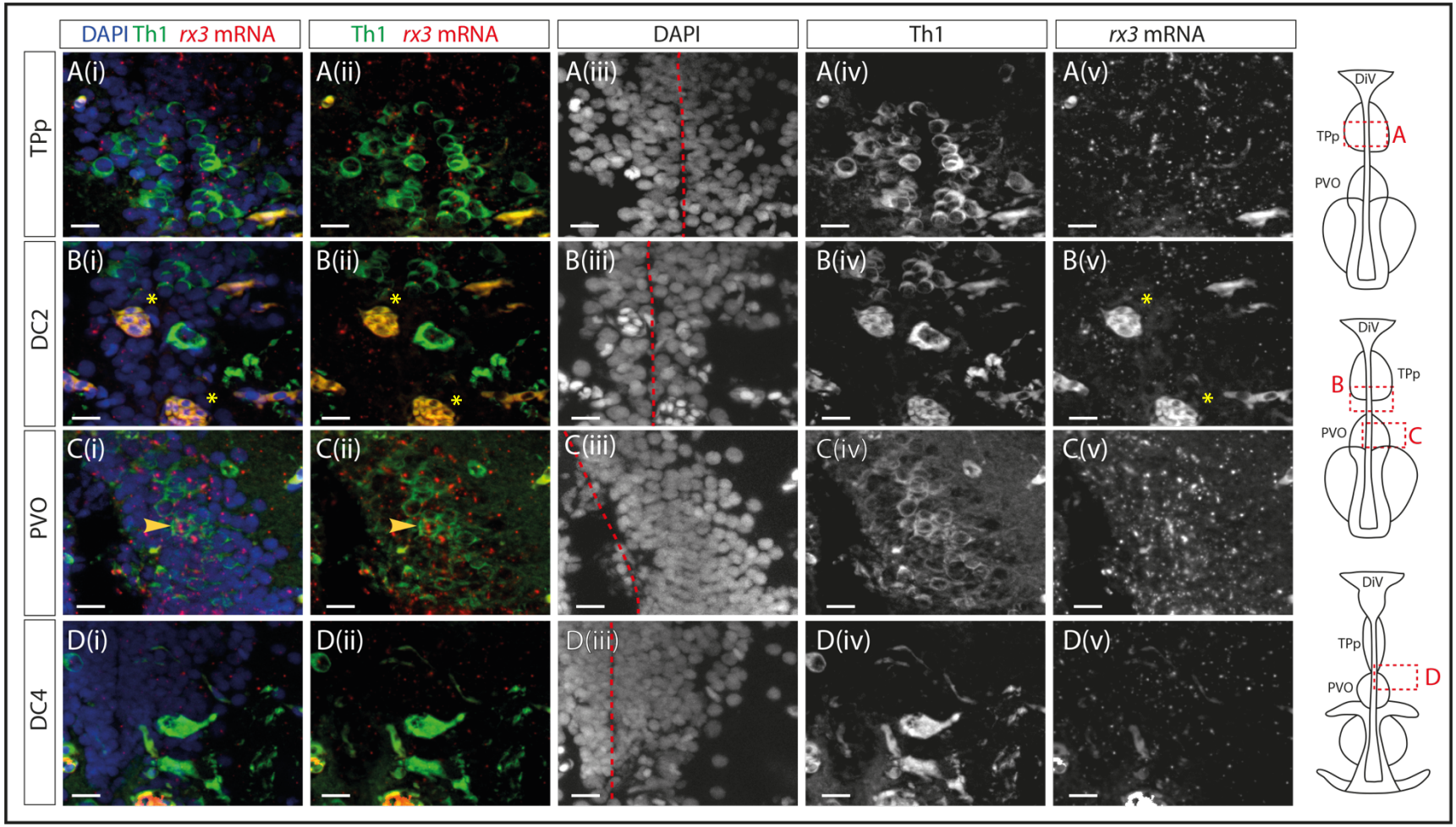
DAPI Th1 rx3 mRNA
Th1 rx3 mRNA
DAPI
Th1
rx3 mRNA
TPp
DC2
PVO
DC4
A(i)
A(ii)
A(iii)
A(iv)
A(v)
B(i)
B(ii)
B(iii)
B(iv)
B(v)
C(i)
C(ii)
C(iii)
C(iv)
C(v)
D(i)
D(ii)
D(iii)
D(iv)
D(v)
DiV
TPp
A
PVO
DiV
B
TPp
PVO
C
DiV
TPp
PVO
D

Fig. 4.6: *rx3* is expressed within the PVO in adulthood

A(i-v). Fluorescent MIP of a transverse section through the TPp of a 6-month old zebrafish, labelled with DAPI (blue), Th1 (green) and *rx3* (red). Th1 and *rx3* are shown without DAPI (ii), DAPI is shown in (iii), Th1 is shown in (iv), *rx3* is shown in (v). DiV is outlined in red. Scale bars represent 10 μm. Low levels of *rx3* expression in the TPp.

B(i-v). Fluorescent MIP of a transverse section through the DC2 population of a 6-month old zebrafish, labelled with DAPI (blue), Th1 (green) and *rx3* (red). Th1 and *rx3* are shown without DAPI (ii), DAPI is shown in (iii), Th1 is shown in (iv), *rx3* is shown in (v). DiV is outlined in red. Yellow asterisks mark non-specific blood vessel labelling by secondary antibody. Scale bars represent 10 μm. No expression of *rx3* in the DC2 domain.

C(i-v). Fluorescent MIP of a transverse section through the PVO of a 6-month old zebrafish, labelled with DAPI (blue), Th1 (green) and *rx3* (red). Th1 and *rx3* are shown without DAPI (ii), DAPI is shown in (iii), Th1 is shown in (iv), *rx3* is shown in (v). DiV is outlined in red. Scale bars represent 10 μm. *rx3* is strongly expressed in DA neurons of the PVO.

D(i-v). Fluorescent MIP of a transverse section through the DC4 population of a 6-month old zebrafish, labelled with DAPI (blue), Th1 (green) and *rx3* (red). Th1 and *rx3* are shown without DAPI (ii), DAPI is shown in (iii), Th1 is shown in (iv), *rx3* is shown in (v). DiV is outlined in red. Scale bars represent 10 μm. No expression of *rx3* in the DC4 domain.

In the adult PT, low levels of *rx3* can be detected in the TPp (Fig.4.6A) and no expression is detected in the $DC2^A$ or $DC4^A$ population (Fig. 4.6B,D). Strong expression of *rx3* is detected within the PVO, where some $Th1^+$ DA neurons appear to co-express *rx3* (Fig. 4.6C, yellow arrowhead). In summary, at larval and adult stages, $rx3^+$ cells can be observed in the rostral PT, within DC3 and PVO DA populations respectively (Fig.4.9 schematic).

Many studies, including our own, have shown that the orthopedia gene, *otp*, and its product, OTP, are expressed in DA-progenitors (Ryu *et al.*, 2007; Fernandes *et al.*, 2013, Muthu et al., 2016). Zebrafish have two paralogous *otp* genes (*otpa* and *otpb*), and expression of both has been extensively characterised in the zebrafish embryo. Briefly, *otpa* and *otpb* expression domains show a high level of overlap, and differences in expression are only observed in the caudal hypothalamus. In the rostral PT, *otpa* and *otpb* are expressed by DC2 and DC4 neurons (and adjacent $Th1^-$ cells), but not by DC1 and DC3 DA neurons (Ryu *et al.*, 2007*b*; Fernandes *et al.*, 2013). OTP is required, in a cell-autonomous manner, for the differentiation of progenitors: loss of function of OTP results in the loss of DC2 and DC4 populations (and also, loss of DC5 and DC6) populations (Ryu *et al.*, 2007*b*; Fernandes *et al.*, 2013). It has not yet been reported whether OTP expression is maintained into adulthood in the PT.

Here, I analysed expression of OTP using an antibody against OTPb (Blechman *et al.*, 2007). I first aimed to describe embryonic OTPb expression in consecutive transverse sections through the rostral PT; previous studies have analysed expression only in wholemount view (Ryu *et al.*, 2007; Fernandes *et al.*, 2013, Muthu et al., 2016). Immunohistochemical analysis of OTPb at 55hpf reveals expression in DC2 and DC4 DA neurons, and in adjacent $Th1^-$cells (Fig.4.7A, B), and shows that OTPb cannot be detected in DC1 or DC3 DA neurons (Fig. 4.7A,B). This data agrees with characterisation provided by previous studies.

I next analysed expression of OTPb in the rostral PT of an adult (6-month) zebrafish. OTPb is expressed in $DC2^A$ and $DC4^A$ DA neurons (Fig.4.8B,D) and is not detected in DA neurons of the PVO (Fig.4.8C). OTPb expression is also detected in $Th1^-$ cells immediately adjacent to these populations. These patterns mirror those in the embryo. Surprisingly, however, and in marked contrast to the embryonic DC1 population, OTPb is also detected in $Th1^+$ DA

neurons in the TPp (Fig.4.8A). Indeed, quantitative analyses suggest that every $Th1^{+}$ DA neuron in the TPp co-expresses OTPb (see Chapter 6). Therefore, DC1 and TPp populations show markedly different progenitor characteristics. Together, these analyses suggest that DC1/TPp populations, DC2/$DC2^{A}$ populations, DC3/PVO populations and DC4/$DC4^{A}$ populations might each derive from distinct progenitor cells with particular characteristics (summarised together in Table 4.1; Fig. 4.9).

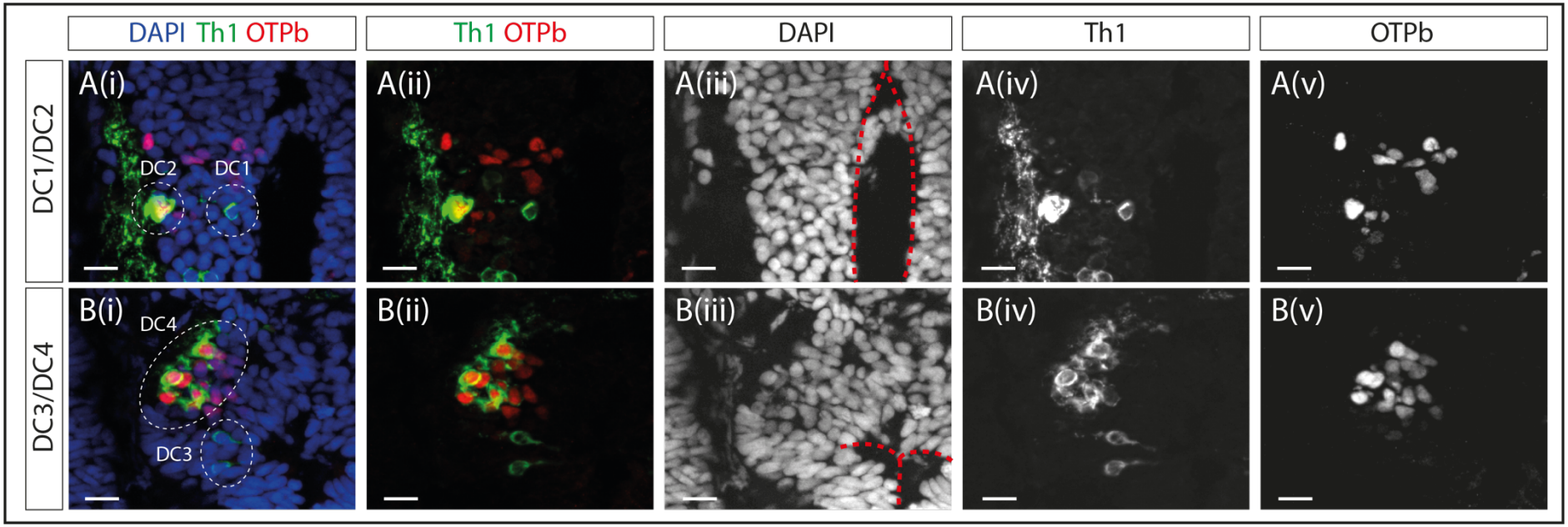
DAPI Th1 OTPb
Th1 OTPb
DAPI
Th1
OTPb
DC1/DC2
DC3/DC4
A(i)
A(ii)
A(iii)
A(iv)
A(v)
B(i)
B(ii)
B(iii)
B(iv)
B(v)
DC2
DC1
DC4
DC3

Fig. 4.7: OTPb is expressed by DC2 and DC4 neurons and by non-Th1-expressing progenitors in the embryonic rostral PT

A(i-v). Fluorescent MIP of a transverse section through DC1 and DC2 populations of 55hpf zebrafish larvae, labelled with DAPI (blue), Th1 (green) and OTPb (red). Th1 and OTPb are shown without DAPI (ii), DAPI is shown in (iii), Th1 is shown in (iv), OTPb is shown in (v). Scale bars represent 10 μm. DA populations are outlined, DiV is outlined in red. DC2 DA neurons co-label with OTPb, DC1 DA neurons do not.

B(i-v). Fluorescent MIP of a transverse section through DC3 and DC4 populations of 55hpf zebrafish larvae, labelled with DAPI (blue), Th1 (green) and OTPb (red). Th1 and OTPb are shown without DAPI (ii), DAPI is shown in (iii), Th1 is shown in (iv), OTPb is shown in (v). Scale bars represent 10 μm. DA populations are outlined, DiV is outlined in red. DC4 DA neurons co-label with OTPb, DC3 DA neurons do not.

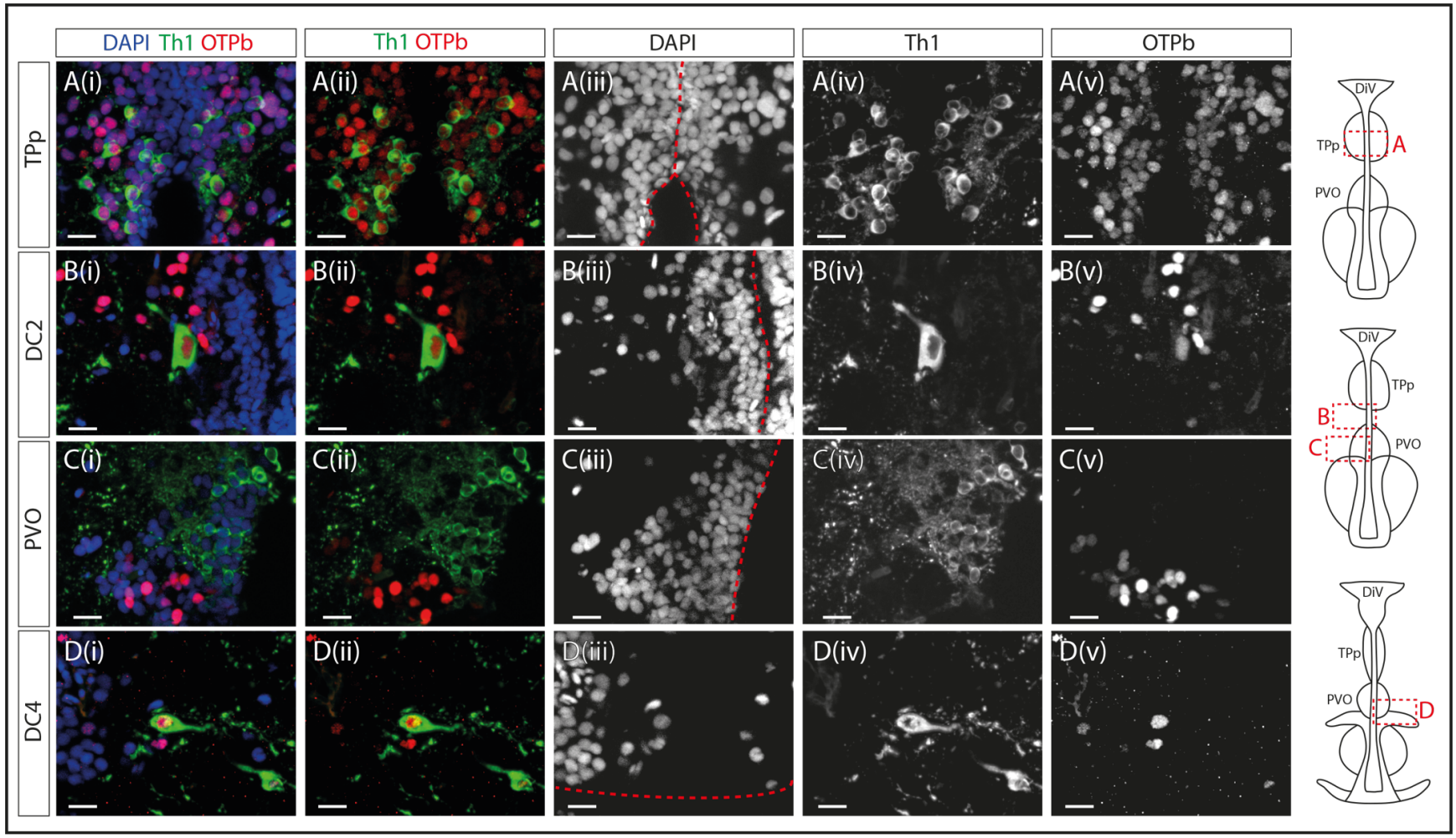
DAPI Th1 OTPb
Th1 OTPb
DAPI
Th1
OTPb
TPp
DC2
PVO
DC4
A(i)
A(ii)
A(iii)
A(iv)
A(v)
B(i)
B(ii)
B(iii)
B(iv)
B(v)
C(i)
C(ii)
C(iii)
C(iv)
C(v)
D(i)
D(ii)
D(iii)
D(iv)
D(v)
DiV
TPp
PVO
A
B
C
D

Fig. 4.8: OTPb expression is detected in the TPp, DC2^{A} and DC4^{A} DA neurons the adult rostral PT.

A(i-v). Fluorescent MIP of a transverse section through the TPp of a 6-month zebrafish, labelled with DAPI (blue), Th1 (green) and OTPb (red). Th1 and OTPb are shown without DAPI (ii), DAPI is shown in (iii), Th1 is shown in (iv), OTPb is shown in (v). DiV is outlined in red. Scale bars represent 10 μm. Schematics on right hand side indicate position of corresponding image in relation the DiV. TPp DA neurons co-express OTPb.

B(i-v). Fluorescent MIP of a transverse section through the DC2 population of a 6-month zebrafish, labelled with DAPI (blue), Th1 (green) and OTPb (red). Th1 and OTPb are shown without DAPI (ii), DAPI is shown in (iii), Th1 is shown in (iv), OTPb is shown in (v). DiV is outlined in red. Scale bars represent 10 μm. Schematics on right hand side indicate position of corresponding image in relation the DiV. DC2 DA neurons co-express OTPb.

C(i-v). Fluorescent MIP of a transverse section through the PVO of a 6-month zebrafish, labelled with DAPI (blue), Th1 (green) and OTPb (red). Th1 and OTPb are shown without DAPI (ii), DAPI is shown in (iii), Th1 is shown in (iv), OTPb is shown in (v). DiV is outlined in red. Scale bars represent 10 μm. Schematics on right hand side indicate position of corresponding image in relation the DiV. PVO DA neurons do not co-express OTPb.

D(i-v). Fluorescent MIP of a transverse section through the DC4 population of a 6-month zebrafish, labelled with DAPI (blue), Th1 (green) and OTPb (red). Th1 and OTPb are shown without DAPI (ii), DAPI is shown in (iii), Th1 is shown in (iv), OTPb is shown in (v). DiV is outlined in red. Scale bars represent 10 μm. Schematics on right hand side indicate position of corresponding image in relation the DiV. DC4 DA neurons co-express OTPb.

Population	Position			Morphology	Position in relation to Nestin+ cells	Position in relation to Her4+ cells	Position in relation to *rx3* + cells	DA neurons OTPb+?	Position in relation to OTPb+Th1- cells
	Antero-ventral	Dorso-ventral	Ventricle						
DC1	Anterior most	Dorsal most	At and beyond ventricle	Small (parvocellular)	Immediately adjacent to numerous	Immediately adjacent to restricted populations	Low *rx3*	No	Adjacent
DC2	Anterior	Dorsal	Beyond ventricle	Large (magnocellular)	Close to numerous	Close to restricted populations	Low *rx3*	Yes	Adjacent
DC3	Anterior	Ventral	At ventricle	Small, bipolar (parvocellular)	Immediately adjacent to numerous	Immediately adjacent to restricted populations	High *rx3*	No	Bordering
DC4	Posterior	Dorsal	Well beyond ventricle	Large (magnocellular)	Close to numerous	Close to restricted populations	No *rx3*	Yes	Adjacent
TPp	Anterior most	Dorsal most	At and beyond ventricle	Small (parvocellular)	Immediately adjacent to numerous	Immediately adjacent to restricted populations	Low *rx3*	Yes	Adjacent
DC2^{A}	Anterior	Dorsal	Beyond ventricle	Large (magnocellular)	Immediately adjacent to numerous	Close to restricted populations	Low *rx3*	Yes	Adjacent
PVO	Anterior	Ventral	At ventricle	Small, bipolar (parvocellular)	Close to distinct isolated Nestin+ cells	Immediately adjacent to distinct "tramline" population	High *rx3*	No	Bordering
DC4^{A}	Posterior	Dorsal	Well beyond ventricle	Large (magnocellular)	Close to numerous	Close to restricted populations	No *rx3*	Yes	Adjacent

Table 4.1: Summary of morphology and position of PT DA neurons in relation to populations of neural stem/progenitor cells.

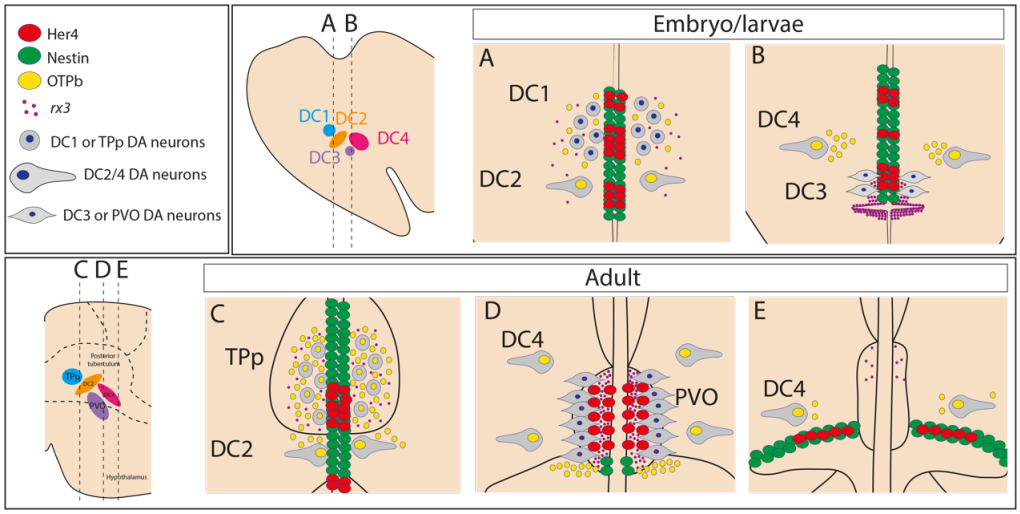

Fig. 4.9: Summary of position of DC1/TPp, DC2/DC2^{A} DC3/PVO and DC4/DC4^{A} DA neurons the adult rostral PT in relation to populations of neural stem/progenitor cells.

Schematics depicting expression domains in DA populations of the rostral PT at embryonic/larval (A,B) and adult (C-E) ages. Red circles: Her4^{+} cells, green circles: Nestin^{+} cells, yellow circles: OTPb^{+} cells, small purple circles: *rx3* mRNA expression, small round grey cells: DC1/TPp DA neurons, large pear shaped cells: DC2/DC2^{A} or DC4/DC4^{A} DA neurons, small bipolar cells: DC3/PVO DA neurons.

4.3: Discussion

The aim of this chapter was to seek evidence for the existence of neural stem/progenitor niches in this region. To achieve this, sections of the adult rostral PT, and sections of the corresponding embryonic/larval region, were analysed using labelling with markers of neural stem and progenitor cells.

First, my analyses of progenitor populations in the embryonic and adult PT using markers of radial glial cells (Nestin and Her4.1), showed that radial glial-like cell populations are present in the embryonic and the adult rostral PT. This data supports the presence of neural stem/progenitor cell populations in the adult rostral PT that retain expression of embryonic radial glial proteins including Nestin and Her4, both of which are pivotal for regulation of stem/progenitor self-renewal (Kageyama *et al.*, 2008; Chapouton *et al.*, 2010; Park *et al.*, 2010). My analyses show that in DC1/TPp, DC2/DC2^{A} and DC4/DC4^{A} populations, Her4 expression is less widespread than Nestin expression. One possibility is that Her4 and Nestin label different populations of stem/progenitor cells; a second possibility is that Her4-expressing cells are a subset of Nestin-expressing cells. This contrasts with the PVO, which is fundamentally different to the rest of the PT. In the PVO, Nestin expression is restricted to one or two cells, and Her4 is expressed in a double tramline appearance, where a proportion of cells are located at a distance from the ventricle and extend a short process towards it. This suggests that PVO DA neurons may derive from a distinct population of progenitor cells compared to DC1/TPp, DC2/DC2^{A} and DC4/DC4^{A} populations. Indeed, studies investigating proliferation in the zebrafish larval PT have shown a dorsal and ventral zone of proliferation, suggesting two distinct neural stem/progenitor niches exist in the PT (Mueller & Wullimann, 2002). Altogether, here my studies provide evidence for distinct neural stem/progenitor populations in the PT, that are established in early life and maintained to adulthood.

Next, I analysed progenitor populations in the adult and embryonic PT using markers involved in DA differentiation, namely *rx3* and OTPb. These studies provided further evidence that distinct progenitor populations are present in the embryonic and adult rostral PT. My analyses of *rx3* expression in the embryo agrees with previous studies (Muthu et al. 2016), that showed *rx3* expression in the anterior hypothalamus (specifically, in two zones, termed zones I and II). I extended these studies by analysing embryonic *rx3* expression with a focus on the PT, and also analysing *rx3* expression in the adult zebrafish PT to determine whether *rx3*-expressing progenitors are retained in adulthood. My data showed that in regions of the PT that are rostral to the anterior hypothalamus, *rx3* is detected at very low levels (DC1/TPp and DC2/DC2^{A}), and is not detected in regions dorsal to the anterior hypothalamus (DC4/DC4^{A}). In regions of the PT that overlap with the anterior hypothalamus (DC3 and the PVO), *rx3* is strongly detected. This adds weight to the idea that DC3 and PVO populations are related (Rink and Wullimann, 2002b; Chapter 3), as both embryonic and adult DA neurons reside in a region of *rx3* expression. Furthermore, as *rx3* expression is detected in the PVO, but little to no expression is observed in other PT populations, this supports my previous observations that the anterior-ventral region of the PT (containing DC3/PVO DA neurons) is fundamentally different to the rest of the PT. Since Rx3 is part of a mechanism that balances stem and progenitor cells in the hypothalamus, this strongly suggests that the anterior-ventral PT should be defined as part of the hypothalamus.

My analyses of OTPb expression agree with previous studies in the zebrafish embryo that show OTPb expression in DC2 and DC4 DA neurons, but not in DC1 or DC3 DA neurons. My analyses add to this data by investigating OTPb expression in sections, where previous studies have analysed wholemount zebrafish embryos (Ryu *et al.*, 2007; Fernandes *et al.*, 2013, Muthu et al., 2016). In addition, my studies extend previous work, by analysing OTPb expression in the adult PT. I show expression is retained in DC2^{A} and DC4^{A} DA neurons, is not expressed by PVO DA neurons, but intriguingly is expressed by TPp DA neurons. Firstly, this adds evidence that DC2 and DC2^{A}; DC3 and PVO; DC4 and DC4^{A} DA neurons are related (Rink and Wullimann, 2002b; Chapter 3), but importantly shows that TPp DA neurons are profoundly distinct to DC1 DA neurons. Previous studies have shown that in embryonic (2dpf) and larval (5dpf) zebrafish, DA neurons in the presumptive TPp and the ventral thalamus form a contiguous population (Rink and Wullimann, 2002b). Therefore, I propose

that DC1 DA neurons at 55hpf are predominately comprised of ventral thalamic DA neurons and TPp DA neurons arise from a different progenitor population, in later life, that express OTPb. Further studies are required to determine at what age OTPb^{+} TPp DA neurons first appear and whether OTPb is required for their specification/differentiation.

In summary, these analyses provide three core conclusions. First, the PT contains populations of neural stem/progenitor cells that can be dorso-ventrally divided into at least two discrete populations: ascending neurons in the dorsal PT, composed of TPp, DC2/DC2^{A} and DC4/DC4^{A} populations and local-projecting neurons in the ventral PT, composed of DC3/PVO DA neurons. Second, the DC3/PVO population is fundamentally different from the rest of the PT: it contains *rx3*-expressing progenitors, it resides at the border of/overlaps with the anterior hypothalamus and it contains a morphologically distinct population of Nestin^{+} and Her4^{+} radial glia. For these reasons, I have proposed that the PVO should be classed as a hypothalamic population, rather than a rostral PT population. Third, differences in OTPb expression show that TPp DA neurons are profoundly different to DC1 neurons. I have therefore proposed that the DC1 population is predominately formed of thalamic DA neurons at embryonic time points and that TPp DA neurons arise from a divergent progenitor population in later life.

Chapter 5

Dopaminergic neurons in the rostral PT are generated throughout life

5.1: Introduction

The analysis outlined in chapter 4 provides initial evidence for the presence of neural stem/progenitor cells in the PT (including the hypothalamic DC3/PVO population) that persist from the developing embryo to adulthood. Recent studies have shown that DA neurons of the caudal hypothalamus are generated in adulthood (McPherson *et al.*, 2016), however, as yet, no study has definitively answered the question of whether DA neurons are added to ascending dopaminergic populations throughout adult life (see introduction section 1.4.3). Therefore, I aimed to assess the generation of DA neurons in the rostral PT, by examining EdU incorporation. In this chapter, I describe experiments in which I analysed EdU labelling in combination with anti-Th1 immunohistochemistry, to detect newborn DA neurons. DA generation at 55hpf was examined, as DA neuron populations are well established at this stage. Further, adult zebrafish aged 3-, 6-, 12- and 22-months were examined, to investigate DA generation across the zebrafish lifespan. I also describe experiments in which I used a genetic conditional lineage tracing strategy to firmly determine the evidence of de novo DA adult neurogenesis.

5.2.1 The generation of dopaminergic neurons in the embryonic rostral PT

A previous study has characterised embryonic generation of DA neurons in the zebrafish, using sequential pulses of EdU to resolve when neurons of specific DA groups become postmitotic during embryogenesis (Mahler *et al.*, 2010). In this study, birthdating analysis (as defined by cells no longer incorporating EdU and expressing Th1) showed that DA neurons in the DC2 population differentiate first, becoming post-mitotic at 16hpf, followed by DC4 DA neurons at 24hpf and DC1 DA neurons at 30hpf. DC3 DA neurons however, continuously label with EdU throughout development, suggesting these neurons arise from proliferating precursor pools throughout embryogenesis (Mahler *et al.*, 2010).

My observations in Chapter 3 that DC1/TPp, DC3/PVO and DC4/DC4^{A} populations increase in size after 55hpf do not support the study by Mahler et al. To resolve this discrepancy I took 31hpf zebrafish embryos, pulsed them with EdU by injection into the yolk sac, chased to 55hpf (Fig. 5.1A,B), and analysed for Th1^{+}EdU^{+} neurons in sections through the rostral PT. In contrast to the Mahler et al. study, Th1^{+}EdU^{+} DA neurons were detected in all rostral PT populations: DC1 (Fig. 5.1C), DC2 (Fig. 5.1D), DC3 (Fig. 5.1E) and DC4 (Fig. 5.1F). To determine the level of DA neuron generation in each population of the rostral PT, the number of Th1^{+}EdU^{+} DA neurons in each population was quantified. This showed high levels of DA neuronal generation in the DC1 population (0.6±0.27 out of 2.4±0.16, 25%;) and the DC3 population (8.8±0.93 out of 15.7±1.13, 56%), lower levels in the DC2 population (0.7±0.34 out of 8.2±0.49, 8.5%) and lowest levels in the DC4 populations (0.2±0.13 out of 8.3±0.82, 2%) (Fig. 5.2). Together, these observations show that DA neurons in populations DC1-4 are still generated between 31 and 55hpf, demonstrating that DC1, DC2 and DC4 populations do not become post-mitotic as early as previously shown. This also shows that DC3 precursors are the most proliferative population at this time point.

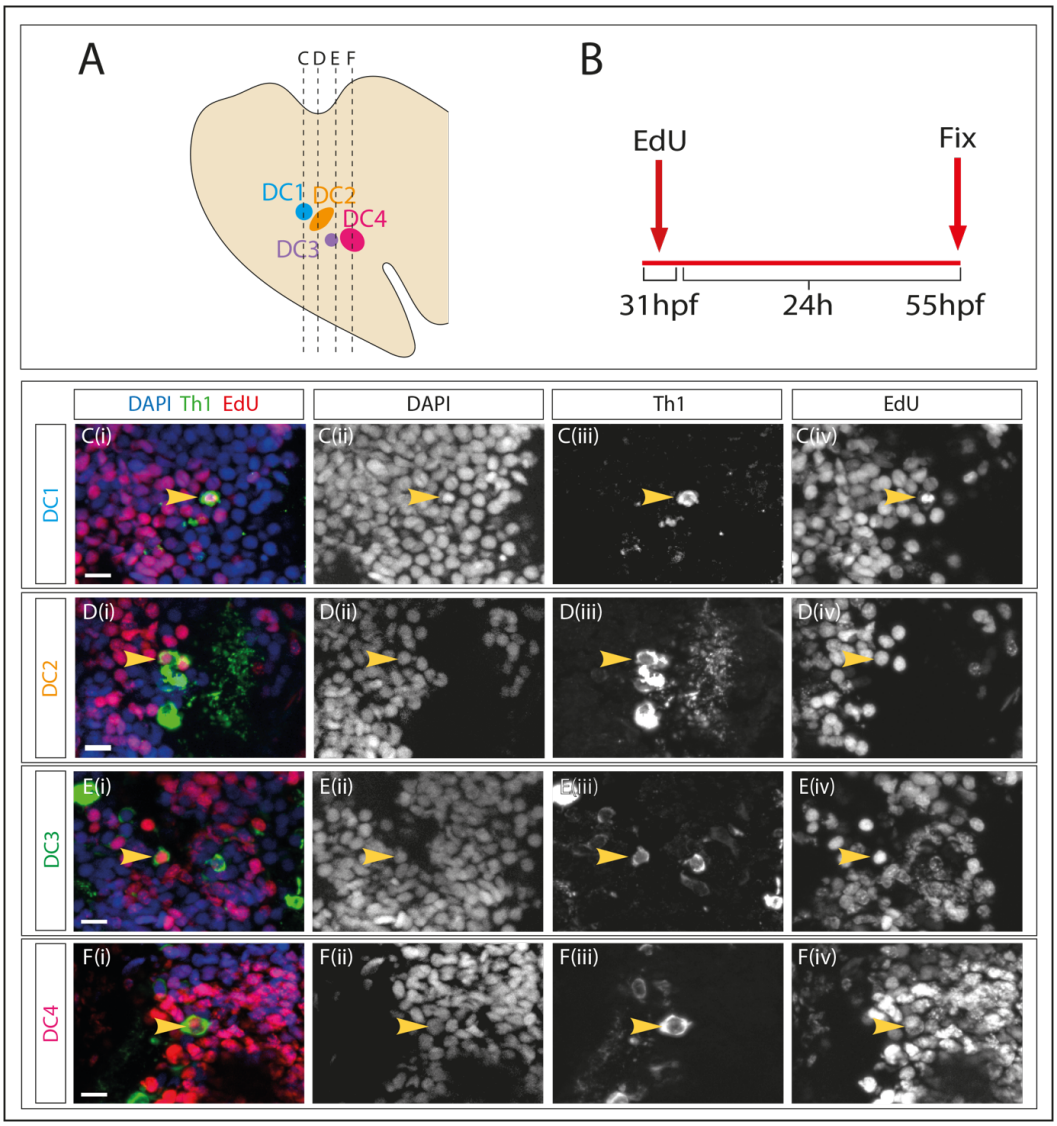
A
C D E F
DC1
DC2
DC4
DC3
B
EdU
Fix
31hpf
24h
55hpf
DAPI Th1 EdU
DAPI
Th1
EdU
DC1
DC2
DC3
DC4
C(i)
C(ii)
C(iii)
C(iv)
D(i)
D(ii)
D(iii)
D(iv)
E(i)
E(ii)
E(iii)
E(iv)
F(i)
F(ii)
F(iii)
F(iv)

Fig. 5.1: Dopaminergic populations in the rostral PT are added to between 31hpf and 55hpf.

A. Schematic showing subpopulations of DA neurons within the embryonic zebrafish rostral PT. Illustration adapted from Rink and Wullimann, 2002.

B. Schematic representing the EdU pulse-chase schedule. Zebrafish embryos were injected with 5nl of 5mM EdU in HBSS at 31hpf and chased to 55hpf where embryos were fixed and sectioned.

C(i-iv). Fluorescent MIP of a transverse section through the DC1 population of the 55hpf EdU injected embryo, labelled with DAPI (blue)(shown individually in (ii)), Th1 (green)(shown individually in (iii)), and EdU (red) (shown individually in (iv)). DC1 DA neurons are newly generated. Scale bar represents 10μm.

D(i-iv). Fluorescent MIP of a transverse section through the DC2 population of the 55hpf EdU injected embryo, labelled with DAPI (blue)(shown individually in (ii)), Th1 (green)(shown individually in (iii)), and EdU (red) (shown individually in (iv)). DC2 DA neurons are newly generated. Scale bar represents 10μm.

E(i-iv). Fluorescent MIP of a transverse section through the DC3 population of the 55hpf EdU injected embryo, labelled with DAPI (blue)(shown individually in (ii)), Th1 (green)(shown individually in (iii)), and EdU (red) (shown individually in (iv)). DC3 DA neurons are newly generated. Scale bar represents 10μm.

F(i-iv). Fluorescent MIP of a transverse section through the DC4 population of the 55hpf EdU injected embryo, labelled with DAPI (blue)(shown individually in (ii)), Th1 (green)(shown individually in (iii)), and EdU (red) (shown individually in (iv)). DC4 DA neurons are newly generated. Scale bar represents 10μm.

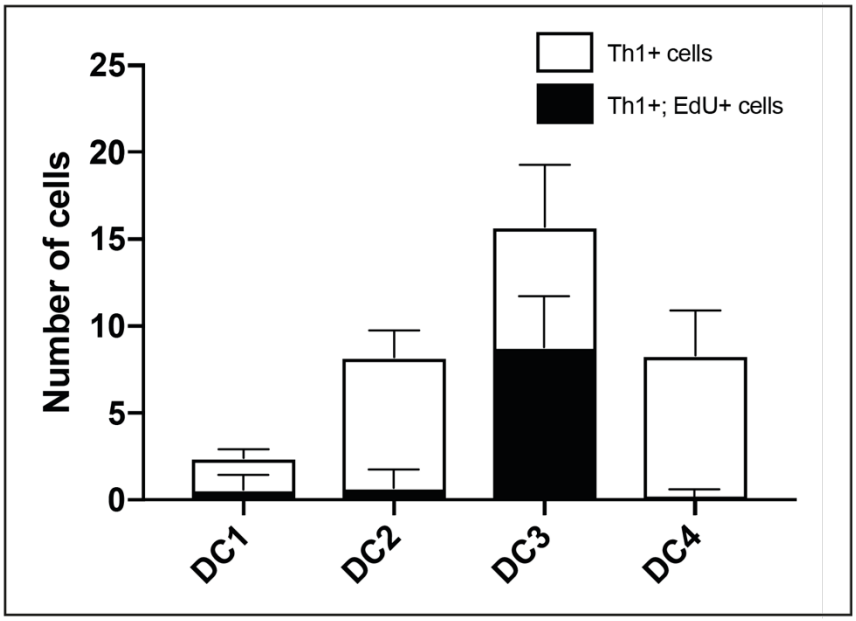

Fig. 5.2: Highest level of generation in DC3 DA neurons.

Bar graphs show the mean number of $EdU^{+}Th1^{+}$ cells and $EdU^{-}Th1^{+}$ cells in each population of the rostral PT (n=10 for each population).

5.2.2 EdU pulse-chase studies provide evidence for the generation of DA neurons in the adult rostral PT

I next sought to determine whether DA neurons of the PT are generated throughout adulthood. To do this, I used Click-iT EdU, in combination with anti-Th1 immunohistochemistry, to detect newborn DA neurons in consecutive sections through the adult rostral PT. Zebrafish at 3-, 6-, 12- and 22-months of age were analysed, to gain a representative view across the lifespan. Zebrafish were injected intraperitoneally (Fig. 5.3A) with EdU once daily for 3 days, and subsequently culled 5-days post injection (Fig. 5.3B). I reasoned that a once-daily EdU injection regime would ensure labelling of infrequently proliferating stem/progenitor cells, and that a 5-day chase period would allow differentiation of cycling progenitors to DA neurons.

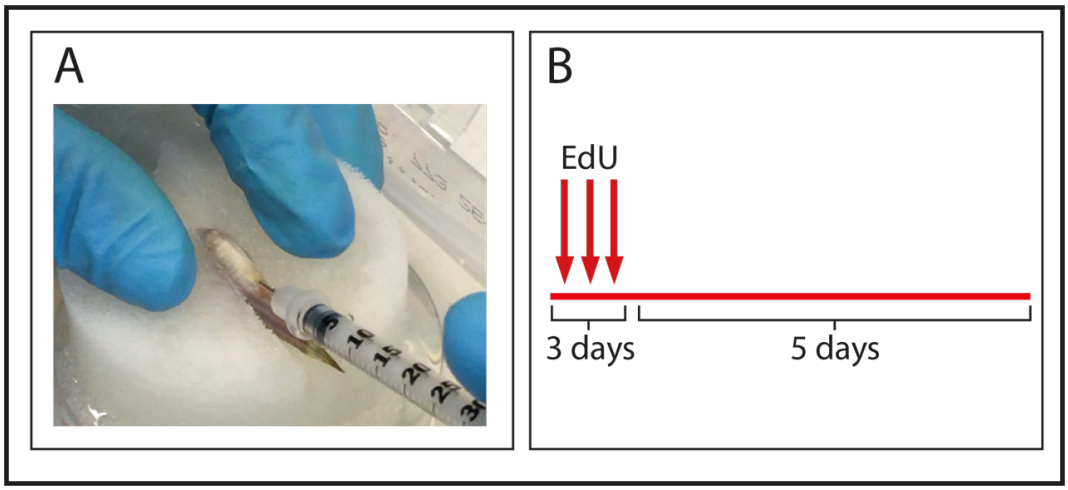

Fig. 5.3: Injection of EdU in adult zebrafish.

A. Photograph showing intraperitoneal injection of EdU into an adult anaesthetised zebrafish. Zebrafish at 3-, 6-, 12- and 22-months old were injected with 5µl of 10mM EdU.
B. Schematic showing EdU pulse-chase schedule. EdU was injected once daily for 3 days, zebrafish were replaced in tanks for 5 days and sacrificed on the 5th day.

In the 3-month old zebrafish, Th1^{+} neurons that were also EdU^{+} could be detected in the TPp (Fig.5.4A,A') and in the PVO (Fig.5.4C,C') (yellow arrowheads). Neither DC2^{A} (Fig.5.4B,B'), nor DC4^{A} (Fig.5.4D,D') DA neurons were ever found to be Th1^{+}EdU^{+}. Similarly, at 6-months of age, Th1^{+} EdU^{+} DA neurons were detected in the TPp (Fig.5.5A,A') and in the PVO (Fig.5.5C,C'), whereas no Th1^{+} DC2^{A} (Fig.5.5B,B') or DC4^{A} (Fig.5.5D,D') DA neurons were EdU^{+}. At 12-months of age, once more the TPp (Fig.5.6A,A') and PVO (Fig.5.6C,C') contained Th1^{+} EdU^{+} DA neurons, with no DC2^{A} (Fig.5.6B,B') or DC4^{A} (Fig.5.6D,D') Th1^{+} DA neurons colabelled with EdU. At 22-months of age however, no Th1^{+} EdU^{+} neurons could be detected in the TPp (Fig. 5.7A,A'), DC2^{A} (Fig.5.7B,B'), PVO (Fig.5.7C,C') or DC4^{A} (Fig.5.7D,D') populations. Together this data shows that DA neurons in the TPp and the PVO are generated in adult life, whereas large magnocellular DC2^{A} and DC4^{A} neurons are not. The lack of EdU incorporation in DA neurons of any population in the rostral PT at 22-months of age suggests an age-related decline in DA neurogenesis.

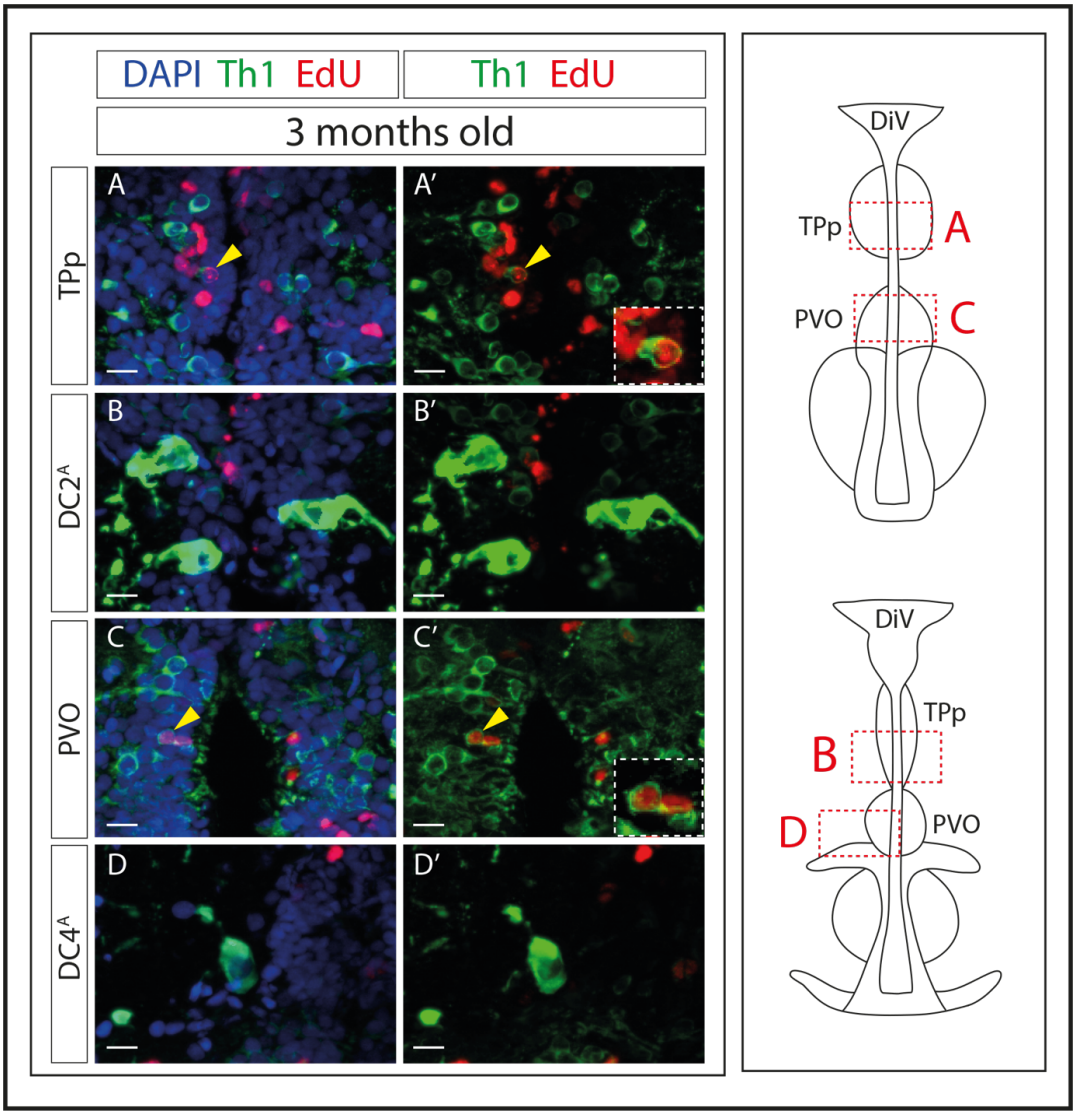
DAPI Th1 EdU
Th1 EdU
3 months old
TPp
DC2A
PVO
DC4A
A
A′
B
B′
C
C′
D
D′
DiV
TPp
A
PVO
C
DiV
TPp
B
D
PVO

Fig. 5.4: DA neurons are generated in the TPp and the PVO of 3-month old zebrafish.

A,A'. Fluorescent MIP of a transverse section through the TPp of the 3-month EdU injected zebrafish, labelled with DAPI (blue), Th1 (green) and EdU (red), shown without DAPI in A'. TPp DA neurons are newly generated. Scale bar represents 10μm. Position of image in relation to DiV is shown in schematic.

B,B'. Fluorescent MIP of a transverse section through the DC2 population of the 3-month EdU injected zebrafish, labelled with DAPI (blue), Th1 (green) and EdU (red), shown without DAPI in B'. DC2 DA neurons are not newly generated. Scale bar represents 10μm. Position of image in relation to DiV is shown in schematic.

C,C'. Fluorescent MIP of a transverse section through the PVO of the 3-month EdU injected zebrafish, labelled with DAPI (blue), Th1 (green) and EdU (red), shown without DAPI in C'. PVO DA neurons are newly generated. Scale bar represents 10μm. Position of image in relation to DiV is shown in schematic.

D,D'. Fluorescent MIP of a transverse section through the DC4 population of the 3-month EdU injected zebrafish, labelled with DAPI (blue), Th1 (green) and EdU (red), shown without DAPI in D'. DC4 DA neurons are not newly generated. Scale bar represents 10μm. Position of image in relation to DiV is shown in schematic.

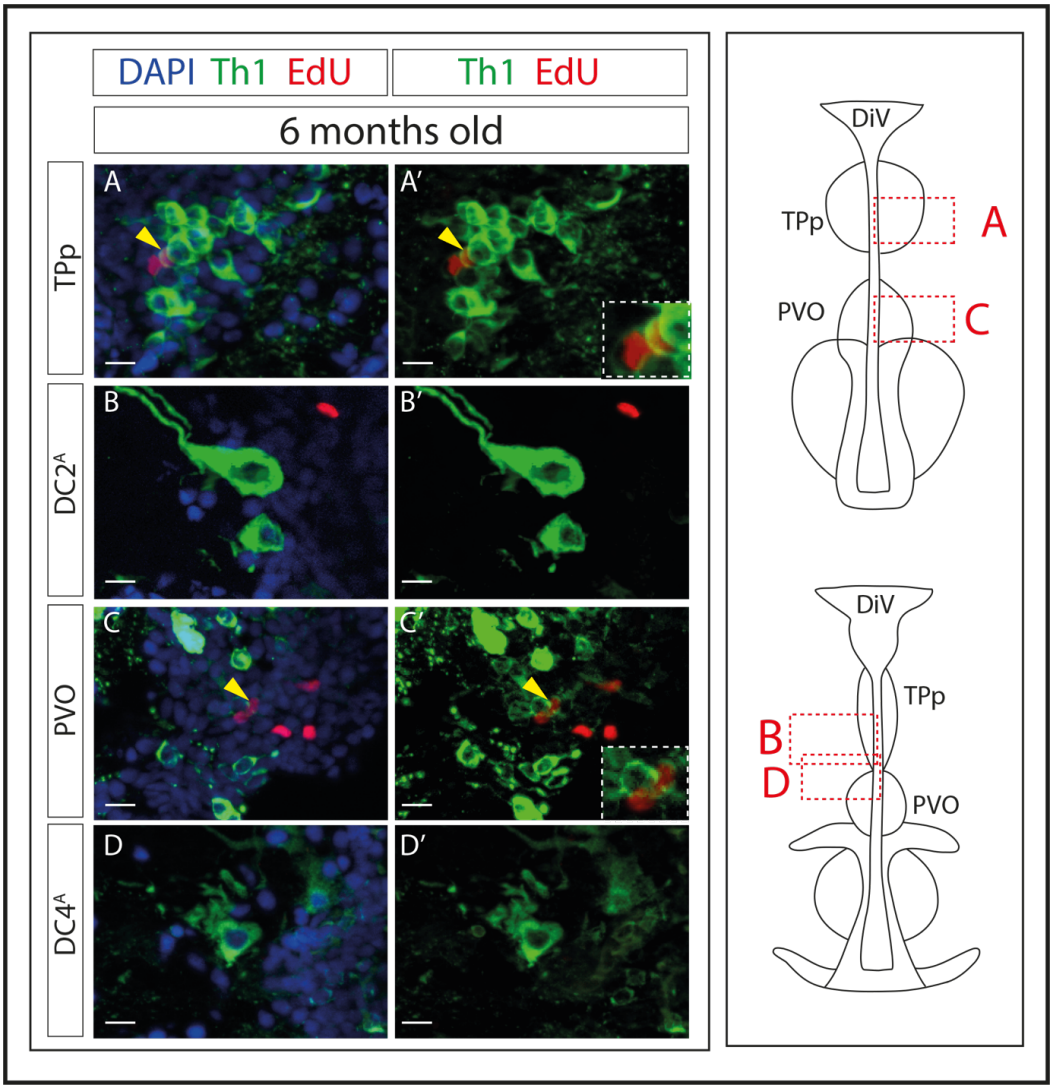
DAPI Th1 EdU
Th1 EdU
6 months old
TPp
DC2A
PVO
DC4A
A
A′
B
B′
C
C′
D
D′
DiV
TPp
A
PVO
C
DiV
TPp
B
D
PVO

Fig. 5.5: DA neurons are generated in the TPp and the PVO of 6-month old zebrafish.

A,A'. Fluorescent MIP of a transverse section through the TPp of the 6-month EdU injected zebrafish, labelled with DAPI (blue), Th1 (green) and EdU (red), shown without DAPI in A'. TPp DA neurons are newly generated. Scale bar represents 10μm. Position of image in relation to DiV is shown in schematic.

B,B'. Fluorescent MIP of a transverse section through the DC2 population of the 6-month EdU injected zebrafish, labelled with DAPI (blue), Th1 (green) and EdU (red), shown without DAPI in B'. DC2 DA neurons are not newly generated. Scale bar represents 10μm. Position of image in relation to DiV is shown in schematic.

C,C'. Fluorescent MIP of a transverse section through the PVO of the 6-month EdU injected zebrafish, labelled with DAPI (blue), Th1 (green) and EdU (red), shown without DAPI in C'. PVO DA neurons are newly generated. Scale bar represents 10μm. Position of image in relation to DiV is shown in schematic.

D,D'. Fluorescent MIP of a transverse section through the DC4 population of the 6-month EdU injected zebrafish, labelled with DAPI (blue), Th1 (green) and EdU (red), shown without DAPI in D'. DC4 DA neurons are not newly generated. Scale bar represents 10μm. Position of image in relation to DiV is shown in schematic.

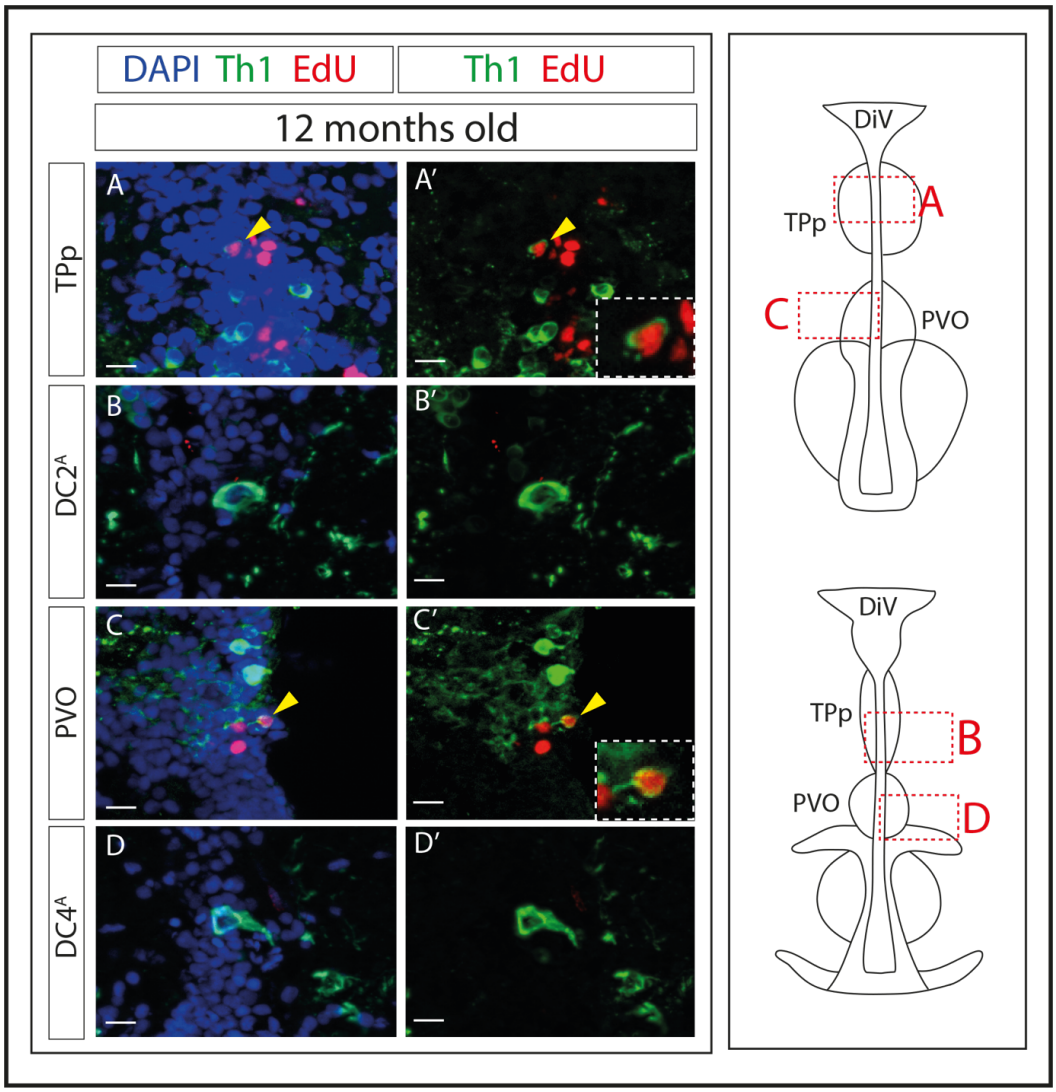
DAPI Th1 EdU
Th1 EdU
12 months old
TPp
DC2A
PVO
DC4A
A
A′
B
B′
C
C′
D
D′
DiV
TPp
A
C
PVO
DiV
TPp
B
PVO
D

Fig. 5.6: DA neurons are generated in the TPp and the PVO of 12-month old zebrafish.

A,A'. Fluorescent MIP of a transverse section through the TPp of the 12-month EdU injected zebrafish, labelled with DAPI (blue), Th1 (green) and EdU (red), shown without DAPI in A'. TPp DA neurons are newly generated. Scale bar represents 10μm. Position of image in relation to DiV is shown in schematic.

B,B'. Fluorescent MIP of a transverse section through the DC2 population of the 12-month EdU injected zebrafish, labelled with DAPI (blue), Th1 (green) and EdU (red), shown without DAPI in B'. DC2 DA neurons are not newly generated. Scale bar represents 10μm. Position of image in relation to DiV is shown in schematic.

C,C'. Fluorescent MIP of a transverse section through the PVO of the 12-month EdU injected zebrafish, labelled with DAPI (blue), Th1 (green) and EdU (red), shown without DAPI in C'. PVO DA neurons are newly generated. Scale bar represents 10μm. Position of image in relation to DiV is shown in schematic.

D,D'. Fluorescent MIP of a transverse section through the DC4 population of the 12-month EdU injected zebrafish, labelled with DAPI (blue), Th1 (green) and EdU (red), shown without DAPI in D'. DC4 DA neurons are not newly generated. Scale bar represents 10μm. Position of image in relation to DiV is shown in schematic.

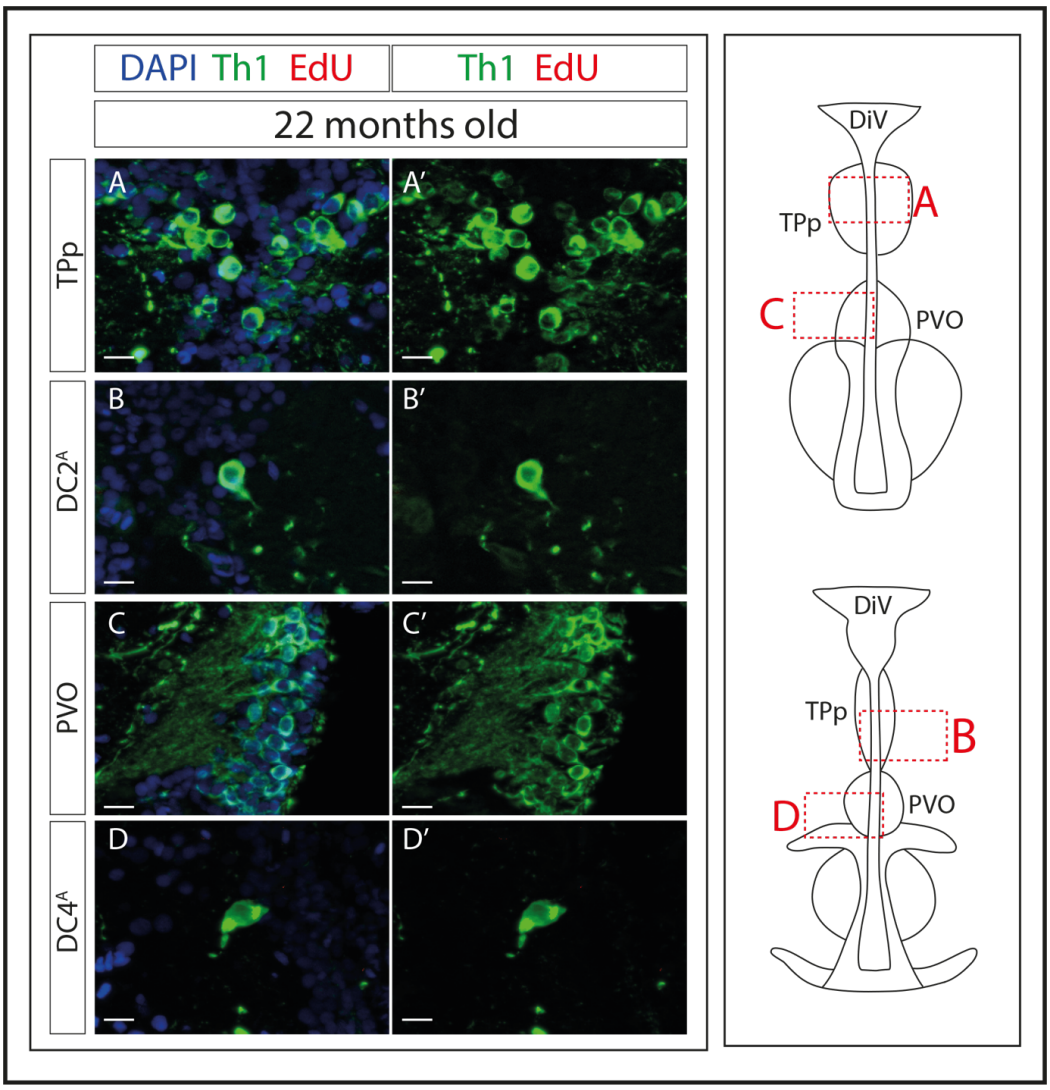
DAPI Th1 EdU
Th1 EdU
22 months old
TPp
DC2A
PVO
DC4A
A
A′
B
B′
C
C′
D
D′
DiV
TPp
A
C
PVO
DiV
TPp
B
D
PVO

Fig. 5.7: DA neurons are not generated in the TPp and the PVO of 22-month old zebrafish.

A,A'. Fluorescent MIP of a transverse section through the TPp of the 22-month EdU injected zebrafish, labelled with DAPI (blue), Th1 (green) and EdU (red), shown without DAPI in A'. TPp DA neurons are not newly generated. Scale bar represents 10μm. Position of image in relation to DiV is shown in schematic.

B,B'. Fluorescent MIP of a transverse section through the DC2 population of the 22-month EdU injected zebrafish, labelled with DAPI (blue), Th1 (green) and EdU (red), shown without DAPI in B'. DC2 DA neurons are not newly generated. Scale bar represents 10μm. Position of image in relation to DiV is shown in schematic.

C,C'. Fluorescent MIP of a transverse section through the PVO of the 22-month EdU injected zebrafish, labelled with DAPI (blue), Th1 (green) and EdU (red), shown without DAPI in C'. PVO DA neurons are not newly generated. Scale bar represents 10μm. Position of image in relation to DiV is shown in schematic.

D,D'. Fluorescent MIP of a transverse section through the DC4 population of the 22-month EdU injected zebrafish, labelled with DAPI (blue), Th1 (green) and EdU (red), shown without DAPI in D'. DC4 DA neurons are not newly generated. Scale bar represents 10μm. Position of image in relation to DiV is shown in schematic.

The lack of de novo neurogenesis of DA neurons in the 22-month zebrafish suggests that the rate of DA generation in the TPp and the PVO declines with age. To investigate this, I quantified $Th1^{+}$ EdU^{+} DA neurons in the TPp (Fig.5.8A) and the PVO (Fig. 5.8B) at 3-, 12- and 22-months of age. This revealed that in the TPp, the number of newly generated DA neurons significantly decreases between 3-months (3±0.37) and 12-months of age (1±0.58) and between 3-months (3±0.37) and 22-months of age (0±0), but does not significantly further decrease between 12-months (1±0.58) and 22-months of age (0±0) (Fig.5.8A). In the PVO, the number of newly generated DA neurons significantly decreases between 3-months (9±0.94) and 12-months of age (2±0.33) and between 3-months (9±0.94) and 22-months of age (0±0), but does not significantly further decrease between 12-months (2±0.33) and 22-months of age (0±0) (Fig.5.8B). This shows that between 3-months of age and 12-months of age, the rate of DA generation significantly declines in both the TPp and the PVO.

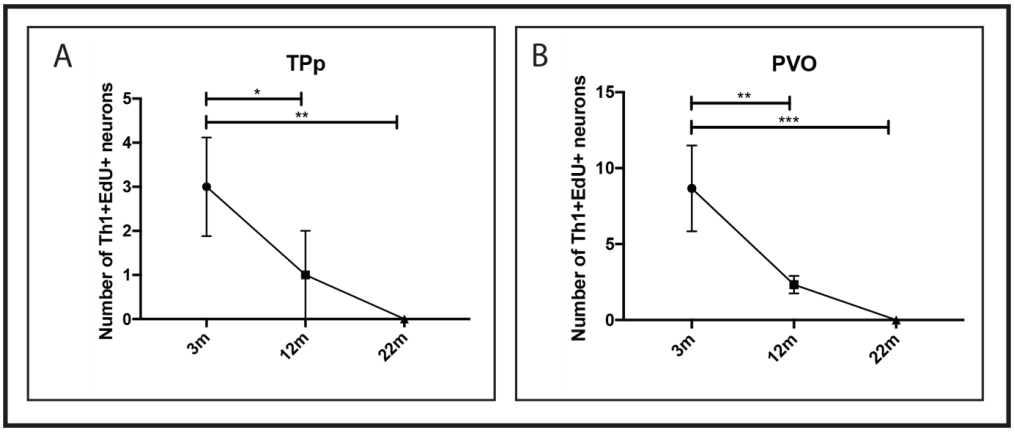

Fig. 5.8: The rate of DA generation declines with age.

A. Mean number of Th1+EdU+ DA neurons in the TPp at 3-, 12- and 22-months of age. The number of newly generated DA neurons is significantly decreased 12-month old zebrafish compared to 3-month old zebrafish (p=0.0277, *, 1-way ANOVA, n=9 for 3-month brains, n=3 for 12-month brains), and in 22-month old zebrafish compared to 3-month old zebrafish (p=0.0019, **, 1-way ANOVA, n=9 for 3-month brains, n=3 for 22-month brains). Error bars represent standard deviation.
B. Mean number of Th1+EdU+ DA neurons in the PVO at 3-, 12- and 22-months of age. The number of newly generated DA neurons is significantly decreased 12-month old zebrafish compared to 3-month old zebrafish (p=0.0039, **, 1-way ANOVA, n=9 for 3-month brains, n=3 for 12-month brains), and in 22-month old zebrafish compared to 3-month old zebrafish (p=<0.001, ***, 1-way ANOVA, n=9 for 3-month brains, n=3 for 22-month brains). Error bars represent standard deviation.

In chapter 3, I showed that there was no significant difference in the total number of DA neurons in rostral PT populations between male and female zebrafish. Previous studies have shown a sexually dimorphic pattern of neurogenesis in the telencephalon in male and female zebrafish (Ampatzis *et al.*, 2012), however it remains unknown whether the generation of DA neurons in the diencephalon is sexually dimorphic. Therefore, I asked whether male and female zebrafish show differences in generation of DA neurons in the adult rostral PT. To do so I quantified $Th1^{+}EdU^{+}$ DA neurons in the TPp and the PVO in male and female 3-month old zebrafish. Quantification showed no significant difference in the number of newly generated DA neurons between the male TPp (3±0.48) and the female TPp (3±0.71) or between the male PVO (8±1.29) and the female PVO (10±1.47). This shows that there are no differences in the level of generation of DA PT neurons between male and female zebrafish.

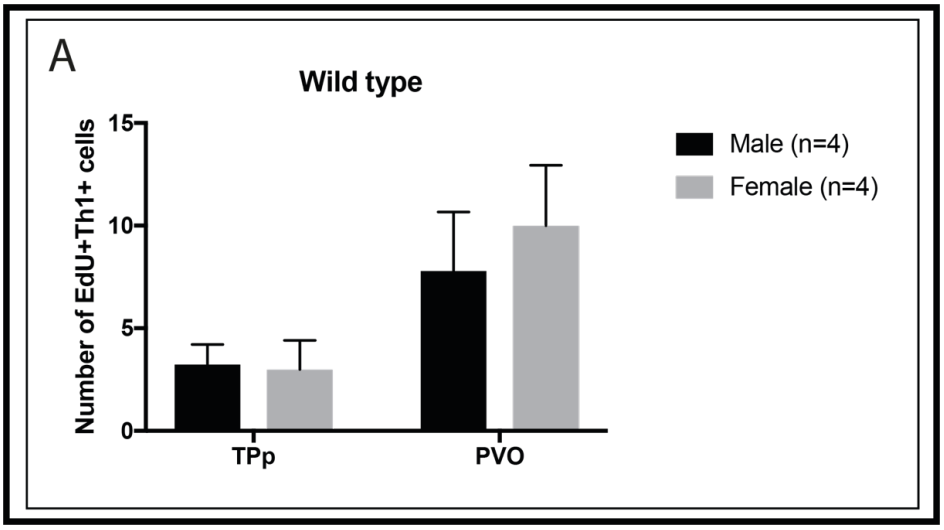

Fig. 5.9: No significant difference in the number of newly generated DA neurons in the TPp or the PVO.

The mean number of Th1+EdU+ cells in the TPp and the PVO are quantified in 15μm sections of 3-month old male and female zebrafish. No significant difference between the number of DA neurons in either subpopulation in male and female zebrafish (error bars represent standard deviation, n=4 males, n=4 females, statistically analysed by unpaired t-test).

5.2.3 De novo DA neurogenesis in the adult rostral PT from Her4^{+} progenitor cells

EdU pulse-chase analysis provides a useful tool for studying cell proliferation, but suffers from the criticism that cells that are undergoing DNA repair, or programmed cell death may incorporate nucleotide analogues (Rakic, 2002; El-Khodor *et al.*, 2003) – i.e. that EdU-labelling does not necessarily mean a cell is new-born. Therefore, to confirm that DA neurons are newly-generated from stem/progenitor cells, I used a conditional lineage tracing strategy to label progenitors and their progeny in the adult PT. Since Her4 is widely expressed by radial-glial like cells lining the ventricle of the adult rostral PT (see Chapter 4 section 4.2.1), I hypothesized that DA neurons adjacent to populations of Her4+ progenitors may arise from these cell populations. A zebrafish line allowing conditional lineage tracing of Her4^{+} progenitors has been previously described. In this line, tamoxifen-inducible Cre recombinase is driven by the *her4* promoter (*Tg*(*her4:ERT2CreERT2))*(Boniface *et al.*, 2009; Dirian *et al.*, 2014). This Her4 line was crossed to an ubiquitous reporter line – *ubi:switch* (*Tg(−3,5ubi:loxP-GFP-loxP-mCherry)*)(Mosimann *et al.*, 2011): in the absence of Cre, the ubiquitous reporter line expresses GFP under control of ubiquitin, and permanently switches to express mCherry after a recombination event. This allows conditional labelling of Her4^{+} progenitors and their progeny (Fig.5.10A, 5.11A). Since EdU studies showed the highest level of DA neuron generation in 3-month old zebrafish, I used 3-month old zebrafish for conditional lineage tracing, to give the best chance of detecting labelled newborn DA neurons.

Tamoxifen, diluted in sunflower oil, or a vehicle control (oil only) were injected once intraperitoneally into 3-month old *Tg(her4:ERT2CreERT2); Tg(−3,5ubi:loxP-GFP-loxP-mCherry)* zebrafish, followed by a 32-day chase period to allow differentiation (Fig. 5.10B, 5.11B). Zebrafish brains were sectioned and anti-mCherry immunohistochemistry in combination with anti-Th1 immunohistochemistry was performed on consecutive sections to allow detection of recombined cells. In the vehicle control injected zebrafish, no expression of mCherry was observed, showing that there were no recombination events in zebrafish that were not treated with tamoxifen (Fig.5.10C,D). When recombination was induced by injection of tamoxifen, mCherry^{+}Th1^{+} DA neurons were observed in both the TPp and in the PVO (Fig.5.11C,D, yellow arrows), showing that these DA neurons were newly generated and derived from Her4^{+} progenitors. This data definitively demonstrates that DA neurons in the TPp and the PVO are generated from Her4^{+} stem/progenitor cells in the adult brain.

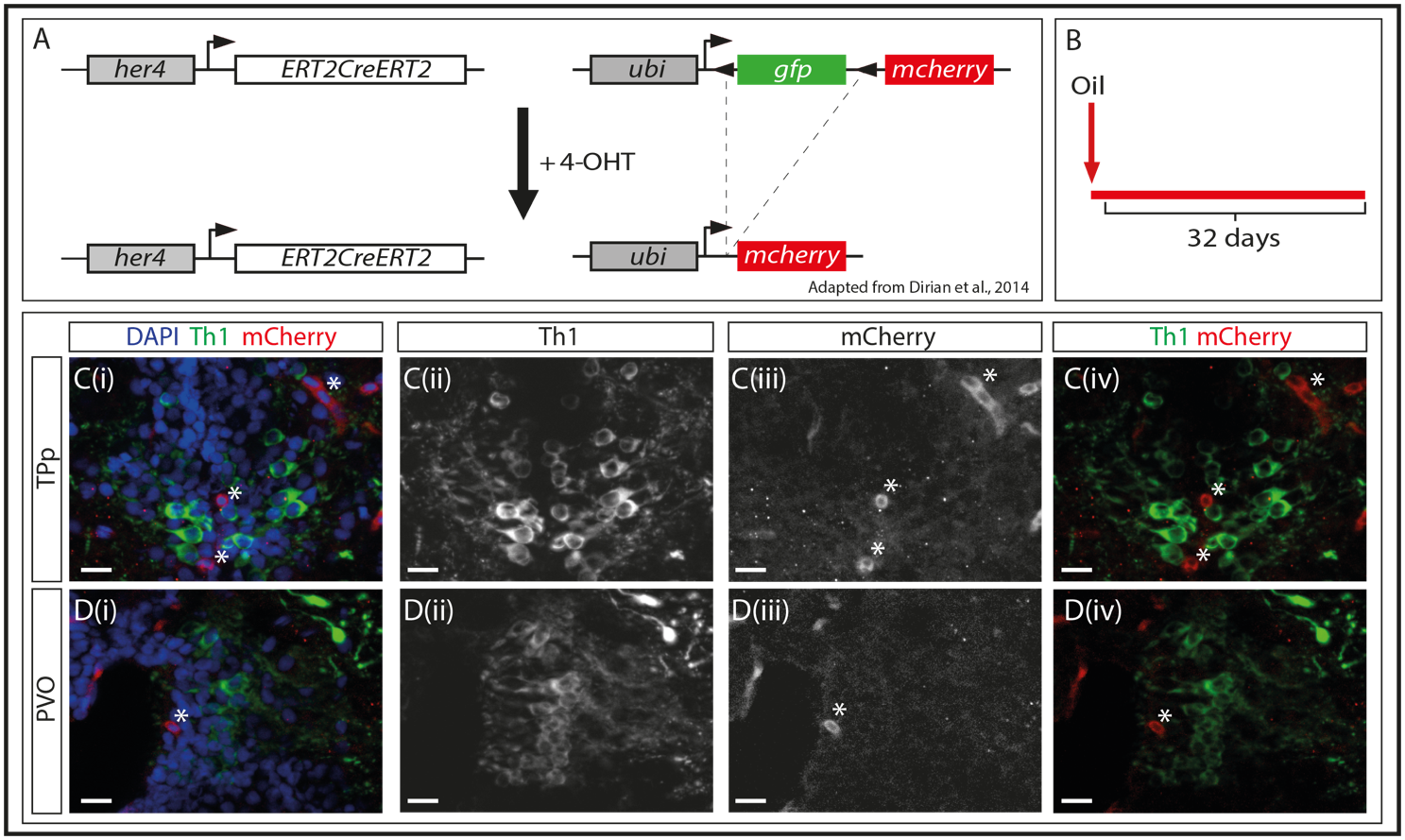
A
her4
ERT2CreERT2
ubi
gfp
mcherry
+4-OHT
her4
ERT2CreERT2
ubi
mcherry
Adapted from Dirian et al., 2014
B
Oil
32 days
DAPI Th1 mCherry
Th1
mCherry
Th1 mCherry
TPp
PVO
C(i)
C(ii)
C(iii)
C(iv)
D(i)
D(ii)
D(iii)
D(iv)

Fig. 5.10: No recombination in vehicle only injected *Tg(her4:ERT2CreERT2); Tg(−3,5ubi:loxP-GFP-loxP-mCherry)* zebrafish

A. Schematic illustrating cross of zebrafish lines: *Tg(her4:ERT2CreERT2)* conditional lineage tracing line was crossed to the ubiquitous reporter line *Tg(−3,5ubi:loxP-GFP-loxP-mCherry)*. Upon addition of tamoxifen (4-OHT, black arrow), *gfp* is excised and cells expressing *her4* will express *mcherry*.

B. Schematic illustrating the injection schedule: in control zebrafish, 5μl of oil with no tamoxifen added was injected intraperitoneally, zebrafish were then chased for 32-days.

C(i-iv). Fluorescent MIP of a transverse section through the TPp of an oil injected 3-month old zebrafish, labelled with DAPI (blue), Th1 (green) and mCherry (red). Th1 is shown as a single channel in (ii), mCherry is shown in (iii). Th1 (green) and mCherry (red) are shown together in (iv). Asterisks label blood vessel non-specific staining. Scale bars represent 10 μm. No recombination in the TPp of oil injected zebrafish.

D(i-iv). Fluorescent MIP of a transverse section through the PVO of an oil injected 3-month old zebrafish, labelled with DAPI (blue), Th1 (green) and mCherry (red). Th1 is shown as a single channel in (ii), mCherry is shown in (iii). Th1 (green) and mCherry (red) are shown together in (iv). Asterisks label blood vessel non-specific staining. Scale bars represent 10 μm. No recombination in the PVO of oil injected zebrafish.

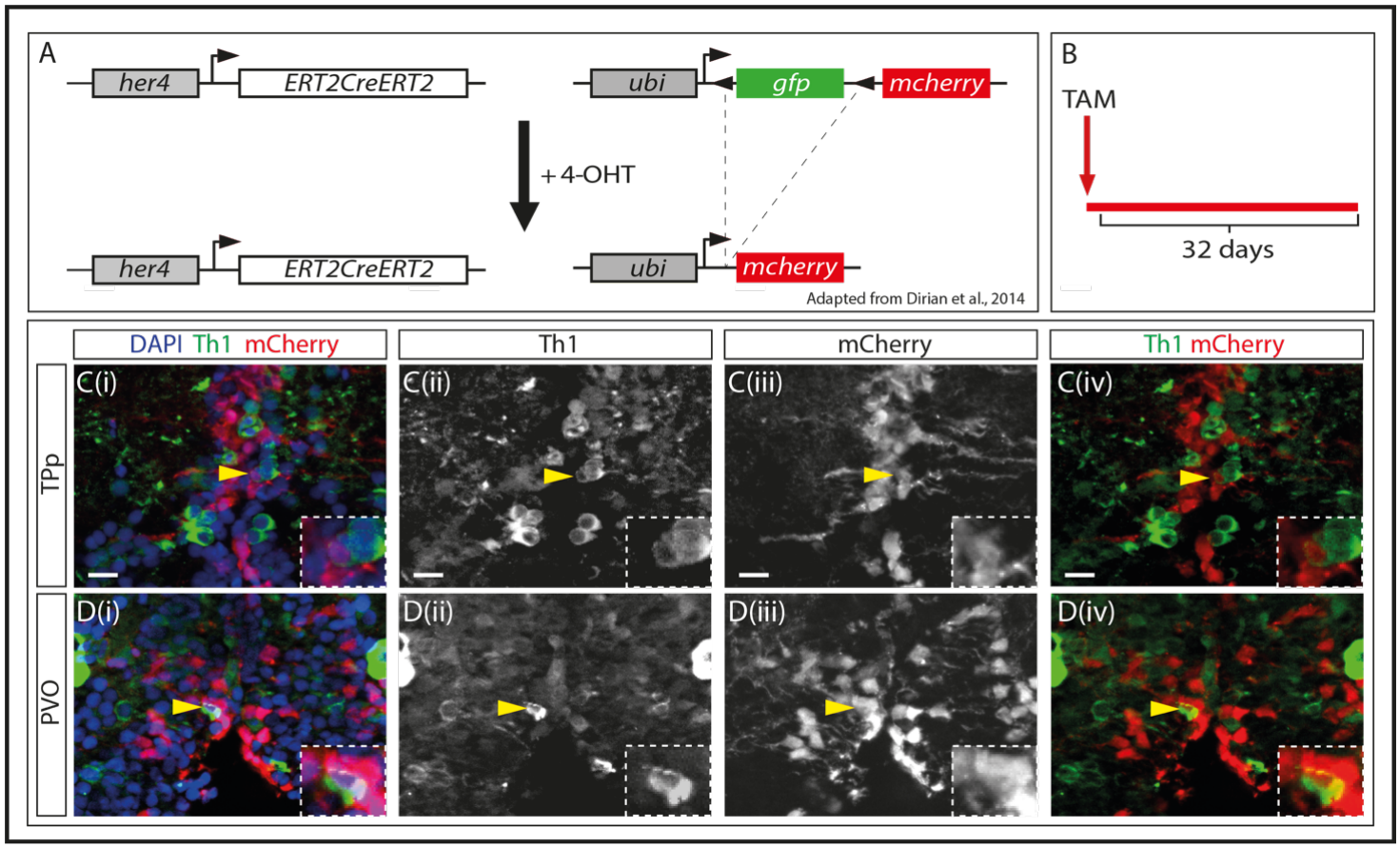
A
her4
ERT2CreERT2
ubi
gfp
mcherry
+4-OHT
her4
ERT2CreERT2
ubi
mcherry
Adapted from Dirian et al., 2014
B
TAM
32 days
DAPI Th1 mCherry
Th1
mCherry
Th1 mCherry
TPp
PVO
C(i)
C(ii)
C(iii)
C(iv)
D(i)
D(ii)
D(iii)
D(iv)

Fig. 5.11: mCherry labels DA neurons in the TPp and the PVO in tamoxifen injected *Tg(her4:ERT2CreERT2); Tg(−3,5ubi:loxP-GFP-loxP-mCherry)* zebrafish

A. Schematic illustrating cross of zebrafish lines: *Tg(her4:ERT2CreERT2)* conditional lineage tracing line was crossed to the ubiquitous reporter line *Tg(−3,5ubi:loxP-GFP-loxP-mCherry)*. Upon addition of tamoxifen (4-OHT, black arrow), *gfp* is excised and cells expressing *her4* will express *mcherry*.

B. Schematic illustrating the injection schedule: 5µl of oil with 10mM tamoxifen was injected intraperitoneally, zebrafish were then chased for 32-days.

C(i-iv). Fluorescent MIP of a transverse section through the TPp of a tamoxifen injected 3-month old zebrafish, labelled with DAPI (blue), Th1 (green) and mCherry (red). Th1 is shown as a single channel in (ii), mCherry is shown in (iii). Th1 (green) and mCherry (red) are shown together in (iv). Scale bars represent 10 μm. mCherry+Th1+ cells are observed in the TPp (yellow arrows).

D(i-iv). Fluorescent MIP of a transverse section through the PVO of an oil injected 3-month old zebrafish, labelled with DAPI (blue), Th1 (green) and mCherry (red). Th1 is shown as a single channel in (ii), mCherry is shown in (iii). Th1 (green) and mCherry (red) are shown together in (iv). Scale bars represent 10 μm. mCherry+Th1+ cells are observed in the PVO (yellow arrows).

5.3 Discussion

The aim of this chapter was to determine whether DA neurons in the rostral PT are generated throughout life in the zebrafish. To achieve this, EdU labelling in combination with anti-Th1 immunohistochemistry, was used to detect newborn DA neurons in the embryo and at various stages throughout adult life. Then, a genetic conditional lineage tracing line was used to confirm de novo DA adult neurogenesis in the adult zebrafish PT.

First, my analyses of DA neuron generation in the embryo using EdU pulse chase analysis revealed that DA neurons in populations DC1-4 are still generated between 31 and 55hpf. This data disagrees with previous studies that show that DC1, DC2 and DC4 have become post-mitotic by 16-18hpf, 24-30hpf and 20-24hpf respectively (Mahler *et al.*, 2010). The discrepancies between my data and the studies performed by Mahler et al. are most likely due to different technical approaches. In my analyses, I injected EdU directly into the yolk sac, and analysed DA populations in consecutive sections. Mahler et al. soaked embryos in EdU for 30 minutes, and analysed DA populations in wholemount tissue. It is possible that EdU soaking is not sufficient to label all proliferating populations, whereas injecting EdU directly into the yolk sac allows continued uptake into proliferating cells, allowing more chance of labelling slowly-proliferating progenitors. Furthermore, it is also possible that double-labelled cells may be not be detected when imaging wholemount embryos.

My analyses in chapter 3 shows a huge expansion in the DC1/TPp population and the DC3/PVO population between 55hpf and 3-months. My embryonic EdU analyses showing DC1 and DC3 DA neurons are still being generated at 55hpf, support these observations from chapter 3. My data shows that DC3 DA neurons are generated at the highest rate between 31 and 55hpf. This suggests that the DC3 population begins to expand in size early in development. In chapter 4, I showed that DC1 (embryonic) DA neurons and TPp (adult) DA neurons are fundamentally different: adult TPp DA neurons express OTPb, and embryonic DC1 DA neurons do not. Therefore, in contrast to DC3, I predict that the TPp undergoes a huge expansion in neuron number after 55hpf, i.e. late in development.

Since I observed no change in the population size of DC2/DC2^{A} neurons (chapter 3), but I observed EdU-labelled DC2 DA neurons at 55hpf, it is likely that the DA neurons added between 31 and 55hpf are the last-generated of the population. From these analyses, however, it remains possible however that these neurons are continuously turned over, rather than added to, and so maintain a constant population size. My observations in chapter 3 showed that the DC4/DC4^{A} DA neuron populations increases in size between 55hpf and 3-months, though to a lesser extent than the TPp and PVO populations, suggesting restricted addition at embryonic/larval and/or juvenile periods. Here, my observation of EdU-labelled DC4 DA neurons at embryonic time points supports this data.

Next, my analyses of the generation of DA neurons in the adult rostral PT using EdU labelling showed for the first time that two DA neuron populations are added to in adulthood. One of these populations, the TPp, contains ascending DA neurons. The other, the PVO, is hypothalamic in nature (chapter 4). Together, this data shows that both the TPp and the PVO are still expanding in size at 3-, 6- and 12-months, but by 22-months show little to no DA neuron generation.

Here, my analyses also show that the large magnocellular ascending DA neurons in DC2^{A} and DC4^{A} populations do not label with EdU in adulthood. This suggests that these magnocellular populations are born early and show little to no generation in adult life. It is therefore most likely that the populations observed in the adult zebrafish, in particular DC2^{A} DA neurons, are the same as those observed in the embryonic/larval zebrafish. It is possible that magnocellular DC2^{A} and DC4^{A} neurons are related to other magnocellular primary neurons, such as Mauthner cells providing motion and depth information, as well as startle response. Future work should characterise similarities in morphology and function between magnocellular neurons in zebrafish.

My observation that no DA neurons are newly generated in 22-month old zebrafish prompted me to quantify the number of newly generated DA neurons in the TPp and the PVO in young adult, adult and aged adult life stages, to determine whether the rate of DA neurogenesis decreases with age. Here, I show for the first time that the rate of DA generation in zebrafish does indeed decline with age. This agrees with previous studies

that show declining rates of neurogenesis in mammals (see introduction section 1.4.4) and in the zebrafish telencephalon (see introduction section 1.4.5). This shows that ageing is a common regulatory factor between mammals and zebrafish, and that ageing results in a reduced ability to generate DA neurons in both ascending and local-projecting populations. Future work should focus on determining whether the declining rate of neuron generation with age is specific to DA neurons. For example, the rate of generation of other neuron populations should be quantified using a generic neuronal marker such as HuC/D. This would also allow control for possible loss of EdU absorption in aged zebrafish.

Finally, since EdU pulse-chase analyses are limited (cells that are undergoing DNA repair, or programmed cell death may incorporate nucleotide analogues and may therefore not be truly newborn), I performed conditional lineage tracing experiments. My data showed for the first time that Her4^{+} progenitors give rise to DA neurons in adulthood in two populations: the ascending TPp, and the local PVO. This is in direct agreement with my EdU analyses, and definitively confirms that DA neurons are generated from resident stem/progenitor cells in the adult brain. Future work should focus on the development of an OTPb-driven conditional lineage tracing line. This would allow direct tracing of OTPb expressing ascending DA neurons in the TPp.

In summary, these analyses provide three main conclusions. First, DA neurons in embryonic rostral PT populations do not become post-mitotic as early as previously shown by other studies. Second, the TPp (one of the ascending DA neuron populations) and the PVO (the locally projecting, hypothalamic DA neuron population) are both generated in adult life from resident stem/progenitor cells, where TPp DA neurons are most likely generated late in development. Third, the magnocellular ascending DA neuron populations (DC2/DC2A and DC4/DC4^{A}) are not generated in adulthood, and are born early, showing little or no change in population size in adult life.

Chapter 6

Impeded generation of adult dopaminergic neurons in the rostral PT in a genetic model of Parkinson's disease

6.1: Introduction

PD is pathologically defined by a reduced number of DA neurons in the substantia nigra. The largest risk factor for developing PD is ageing; however monogenic-inherited mutations have been shown to cause PD in around 10% of cases (see introduction section 1.2.1). Many studies in the past 20 years have begun to shed light onto the pathogenesis of PD, and it is clear from these that PD is a complex multisystem disorder, most likely with converging and common mechanisms involved in the correct regulation of DA neurons. Any alterations that disturb these common mechanisms, and subsequently the number or function of DA neurons, could contribute to disease onset or progression. However, we still do not have a clear understanding of underlying mechanisms.

Recent evidence has shown that PD genes – i.e. genes whose dysfunction/dysregulation leads to PD - regulate neural stem/progenitor cells in the adult brain (see introduction section 1.4.5). It has therefore been hypothesized that PD may involve dysregulated neurogenesis as an underlying pathological mechanism, and indeed several studies have begun to describe dysregulated neurogenesis in various brain regions in models of PD (Introduction section 1.4.6). However, as yet, no study has investigated whether in vivo adult generation of ascending DA neurons is impaired in a genetic model of PD. This is perhaps in part due to the limited number of robust rodent PD models: many rodent PD lines do not recapitulate genetic forms of the disease (introduction section 1.3.1). The work that I describe in Chapter 5, showing that ascending DA neurons are generated in the adult rostral PT, shows that the zebrafish provides an excellent model system in which to study in vivo adult DA neurogenesis. Importantly, a *pink1* knockout zebrafish line that robustly models PD has previously been created by the Bandmann lab (Flinn *et al.*, 2013).

In humans, PINK1 is expressed throughout the brain and autosomal recessive inherited loss of function mutations in *PINK1* cause early onset PD (Valente *et al.*, 2004; Gandhi *et al.*, 2006). Although PINK1 has been linked to regulation of mitophagy, mitochondrial function and oxidative stress, the underlying mechanisms of PINK1-mediated PD are not yet fully understood (discussed in detail in section 1.2.4). *Pink1* knockout mice do not display reductions in DA neuron number in the substantia nigra, and so do not robustly model PD.

The *pink1* knockout zebrafish line was established in the Bandmann lab using the targeting induced local lesions in genomes (TILLING) method of mutation. This resulted in the introduction of a premature stop codon in the kinase domain of the zebrafish *pink1* gene, and consequently inactivation of kinase activity and decreased *pink1* mRNA stability. Pink1 deficiency in zebrafish closely models manifestations of the human disease, with reduced numbers of dopaminergic neurons in adult zebrafish and mitochondrial impairment (Flinn *et al.*, 2013). It remains unclear whether reduced DA neurogenesis contributes to this phenotype.

I therefore next aimed to determine whether de novo DA neuron generation is altered in the *pink1*-/- zebrafish. In this chapter, I describe experiments in which I analyse neurogenesis of DA neurons in *pink1*+/+ and *pink1*-/- zebrafish by quantification of DA population sizes throughout life, EdU pulse-chase experiments, investigations into cell death and analyses of progenitor populations. The key aim was to determine whether zebrafish with mutations in *pink1* display reduced DA generation.

6.2: Results

6.2.1 Impeded increase in DA neuronal population sizes in *pink1*-/- zebrafish

In chapter 5, I showed that new DA neurons are generated in adulthood at a rate that decreases with age. It is not clear from these analyses however, whether newborn neurons are added to existing populations, resulting in expansion in DA neuron number, or whether new neurons replace existing neurons resulting in a static population size. I therefore first quantified the number of DA neurons at 55hpf, 3 months and 24-months of age in each rostral PT subpopulation in *pink1+/+* zebrafish, expanding the quantification performed at 55hpf and 3 months by increasing the number of replicates (see Chapter 3: Fig.3.8).

Since DA neurons are generated in the TPp and the PVO throughout life (Chapter 5), I first counted DA neuronal numbers in these two populations. Additionally, since I have shown that DC1 and TPp DA neuronal populations are fundamentally different (Chapter 4), here the quantification of the number of TPp DA neurons at 55hpf is 0. Analysis of the number of $Th1^{+}$ DA neurons in the TPp shows that in *pink1+/+* zebrafish, DA neuron population size significantly increases between 55hpf and 3-months from 0 (±0) to 341 (±42.51), and increases further between 3- and 24-months of age from 341 (±42.51) to 434(±28.27) (Fig.6.1A). Similarly, in the *pink1*+/+ PVO, the number of DA neurons increases between 55hpf and 3-months, from 16 (±3.56) to 377 (±47.16), with further increase between 3- and 24-months from 377 (±47.16) to 485 (±58.58) (Fig. 6.1A). Therefore, DA neuronal numbers increase in the TPp and the PVO in adulthood. In chapter 5, I showed that magnocellular $DC2^{A}$ and $DC4^{A}$ neurons do not label with EdU at 3-, 6-, 12- or 22-months of age and so do not appear to be generated in adult life. To provide an independent assessment of this, I next analysed the size of these PT populations. Analysis of the DC2/$DC2^{A}$ population in *pink1*+/+ zebrafish shows that the number of $Th1^{+}$ DA neurons does not significantly increase between 55hpf and 3-months of age (from 8±1.55 to 9±1.05), or between 3- and 24-months of age (from 9±1.05 to 9±1.55) (Fig.6.1C). However, the number of DA neurons in the *pink1*+/+ DC4/$DC4^{A}$ population significantly increases between 55hpf and 3-months of age, from 8(±2.58) to 20(±1.35), although it does not further increase between 3-months and 24-months of age (20±1.35 to 21±1.17) (Fig.6.4D). These data support my EdU analyses, showing that DA neuronal numbers do not increase in the $DC2^{A}$ or the $DC4^{A}$ populations in adulthood. Additionally, this data strengthens my quantification in section 3.2.2, as both sets of quantifications were performed at different times and on different samples yet give comparable results. This suggests robust quantification methodology.

Next, I counted DA neuronal population sizes at the same time-points in *pink1*-/- zebrafish to ask how the numbers compare to the *pink1+/+* fish. In the TPp of *pink1*-/- zebrafish, the number of DA neurons increases between 55hpf and 3-months from 0(±0) to 330(±72.74) but shows no further significant increase between 3-months to 24-months (330±72.74 to 364±54.27) (Fig.6.1A). Comparison of the total number of DA neurons in the TPp at each time point between *pink1+/+* and *pink1*-/- zebrafish shows that *pink1*-/- zebrafish have significantly fewer DA neurons in the TPp at 2-years of age (434±28.27 compared to

364±54.27, a 16.1% reduction), but show no difference at 55hpf or 3-months of age (Fig.6.1B). Similarly in the *pink1*-/- PVO, the number of DA neurons increases between 55hpf and 3-months, from 14(±3.41) to 343(±37.58), but does not significantly increase between 3- and 24-months (from 343±37.58 to 314±64.01)(Fig6.1B). Comparison of the total number of DA neurons at each time point between *pink1+/+* and *pink1*-/- zebrafish shows that *pink1*-/- zebrafish have significantly fewer DA neurons in the PVO at 2-years of age (485±58.58 compared to 314±64.01, a 35.3% reduction), but show no difference at 55hpf or 3-months of age (Fig.6.1B). This suggests that loss of PINK1 does not alter the generation of TPp and PVO neurons in early life but has a significant effect in adulthood: in contrast to *pink1+/+* zebrafish, the TPp and PVO populations do not expand in adult life in *pink1*-/- zebrafish, resulting in fewer DA neurons in aged zebrafish.

Quantification of DC2/DC2^{A} DA neurons in the *pink1*-/- zebrafish shows that the number of DC2/DC2^{A} DA neurons does not increase between 55hpf and 3-months of age (7±1.37 to 9±1.57). However, between 3-months and 24-months, the number of DA neurons in the DC2^{A} population significantly decreases from 9(±1.57) to 7(±0.85) (Fig.6.1C). Comparison of the total number of DA neurons at each time point between *pink1+/+* and *pink1*-/- zebrafish shows that *pink1*-/- zebrafish have significantly fewer DA neurons in the DC2^{A} population at 2-years of age (9±1.55 compared to 7±0.85, 22.2% reduction), but show no difference at 55hpf or 3-months of age (Fig.6.1C). Quantification of DC4/DC4^{A} DA neurons in the *pink1*-/- zebrafish shows that the number significantly increases between 55hpf and 3-months, from 8(±1.95) to 17(±2.35) but does not increase between 3- and 24-months of age (17±2.35 to 17±2.15) (Fig.6.1D). Comparison of the total number of DA neurons at each time point between *pink1+/+* and *pink1*-/- zebrafish shows that *pink1*-/- zebrafish have significantly fewer DA neurons in the DC4/DC4^{A} population at 3-months of age (20±1.35 compared to 17±2.35, a 15% reduction) and at 2-years of age (22±1.17 compared to 17±2.15, a 22.7% reduction), but show no difference at 55hpf (Fig.6.1D).

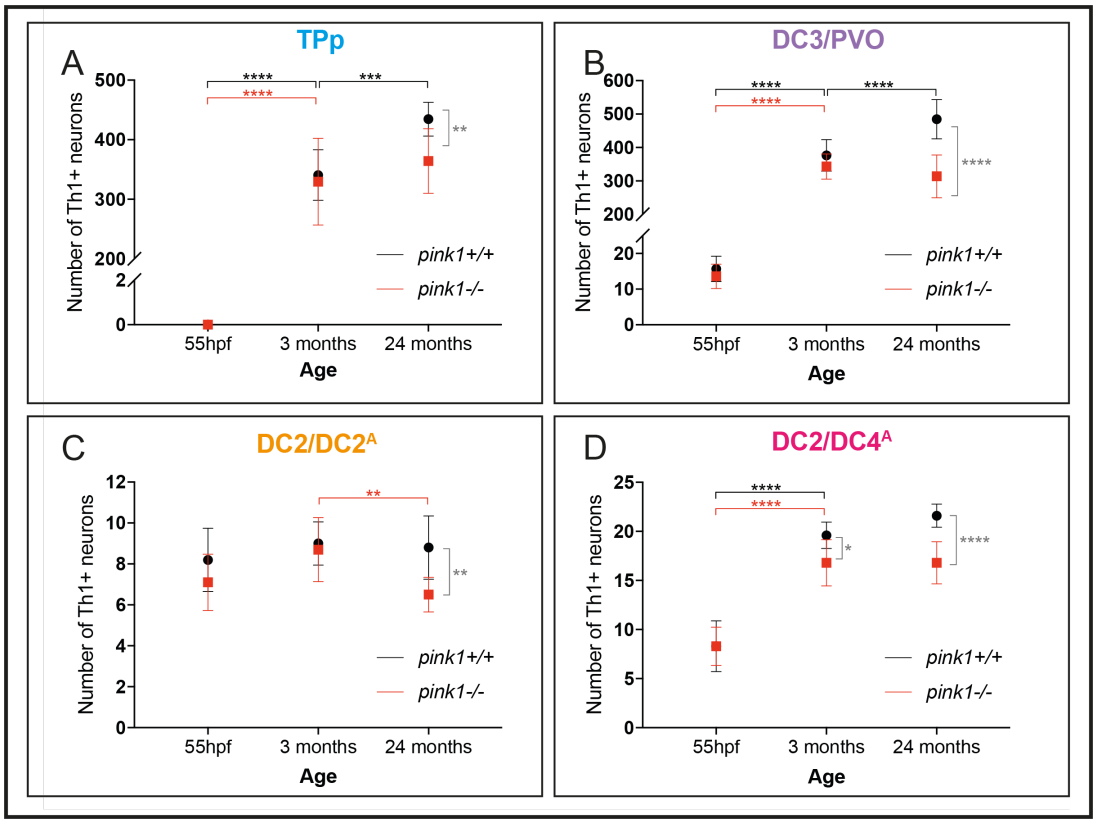

Fig. 6.1: Rostral PT DA neuron population sizes throughout life in *pink1*+/+ and *pink1*-/- zebrafish.

A. Mean number of $Th1^+$ DA neurons in the TPp at 55hpf, 3- and 24-months of age. In *pink1*+/+ zebrafish (black), the number of DA neurons significantly increases between 55hpf and 3-months (p=<0.0001,****, 2-way ANOVA, n=10 for both) and between 3-months and 24-months (p=0.0001,****, 2-way ANOVA, n=10 for both). In *pink1*-/- zebrafish (red), the number of DA neurons significantly increases between 55hpf and 3-months (p=<0.0001,****, 2-way ANOVA, n=10 for both) but not between 3-months and 24-months. *pink1*-/- zebrafish have significantly fewer DA neurons than *pink1*+/+ zebrafish in the TPp at 2-years of age (p=0.0065,**, 2-way ANOVA, n=10 for both). Error bars represent standard deviation.

B. Mean number of $Th1^+$ DA neurons in the PVO at 55hpf, 3- and 24-months of age. In *pink1*+/+ zebrafish (black), the number of DA neurons significantly increases between 55hpf and 3-months (p=<0.0001,****, 2-way ANOVA, n=10 for both) and between 3-months and 24-months (p=<0.0001,****, 2-way ANOVA, n=10 for both). In *pink1*-/- zebrafish (red), the number of DA neurons significantly increases between 55hpf and 3-months (p=<0.0001,****, 2-way ANOVA, n=10 for both) but not between 3-months and 24-months. *pink1*-/- zebrafish have significantly fewer DA neurons than *pink1*+/+ zebrafish in the PVO at 2-years of age (p=<0.0001,****, 2-way ANOVA, n=10 for both). Error bars represent standard deviation.

C. Mean number of $Th1^+$ DA neurons in the $DC2/DC2^A$ population at 55hpf, 3- and 24-months of age. In *pink1*+/+ zebrafish (black), the number of DA neurons does not significantly increase between 55hpf and 3-months, or between 3-months and 24-months. In *pink1*-/- zebrafish (red), the number of DA neurons does not significantly increase between 55hpf and 3-months, but significantly decreases between 3-months and 24-months (p=0.0077,**, 2-way ANOVA, n=10 for both). *pink1*-/- zebrafish have significantly fewer DA neurons than *pink1*+/+ zebrafish in the $DC2^A$ population at 2-

years of age (p=0.0065,**, 2-way ANOVA, n=10 for both). Error bars represent standard deviation.

D. Mean number of $Th1^{+}$ DA neurons in the DC4/$DC4^{A}$ population at 55hpf, 3- and 24-months of age. In *pink1*+/+ zebrafish (black), the number of DA neurons significantly increases between 55hpf and 3-months (p=<0.0001,****, 2-way ANOVA, n=10 for both) but not between 3-months and 24-months. In *pink1*-/- zebrafish (red), the number of DA neurons significantly increases between 55hpf and 3-months (p=<0.0001,****, 2-way ANOVA, n=10 for both) but not between 3-months and 24-months. *pink1*-/- zebrafish have significantly fewer DA neurons than *pink1*+/+ zebrafish in the $DC4^{A}$ population at 3-months (p=0.0308,*, 2-way ANOVA, n=10 for both) and at 2-years of age (p=<0.0001,****, 2-way ANOVA, n=10 for both). Error bars represent standard deviation.

Together these analyses show firstly that, like the *pink1+/+* wild type, the *pink1*-/- zebrafish does not appear to add to existing DC2/$DC2^{A}$ DA neuron populations, but in contrast to the wild type, displays loss of $DC2^{A}$ DA neurons in later life. Secondly, although the DC4/$DC4^{A}$ population expands between 55hpf and 3-months in the *pink1*-/- zebrafish, at 3-months the number of DA neurons in this population does not reach that of the *pink1*+/+ zebrafish, suggesting reduced early-life generation of these neurons.

Overall, this data shows that in *pink1*+/+ zebrafish, TPp and the PVO DA neuron populations expand with age, whereas the DC2/$DC2^{A}$ population size does not increase and the DC4/$DC4^{A}$ population displays restricted expansion in early stages of life (i.e. before 3-months of age) but not in later stages. My analyses also show that *pink1*-/- zebrafish display comparable expansion of DA neuron populations in early life stages in the TPp and PVO, but fail to expand these populations in later stages of life. Furthermore, although the DC4/$DC4^{A}$ population increases in size in early life stages in the *pink1-/-* zebrafish, the maximum number of DA neurons is lower than that of *pink1*+/+ zebrafish. Finally, in *pink1*-/- zebrafish, the $DC2^{A}$ population display a small reduction of the number of DA neurons in later life stages, suggesting that $DC2^{A}$ DA neurons may be degenerating in zebrafish lacking functional Pink1.

6.2.2 Impeded adult DA neuron generation in the TPp and PVO of *pink1*-/- zebrafish

Since my observations show reduced DA neuronal populations in the TPp and the PVO between 3- and 24-months of age, I next performed EdU pulse-chase analyses on *pink1*+/+ and *pink1*-/- zebrafish at 3-months of age to directly compare adult DA neuronal generation in these populations. To achieve this, *pink1*+/+ and *pink1*-/- zebrafish were injected with EdU once daily for 3-days and culled 5-days post injection, and the number of $Th1^{+}EdU^{+}$ neurons was quantified in consecutive sections through the TPp and the PVO. Quantification shows that the number of newly generated $Th1^{+}EdU^{+}$ DA neurons is significantly decreased, both in the TPp of *pink1*-/- zebrafish (1.5±0.29) compared to *pink1*+/+ zebrafish (3.0±0.37)(Fig.6.2A), and in the PVO of *pink1*-/- zebrafish (4.9±0.46) compared to *pink1*+/+ zebrafish (8.6±0.94)(Fig.6.2B). This confirms that generation of DA neurons is impeded in the TPp and the PVO of adult *pink1*-/- zebrafish.

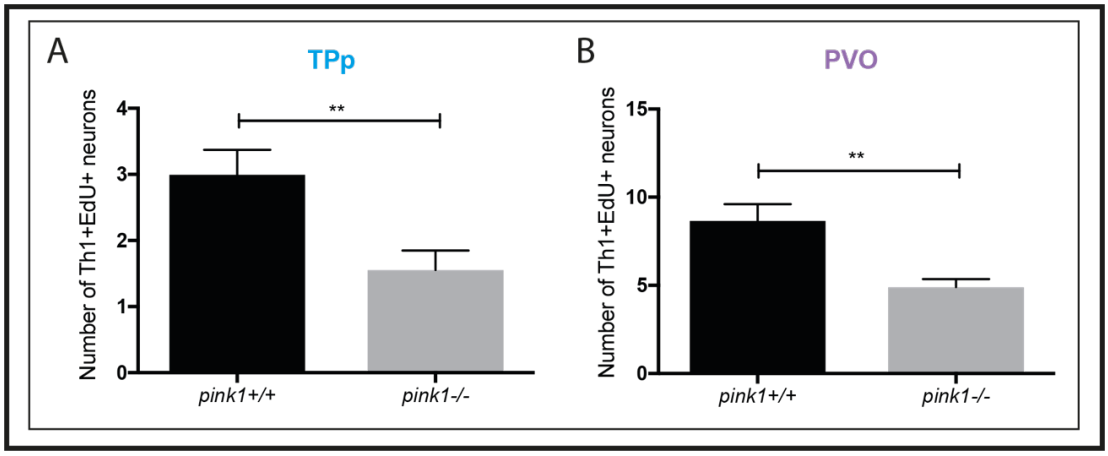

Fig. 6.2: Zebrafish lacking functional Pink1 have impeded generation of DA neurons in the TPp and the PVO of the rostral PT.

A. Mean number of Th1+EdU+ DA neurons in the TPp at 3-months of age. The number of newly generated DA neurons is significantly decreased *pink1*-/- zebrafish compared to *pink1*+/+ zebrafish (p=0.0078, **, unpaired t-test, n=9). Error bars represent standard deviation.
B. Mean number of Th1+EdU+ DA neurons in the PVO at 3-months of age. The number of newly generated DA neurons is significantly decreased *pink1*-/- zebrafish compared to *pink1*+/+ zebrafish (p=0.0017, **, unpaired t-test, n=9). Error bars represent standard deviation.

I next asked whether loss of Pink1 results in overall defects in proliferation in the TPp and PVO. To analyse this, I quantified the number of EdU^+ cells in the TPp and the PVO in 3-month old *pink1*+/+ and *pink1*-/- zebrafish. This shows no significant difference in the number of EdU^+ cells in the TPp of *pink1*-/- zebrafish (149±16.95) compared to *pink1*+/+ zebrafish (171.8±16.50)(Fig. 6.3A) or in the PVO of *pink1*-/- zebrafish (128±8.95) compared to *pink1*+/+ zebrafish (142±12.02)(Fig. 6.3B). This shows that, although loss of Pink1 results in impeded generation of DA neurons in adult zebrafish, its loss does not alter overall levels of proliferation in the rostral PT.

Together this data shows that the generation of adult DA neurons is impeded in the TPp and the PVO of *pink1*-/- zebrafish, but this is not caused by overall decreases in proliferation.

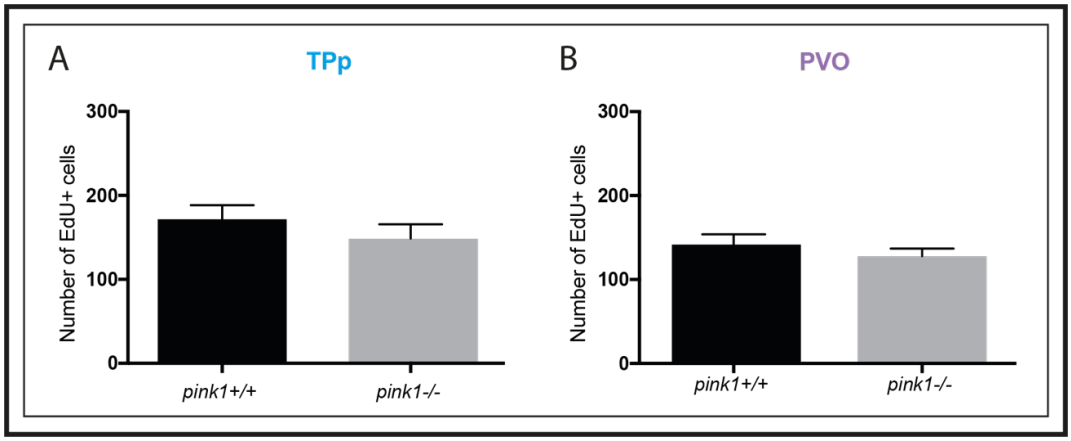

Fig. 6.3: Loss of functional Pink1 does not alter overall levels of proliferation in the TPp and the PVO of the rostral PT.

A. Mean number of EdU+ cells in the TPp at 3-months of age. The overall number of newly generated cells is not significantly different in *pink1*-/- zebrafish compared to *pink1*+/+ zebrafish. Error bars represent standard deviation. Statistically analysed by unpaired t-test, n=9 for both genotypes.
B. Mean number of EdU+ cells in the PVO at 3-months of age. The overall number of newly generated cells is not significantly different in *pink1*-/- zebrafish compared to *pink1*+/+ zebrafish. Error bars represent standard deviation. Statistically analysed by unpaired t-test, n=9 for both genotypes.

6.2.3 Analysis of cell death in *pink*+/+ and *pink1*-/- zebrafish

My analyses (section 6.2.1) show that *pink1*-/- zebrafish fail to expand DA neuronal population sizes in the rostral PT after 3-months of age and show (section 6.2.2) that this is due, at least in part, to the decreased de novo generation of DA neurons in adulthood. Nonetheless, this does not preclude the possibility that loss of functional Pink1 may also result in reduced survival of newborn neurons. The apoptosis of differentiated neurons may accompany impeded DA generation, resulting in a shift in the balance of generation and degeneration. To determine whether newly generated DA neurons undergo apoptosis (programmed cell death) in *pink1*-/- zebrafish, I performed antibody labelling with cleaved caspase-3 (cCaspase) in zebrafish injected with EdU (as in section 6.2.2). Cleaved caspase-3 is an indicator of apoptotic events and is a widely-used marker for cells undergoing programmed cell death (Porter & Jänicke, 1999). A positive control is crucial when performing apoptosis experiments, to ensure that any negative observations are not due to failure of apoptotic assay. Therefore, I first aimed to determine that I could demonstrate robust cCaspase labelling.

Zebrafish embryos with an *rx3* gene knockout (also termed *chk* mutants) have been previously shown to display increased cell death in the hypothalamus (Muthu *et al.*, 2016), therefore I used this line as a positive control for cCaspase labelling. Brain sections from *chk*-/- 55hpf zebrafish embryos (as used in Muthu *et al.*, 2016) show clear examples of cCaspase+ cells in the hypothalamus, compared to no labelling in *chk*+/+ embryos (Fig.6.4A,B, yellow arrowheads). This shows that I can robustly demonstrate cCaspase labelling in a positive control. Next, I performed cCaspase labelling on 3-month old *pink1+/+* zebrafish injected with EdU (as in section 6.2.2). No $cCaspase^{+}EdU^{+}Th1^{+}$ cells were observed in either the TPp (Fig.6.5Ai-iv, yellow arrowheads) or the PVO (Fig.6.5Bi-iv, yellow arrowheads) in 3-month old zebrafish, suggesting newborn DA neurons are not undergoing apoptosis in *pink1*-/- zebrafish.

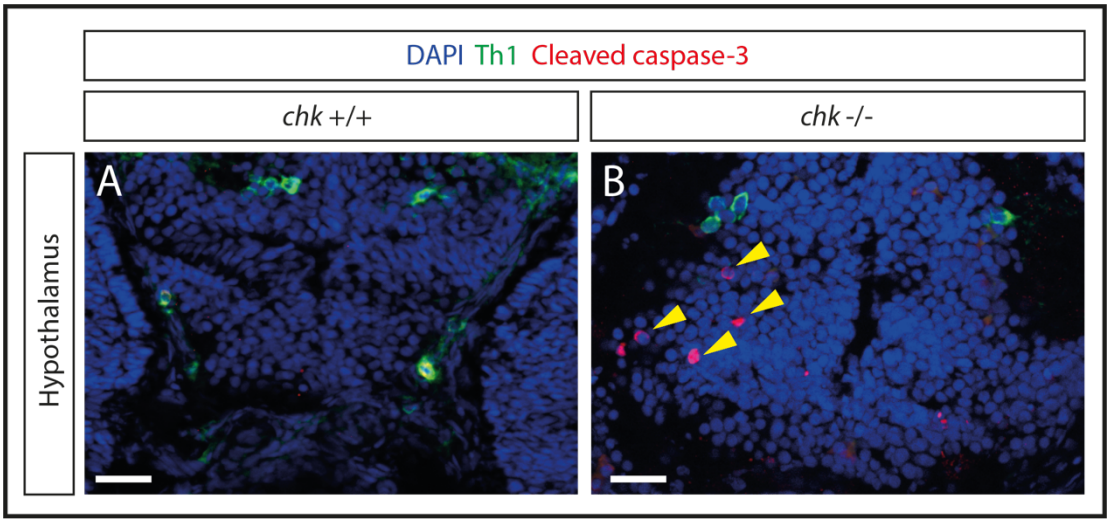

Fig. 6.4: Cleaved caspase-3 labelling in *chk*-/- zebrafish embryos as a positive control.

A. Fluorescent MIP of a transverse section through the hypothalamus of the 55hpf *chk*+/+ embryo, labelled with DAPI (blue), Th1 (green) and cleaved caspase-3 (red). No cleaved caspase-3+ cells are observed in the hypothalamus of *chk*+/+ zebrafish embryos. Scale bar represents 20μm.
B. Fluorescent MIP of a transverse section through the hypothalamus of the 55hpf *chk*-/- embryo, labelled with DAPI (blue), Th1 (green) and cleaved caspase-3 (red). Cleaved caspase-3+ cells are observed in the hypothalamus of *chk*-/- zebrafish embryos. Scale bar represents 20μm.

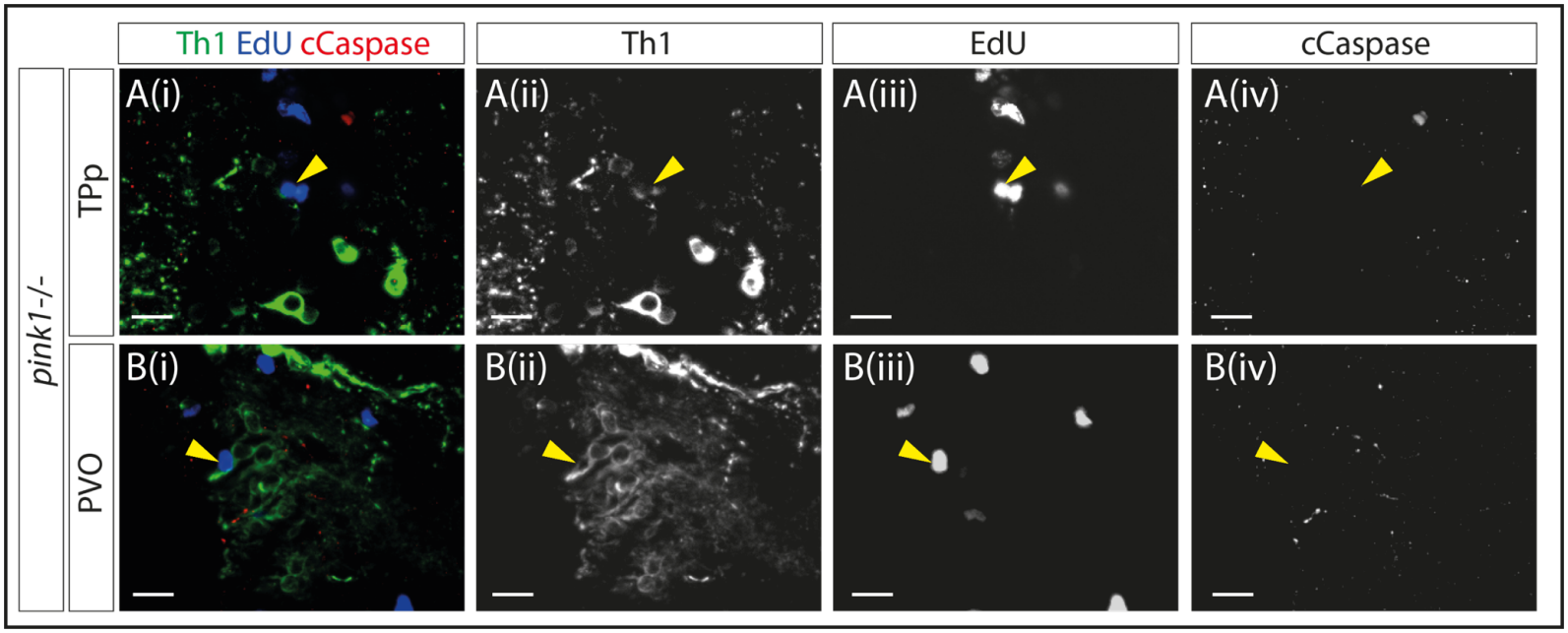

Fig. 6.5: Newly generated DA neurons in the TPp and the PVO do not undergo apoptosis in *pink1*-/- zebrafish.

A(i-iv). Fluorescent MIP of a transverse section through the TPp of the 3-month old *pink1*-/- EdU injected zebrafish, labelled with Th1 (green)(shown individually in (ii)), EdU (blue)(shown individually in (iii)), and cleaved caspase-3 (cCaspase) (red) (shown individually in (iv)). Th1+EdU+ DA neurons do not label with cCaspase in the TPp. Scale bar represents 10μm, n=3.

B(i-iv). Fluorescent MIP of a transverse section through the PVO of the 3-month old *pink1*-/- EdU injected zebrafish, labelled with Th1 (green)(shown individually in (ii)), EdU (blue)(shown individually in (iii)), and cleaved caspase-3 (cCaspase) (red) (shown individually in (iv)). Th1+EdU+ DA neurons do not label with cCaspase in the PVO. Scale bar represents 10μm, n=3.

To ask whether the absence of Pink1 promotes or triggers apoptosis, I performed cCaspase labelling of DA at three stages throughout adult life: 3-, 6- and 24-months, and quantified the number of cCaspase^{+}Th1^{+} cells in all four populations of the rostral PT in both *pink1+/+* and pink1-/- zebrafish. No cCaspase^{+}Th1^{+} cells were detected in TPp, DC2^{A} or DC4^{A} DA neuron populations at any time point (not shown) in fish of either genotype. In the 3-month old PVO a low number of cCaspase^{+}Th1^{+} cells were detected in *pink1*+/+ zebrafish (1±0.55), with a higher number detected in *pink1*-/- zebrafish (7±4.75)(Fig6.6A), although this did not reach significance. This data is skewed by one individual, in which a high number of cCaspase^{+}Th1^{+} cells were detected in the PVO (an example of a section through the PVO of this individual is shown in Fig.6.7, yellow arrowheads). At 6-months of age, a low number of cCaspase^{+}Th1^{+} cells were detected in the PVO in both *pink1*+/+ (1.5±0.5) and *pink1*-/- zebrafish (1.5±0.5)(Fig.6.6B), with no statistical difference between genotypes. At 24-months of age, a low number of cCaspase^{+}Th1^{+} cells were detected in the PVO in both *pink1*+/+ (0.5±0.5) and *pink1*-/- zebrafish (0.5±0.5)(Fig.6.6C), again with no statistical difference between genotypes.

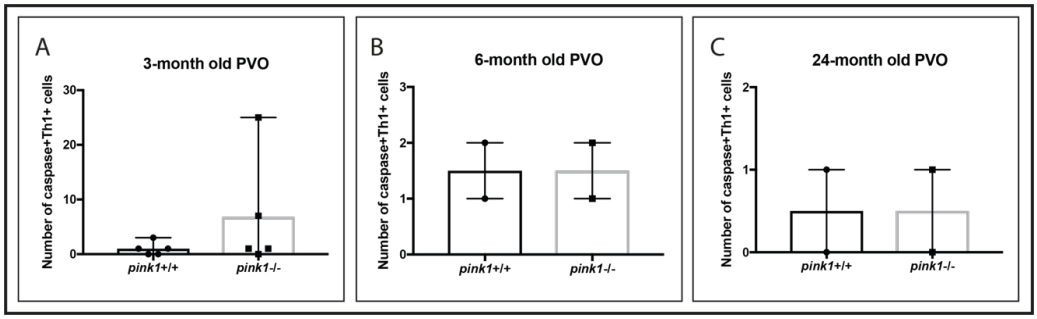

Fig. 6.6: Both *pink1*+/+ and *pink1*-/- zebrafish show low levels of apoptosis in the PVO throughout life, where a small number of *pink1*-/- zebrafish display increased apoptosis in the 3-month PVO.

A. Mean number of $Th1^{+}cCaspase^{+}$ DA neurons in the PVO at 3-months of age. The number of apoptotic DA neurons is not significantly different in *pink1*-/- zebrafish compared to *pink1*+/+ zebrafish. One individual skews the data. Error bars represent range, n=5 for both genotypes.
B. Mean number of $Th1^{+}cCaspase^{+}$ DA neurons in the PVO at 6-months of age. The number of apoptotic DA neurons is not significantly different in *pink1*-/- zebrafish compared to *pink1*+/+ zebrafish. Error bars represent range, n=2 for both genotypes.
C. Mean number of $Th1^{+}cCaspase^{+}$ DA neurons in the PVO at 24-months of age. The number of apoptotic DA neurons is not significantly different in *pink1*-/- zebrafish compared to *pink1*+/+ zebrafish. Error bars represent range, n=2 for both genotypes.

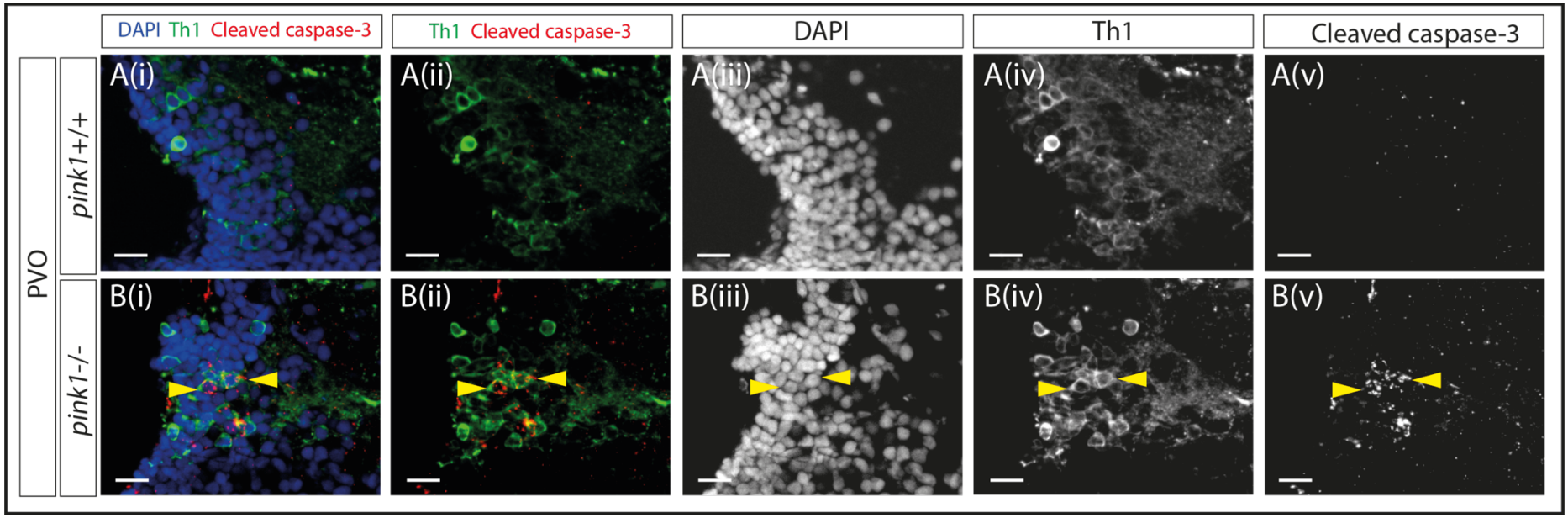

Fig. 6.7: Example of a 3-month old *pink1*-/- zebrafish displaying increased apoptosis of DA neurons in the PVO.

A(i-iv). Fluorescent MIP of a transverse section through the PVO of the 3-month old *pink1*+/+ zebrafish, labelled with DAPI (blue)(shown individually in (iii)), Th1 (green)(shown individually in (iv)), and cleaved caspase-3 (cCaspase) (red) (shown individually in (v)). DA neurons do not label with cCaspase in the PVO in the *pink1*+/+ zebrafish. Scale bar represents 10μm.

B(i-iv). Fluorescent MIP of a transverse section through the PVO of the 3-month old *pink1*-/- zebrafish, labelled with DAPI (blue)(shown individually in (iii)), Th1 (green)(shown individually in (iv)), and cleaved caspase-3 (cCaspase) (red) (shown individually in (v)). DA neurons label with cCaspase in the PVO in a *pink1*-/- zebrafish. Scale bar represents 10μm.

Together, this data shows that there is no evidence that newly generated DA neurons in the TPp and the PVO undergo apoptosis in the adult *pink1*-/- zebrafish. Furthermore, there is no evidence for increased apoptosis of any ascending DA neuron (i.e. either newly-born or previously generated neuron in the TPp, $DC2^{A}$ and $DC4^{A}$ populations) in the *pink1*-/- zebrafish at young or late adult stages. In the locally projecting PVO, DA neuron apoptosis was observed in a *pink1*-/- individual at 3-months of age. This suggests loss of Pink1 may result in increased cell death in the PVO in a small number of individuals, though this requires further investigation.

6.2.4 Analysis of progenitor populations in *pink*+/+ and *pink1*-/- zebrafish

My analysis of the generation of DA neurons in *pink1-/-* zebrafish shows that adult DA neurogenesis is impeded with loss of functional Pink1, whereas developmental generation of DA neurons appears to be unaltered. Therefore, I next hypothesised that the impeded adult generation of DA neurons in *pink1*-/- zebrafish may result from alterations to a distinct population of adult DA progenitors.

In chapter 4, I showed that OTPb is expressed in DA neurons in the TPp (i.e. the large population of ascending neurons that display de novo neurogenesis throughout life) in adulthood, but not in DC1 DA neurons during development. This suggests that adult TPp DA neurons may arise from progenitors that are distinct from embryonic DC1 DA neuron progenitors. I therefore aimed to quantify $OTPb^{+}$ progenitors in *pink1*+/+ and *pink1-/-* zebrafish at an early adult time-point (when there are no obvious differences in TPp DA population size in the two genotypes) and a late adult time-point (when there are difference in TPp DA population size in the two genotypes). To achieve this, anti-Th1 and anti-OTPb immunohistochemistry was performed in brain sections through the TPp of 3-month old and 24-month old *pink1*+/+ and *pink1-/-* zebrafish. Subsequently, the number of $OTPb^{+}$ $Th1^{+}$ DA neurons and the number of $OTPb^{+}$ $Th1^{-}$ progenitors was quantified in the TPp at both ages. At 3-months of age, *pink1-/-* zebrafish have a reduced population of $OTPb^{+}$ $Th1^{-}$ progenitors in the TPp (844±26.5) compared to *pink1*+/+ siblings (1342±83) but there is no difference in the number of $OTPb^{+}$ $Th1^{+}$ DA neurons in *pink1-/-* zebrafish (271.5±31.5) compared to *pink1*+/+ siblings (271.5±31.5)(Fig.6.8A). By contrast, at 2-years

of age, *pink1-/-* zebrafish have reduced populations, both of $OTPb^{+}$ $Th1^{-}$ progenitors (730.3±142.8) compared to *pink1*+/+ siblings (1237±96.29), and of $OTPb^{+}$ $Th1^{+}$ DA neurons (435±37.73) compared to *pink1*+/+ siblings (315.3±28.89)(Fig.6.8B). Thus, *pink1-/-* zebrafish have a reduced population of $OTPb^{+}$ progenitors in the TPp at both early adult and late adult life stages and a reduced population of $OTPb^{+}Th1^{+}$ DA neurons in later life. Together this suggests that Pink1 is required for the generation of an adult $OTPb^{+}$ population of DA progenitors.

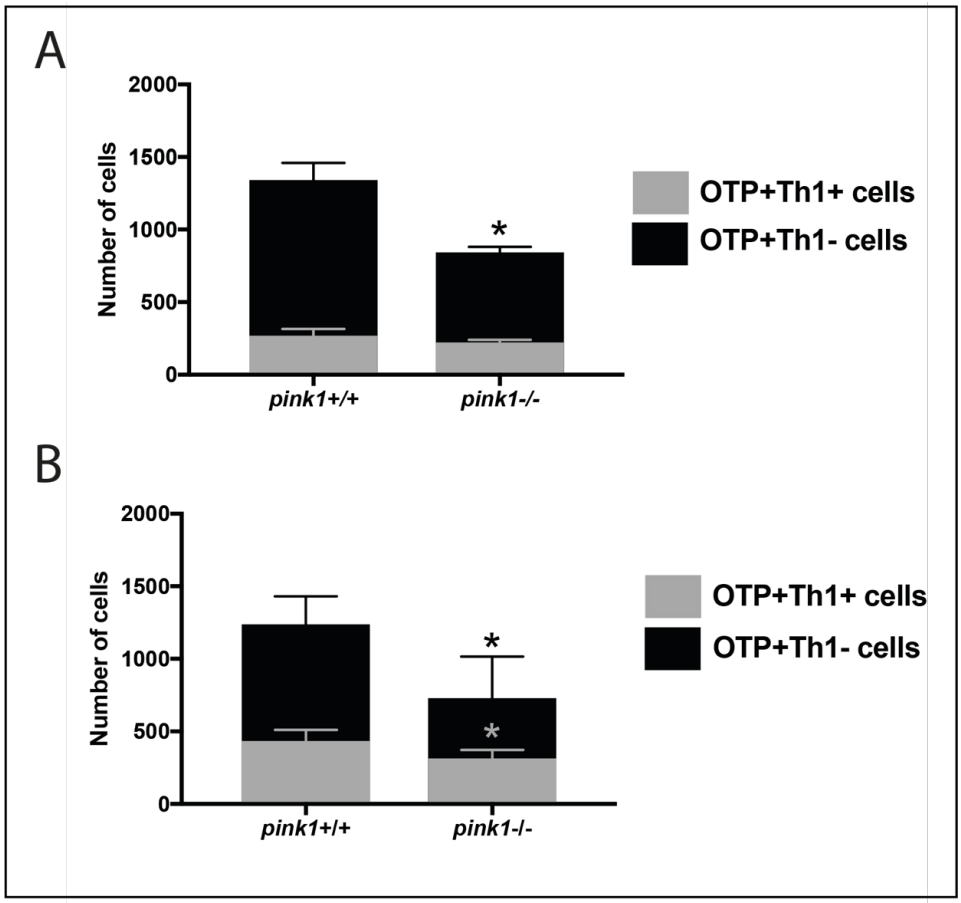

Fig. 6.8: Reduced population of OTPb^{+} progenitors in the TPp of *pink1*-/- zebrafish at 3-months and 24-months of age.

A. Mean number of OTP^{+}Th1^{-} progenitors and OTP^{+}Th1^{+} DA neurons in the TPp at 3-months of age. The number of OTP^{+}Th1^{-} progenitors is significantly decreased in the TPp of *pink1*-/- zebrafish compared to *pink1*+/+ zebrafish (p=0.0292,*, unpaired t-test), but no significant difference in the number of OTP^{+}Th1^{+} DA neurons. Error bars represent standard deviation, n=2 for both genotypes.
B. Mean number of OTP^{+}Th1^{-} progenitors and OTP^{+}Th1^{+} DA neurons in the TPp at 24-months of age. The number of OTP^{+}Th1^{-} progenitors is significantly decreased in the TPp of *pink1*-/- zebrafish compared to *pink1*+/+ zebrafish (p=0.0259,*, unpaired t-test), and the number of OTP^{+}Th1^{+} DA neurons is significantly decreased (p=0.0453,*, unpaired t-test). Error bars represent standard deviation, n=4 for both genotypes.

6.3: Discussion

In chapter 5, I showed that new DA neurons are newly generated in adulthood in two rostral PT populations: the ascending TPp and the locally projecting, hypothalamic-like, PVO. The aim of this chapter was to determine whether de novo DA neuronal generation is altered in a model of PD, the *pink1*-/- zebrafish. To achieve this, neurogenesis of DA neurons in *pink1*+/+ and *pink1*-/- zebrafish was analysed by quantification of DA population size, EdU pulse-chase experiments, investigations into cell death and analyses of progenitor populations.

First, my analyses of DA neuronal population size in the rostral PT showed that in *pink1*+/+ zebrafish, TPp and the PVO DA neuron populations expand with age, whereas the DC2/DC2^{A} population size does not increase and the DC4/DC4^{A} population displays restricted expansion in early stages of life, but not in adulthood. The growth in size of the TPp and the PVO suggests that DA neurons are added to existing populations, rather than replacing DA neurons in the population. This data agrees with my EdU pulse-chase analyses of DA neuron generation (section 5.2.2), which shows that DA neurons are generated in the TPp and the PVO at 3, 6 and 12-months of age. In contrast, magnocellular DA neuron populations show little or no increase in population size in adulthood. Together with my EdU analyses in chapter 5 (section 5.2.2) demonstrating no EdU labelling in DC2^{A} or DC4^{A} populations, this suggests that new DA neurons are not added to these populations in adult life. This further suggests that the same, relatively small populations of, DC2^{A} or DC4^{A} DA neurons are retained throughout adult life and are not turned over.

Next, my analyses of DA neuronal population size in *pink1*-/- zebrafish revealed that *pink1*-/- zebrafish display comparable expansion of DA neuron populations in early life stages in the TPp and PVO, but fail to expand these populations in adult stages of life (i.e. between 3- and 24-months). This suggests that loss of Pink1 results in impeded adult generation of DA neurons in these populations, resulting in a smaller population sizes at 24-months. This equates to around a 16% reduction in the TPp, and around 35% reduction in the PVO. This could have significant impact on DA function.

Furthermore, my data shows that, although the DC4/DC4^{A} population increases in size in early life stages in the *pink1-/-* zebrafish, the number of DA neurons at 3-months is lower than that of *pink1*+/+ zebrafish. This suggests that loss of Pink1 results in impeded early life expansion of DC4 DA neurons, resulting in a smaller population size at 3-months and at 24-months. This equates to a 15-22% difference in population size. Additionally, my data shows that in *pink1*-/- zebrafish, the DC2^{A} population equally does not increase size in early life, but displays a small reduction in size in later life stages (i.e. between 3- and 24-months). This suggests that DC2^{A} DA neurons may be degenerating in zebrafish lacking functional Pink1. Since my analyses in *pink1*+/+ zebrafish shows that DC2 DA neurons are generated early and the population does not appear to turn over, this suggests that the DC2/DC2^{A} population may be particularly susceptible to degeneration, where lost DA neurons are not replaced. The relatively small size of the DC2/DC2^{A} population means that a loss of even a small number of DA neurons in the *pink1-/-* zebrafish, equates to around a 22% reduction in population size. Again, this could have significant impact on DA function.

Since my observations showed reduced DA neuron population size in the TPp and the PVO, I next assessed DA neuron generation directly by EdU analyses in *pink1*+/+ and *pink1*-/- zebrafish. My studies showed reduced generation of DA neurons in the TPp and the PVO of *pink1*-/- zebrafish, compared to *pink1*+/+ zebrafish. This agrees with my data from section 6.2.1, confirming that loss of functional Pink1 results impedes generation of DA neurons in one ascending DA neuron population (the TPp) and in one hypothalamic-like population (the PVO). My data further show that there is no difference in overall levels of proliferation in *pink1*+/+ and *pink1*-/- zebrafish in the PT, suggesting that loss of Pink1 does not interfere with proliferative mechanisms in a non-specific manner.

My analyses (section 6.2.1) show that *pink1*-/- zebrafish fail to expand DA neuronal population sizes in the rostral PT after 3-months of age and show (section 6.2.2) that this is due, at least in part, to that the decreased de novo generation of DA neurons in adulthood. I next assessed whether loss of functional Pink1 also increased cell death, contributing to a shift in the balance of generation and degeneration, either by the reduced survival of newborn neurons, or by increased apoptosis of existing populations. My data shows no

evidence that newly generated DA neurons in the TPp and the PVO undergo apoptosis in the adult *pink1*-/- zebrafish. This suggests that the impeded generation of DA neurons observed in *pink1*-/- zebrafish is not due to reduced survival of newly generated neurons.

Furthermore, my data shows no evidence for increased apoptosis of any ascending DA neuron (i.e. either newly-born or previously generated neuron in the TPp, $DC2^{A}$ and $DC4^{A}$ populations) in the *pink1*-/- zebrafish at young or late adult stages. For the $DC2^{A}$ DA neuron population, this result does not agree with my previous data that shows no generation of $DC2^{A}$ DA neurons but a reduced population size in *pink1*-/- zebrafish. However, the reduction in population size was small, equating to around 2 neurons. It is likely that DA neuronal death occurred at an age that I did not investigate: indeed, the cCaspase assay is limited in providing a 'snapshot' of cell death at the time of fixation. Likewise, it is possible that this assay also did not allow labelling of cell death in the $DC4^{A}$ population, which showed a modest reduction in population size of around 3-5 DA neurons in *pink1*-/- zebrafish. In the third and largest population of ascending DA neurons (the TPp) however, my observation of no cell death together with my observation of reduced generation (section 6.2.2) suggests that the reduced population sizes of these neurons in *pink1*-/- zebrafish may be caused by impeded DA generation, rather than solely by high levels of cell death.

In the locally projecting, hypothalamic-like PVO, a high level of DA neuron apoptosis was observed in one *pink1*-/- individual at 3-months of age. This suggests that loss of Pink1 may result in increased cell death in the PVO in a small number of individuals. Indeed, the PVO in *pink1*-/- zebrafish displayed the largest reduction in population size in aged fish, equating to around a 35% decrease. This suggests that increased cell death of PVO DA neurons may accompany their impeded generation (section 6.2.2). It is possible that the position and morphology of DA neurons in the PVO contributes to their susceptibility to cell death, as these neurons contact the CSF, and so may be directly influenced by CSF-signals. Since I only observed the increase in cell death in one individual, this requires further investigation. However, since this population is not part of the ascending DA neuron system and is more hypothalamic in nature, I did not pursue this further.

In chapter 4, I showed that OTPb is expressed in DA neurons in the TPp in adulthood, but not by DC1 DA neurons during development. Therefore, my data suggests that adult TPp DA neurons most likely arise from OTPb-expressing progenitors that are distinct from embryonic DC1 DA neuronal progenitors. I therefore aimed to quantify $OTPb^{+}$ progenitors in *pink1*+/+ and *pink1-/-* zebrafish at an early adult time-point (when there are no obvious differences in TPp DA population size between the two genotypes) and a late adult time-point (when there are differences in TPp DA population size between the two genotypes). My analyses showed that *pink1-/-* zebrafish have a reduced population of $OTPb^{+}$ progenitors in the TPp at both early adult and late adult life stages. This suggests that Pink1 is required for the generation of an adult $OTPb^{+}$ population of progenitors. Together, this suggests that loss of Pink1 results in a reduced population of OTPb progenitors in early life, which may directly result in reduced generation of DA neurons. Reduced generation may consequently result in failed expansion of the ascending population of TPp DA neurons, and subsequently a reduced population size in later life.

In summary, these analyses provide four main conclusions. First, whilst one of the ascending populations (the TPp) and the local-projecting PVO expand in adulthood in *pink1*+/+ zebrafish, in *pink1*-/- zebrafish, these populations fail to expand in adult life. Furthermore, ascending $DC2^{A}$ DA neurons are lost in adult life in *pink1*-/- zebrafish. Second, *pink1*-/- zebrafish have reduced adult generation of TPp and PVO DA neurons. Third, newly generated ascending DA neurons in *pink1*-/- zebrafish do not undergo apoptosis, and there is no increased cell death in the TPp, suggesting that reduced population size of the TPp is not caused by high levels of cell death. In the locally projecting PVO however, increased cell death may accompany impeded generation. Fourth, Pink1 is required for the generation of adult OTPb-expressing progenitors.

Chapter 7

The zebrafish as a model for Leucine-rich Repeat Kinase-2 (Lrrk2) deficiency

7.1: Introduction

Mutations in the leucine-rich repeat kinase 2 (*LRRK2)* are the most common known cause of monogenic-inherited PD, explaining between 5-13% of familial and 1-5% of sporadic PD. Patients with *LRRK2* mutations typically develop late-onset PD, presenting with the classical symptoms and signs of the disease (Kumari & Tan, 2009). The most common *LRRK2* mutation, the G2019S mutation, results in increased kinase activity, due to the mutation introducing a phosphorylation site in the kinase domain of the protein (Luzón-Toro *et al.*, 2007). Although gain of function mutations show the role of LRRK2 in PD, the biological role of LRRK2 remains relatively unclear. I therefore aimed to generate a zebrafish *lrrk2* knockout line, to allow future investigations into the function of Lrrk2 in vivo.

7.2: Zebrafish *lrrk2* orthologue identification and expression

To identify the zebrafish orthologue of *LRRK2*, the sequence of the human protein (ENSP00000298910) was aligned to the zebrafish proteome using BLASTP software. The top hit of this search was annotated as Lrrk2 in the zebrafish proteome (ENSDARP00000018692), with approximately 54% homology to the human LRRK2 protein. To further validate this, the zebrafish Lrrk2 orthologue sequence was aligned to the human proteome, identifying the top hit as the human LRRK2 protein (ENSP00000298910). From ENSEMBL software, human *LRRK2* and zebrafish *lrrk2* have similar genetic structures: a similar protein size (human 2527aa and zebrafish 2532aa), exon number (human 51 exons, zebrafish 52 exons) and transcript length (human 9158bp, zebrafish 8042bp). Furthermore, human LRRK2 and Zebrafish Lrrk2 both contain comparable protein domains, namely, an Ankyrin repeat domain (ANK), a leucine-rich repeat domain (LRR), a Roc domain, a C-terminal of Roc (COR) domain, a kinase domain and a WD40-repeat-containing domain (figure 7.1).

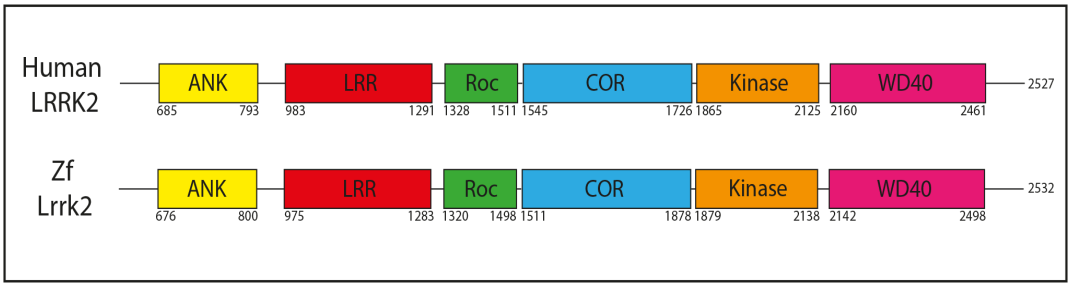

Figure 7.1: Protein domains of human and zebrafish LRRK2/Lrrk2.

Schematic demonstrating domains within human LRRK2 (top) and zebrafish (Zf) Lrrk2 (bottom).

Human LRRK2 may be alternatively spliced into 4 protein coding variants, ranging in size from 521-2527 amino acids, where the major isoform is 2527 amino acids in length. Zebrafish Lrrk2 may be alternatively spliced into 3 different protein coding isoforms, all of which are 2532 amino acids in length. To further validate orthology, zebrafish *lrrk2* and human *LRRK2* genetic loci were compared, to determine whether synteny exists between genes. *SLC2A13* was found to be present in both organisms, located upstream of human *LRRK2*, yet downstream of *lrrk2* in zebrafish. No other genes could be located up to 500kb upstream or downstream of *LRRK2/lrrk2* that were present in both humans and zebrafish (figure 7.2).

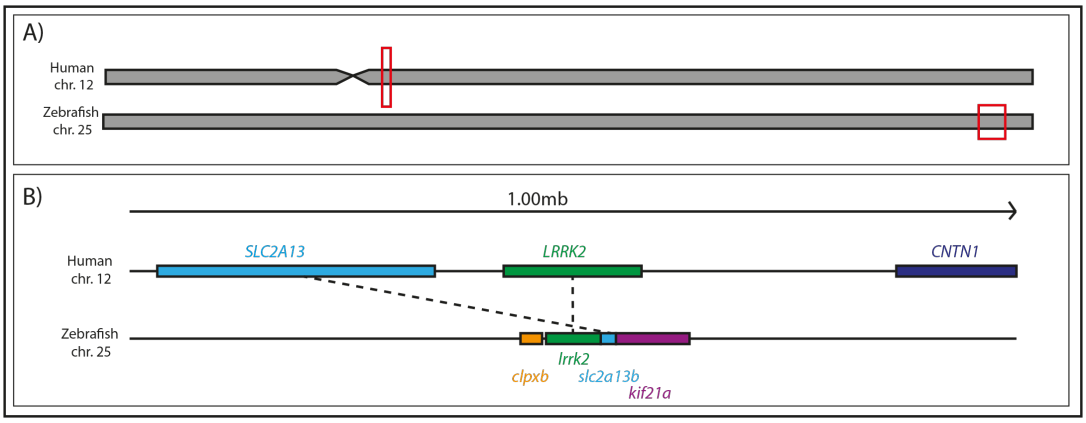

Figure 7.2: Genomic loci of human and zebrafish *LRRK2/lrrk2*.

A: schematic demonstrating position of human LRRK2 and zebrafish lrrk2 within respective chromosomes (indicated by red box).

B: schematic comparing genomic loci of human *LRRK2* (top) and zebrafish *lrrk2* (bottom) orthologues, coloured boxes indicate surrounding protein coding genes

To determine whether *lrrk2* is expressed during development and during adulthood, *lrrk2* cDNA from zebrafish embryos (aged 1-,2-,3-,4- and-5-dpf) and *lrrk2* cDNA from adult brains (3-,6-,9-,12- and 24-months of age) was amplified using RT-PCR. Expression of *lrrk2* was detected at a constant level in zebrafish aged from 1-5dpf, with slightly higher expression detected in adult zebrafish brains. Expression of *lrrk2* between 3- and 24-months of age remained relatively constant (figure 7.3).

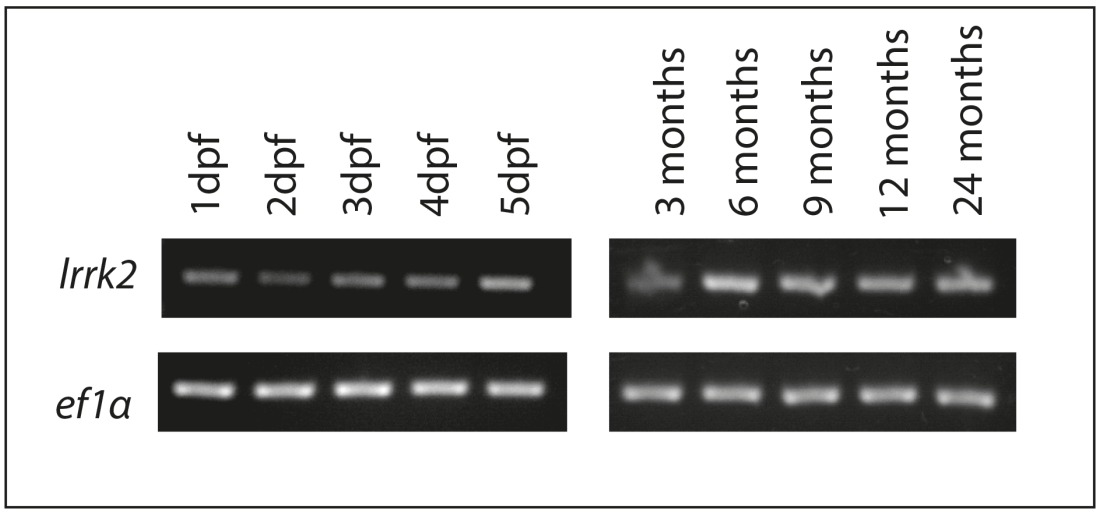

Figure 7.3: Expression of *lrrk2* during embryonic development and in entire brains from adult zebrafish at various ages.

RT-PCR using cDNA from 1-5dpf zebrafish (left) and brains from 3-24-month zebrafish (right), with *ef1α* as a loading control.

7.3: Using the CRISPR/Cas9 system to generate a *lrrk2* knockout zebrafish line

7.3.1: Introduction to CRISPR/Cas9 genome editing

In recent years, genome editing techniques have advanced greatly, allowing the introduction of site-specific mutations within target genes. One such technique, CRISPR (clustered regularly interspaced short palindromic repeats)/Cas9 (CRISPR-associated protein-9), has become a widely-used device for research in genetic disease. CRISPR/Cas is a system that is present in bacteria, as part of prokaryotic immunity against viral integration into the bacterial genome. Briefly, short fragments of viral DNA are incorporated into the bacterial genome between short palindromic repeats. Transcribed RNA from these sequences are used as guide RNA, and in conjunction with Cas proteins, allow recognition and cleavage of any invading nucleic acids. This provides an adaptive immune system against viral infection (Bhaya *et al.*, 2011).

This system has recently been adapted to use in eukaryotes, including model organisms, to generate site-specific mutations in model organisms. In this adaption, the guide RNA sequence is altered, to allow targeted binding and cleavage of genomic DNA. To achieve this, an ultramer is generated, containing a T7 promoter, a target sequence and a guide RNA (gRNA) scaffold (figure 7.4). The target sequence must be unique, thus only resulting in site-specific cleavage, and must be immediately upstream of a protospacer adjacent motif (PAM) site, to allow binding of the gRNA-Cas9 complex (for Cas9, the PAM sequence is 5' NGG). The target sequence binds to the desired site within genomic DNA, and the guide RNA scaffold recruits Cas9 endonuclease. Cas9 cleaves the DNA 3 nucleotide bases upstream of the PAM site (figure 7.5). This cleavage results in activation of error prone DNA repair mechanisms, introducing mutations into the targeted site (Wang *et al.*, 2016).

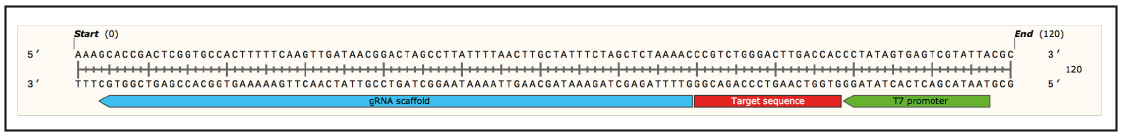

Figure 7.4: The CRISPR/Cas9 genome editing system – structure of ultramer.

Schematic showing the structure of an ultramer, containing a T7 promoter (green), a customized target sequence (red) and a gRNA scaffold (blue). This ultramer allows transcription of the guide RNA that can be injected into model organisms

.

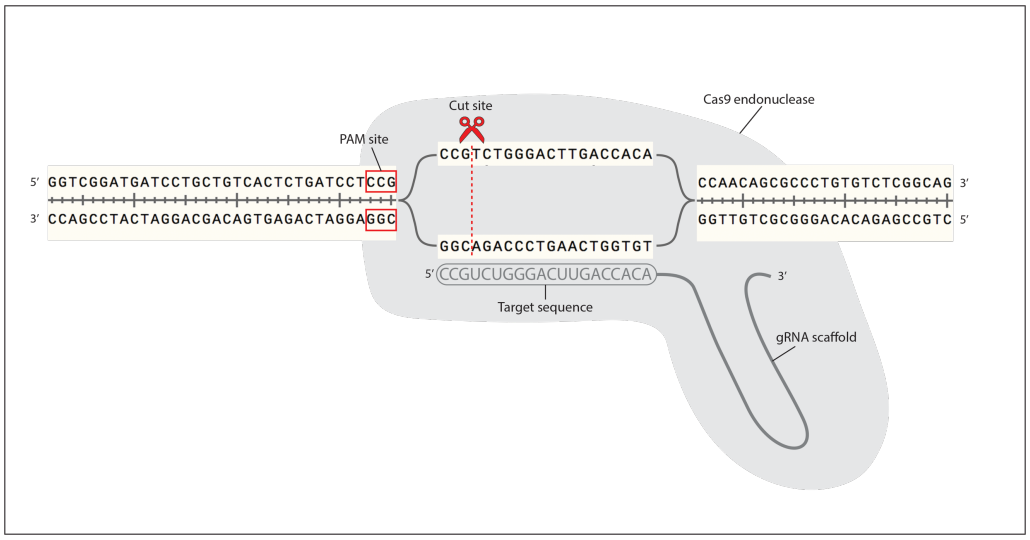

Figure 7.5: Mechanism of CRISPR/Cas9 cleavage.

Schematic showing the guide RNA binding to the target sequence, allowing recruitment of Cas9 endonuclease and resulting in site-specific cleavage of genomic DNA

7.3.2: Design of CRISPR/Cas9 target site in the *lrrk2* gene

To allow identification of successful CRISPR/Cas9-mediated mutation, PAM sites located close to large restriction enzyme sites (such as *Mwo1* and *Bsl1*) are preferable, so that successful mutation will result in disruption of the restriction enzyme cut site. Since *Bsl1* sites contain PAM sites within the recognition sequence (CCNNNNNNNGG), a gRNA was designed to a *Bsl1* restriction enzyme site in exon 20 of the zebrafish *lrrk2* gene (figure 7.6). Targeting this region should result in cleavage of gDNA within the *Bsl1* restriction site, with introduced mutations resulting in disruption of this recognition sequence, and an inability of *Bsl1* to cut the DNA. According to Ensembl software, exon 20 encodes a region of the Ankyrin repeat domain, the first Lrrk2 protein domain. The aim of targeting this exon was to create a deletion or insertion, causing a frameshift mutation and introducing a premature stop codon. This would theoretically ultimately result in a truncated Lrrk2 protein.

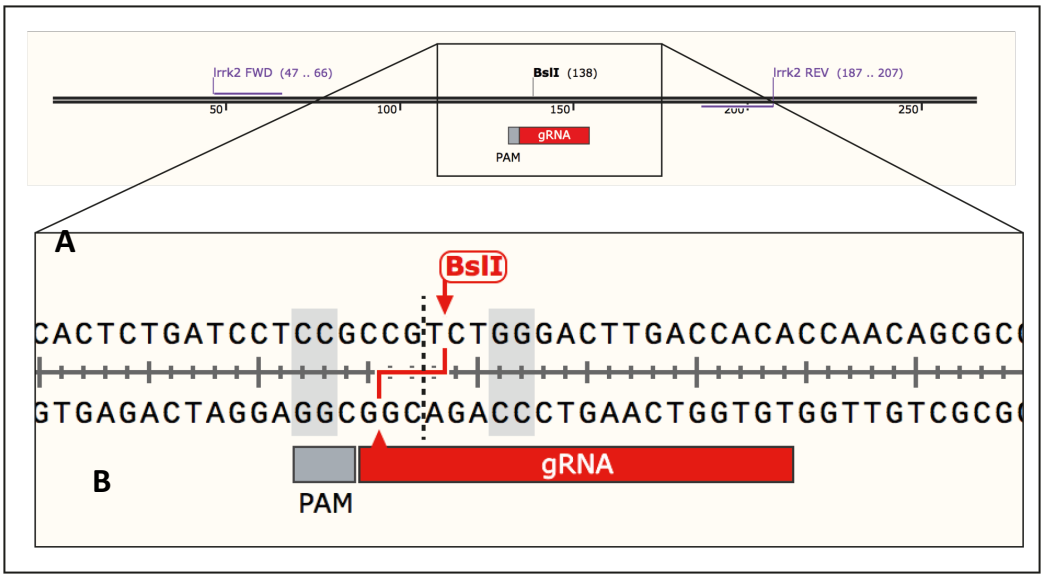

Figure 7.6: CRISPR sites in the zebrafish *lrrk2* gene.

A: Schematic showing an overview of *lrrk2* exon 20, showing primer sites (purple), PAM site (grey box) and gRNA binding site (red box). Bsl1 restriction site is also shown.

B: Schematic showing CRISPR binding site in more detail, where the Bsl1 restriction enzyme recognition sequence is shaded grey on the DNA and the cut site is illustrated with a red line. The CRISPR PAM site is illustrated with a grey box below the sequence, and the gRNA site with a red box below the sequence. The CRISPR/Cas9 cut site is illustrated with a black dotted line

7.3.3: Injection and testing efficiency of CRISPR/Cas9–mediated mutation of *lrrk2*

The gRNA was injected into one-cell stage wild-type zebrafish embryos, and to test the efficiency of the CRISPR, genomic DNA (gDNA) was extracted from 24hpf injected and uninjected control zebrafish. Exon 20 of *lrrk2* was amplified by PCR and digested with *Bsl1*, and PCR products were run on an analytical gel to determine if the restriction site had been disrupted in CRISPR-injected zebrafish (figure 7.7). PCR products from uninjected and undigested embryos produced a 160bp fragment, whereas PCR products from uninjected and *Bsl1* treated embryos were almost completely digested, giving fragments of 90bp + 70bp. PCR products from CRISPR injected and *Bsl1* treated embryos showed incomplete digestion in 6 out of 7 embryos examined, showing the CRISPR efficiently introduced mutations into exon 20, disrupting the *Bsl1* recognition sequence in almost all embryos examined.

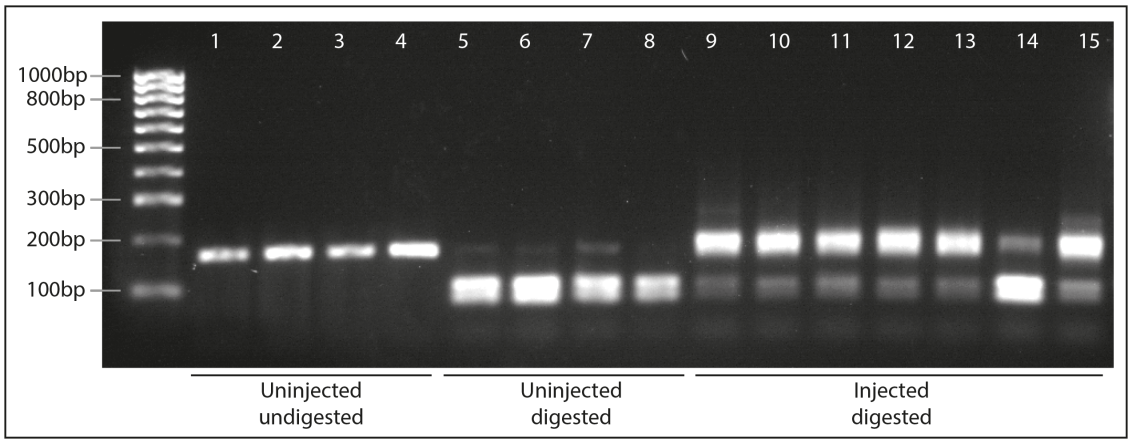

Figure 7.7: CRISPR analytical restriction digest.

To test the efficiency of the *lrrk2* CRISPR, gDNA was extracted from CRISPR injected and control uninjected 1dpf embryos. The CRISPR target site was amplified by PCR and DNA was digested with *BslI* enzyme. Uninjected and undigested DNA produced a band of approximately 160bp (lanes 1-4). Uninjected controls digested with *BslI* produced two bands of approximately 90bp + 70bp (lanes 5-8). CRISPR injected PCR product digested with *BslI* resulted in incomplete digestion in 6/7 embryos examined (lanes 9-15), showing the *BslI* restriction site was mutated in a highly efficient manner.

7.3.4: *lrrk2* CRISPR founder identification

To determine whether CRISPR-induced mutations were transmitted to the germ line, CRISPR injected embryos (F0) were raised to breeding age and outcrossed to wild type zebrafish. Offspring from this outcross were raised in separate tanks and finclipped to identify founder individuals. DNA was extracted from F1 fin clips and amplified by PCR. PCR products were run on analytical gels to identify large deletions or insertions. PCR products from the first tank of F1 fish revealed two samples containing deletions (figure 7.8a). These samples were sequenced, revealing an 18bp deletion in exon 20 (figure 7.8b). This deletion however, was in frame, deeming these founders unsuitable.

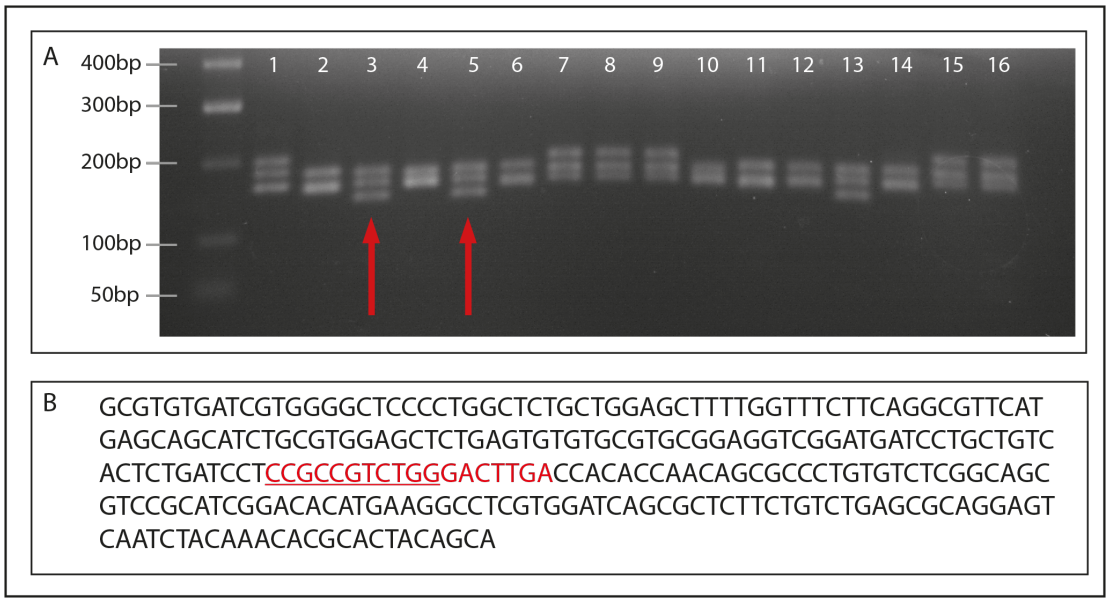

Figure 7.8: Founder identification by PCR.

CRISPR/Cas9 injected adults (F0) were outcrossed to wild type individuals. DNA was extracted from the progeny and amplified by PCR. PCR products were run on an analytical gel to identify any large deletions or insertions. PCR products with potential deletions/insertions were sequenced. A: An example of PCRs of gDNA from finclips of 16 F1 individuals (lanes 1-16). Wild type PCR product gives a band at 160bp. Arrows indicate PCR products of interest (lanes 3 and 5), showing potential deletions – these PCR products were sequenced. B: Sequencing of PCR products revealed a 18bp deletion (red) in both products sequenced. Underlined text demonstrates CRISPR target sequence. This deletion was in frame so these fish were not selected as founders.

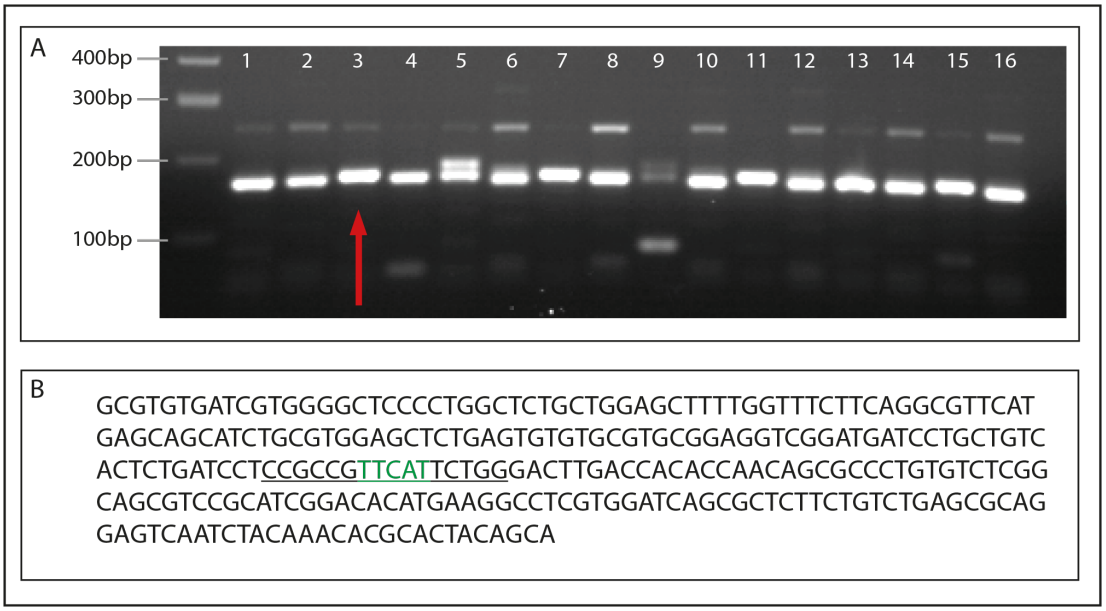

Figure 7.9: Founder identification by PCR.

CRISPR/Cas9 injected adults (F0) were outcrossed to wild type individuals. DNA was extracted from the progeny and amplified by PCR. PCR products were run on an analytical gel to identify any large deletions or insertions. PCR products with potential deletions/insertions were sequenced. A: An example of PCRs of gDNA from finclips of 16 F1 individuals (lanes 1-16). Wild type PCR product gives a band at 160bp. Arrow indicates PCR product of interest (lane 3), showing a potential insertion – this PCR product was sequenced. B: Sequencing of PCR products revealed a 5bp insertion (green) causing a frame shift and disruption of *BsI1* restriction site. Underlined text demonstrates CRISPR target sequence

.

PCR products from the second tank of F1 fish revealed a sample appearing to contain an insertion (figure 7.9a). This sample was sequenced, revealing a 5bp insertion (figure 7.9b). This insertion disrupts the *Bsl1* restriction site in exon 20, allowing relatively easy genotyping (figure 7.10), and causes a frameshift. An online Attotron Transcription and Translation tool was used to calculate the predicted protein of the F1 5bp insertion mutated DNA sequence (table 7.1). This predicted a frame shift, resulting in altered amino acids and introduction of a premature stop codon. This suggests this mutation may produce a truncated protein.

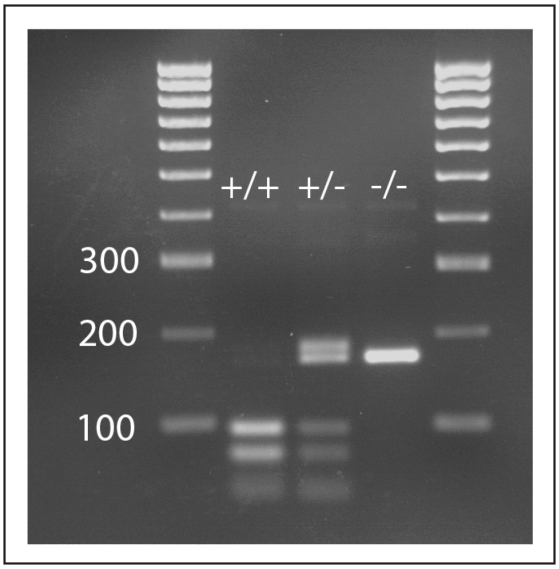

Figure 7.10: Genotyping of *lrrk2* mutation by *Bsl1* restriction digest.

DNA was extracted and amplified by PCR from *lrrk2+/+*, *lrrk2+/-*, and *lrrk2-/-* individuals. PCR product was digested with Bsl1 enzyme. Wild type *lrrk2* (+/+) is fully digested by *Bsl1*, giving two fragments of 90bp + 70bp. Individuals that are heterozygous for the 5bp insertion (+/-) are partially digested by *Bsl1*, giving fragments of 90bp + 70bp + 160bp. The band at 160bp forms a heteroduplex caused by genetic recombination of the wild type and mutated DNA strand. DNA from Individuals homozygous for the 5bp insertion (-/-) are not digested by *Bsl1*.

	DNA sequence	Predicted protein sequence
Wild type exon 20	GCGTGTGATCGTGGGGCTCCCCTGG CTCTGCTGGAGCTTTTGGTTTCTTC AGGCGTTCATGAGCAGCATCTGCGT GGAGCTCTGAGTGTGTGCGTGCGG AGGTCGGATGATCCTGCTGTCACTC TGATCCTCCGCCGTCTGGGACTTGA CCACACCAACAGCGCCCTGTGTCTC GGCAGCGTCCGCATCGGACACATGA AGGCCTCGTGGATCAGCGCTCTTCT GTCTGAGCGCAGGAGTCAATCTACA AACACGCACTACAGCA	ACDRGAPLALLELLVSSGVHEQHLRG ALSVCVRRSDDPAVTLILRRLGLDHTN SALCLGSVRIGHMKASWISALLSERRS QSTNTHYS
CRISPR exon 20	GCGTGTGATCGTGGGGCTCCCCTGG CTCTGCTGGAGCTTTTGGTTTCTTC AGGCGTTCATGAGCAGCATCTGCGT GGAGCTCTGAGTGTGTGCGTGCGG AGGTCGGATGATCCTGCTGTCACTC TGATCCTCCGCCGTTCATTCTGGGA CTTGACCACACCAACAGCGCCCTGT GTCTCGGCAGCGTCCGCATCGGACA CATGAAGGCCTCGTGGATCAGCGCT CTTCTGTCTGAGCGCAGGAGTCAAT CTACAAACACGCACTACAGCA	ACDRGAPLALLELLVSSGVHEQHLRG ALSVCVRRSDDPAVTLILRR*SFWDLTT* *PTAPCVSAASASDT---RPRGSALFCLSA* *GVNLQTRTTA*

Table 7.1: Predicted exon 20 protein sequence with 5bp insertion.

The predicted protein amino acid sequence of wild type exon 20 DNA sequence and of CRISPR-induced 5bp insertion (green) DNA sequence. The 5bp insertion results in predicted alteration of amino acids (italic) compared to wild type, and introduction of a premature stop codon (indicated by "---" in protein sequence, highlighted in red and underlined). CRISPR target site is also indicated in DNA sequence by underlining DNA bases.

7.3.5: Confirmation of *lrrk2* knockout

The 5bp insertion leads to frameshift and introduction of a premature stop codon in exon 20 of *lrrk2*, potentially resulting in a truncated Lrrk2 protein. qPCR was used to demonstrate that the premature stop codon leads to nonsense mediated decay of *lrrk2* transcript. RNA was extracted from 3-month old *lrrk2+/+* and *lrrk2-/-* zebrafish brains (1 brain per replicate, 3 replicates per genotype), and cDNA was generated from the RNA. qPCR on *lrrk2+/+* and *lrrk2-/-* brains showed a 95% decrease (p=0.0111) in *lrrk2* transcript level in *lrrk2-/-* brains, compared to *lrrk2+/+* controls (figure 7.11). This indicates that *lrrk2* mRNA trancript is unstable, due to the introduction of the premature stop codon, furthermore suggesting loss of function of Lrrk2 protein. The qPCR primers are predicted to amplify all three varients of Lrrk2, suggesting effective knockdown of all *lrrk2* transcript.

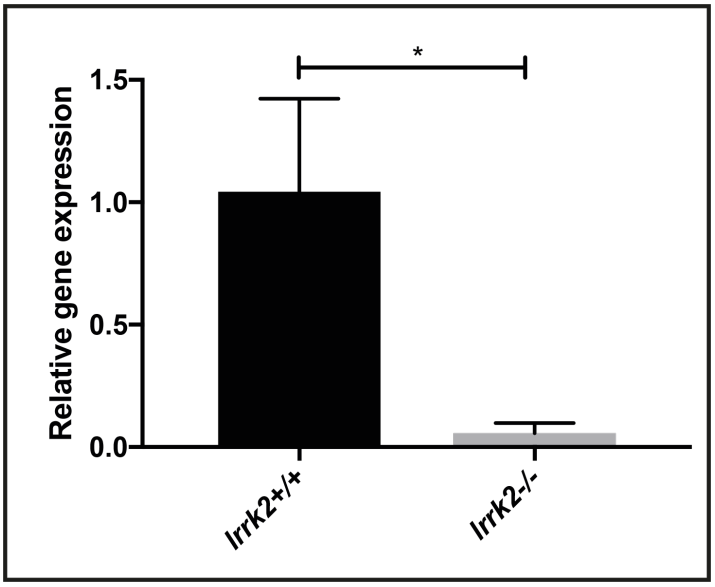

Figure 7.11: qPCR of *lrrk2* transcript in *lrrk+/+* and *lrrk2-/-* brains.

qPCR was used to investigate the effect of the 5bp insertion on the *lrrk2* mRNA transcript. qPCR on *lrrk2+/+* and *lrrk2-/-* brains showed a 95% decrease (p=0.0111, unpaired t-test) in *lrrk2* transcript level in *lrrk2-/-* brains, compared to *lrrk2+/+* controls. Data normalised to the reference gene, *ef1α.*

.

7.4: Discussion

The aim of this study was to generate a *lrrk2* deficient zebrafish line. To do this, *lrrk2* expression was evaluated in embryonic and adult zebrafish, and a *lrrk2* knockout line was generated using CRISPR/Cas9 technology.

Zebrafish were found to possess a *lrrk2* orthologue, with conserved protein structure and similarities in protein size, exon number and transcript length. Furthermore, zebrafish *lrrk2* also has relatively well conserved gene synteny. Expression of *lrrk2* in zebrafish embryos was constant from 1dpf to 5dpf, and was found to persist throughout adult stages of life.

A zebrafish *lrrk2* knockout was successfully generated in this study by use of CRISPR/Cas9 technology. Exon 20 of the zebrafish *lrrk2* gene was targeted by CRISPR/Cas9, resulting in introduction of a 5bp insertion. This insertion disrupted a *BsI1* restriction site and resulted in a frameshift. This insertion was predicted to result in the introduction of a premature stop codon and protein sequencing predicted a truncated Lrrk2 protein. Knockout of *lrrk2* was confirmed using qPCR, which showed a 95% decrease in *lrrk2* mRNA transcript levels in *lrrk2-/-* zebrafish.

Future work is required to determine the role of Lrrk2 in regulation of neurogenesis in PD. The *lrrk2* knockout zebrafish line generated in this study would not be appropriate for directly modelling PD, as the most common mutations in *lrrk2* in PD result in gain of function of kinase activity (see section 1.2.5). This *lrrk2* knockout zebrafish line however, would be a valuable tool for analysing the complex biological role of Lrrk2 in the regulation of dopaminergic neurogenesis. For example, previous studies in midbrain-derived neural progenitor cell cultures have shown *LRRK2* knockdown results in impeded differentiation of DA neurons (Milosevic *et al.*, 2009). It would certainly be interesting to determine whether differentiation or generation of ascending DA neuron populations was impeded in this *lrrk2* knockout zebrafish line. To investigate this, EdU analysis and genetic lineage

tracing of PT DA neurons should be performed on *lrrk2* knockout zebrafish, followed by analysis of stem/progenitor populations.

In the course of performing my studies, another *lrrk2* knockout zebrafish line was created (Suzzi *et al.*, 2017). In this line, the authors used the CRISPR/Cas9 technique to remove the entire coding domain of *lrrk2*. This contrasts with my *lrrk2* knockout zebrafish line, which contains a 5bp insertion, resulting in frameshift and nonsense mediated decay of mRNA transcript. My zebrafish line requires further characterisation, to determine whether *lrrk2* knockout zebrafish have fewer DA neurons in the PT. However, it would be interesting to identify variances in phenotype caused by the different mutation types. Furthermore, recent advances in CRISPR/Cas9-mediated homology that direct knock-in of point mutations in zebrafish, can allow site directed editing of single nucleotides (Armstrong *et al.*, 2016). In this case, the generation of a G2019S point mutation zebrafish is possible, potentially allowing overexpression of Lrrk2. It would therefore be fascinating to determine whether *lrrk2* overexpression resulted in alterations to DA neurogenesis in embryonic and adult zebrafish.

Chapter 8

Final Discussion

In the studies presented in this thesis I have:

1. Robustly defined and compared morphological and positional similarities between embryonic and adult PT DA neuron populations.
2. Shown through analysis of stem/progenitor markers that distinct populations of stem and progenitor cells reside in the adult PT. Moreover, on the basis of expression of stem/progenitor markers, I have demonstrated (a) that the PVO is fundamentally different from the rest of the PT and is likely to be hypothalamic in nature, and (b) that adult TPp DA neurons are profoundly different from embryonic DC1 DA neurons due to differences in OTPb expression.
3. Shown that DA neurons are newly-generated in one of the ascending DA neuron populations (the TPp) and the local-projecting PVO population in adult life from resident stem/progenitor cells, whereas magnocellular DA neurons are not. I have further shown that DA neurons in embryonic PT populations do not become post-mitotic as early as previously suggested by other studies.
4. Demonstrated that loss of Pink1 results in failed expansion of the ascending TPp and the local-projecting PVO in adult life, and results in a loss of ascending magnocellular $DC2^{A}$ DA neurons in adult life. I have further shown that the smaller population size of the TPp in *pink1*-/- zebrafish is not caused by increased cell death, and have provided evidence that loss of Pink1 results in the impeded adult generation of ascending DA neurons due to failed generation of adult populations of progenitors.

8.1: Discussion

8.1.1 Ascending DA neurons are generated in adult life

In rodent models, previous attempts have been made to determine whether there is de novo generation of ascending dopaminergic neurons in the substantia nigra, but the conclusions of these studies have been conflicting (Kay & Blum, 2000; Lie *et al.*, 2002; Zhao *et al.*, 2003; Frielingsdorf *et al.*, 2004; Yoshimi *et al.*, 2005; Shan *et al.*, 2006). Moreover, no study has used conditional lineage tracing to determine whether de novo generation of ascending DA neurons occurs from identified populations of stem/progenitor cells.

Using conditional lineage tracing, together with EdU analyses, I have shown for the first time that DA neurons in the largest ascending population, the TPp, are newly generated from Her4-expressing stem/progenitor cells in adult zebrafish. I have further shown that the TPp expands in size during development, and continues to expand in adult life. The growth of this population suggests that DA neurons are added to the existing population, rather than replacing DA neurons. Importantly, I have also demonstrated that there is very little or no death of DA neurons in the TPp, further suggesting that the TPp undergoes growth not replacement of DA neurons. The wider significance of these results will be discussed below.

My studies show that DA neurons in the zebrafish ascending TPp are added to in adult life. It is generally accepted that DA neurons in the TPp (together with DC2/DC2^{A} and DC4/DC4^{A} DA neurons) represent the mammalian ascending nigrostriatal system. This is due to the fact that DA neurons within these populations project to a region of the ventral telencephalon termed the subpallium, thought to be homologous to the striatum (Rink & Wullimann, 2001*b*; Ganz *et al.*, 2010*a*). The substantia nigra is a region that degenerates in PD, therefore stimulation of endogenous DA neurogenesis in the adult brain offers an attractive target for PD treatment. In mouse models, the low rate of neurogenesis has made studying generation of ascending DA neurons difficult. In contrast, zebrafish have a higher rate of constitutive neurogenesis, allowing investigation into DA generation.

It should be noted however, that key differences exist between mammals and zebrafish. First, the exact homology between DA populations in both species is not yet fully understood. From fish to mammals, the DA systems have significantly evolved: mammals develop DA neurons in the midbrain, whereas zebrafish develop DA neurons only in the forebrain (Smeets & González, 2000). Importantly, signalling pathways shown to be crucial for the development of ventral midbrain (VM) DA neurons in mammals do not appear to regulate ventral diencephalic (vDC) neurons in a comparable manner. For example, in mammals Nurr1 and Pitx3 are specifically required for the transition of VM DA progenitors to DA neurons: loss of Nurr1 results in failed VM dopaminergic specification, while loss of Pitx3 results in the absence of SNpc DA neurons (Hwang *et al.*, 2003; Smits *et al.*, 2003; Hegarty *et al.*, 2013). However in zebrafish, loss of Nurr1 results in altered spatial organisation of vDC DA neuron populations but does not reduce population numbers, and loss of Pitx3 has no effect on the number of vDC DA neurons (Filippi *et al.*, 2007). It is therefore likely that some transcriptional regulatory mechanisms of ascending DA neuron development are not fully evolutionarily conserved between mammals and zebrafish.

One transcription factor that is crucial to the development of ascending DA neuronal populations in zebrafish is OTP. In zebrafish, OTP is required for the development of the ascending DC2 and DC4 DA populations and also the hypothalamic DC5 and DC6 DA populations (Ryu *et al.*, 2007*a*). Here, I have shown for the first time that ascending TPp DA neurons also express OTPb in the adult zebrafish, although embryonic DC1 neurons do not. This shows that, in zebrafish, the largest ascending DA neuron population expressed OTPb and arises later in development. However, two issues remain outstanding and require further study. First, as yet, no study has ascertained if the TPp DA population is lost in the absence of OTP. Second, it is not clear whether ascending OTPb^{+} DA neurons exist in other species. In the embryonic mouse, OTP is expressed in, and required for the development of the hypothalamic A11 DA population, but there is little evidence to suggest that OTP is expressed in, or required for the development of DA neurons of the substantia nigra (Ryu *et al.*, 2007*a*). This suggests two possibilities: either (a) OTP-dependent DA neurons are not represented in the mammalian substantia nigra or (b) OTP is required only for generation of DA populations that arise later in development, and have therefore been missed in previous studies (the Ryu et al. study analyses OTP expression in embryonic periods). In support of the latter possibility, one study has, in fact, shown that OTP is expressed by a

small population of neurons within the nigrostriatal bundle of the postnatal mouse VM (Wang & Lufkin, 2000). Although it is not clear whether these are DA neurons, it is possible that an OTP-dependent nigrostriatal DA population arises in late prenatal/postnatal life in mammals. Further characterisation of the molecular characteristics of VM and vDC DA neurons will help to further elucidate homology between zebrafish and mammalian DA populations.

The second key difference between mammals and zebrafish is the growth of ascending DA neuron populations in the adult brain. A study by Zhao et al. demonstrated that the number of DA neurons in the substantia nigra of the mouse stayed constant in adult life. This suggests that, if DA neurogenesis does occur in the mammalian substantia nigra, it acts to maintain a static population size, potentially balancing apoptosis. By contrast, in zebrafish, my analyses of population size and cell death show that new DA neurons add to, rather than replace, existing DA neuron populations in the adult zebrafish TPp. This highlights a significant regulatory difference between mammals and zebrafish, agreeing with multiple studies in the telencephalon that show the zebrafish displays a more constitutive form of neurogenesis (Grandel *et al.*, 2006; Chapouton *et al.*, 2011). Further studies are required to determine the mechanisms that allow additive DA neurogenesis in the zebrafish PT compared to the mammalian substantia nigra. My data, showing that no cell death of ascending DA neurons occurs in the zebrafish, contrasts with studies in mammals, where cell death of ascending DA neurons is observed and suggests that regulation of programmed cell death could be one mechanistic difference.

A third difference between mammalian and zebrafish ascending neurons is the position of ascending DA neurons. My analyses from chapter 4 show that neurons in the neurogenic populations of the zebrafish PT (the TPp and the PVO) both reside immediately adjacent to the diencephalic ventricle and to radial glial progenitors. This spatial organisation may provide a more permissive environment for dopaminergic neurogenesis, potentially allowing newborn DA neurons to survive or stimulating resident stem/progenitor cells to generate DA neurons.

Studies of proliferative zones in the telencephalon have shown that the rate of formation of new cells depends on dorso-ventral position of the region in question. The most proliferative region is found in the medial subpallium (Vv) (Adolf *et al.*, 2006; Grandel *et al.*, 2006), where progenitors in this zone, but not in more dorsal regions, have been shown to be directly regulated by FGF signalling (Ganz *et al.*, 2010*a*). This suggests FGF signalling could be the cause of a higher proliferation rate in this region of the telencephalon. It is not clear whether growth factors such as FGF regulate proliferation in the zebrafish PT or the mammalian substantia nigra, however FGF has been shown to stimulate neurogenesis in other regions of the mammalian brain, such as the hypothalamus (Robins *et al.*, 2013). This highlights FGF as a potential stimulant for adult neurogenesis of DA neurons, though this requires further investigation. Future studies in both species could elucidate the differences in mechanisms that regulate different rates of neurogenesis. Understanding this is crucial to the development of new treatments that stimulate endogenous neurogenesis to replenish neurons in adult life, which could offer appealing new strategies to treat neurodegenerative disease.

8.1.2 DA neurogenesis is impeded in PD

A recent study showed that loss of Pink1 results in reduced neurogenesis in the mouse hippocampus (Agnihotri *et al.*, 2017) and numerous studies have shown that PD genes can regulate neural stem/progenitor cells in the adult brain (Le Grand *et al.*, 2015). However, until now, no study has investigated whether in vivo generation of ascending DA neurons is reduced in PD. Here, my analyses show that loss of Pink1 results in impeded in vivo adult generation of ascending DA neurons and of local-projecting DA neurons. How could this be relevant for the development or progression of PD?

Firstly, any disruption in the number of DA neurons could significantly disrupt DA system function. In PD, loss of dopamine signalling due to loss of DA neurons, results in the cardinal motor features of PD. Thus, impeded generation of DA neurons could contribute to DA neuronal loss in PD. In chapter 6, I showed that zebrafish lacking functional Pink1 fail to expand both the ascending TPp and the local-projecting PVO DA neuron populations in adulthood. This resulted in a significant reduction in population size by 2-years of age. This

suggests that failed adult generation of ascending DA neurons results in a smaller population size, and consequently could result in reduced dopaminergic signalling. As discussed above, I have shown that zebrafish ascending DA populations undergo growth, not replacement. In this respect, any reductions in DA neurogenesis would be even more significant. For instance, if DA neurons apoptose and are not efficiently replaced, this would result in a net loss of DA neuron number.

As mentioned above, Agnihortri et al. (2017) showed that loss of Pink1 in the adult mouse hippocampus results in impeded differentiation to neurons, reduced generation of late stage progenitors and increased generation of oligodendrocytes. This suggests that loss of Pink1 does not solely reduce DA neurogenesis. Nonetheless, this finding is significant, as the non-motor symptoms that characterise PD are not thought to be directly related to degeneration of the nigrostriatal DA system. Instead, non-motor processes that are affected in PD, including sense of smell, mood and regulation of sleep cycle, directly rely on the function of regions such as the olfactory system, hippocampus and hypothalamus (Winner *et al.*, 2011*a*). It is therefore feasible that dysfunctional neurogenesis in these systems could contribute to non-motor symptoms in PD, though this certainly requires further investigation.

Understanding the mechanisms that cause reduced neurogenesis in organisms with mutations in PD-genes could help to direct future research. The study by Agnihortri et al. elucidates one potential mechanism for reduced hippocampal neurogenesis in mice lacking functional PINK1. Here the authors show that neural stem cells (NSCs) from *PINK1* knockout mice display decreased mitochondrial membrane potential and elevated glycolysis, suggesting that loss of PINK1 results in deficits in mitochondrial function in NSCs (Agnihotri *et al.*, 2017). As discussed in the Introduction, previous studies have shown that PINK1 is crucial to mitophagy in DA neurons: PINK1 functions with Parkin to initiate mitophagy, labelling dysfunctional mitochondria for recycling. However, the PINK1/Parkin pathway can also regulate mitochondrial dynamics, increasing mitochondrial fusion at the expense of fission (Poole *et al.*, 2008). Though the exact mechanism of this is not known, it is thought that the PINK1/Parkin pathway may regulate the ubiquitination of proteins involved in mitochondrial fusion, such as Mitofusin 1/2 (Mfn1/2) (Poole *et al.*, 2008; Gegg

et al., 2010; Yu *et al.*, 2011). Therefore, lack of functional PINK1 results in a tip in the balance of mitochondrial fusion/fission dynamics toward more fusion.

Mitochondria continually change shape through combined actions of fusion (a process of fusing mitochondria together, forming a single closed network) and fission (a process of mitochondrial fragmentation, resulting in large numbers of small mitochondria)(Bliek *et al.*, 2013). One major role of mitochondrial dynamics is likely to be to share organelle contents, to replace damaged or lost components; another is to allow fragmentation of mitochondria upon programmed cell death (Scott & Youle, 2010). However, recently, regulation of mitochondrial fusion and fission has also been implicated in the regulation of adult NSCs. One study has shown that mitochondrial dynamics are crucial to regulation of neural stem cell identity and fate decisions, where deletion of Mfn1/2 in the adult hippocampus resulted in depletion of NSCs and reduced neurogenesis (Khacho *et al.*, 2016). This suggests that mitochondrial fusion is necessary for maintenance of NSC self-renewal. Thus, loss of functional PINK1 could result in a tip in the balance of mitochondrial dynamics toward fusion, and subsequently push NSCs toward self-renewal at the expense of generation of progenitors. In this respect, it is most likely that there would already be a reduced population of progenitors in early life, as NSCs would fail to generate extensive progenitor pools in development. My analyses disagree with this, as I have shown that loss of Pink1 does not alter embryonic/juvenile generation of DA neurons.

However, there is an alternative hypothesis for the mechanism of reduced neurogenesis associated with lack of functional PINK1. In the introductory section 1.4.6, I discussed a study that showed that PINK1 can interact with Notch in a non-canonical pathway in *Drosophila*. In this pathway, PINK1 is involved in the recruitment of Notch to the mitochondrial membrane, resulting in activation of mTORC2/AKT signalling, and promotion of self-renewal (Lee *et al.*, 2013). In this case, loss of PINK1 could result in reduced Notch/mTORC2/AKT signalling, reduced self-renewal and subsequently an exhaustion of the NSC pool. This phenotype could result in initial generation of neurons and progenitors in early life from proliferating progenitor pools, but an exhaustion in later life. My studies showing normal embryonic/juvenile development, followed by failed expansion of neuronal populations in later life support this hypothesis. Indeed, I have also shown that

DA neurons in the wild type TPp and PVO arise from resident stem/progenitor cells that express *her4*, a gene that is directly regulated by Notch signalling (Kageyama *et al.*, 2008), further implicating an involvement for Notch in the regulation of PT DA neurogenesis. Thus, here I propose that loss of Pink1 results in reduced non-canonical Notch signalling, reduced mTORC2/AKT signalling, reduced self-renewal capacity and exhaustion of NSC populations (Figure 8.1). Further studies are required to test this hypothesis, and these will be discussed below.

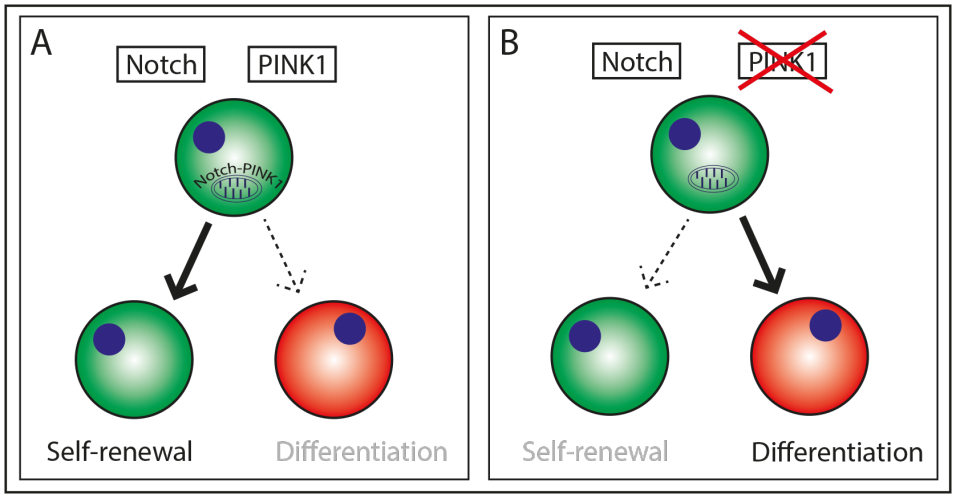

Figure 8.1: Schematic illustrating a proposed mechanism of reduced DA neurogenesis in adult life in *pink1* knockout zebrafish.

8.2 Future directions

8.2.1 Dopaminergic populations in the zebrafish and mammalian brain

The zebrafish is a powerful tool to study DA neurogenesis. For example, zebrafish and mammals share similar functional organisation of the DA neuron system and also share many of the mechanisms that regulate neurogenesis.

Furthermore, there are several readily-available conditional lineage tracing lines that allow reliable and robust analysis of neurogenic potential. My analyses of DA neurogenesis begin to provide evidence that ascending DA neurons can be generated in the adult vertebrate brain. However, as discussed above, the exact homology between mammalian and zebrafish DA neuron populations is yet to be fully elucidated. Furthermore, the precise role and function of each DA neuron population in the zebrafish brain is not yet known. Understanding this could provide novel insight into the neurogenic potential of ascending DA neuron populations. To this end, future studies should be directed towards analysing the molecular characteristics of ascending DA neurons in the adult mammalian and zebrafish brain. An initial study could focus on determining whether a subset of DA neurons in the adult mammalian substantia nigra express OTP. Further analyses of the molecular characteristics of DA populations in the adult zebrafish brain could allow generation of conditional knockout zebrafish lines, allowing interpretation of the functional implication of loss of particular DA neuron subsets. Future studies should also be directed towards understanding the differences in proliferative and neurogenic potential between zebrafish and mammals. Here, an initial study could focus on assessing whether growth factors, such as FGF, are expressed in the PT and the substantia nigra. Certainly, in the embryo, *Fgf3* is expressed in the PT (Muthu et al., 2016), while in mammals, FGF2 and FGF20 are expressed in the substantia nigra and have been implicated in the survival of midbrain DA neurons (Ohmachi *et al.*, 2000; Timmer *et al.*, 2007). However, as yet, no study has systematically characterised FGF signalling through life, or examined its potential role in the maintenance of stem/progenitor populations.

8.2.2 The functional role of adult DA neurogenesis and the implications of its dysregulation in PD

In chapter 5, I showed that DA neurons in ascending and locally projecting populations of the zebrafish PT are generated in adulthood. Subsequently, in chapter 6, I demonstrated that adult DA neurogenesis of these populations of DA neurons was reduced in zebrafish lacking functional Pink1. On this basis, I hypothesise that reduced DA neurogenesis contributes to the pathogenesis of PD. However, this raises several important questions: (a) are newly generated DA neurons incorporated into existing neuronal networks?; (b) what is the functional significance of adult DA neurogenesis?; (c) does disruption of DA neurogenesis contribute to reduced DA signalling in PD? Thus, future experiments should be directed at answering these questions. Further, and on a smaller scale, I hypothesise that reduced DA neurogenesis in zebrafish lacking functional Pink1 is in part caused by reduced non-canonical Notch signalling and subsequently reduced self-renewal of NSCs. Further experiments could be performed to test this hypothesis. An initial study could focus on crossing the Her4 conditional lineage tracing line to the *pink1* knockout zebrafish line, to quantify the number of DA neurons arising from Her4-expressing stem/progenitor cells in *pink1*+/+ and *pink1*-/- zebrafish. These types of study will help to move forwards our understanding of the role of de novo neurogenesis in the adult brain, and the impact of its dysregulation in neurodegenerative disease.

Bibliography

Aarsland D, Brønnick K, Ehrt U, Deyn PPD, Tekin S, Emre M & Cummings JL (2007). Neuropsychiatric symptoms in patients with Parkinson's disease and dementia: frequency, profile and associated care giver stress. *J Neurol Neurosurg Psychiatry* **78,** 36–42.

Aasly JO, Vilariño-Güell C, Dachsel JC, Webber PJ, West AB, Haugarvoll K, Johansen KK, Toft M, Nutt JG, Payami H, Kachergus JM, Lincoln SJ, Felic A, Wider C, Soto-Ortolaza AI, Cobb SA, White LR, Ross OA & Farrer MJ (2010). Novel pathogenic LRRK2 p.Asn1437His substitution in familial Parkinson's disease. *Mov Disord Off J Mov Disord Soc* **25,** 2156–2163.

Abbott RD, Petrovitch H, White LR, Masaki KH, Tanner CM, Curb JD, Grandinetti A, Blanchette PL, Popper JS & Ross GW (2001). Frequency of bowel movements and the future risk of Parkinson's disease. *Neurology* **57,** 456–462.

Adolf B, Chapouton P, Lam CS, Topp S, Tannhäuser B, Strähle U, Götz M & Bally-Cuif L (2006). Conserved and acquired features of adult neurogenesis in the zebrafish telencephalon. *Dev Biol* **295,** 278–293.

Agnihotri SK, Shen R, Li J, Gao X & Büeler H (2017). Loss of PINK1 leads to metabolic deficits in adult neural stem cells and impedes differentiation of newborn neurons in the mouse hippocampus. *FASEB J Off Publ Fed Am Soc Exp Biol* **31,** 2839–2853.

Alcalay RN et al. (2010). Frequency of known mutations in early-onset Parkinson disease: implication for genetic counseling: the consortium on risk for early onset Parkinson disease study. *Arch Neurol* **67,** 1116–1122.

Altman J (1969). Autoradiographic and histological studies of postnatal neurogenesis. IV. Cell proliferation and migration in the anterior forebrain, with special reference to persisting neurogenesis in the olfactory bulb. *J Comp Neurol* **137,** 433–457.

Altman J & Das GD (1965). Autoradiographic and histological evidence of postnatal hippocampal neurogenesis in rats. *J Comp Neurol* **124,** 319–335.

Altman J & Das GD (1966). Autoradiographic and histological studies of postnatal neurogenesis. I. A longitudinal investigation of the kinetics, migration and transformation of cells incorporating tritiated thymidine in neonate rats, with special reference to postnatal neurogenesis in some brain regions. *J Comp Neurol* **126,** 337–389.

Alunni A & Bally-Cuif L (2016). A comparative view of regenerative neurogenesis in vertebrates. *Development* **143,** 741–753.

Alunni A, Krecsmarik M, Bosco A, Galant S, Pan L, Moens CB & Bally-Cuif L (2013). Notch3 signaling gates cell cycle entry and limits neural stem cell amplification in the adult pallium. *Dev Camb Engl* **140,** 3335–3347.

Alvarez-Buylla A, García-Verdugo JM & Tramontin AD (2001). A unified hypothesis on the lineage of neural stem cells. *Nat Rev Neurosci* **2,** 287–293.

Ampatzis K, Makantasi P & Dermon CR (2012). Cell proliferation pattern in adult zebrafish forebrain is sexually dimorphic. *Neuroscience* **226,** 367–381.

Andres-Mateos E, Mejias R, Sasaki M, Li X, Lin BM, Biskup S, Zhang L, Banerjee R, Thomas B, Yang L, Liu G, Beal MF, Huso DL, Dawson TM & Dawson VL (2009). Unexpected lack of hypersensitivity in LRRK2 knock-out mice to MPTP (1-methyl-4-phenyl-1,2,3,6-tetrahydropyridine). *J Neurosci Off J Soc Neurosci* **29,** 15846–15850.

Anichtchik O, Diekmann H, Fleming A, Roach A, Goldsmith P & Rubinsztein DC (2008). Loss of PINK1 function affects development and results in neurodegeneration in zebrafish. *J Neurosci Off J Soc Neurosci* **28,** 8199–8207.

Armstrong GAB, Liao M, You Z, Lissouba A, Chen BE & Drapeau P (2016). Homology Directed Knockin of Point Mutations in the Zebrafish tardbp and fus Genes in ALS Using the CRISPR/Cas9 System. *PLOS ONE* **11,** e0150188.

Atmaca M (2014). Drug-induced impulse control disorders: a review. *Curr Clin Pharmacol* **9,** 70–74.

Ayano G (2016). Dopamine: Receptors, Functions, Synthesis, Pathways, Locations and Mental Disorders: Review of Literatures. *J Ment Disord Treat*; DOI: 10.4172/2471-271X.1000120.

Bach J-P, Ziegler U, Deuschl G, Dodel R & Doblhammer-Reiter G (2011). Projected numbers of people with movement disorders in the years 2030 and 2050. *Mov Disord Off J Mov Disord Soc* **26,** 2286–2290.

Bailey TJ, El-Hodiri H, Zhang L, Shah R, Mathers PH & Jamrich M (2004). Regulation of vertebrate eye development by Rx genes. *Int J Dev Biol* **48,** 761–770.

Balordi F & Fishell G (2007). Hedgehog signaling in the subventricular zone is required for both the maintenance of stem cells and the migration of newborn neurons. *J Neurosci Off J Soc Neurosci* **27,** 5936–5947.

Baptista MAS, Dave KD, Frasier MA, Sherer TB, Greeley M, Beck MJ, Varsho JS, Parker GA, Moore C, Churchill MJ, Meshul CK & Fiske BK (2013). Loss of leucine-rich repeat kinase 2 (LRRK2) in rats leads to progressive abnormal phenotypes in peripheral organs. *PloS One* **8,** e80705.

Barbeau A, Roy M, Bernier G, Campanella G & Paris S (1987). Ecogenetics of Parkinson's disease: prevalence and environmental aspects in rural areas. *Can J Neurol Sci J Can Sci Neurol* **14,** 36–41.

Basak O & Taylor V (2007). Identification of self-replicating multipotent progenitors in the embryonic nervous system by high Notch activity and Hes5 expression. *Eur J Neurosci* **25,** 1006–1022.

Bayer SA, Yackel JW & Puri PS (1982). Neurons in the rat dentate gyrus granular layer substantially increase during juvenile and adult life. *Science* **216,** 890–892.

Bédard A, Gravel C & Parent A (2006). Chemical characterization of newly generated neurons in the striatum of adult primates. *Exp Brain Res* **170,** 501–512.

Bernier PJ, Bedard A, Vinet J, Levesque M & Parent A (2002). Newly generated neurons in the amygdala and adjoining cortex of adult primates. *Proc Natl Acad Sci U S A* **99,** 11464–11469.

Berwick DC & Harvey K (2012). LRRK2 functions as a Wnt signaling scaffold, bridging cytosolic proteins and membrane-localized LRP6. *Hum Mol Genet* **21,** 4966–4979.

Betarbet R, Sherer TB, MacKenzie G, Garcia-Osuna M, Panov AV & Greenamyre JT (2000). Chronic systemic pesticide exposure reproduces features of Parkinson's disease. *Nat Neurosci* **3,** 1301–1306.

Bhaya D, Davison M & Barrangou R (2011). CRISPR-Cas Systems in Bacteria and Archaea: Versatile Small RNAs for Adaptive Defense and Regulation. *Annu Rev Genet* **45,** 273–297.

Biebl M, Cooper CM, Winkler J & Kuhn HG (2000). Analysis of neurogenesis and programmed cell death reveals a self-renewing capacity in the adult rat brain. *Neurosci Lett* **291,** 17–20.

Bielen H & Houart C (2014). The Wnt cries many: Wnt regulation of neurogenesis through tissue patterning, proliferation, and asymmetric cell division. *Dev Neurobiol* **74,** 772–780.

Blackinton JG, Anvret A, Beilina A, Olson L, Cookson MR & Galter D (2007). Expression of PINK1 mRNA in human and rodent brain and in Parkinson's disease. *Brain Res* **1184,** 10–16.

Blechman J, Borodovsky N, Eisenberg M, Nabel-Rosen H, Grimm J & Levkowitz G (2007). Specification of hypothalamic neurons by dual regulation of the homeodomain protein Orthopedia. *Development* **134,** 4417–4426.

Bliek AM van der, Shen Q & Kawajiri S (2013). Mechanisms of Mitochondrial Fission and Fusion. *Cold Spring Harb Perspect Biol* **5,** a011072.

Bonaguidi MA, McGuire T, Hu M, Kan L, Samanta J & Kessler JA (2005). LIF and BMP signaling generate separate and discrete types of GFAP-expressing cells. *Dev Camb Engl* **132,** 5503–5514.

Bond AM, Bhalala OG & Kessler JA (2012). The Dynamic Role of Bone Morphogenetic Proteins in Neural Stem Cell Fate and Maturation. *Dev Neurobiol* **72,** 1068–1084.

Boniface EJ, Lu J, Victoroff T, Zhu M & Chen W (2009). FlEx-based transgenic reporter lines for visualization of Cre and Flp activity in live zebrafish. *Genes N Y N 2000* **47,** 484–491.

Borek LL, Kohn R & Friedman JH (2007). Phenomenology of dreams in Parkinson's disease. *Mov Disord Off J Mov Disord Soc* **22,** 198–202.

Bostantjopoulou S, Katsarou Z, Papadimitriou A, Veletza V, Hatzigeorgiou G & Lees A (2001). Clinical features of parkinsonian patients with the alpha-synuclein (G209A) mutation. *Mov Disord Off J Mov Disord Soc* **16,** 1007–1013.

Bravo-San Pedro JM, Niso-Santano M, Gómez-Sánchez R, Pizarro-Estrella E, Aiastui-Pujana A, Gorostidi A, Climent V, López de Maturana R, Sanchez-Pernaute R, López de Munain A, Fuentes JM & González-Polo RA (2013). The LRRK2 G2019S mutant exacerbates basal autophagy through activation of the MEK/ERK pathway. *Cell Mol Life Sci CMLS* **70,** 121–136.

Brenowitz EA & Larson TA (2015). Neurogenesis in the Adult Avian Song-Control System. *Cold Spring Harb Perspect Biol* **7,** a019000.

Bretaud S, Lee S & Guo S (2004). Sensitivity of zebrafish to environmental toxins implicated in Parkinson's disease. *Neurotoxicol Teratol* **26,** 857–864.

Brooks J, Ding J, Simon-Sanchez J, Paisan-Ruiz C, Singleton AB & Scholz SW (2009). Parkin and PINK1 mutations in early-onset Parkinson's disease: comprehensive screening in publicly available cases and control. *J Med Genet* **46,** 375–381.

Cameron HA & McKay RD (1999). Restoring production of hippocampal neurons in old age. *Nat Neurosci* **2,** 894–897.

Cameron HA & McKay RD (2001). Adult neurogenesis produces a large pool of new granule cells in the dentate gyrus. *J Comp Neurol* **435,** 406–417.

Capilla-Gonzalez V, Herranz-Pérez V & García-Verdugo JM (2015). The aged brain: genesis and fate of residual progenitor cells in the subventricular zone. *Front Cell Neurosci*; DOI: 10.3389/fncel.2015.00365.

Cau E, Gradwohl G, Casarosa S, Kageyama R & Guillemot F (2000). Hes genes regulate sequential stages of neurogenesis in the olfactory epithelium. *Dev Camb Engl* **127,** 2323–2332.

Chang D, Nalls MA, Hallgrímsdóttir IB, Hunkapiller J, van der Brug M, Cai F, International Parkinson's Disease Genomics Consortium, 23andMe Research Team, Kerchner GA, Ayalon G, Bingol B, Sheng M, Hinds D, Behrens TW, Singleton AB, Bhangale TR & Graham RR (2017). A meta-analysis of genome-wide association studies identifies 17 new Parkinson's disease risk loci. *Nat Genet* **49,** 1511–1516.

Chapouton P, Skupien P, Hesl B, Coolen M, Moore JC, Madelaine R, Kremmer E, Faus-Kessler T, Blader P, Lawson ND & Bally-Cuif L (2010). Notch activity levels control the balance between quiescence and recruitment of adult neural stem cells. *J Neurosci Off J Soc Neurosci* **30,** 7961–7974.

Chapouton P, Webb KJ, Stigloher C, Alunni A, Adolf B, Hesl B, Topp S, Kremmer E & Bally-Cuif L (2011). Expression of Hairy/enhancer of split genes in neural progenitors and neurogenesis domains of the adult zebrafish brain. *J Comp Neurol* **519,** 1748–1769.

Chen H-L, Yuh C-H & Wu KK (2010). Nestin Is Essential for Zebrafish Brain and Eye Development through Control of Progenitor Cell Apoptosis. *PLOS ONE* **5,** e9318.

Chesselet M-F (2008). In vivo alpha-synuclein overexpression in rodents: a useful model of Parkinson's disease? *Exp Neurol* **209,** 22–27.

Chishti MA, Bohlega S, Ahmed M, Loualich A, Carroll P, Sato C, St George-Hyslop P, Westaway D & Rogaeva E (2006). T313M PINK1 mutation in an extended highly consanguineous Saudi family with early-onset Parkinson disease. *Arch Neurol* **63,** 1483–1485.

Cho HJ, Liu G, Jin SM, Parisiadou L, Xie C, Yu J, Sun L, Ma B, Ding J, Vancraenenbroeck R, Lobbestael E, Baekelandt V, Taymans J-M, He P, Troncoso JC, Shen Y & Cai H (2013). MicroRNA-205 regulates the expression of Parkinson's disease-related leucine-rich repeat kinase 2 protein. *Hum Mol Genet* **22,** 608–620.

Choi JM et al. (2008). Analysis of PARK genes in a Korean cohort of early-onset Parkinson disease. *Neurogenetics* **9,** 263–269.

Clark IE, Dodson MW, Jiang C, Cao JH, Huh JR, Seol JH, Yoo SJ, Hay BA & Guo M (2006). Drosophila pink1 is required for mitochondrial function and interacts genetically with parkin. *Nature* **441,** 1162–1166.

Connolly BS & Lang AE (2014). Pharmacological treatment of Parkinson disease: a review. *JAMA* **311,** 1670–1683.

Correia Guedes L, Ferreira JJ, Rosa MM, Coelho M, Bonifati V & Sampaio C (2010). Worldwide frequency of G2019S LRRK2 mutation in Parkinson's disease: a systematic review. *Parkinsonism Relat Disord* **16,** 237–242.

Crespo D, Stanfield BB & Cowan WM (1986). Evidence that late-generated granule cells do not simply replace earlier formed neurons in the rat dentate gyrus. *Exp Brain Res* **62,** 541–548.

Dawson TM & Dawson VL (2010). The Role of Parkin in Familial and Sporadic Parkinson's Disease. *Mov Disord Off J Mov Disord Soc* **25,** S32–S39.

Dayer AG, Cleaver KM, Abouantoun T & Cameron HA (2005). New GABAergic interneurons in the adult neocortex and striatum are generated from different precursors. *J Cell Biol* **168,** 415–427.

Deas E, Plun-Favreau H, Gandhi S, Desmond H, Kjaer S, Loh SHY, Renton AEM, Harvey RJ, Whitworth AJ, Martins LM, Abramov AY & Wood NW (2011). PINK1 cleavage at position A103 by the mitochondrial protease PARL. *Hum Mol Genet* **20,** 867–879.

Deng H, Jankovic J, Guo Y, Xie W & Le W (2005). Small interfering RNA targeting the PINK1 induces apoptosis in dopaminergic cells SH-SY5Y. *Biochem Biophys Res Commun* **337,** 1133–1138.

Dirian L, Galant S, Coolen M, Chen W, Bedu S, Houart C, Bally-Cuif L & Foucher I (2014). Spatial Regionalization and Heterochrony in the Formation of Adult Pallial Neural Stem Cells. *Dev Cell* **30,** 123–136.

Doetsch F, Caillé I, Lim DA, García-Verdugo JM & Alvarez-Buylla A (1999). Subventricular Zone Astrocytes Are Neural Stem Cells in the Adult Mammalian Brain. *Cell* **97,** 703–716.

Edelmann K, Glashauser L, Sprungala S, Hesl B, Fritschle M, Ninkovic J, Godinho L & Chapouton P (2013). Increased radial glia quiescence, decreased reactivation upon injury and unaltered neuroblast behavior underlie decreased neurogenesis in the aging zebrafish telencephalon. *J Comp Neurol* **521,** 3099–3115.

Ehninger D & Kempermann G (2003). Regional effects of wheel running and environmental enrichment on cell genesis and microglia proliferation in the adult murine neocortex. *Cereb Cortex N Y N 1991* **13,** 845–851.

El-Khodor BF, Oo TF, Kholodilov N & Burke RE (2003). Ectopic expression of cell cycle markers in models of induced programmed cell death in dopamine neurons of the rat substantia nigra pars compacta. *Exp Neurol* **179,** 17–27.

Enwere E, Shingo T, Gregg C, Fujikawa H, Ohta S & Weiss S (2004). Aging results in reduced epidermal growth factor receptor signaling, diminished olfactory neurogenesis, and deficits in fine olfactory discrimination. *J Neurosci Off J Soc Neurosci* **24,** 8354–8365.

Eriksson PS, Perfilieva E, Björk-Eriksson T, Alborn A-M, Nordborg C, Peterson DA & Gage FH (1998). Neurogenesis in the adult human hippocampus. *Nat Med* **4,** 1313–1317.

Fabre E, Monserrat J, Herrero A, Barja G & Leret ML (1999). Effect of MPTP on brain mitochondrial H2O2 and ATP production and on dopamine and DOPAC in the striatum. *J Physiol Biochem* **55,** 325–331.

Fahn S (2000). The spectrum of levodopa-induced dyskinesias. *Ann Neurol* **47,** S2-9; discussion S9-11.

Fahn S (2003). Description of Parkinson's Disease as a Clinical Syndrome. *Ann N Y Acad Sci* **991,** 1–14.

Fall PA, Fredrikson M, Axelson O & Granérus AK (1999). Nutritional and occupational factors influencing the risk of Parkinson's disease: a case-control study in southeastern Sweden. *Mov Disord Off J Mov Disord Soc* **14,** 28–37.

Fernandes AM, Beddows E, Filippi A & Driever W (2013). Orthopedia transcription factor otpa and otpb paralogous genes function during dopaminergic and neuroendocrine cell specification in larval zebrafish. *PloS One* **8,** e75002.

Filippi A, Dürr K, Ryu S, Willaredt M, Holzschuh J & Driever W (2007). Expression and function of nr4a2, lmx1b, and pitx3 in zebrafish dopaminergic and noradrenergic neuronal development. *BMC Dev Biol* **7,** 135.

Fleming L, Mann JB, Bean J, Briggle T & Sanchez-Ramos JR (1994). Parkinson's disease and brain levels of organochlorine pesticides. *Ann Neurol* **36,** 100–103.

Flinn L, Mortiboys H, Volkmann K, Köster RW, Ingham PW & Bandmann O (2009). Complex I deficiency and dopaminergic neuronal cell loss in parkin-deficient zebrafish (Danio rerio). *Brain J Neurol* **132,** 1613–1623.

Flinn LJ, Keatinge M, Bretaud S, Mortiboys H, Matsui H, De Felice E, Woodroof HI, Brown L, McTighe A, Soellner R, Allen CE, Heath PR, Milo M, Muqit MMK, Reichert AS,

Köster RW, Ingham PW & Bandmann O (2013). TigarB causes mitochondrial dysfunction and neuronal loss in PINK1 deficiency. *Ann Neurol* **74,** 837–847.

Frielingsdorf H, Schwarz K, Brundin P & Mohapel P (2004). No evidence for new dopaminergic neurons in the adult mammalian substantia nigra. *Proc Natl Acad Sci U S A* **101,** 10177–10182.

Fronczek R, Overeem S, Lee SYY, Hegeman IM, van Pelt J, Duinen V, G S, Lammers GJ & Swaab DF (2007). Hypocretin (orexin) loss in Parkinson's disease. *Brain* **130,** 1577–1585.

Gandhi S, Muqit MMK, Stanyer L, Healy DG, Abou-Sleiman PM, Hargreaves I, Heales S, Ganguly M, Parsons L, Lees AJ, Latchman DS, Holton JL, Wood NW & Revesz T (2006). PINK1 protein in normal human brain and Parkinson's disease. *Brain J Neurol* **129,** 1720–1731.

Ganz J, Kaslin J, Hochmann S, Freudenreich D & Brand M (2010*a*). Heterogeneity and Fgf dependence of adult neural progenitors in the zebrafish telencephalon. *Glia* **58,** 1345–1363.

Ganz J, Kaslin J, Hochmann S, Freudenreich D & Brand M (2010*b*). Heterogeneity and Fgf dependence of adult neural progenitors in the zebrafish telencephalon. *Glia* **58,** 1345–1363.

Gautier CA, Kitada T & Shen J (2008). Loss of PINK1 causes mitochondrial functional defects and increased sensitivity to oxidative stress. *Proc Natl Acad Sci U S A* **105,** 11364–11369.

Gehrke S, Imai Y, Sokol N & Lu B (2010). Pathogenic LRRK2 negatively regulates microRNA-mediated translational repression. *Nature* **466,** 637–641.

Gispert S et al. (2009). Parkinson phenotype in aged PINK1-deficient mice is accompanied by progressive mitochondrial dysfunction in absence of neurodegeneration. *PloS One* **4,** e5777.

Gjerstad MD, Wentzel-Larsen T, Aarsland D & Larsen JP (2007). Insomnia in Parkinson's disease: frequency and progression over time. *J Neurol Neurosurg Psychiatry* **78,** 476–479.

Golbe LI (1991). Young-onset Parkinson's disease: a clinical review. *Neurology* **41,** 168–173.

Golbe LI, Di Iorio G, Sanges G, Lazzarini AM, La Sala S, Bonavita V & Duvoisin RC (1996). Clinical genetic analysis of Parkinson's disease in the Contursi kindred. *Ann Neurol* **40,** 767–775.

Goldberg MS, Fleming SM, Palacino JJ, Cepeda C, Lam HA, Bhatnagar A, Meloni EG, Wu N, Ackerson LC, Klapstein GJ, Gajendiran M, Roth BL, Chesselet M-F, Maidment NT, Levine MS & Shen J (2003). Parkin-deficient mice exhibit nigrostriatal deficits but not loss of dopaminergic neurons. *J Biol Chem* **278,** 43628–43635.

González-Fernández MC, Lezcano E, Ross OA, Gómez-Esteban JC, Gómez-Busto F, Velasco F, Alvarez-Alvarez M, Rodríguez-Martínez MB, Ciordia R, Zarranz JJ, Farrer MJ,

Mata IF & de Pancorbo MM (2007). Lrrk2-associated parkinsonism is a major cause of disease in Northern Spain. *Parkinsonism Relat Disord* **13,** 509–515.

Gorrell JM, DiMonte D & Graham D (1996). The role of the environment in Parkinson's disease. *Environ Health Perspect* **104,** 652–654.

Gould E (2007). How widespread is adult neurogenesis in mammals? *Nat Rev Neurosci* **8,** 481.

Gould E, Reeves AJ, Graziano MS & Gross CG (1999). Neurogenesis in the neocortex of adult primates. *Science* **286,** 548–552.

Gould E, Vail N, Wagers M & Gross CG (2001). Adult-generated hippocampal and neocortical neurons in macaques have a transient existence. *Proc Natl Acad Sci U S A* **98,** 10910–10917.

Grandel H, Kaslin J, Ganz J, Wenzel I & Brand M (2006). Neural stem cells and neurogenesis in the adult zebrafish brain: Origin, proliferation dynamics, migration and cell fate. *Dev Biol* **295,** 263–277.

Groiss SJ, Wojtecki L, Südmeyer M & Schnitzler A (2009). Review: Deep brain stimulation in Parkinson's disease. *Ther Adv Neurol Disord* **2,** 379–391.

Haan N, Goodman T, Najdi-Samiei A, Stratford CM, Rice R, El Agha E, Bellusci S & Hajihosseini MK (2013). Fgf10-expressing tanycytes add new neurons to the appetite/energy-balance regulating centers of the postnatal and adult hypothalamus. *J Neurosci Off J Soc Neurosci* **33,** 6170–6180.

Hakimi M, Selvanantham T, Swinton E, Padmore RF, Tong Y, Kabbach G, Venderova K, Girardin SE, Bulman DE, Scherzer CR, LaVoie MJ, Gris D, Park DS, Angel JB, Shen J, Philpott DJ & Schlossmacher MG (2011). Parkinson's disease-linked LRRK2 is expressed in circulating and tissue immune cells and upregulated following recognition of microbial structures. *J Neural Transm* **118,** 795–808.

Han Y-G, Spassky N, Romaguera-Ros M, Garcia-Verdugo J-M, Aguilar A, Schneider-Maunoury S & Alvarez-Buylla A (2008). Hedgehog signaling and primary cilia are required for the formation of adult neural stem cells. *Nat Neurosci* **11,** 277–284.

Hawkes CH (2008). The Prodromal Phase of Sporadic Parkinson's Disease: Does It Exist and If So How Long Is It? *Mov Disord* **23,** 1799–1807.

Hegarty SV, Sullivan AM & O'Keeffe GW (2013). Midbrain dopaminergic neurons: A review of the molecular circuitry that regulates their development. *Dev Biol* **379,** 123–138.

Hershko A & Ciechanover A (1998). The ubiquitin system. *Annu Rev Biochem* **67,** 425–479.

Herzig MC et al. (2011). LRRK2 protein levels are determined by kinase function and are crucial for kidney and lung homeostasis in mice. *Hum Mol Genet* **20,** 4209–4223.

Hinkle KM, Yue M, Behrouz B, Dächsel JC, Lincoln SJ, Bowles EE, Beevers JE, Dugger B, Winner B, Prots I, Kent CB, Nishioka K, Lin W-L, Dickson DW, Janus CJ, Farrer MJ & Melrose HL (2012). LRRK2 knockout mice have an intact dopaminergic system but

display alterations in exploratory and motor co-ordination behaviors. *Mol Neurodegener* **7,** 25.

Hwang D-Y, Ardayfio P, Kang UJ, Semina EV & Kim K-S (2003). Selective loss of dopaminergic neurons in the substantia nigra of Pitx3-deficient aphakia mice. *Brain Res Mol Brain Res* **114,** 123–131.

Ibáñez P, Bonnet A-M, Débarges B, Lohmann E, Tison F, Pollak P, Agid Y, Dürr A & Brice A (2004). Causal relation between alpha-synuclein gene duplication and familial Parkinson's disease. *Lancet Lond Engl* **364,** 1169–1171.

Imayoshi I, Sakamoto M, Ohtsuka T & Kageyama R (2009). Continuous neurogenesis in the adult brain. *Dev Growth Differ* **51,** 379–386.

Imayoshi I, Sakamoto M, Ohtsuka T, Takao K, Miyakawa T, Yamaguchi M, Mori K, Ikeda T, Itohara S & Kageyama R (2008). Roles of continuous neurogenesis in the structural and functional integrity of the adult forebrain. *Nat Neurosci* **11,** 1153.

Imayoshi I, Sakamoto M, Yamaguchi M, Mori K & Kageyama R (2010). Essential roles of Notch signaling in maintenance of neural stem cells in developing and adult brains. *J Neurosci Off J Soc Neurosci* **30,** 3489–3498.

Ingham PW & Placzek M (2006). Orchestrating ontogenesis: variations on a theme by sonic hedgehog. *Nat Rev Genet* **7,** 841–850.

Jager WADH & Bethlem J (1960). THE DISTRIBUTION OF LEWY BODIES IN THE CENTRAL AND AUTONOMIC NERVOUS SYSTEMS IN IDIOPATHIC PARALYSIS AGITANS. *J Neurol Neurosurg Psychiatry* **23,** 283–290.

Jankovic J (2008). Parkinson's disease: clinical features and diagnosis. *J Neurol Neurosurg Psychiatry* **79,** 368–376.

Jankovic J & Aguilar LG (2008). Current approaches to the treatment of Parkinson's disease. *Neuropsychiatr Dis Treat* **4,** 743–757.

Jin K, Sun Y, Xie L, Batteur S, Mao XO, Smelick C, Logvinova A & Greenberg DA (2003). Neurogenesis and aging: FGF-2 and HB-EGF restore neurogenesis in hippocampus and subventricular zone of aged mice. *Aging Cell* **2,** 175–183.

Jin SM, Lazarou M, Wang C, Kane LA, Narendra DP & Youle RJ (2010). Mitochondrial membrane potential regulates PINK1 import and proteolytic destabilization by PARL. *J Cell Biol* **191,** 933–942.

Kageyama R, Ohtsuka T & Kobayashi T (2008). Roles of Hes genes in neural development. *Dev Growth Differ* **50 Suppl 1,** S97-103.

Kaplan MS, McNelly NA & Hinds JW (1985). Population dynamics of adult-formed granule neurons of the rat olfactory bulb. *J Comp Neurol* **239,** 117–125.

Kay JN & Blum M (2000). Differential response of ventral midbrain and striatal progenitor cells to lesions of the nigrostriatal dopaminergic projection. *Dev Neurosci* **22,** 56–67.

Kempermann G, Gast D & Gage FH (2002). Neuroplasticity in old age: sustained fivefold induction of hippocampal neurogenesis by long-term environmental enrichment. *Ann Neurol* **52,** 135–143.

Kempermann G, Gast D, Kronenberg G, Yamaguchi M & Gage FH (2003). Early determination and long-term persistence of adult-generated new neurons in the hippocampus of mice. *Dev Camb Engl* **130,** 391–399.

Kennedy BN, Stearns GW, Smyth VA, Ramamurthy V, van Eeden F, Ankoudinova I, Raible D, Hurley JB & Brockerhoff SE (2004). Zebrafish rx3 and mab21l2 are required during eye morphogenesis. *Dev Biol* **270,** 336–349.

Khacho M, Clark A, Svoboda DS, Azzi J, MacLaurin JG, Meghaizel C, Sesaki H, Lagace DC, Germain M, Harper M-E, Park DS & Slack RS (2016). Mitochondrial Dynamics Impacts Stem Cell Identity and Fate Decisions by Regulating a Nuclear Transcriptional Program. *Cell Stem Cell* **19,** 232–247.

Ki C-S, Stavrou EF, Davanos N, Lee WY, Chung EJ, Kim J-Y & Athanassiadou A (2007). The Ala53Thr mutation in the alpha-synuclein gene in a Korean family with Parkinson disease. *Clin Genet* **71,** 471–473.

Kitada T, Asakawa S, Hattori N, Matsumine H, Yamamura Y, Minoshima S, Yokochi M, Mizuno Y & Shimizu N (1998). Mutations in the parkin gene cause autosomal recessive juvenile parkinsonism. *Nature* **392,** 605–608.

Kokoeva MV, Yin H & Flier JS (2005). Neurogenesis in the hypothalamus of adult mice: potential role in energy balance. *Science* **310,** 679–683.

Kornack DR & Rakic P (2001). Cell proliferation without neurogenesis in adult primate neocortex. *Science* **294,** 2127–2130.

Kowal SL, Dall TM, Chakrabarti R, Storm MV & Jain A (2013). The current and projected economic burden of Parkinson's disease in the United States. *Mov Disord Off J Mov Disord Soc* **28,** 311–318.

Kretzschmar K & Watt FM (2012). Lineage Tracing. *Cell* **148,** 33–45.

Kriegstein A & Alvarez-Buylla A (2009). The glial nature of embryonic and adult neural stem cells. *Annu Rev Neurosci* **32,** 149–184.

Kroehne V, Freudenreich D, Hans S, Kaslin J & Brand M (2011). Regeneration of the adult zebrafish brain from neurogenic radial glia-type progenitors. *Development* **138,** 4831–4841.

Krüger R, Kuhn W, Müller T, Woitalla D, Graeber M, Kösel S, Przuntek H, Epplen JT, Schols L & Riess O (1998). AlaSOPro mutation in the gene encoding α-synuclein in Parkinson's disease. *Nat Genet* **18,** 106–108.

Kuhn HG, Dickinson-Anson H & Gage FH (1996). Neurogenesis in the dentate gyrus of the adult rat: age-related decrease of neuronal progenitor proliferation. *J Neurosci Off J Soc Neurosci* **16,** 2027–2033.

Kuhn HG, Winkler J, Kempermann G, Thal LJ & Gage FH (1997). Epidermal growth factor and fibroblast growth factor-2 have different effects on neural progenitors in the adult rat brain. *J Neurosci Off J Soc Neurosci* **17,** 5820–5829.

Kumari U & Tan EK (2009). LRRK2 in Parkinson's disease: genetic and clinical studies from patients. *FEBS J* **276,** 6455–6463.

Kurowska M, Daszkowska-Golec A, Gruszka D, Marzec M, Szurman M, Szarejko I & Maluszynski M (2011). TILLING - a shortcut in functional genomics. *J Appl Genet* **52,** 371–390.

Lam CS, März M & Strähle U (2009). gfap and nestin reporter lines reveal characteristics of neural progenitors in the adult zebrafish brain. *Dev Dyn* **238,** 475–486.

Lam Hoa A., Wu Nanping, Cely Ingrid, Kelly Rachel L., Hean Sindalana, Richter Franziska, Magen Iddo, Cepeda Carlos, Ackerson Larry C., Walwyn Wendy, Masliah Eliezer, Chesselet Marie-Françoise, Levine Michael S. & Maidment Nigel T. (2011). Elevated tonic extracellular dopamine concentration and altered dopamine modulation of synaptic activity precede dopamine loss in the striatum of mice overexpressing human α-synuclein. *J Neurosci Res* **89,** 1091–1102.

Lasky JL & Wu H (2005). Notch signaling, brain development, and human disease. *Pediatr Res* **57,** 104R-109R.

de Lau LM & Breteler MM (2006). Epidemiology of Parkinson's disease. *Lancet Neurol* **5,** 525–535.

Le Grand JN, Gonzalez-Cano L, Pavlou MA & Schwamborn JC (2015). Neural stem cells in Parkinson's disease: a role for neurogenesis defects in onset and progression. *Cell Mol Life Sci CMLS* **72,** 773–797.

Lee K-S, Wu Z, Song Y, Mitra SS, Feroze AH, Cheshier SH & Lu B (2013). Roles of PINK1, mTORC2, and mitochondria in preserving brain tumor-forming stem cells in a noncanonical Notch signaling pathway. *Genes Dev* **27,** 2642–2647.

Lee SB, Kim W, Lee S & Chung J (2007). Loss of LRRK2/PARK8 induces degeneration of dopaminergic neurons in Drosophila. *Biochem Biophys Res Commun* **358,** 534–539.

Lesage S & Brice A (2009). Parkinson's disease: from monogenic forms to genetic susceptibility factors. *Hum Mol Genet* **18,** R48-59.

Lesage S, Dürr A, Tazir M, Lohmann E, Leutenegger A-L, Janin S, Pollak P, Brice A & French Parkinson's Disease Genetics Study Group (2006). LRRK2 G2019S as a cause of Parkinson's disease in North African Arabs. *N Engl J Med* **354,** 422–423.

Li X, Patel JC, Wang J, Avshalumov MV, Nicholson C, Buxbaum JD, Elder GA, Rice ME & Yue Z (2010). Enhanced striatal dopamine transmission and motor performance with LRRK2 overexpression in mice is eliminated by familial Parkinson's disease mutation G2019S. *J Neurosci Off J Soc Neurosci* **30,** 1788–1797.

Li Y, Liu W, Oo TF, Wang L, Tang Y, Jackson-Lewis V, Zhou C, Geghman K, Bogdanov M, Przedborski S, Beal MF, Burke RE & Li C (2009). Mutant LRRK2(R1441G) BAC

transgenic mice recapitulate cardinal features of Parkinson's disease. *Nat Neurosci* **12,** 826–828.

Lichtenwalner RJ, Forbes ME, Bennett SA, Lynch CD, Sonntag WE & Riddle DR (2001). Intracerebroventricular infusion of insulin-like growth factor-I ameliorates the age-related decline in hippocampal neurogenesis. *Neuroscience* **107,** 603–613.

Lie D-C, Colamarino SA, Song H-J, Désiré L, Mira H, Consiglio A, Lein ES, Jessberger S, Lansford H, Dearie AR & Gage FH (2005). Wnt signalling regulates adult hippocampal neurogenesis. *Nature* **437,** 1370–1375.

Lie DC, Dziewczapolski G, Willhoite AR, Kaspar BK, Shults CW & Gage FH (2002). The adult substantia nigra contains progenitor cells with neurogenic potential. *J Neurosci Off J Soc Neurosci* **22,** 6639–6649.

Lim K-L & Tan JM (2007). Role of the ubiquitin proteasome system in Parkinson's disease. *BMC Biochem* **8,** S13.

Lin W & Kang UJ (2008). Characterization of PINK1 processing, stability, and subcellular localization. *J Neurochem* **106,** 464–474.

Liu Z, Wang X, Yu Y, Li X, Wang T, Jiang H, Ren Q, Jiao Y, Sawa A, Moran T, Ross CA, Montell C & Smith WW (2008). A Drosophila model for LRRK2-linked parkinsonism. *Proc Natl Acad Sci U S A* **105,** 2693–2698.

Loosli F, Staub W, Finger-Baier KC, Ober EA, Verkade H, Wittbrodt J & Baier H (2003). Loss of eyes in zebrafish caused by mutation of chokh/rx3. *EMBO Rep* **4,** 894–899.

Lücking CB, Dürr A, Bonifati V, Vaughan J, De Michele G, Gasser T, Harhangi BS, Meco G, Denèfle P, Wood NW, Agid Y, Brice A, French Parkinson's Disease Genetics Study Group & European Consortium on Genetic Susceptibility in Parkinson's Disease (2000). Association between early-onset Parkinson's disease and mutations in the parkin gene. *N Engl J Med* **342,** 1560–1567.

Lugert S, Basak O, Knuckles P, Haussler U, Fabel K, Götz M, Haas CA, Kempermann G, Taylor V & Giachino C (2010). Quiescent and active hippocampal neural stem cells with distinct morphologies respond selectively to physiological and pathological stimuli and aging. *Cell Stem Cell* **6,** 445–456.

Luo J, Daniels SB, Lennington JB, Notti RQ & Conover JC (2006). The aging neurogenic subventricular zone. *Aging Cell* **5,** 139–152.

Luzón-Toro B, Rubio de la Torre E, Delgado A, Pérez-Tur J & Hilfiker S (2007). Mechanistic insight into the dominant mode of the Parkinson's disease-associated G2019S LRRK2 mutation. *Hum Mol Genet* **16,** 2031–2039.

Luzzati F, De Marchis S, Fasolo A & Peretto P (2006). Neurogenesis in the caudate nucleus of the adult rabbit. *J Neurosci Off J Soc Neurosci* **26,** 609–621.

MacLeod DA, Rhinn H, Kuwahara T, Zolin A, Di Paolo G, McCabe BD, MacCabe BD, Marder KS, Honig LS, Clark LN, Small SA & Abeliovich A (2013). RAB7L1 interacts with LRRK2 to modify intraneuronal protein sorting and Parkinson's disease risk. *Neuron* **77,** 425–439.

Mahler J, Filippi A & Driever W (2010). DeltaA/DeltaD regulate multiple and temporally distinct phases of notch signaling during dopaminergic neurogenesis in zebrafish. *J Neurosci Off J Soc Neurosci* **30,** 16621–16635.

Marsden CD (1990). Parkinson's disease. *Lancet Lond Engl* **335,** 948–952.

Mata IF, Kachergus JM, Taylor JP, Lincoln S, Aasly J, Lynch T, Hulihan MM, Cobb SA, Wu R-M, Lu C-S, Lahoz C, Wszolek ZK & Farrer MJ (2005). Lrrk2 pathogenic substitutions in Parkinson's disease. *Neurogenetics* **6,** 171–177.

Mathers PH, Grinberg A, Mahon KA & Jamrich M (1997). The Rx homeobox gene is essential for vertebrate eye development. *Nature* **387,** 603–607.

Matsuda S, Kitagishi Y & Kobayashi M (2013). Function and Characteristics of PINK1 in Mitochondria. *Oxid Med Cell Longev*; DOI: 10.1155/2013/601587.

Matsuzaki K, Katakura M, Hara T, Li G, Hashimoto M & Shido O (2009). Proliferation of neuronal progenitor cells and neuronal differentiation in the hypothalamus are enhanced in heat-acclimated rats. *Pflugers Arch* **458,** 661–673.

Matta S et al. (2012). LRRK2 controls an EndoA phosphorylation cycle in synaptic endocytosis. *Neuron* **75,** 1008–1021.

McPherson AD, Barrios JP, Luks-Morgan SJ, Manfredi JP, Bonkowsky JL, Douglass AD & Dorsky RI (2016). Motor Behavior Mediated by Continuously Generated Dopaminergic Neurons in the Zebrafish Hypothalamus Recovers after Cell Ablation. *Curr Biol CB*; DOI: 10.1016/j.cub.2015.11.064.

Medina-Martinez O, Amaya-Manzanares F, Liu C, Mendoza M, Shah R, Zhang L, Behringer RR, Mahon KA & Jamrich M (2009). Cell-Autonomous Requirement for Rx Function in the Mammalian Retina and Posterior Pituitary. *PLOS ONE* **4,** e4513.

Menuet A, Pellegrini E, Brion F, Gueguen M-M, Anglade I, Pakdel F & Kah O (2005). Expression and estrogen-dependent regulation of the zebrafish brain aromatase gene. *J Comp Neurol* **485,** 304–320.

Michell AW, Barker RA, Raha SK & Raha-Chowdhury R (2005). A case of late onset sporadic Parkinson's disease with an A53T mutation in alpha-synuclein. *J Neurol Neurosurg Psychiatry* **76,** 596–597.

Migaud M, Batailler M, Segura S, Duittoz A, Franceschini I & Pillon D (2010). Emerging new sites for adult neurogenesis in the mammalian brain: a comparative study between the hypothalamus and the classical neurogenic zones. *Eur J Neurosci* **32,** 2042–2052.

Mills RD, Sim CH, Mok SS, Mulhern TD, Culvenor JG & Cheng H-C (2008). Biochemical aspects of the neuroprotective mechanism of PTEN-induced kinase-1 (PINK1). *J Neurochem* **105,** 18–33.

Milosevic J, Schwarz SC, Ogunlade V, Meyer AK, Storch A & Schwarz J (2009). Emerging role of LRRK2 in human neural progenitor cell cycle progression, survival and differentiation. *Mol Neurodegener* **4,** 25.

Ming G & Song H (2005). Adult Neurogenesis in the Mammalian Central Nervous System. *Annu Rev Neurosci* **28,** 223–250.

Ming G-L & Song H (2011). Adult neurogenesis in the mammalian brain: significant answers and significant questions. *Neuron* **70,** 687–702.

Mizuno Y, Sone N & Saitoh T (1987). Effects of 1-methyl-4-phenyl-1,2,3,6-tetrahydropyridine and 1-methyl-4-phenylpyridinium ion on activities of the enzymes in the electron transport system in mouse brain. *J Neurochem* **48,** 1787–1793.

Moehle MS, Webber PJ, Tse T, Sukar N, Standaert DG, DeSilva TM, Cowell RM & West AB (2012). LRRK2 Inhibition Attenuates Microglial Inflammatory Responses. *J Neurosci Off J Soc Neurosci* **32,** 1602–1611.

Moon HE & Paek SH (2015). Mitochondrial Dysfunction in Parkinson's Disease. *Exp Neurobiol* **24,** 103–116.

Mosimann C, Kaufman CK, Li P, Pugach EK, Tamplin OJ & Zon LI (2011). Ubiquitous transgene expression and Cre-based recombination driven by the ubiquitin promoter in zebrafish. *Dev Camb Engl* **138,** 169–177.

Mueller T & Wullimann MF (2002). BrdU-, neuroD (nrd)- and Hu-studies reveal unusual non-ventricular neurogenesis in the postembryonic zebrafish forebrain. *Mech Dev* **117,** 123–135.

Muranishi Y, Terada K & Furukawa T (2012). An essential role for Rax in retina and neuroendocrine system development. *Dev Growth Differ* **54,** 341–348.

Muthu V, Eachus H, Ellis P, Brown S & Placzek M (2016). Rx3 and Shh direct anisotropic growth and specification in the zebrafish tuberal/anterior hypothalamus. *Dev Camb Engl*; DOI: 10.1242/dev.138305.

Nalls MA et al. (2014). Large-scale meta-analysis of genome-wide association data identifies six new risk loci for Parkinson's disease. *Nat Genet* **46,** 989–993.

Nascimento LFR, Souza GFP, Morari J, Barbosa GO, Solon C, Moura RF, Victório SC, Ignácio-Souza LM, Razolli DS, Carvalho HF & Velloso LA (2016). n-3 Fatty Acids Induce Neurogenesis of Predominantly POMC-Expressing Cells in the Hypothalamus. *Diabetes* **65,** 673–686.

Ness D, Ren Z, Gardai S, Sharpnack D, Johnson VJ, Brennan RJ, Brigham EF & Olaharski AJ (2013). Leucine-rich repeat kinase 2 (LRRK2)-deficient rats exhibit renal tubule injury and perturbations in metabolic and immunological homeostasis. *PloS One* **8,** e66164.

Niwa A, Nishibori M, Hamasaki S, Kobori T, Liu K, Wake H, Mori S, Yoshino T & Takahashi H (2016). Voluntary exercise induces neurogenesis in the hypothalamus and ependymal lining of the third ventricle. *Brain Struct Funct* **221,** 1653–1666.

Noelanders R & Vleminckx K (2017). How Wnt Signaling Builds the Brain: Bridging Development and Disease. *The Neuroscientist* **23,** 314–329.

Nomura T, Göritz C, Catchpole T, Henkemeyer M & Frisén J (2010). EphB signaling controls lineage plasticity of adult neural stem cell niche cells. *Cell Stem Cell* **7,** 730–743.

Nottebohm F (1980). Testosterone triggers growth of brain vocal control nuclei in adult female canaries. *Brain Res* **189,** 429–436.

Nuber S et al. (2008). Neurodegeneration and Motor Dysfunction in a Conditional Model of Parkinson's Disease. *J Neurosci* **28,** 2471–2484.

Ohama E & Ikuta F (1976). Parkinson's disease: Distribution of Lewy bodies and monoamine neuron system. *Acta Neuropathol (Berl)* **34,** 311–319.

Ohmachi S, Watanabe Y, Mikami T, Kusu N, Ibi T, Akaike A & Itoh N (2000). FGF-20, a novel neurotrophic factor, preferentially expressed in the substantia nigra pars compacta of rat brain. *Biochem Biophys Res Commun* **277,** 355–360.

Okatsu K et al. (2012). PINK1 autophosphorylation upon membrane potential dissipation is essential for Parkin recruitment to damaged mitochondria. *Nat Commun* **3,** 1016.

Olanow CW, Perl DP, DeMartino GN & McNaught KSP (2004). Lewy-body formation is an aggresome-related process: a hypothesis. *Lancet Neurol* **3,** 496–503.

Oyanagi K, Wakabayashi K, Ohama E, Takeda S, Horikawa Y, Morita T & Ikuta F (1990). Lewy bodies in the lower sacral parasympathetic neurons of a patient with Parkinson's disease. *Acta Neuropathol (Berl)* **80,** 558–559.

Ozelius LJ, Senthil G, Saunders-Pullman R, Ohmann E, Deligtisch A, Tagliati M, Hunt AL, Klein C, Henick B, Hailpern SM, Lipton RB, Soto-Valencia J, Risch N & Bressman SB (2006). LRRK2 G2019S as a cause of Parkinson's disease in Ashkenazi Jews. *N Engl J Med* **354,** 424–425.

Paisán-Ruiz C, Lewis PA & Singleton AB (2013). LRRK2: Cause, Risk, and Mechanism. *J Park Dis* **3,** 85–103.

Paisán-Ruíz C et al. (2004). Cloning of the Gene Containing Mutations that Cause PARK8-Linked Parkinson's Disease. *Neuron* **44,** 595–600.

Palacino JJ, Sagi D, Goldberg MS, Krauss S, Motz C, Wacker M, Klose J & Shen J (2004). Mitochondrial dysfunction and oxidative damage in parkin-deficient mice. *J Biol Chem* **279,** 18614–18622.

Papadimitriou A, Veletza V, Hadjigeorgiou GM, Patrikiou A, Hirano M & Anastasopoulos I (1999). Mutated alpha-synuclein gene in two Greek kindreds with familial PD: incomplete penetrance? *Neurology* **52,** 651–654.

Papapetropoulos S, Paschalis C, Athanassiadou A, Papadimitriou A, Ellul J, Polymeropoulos MH & Papapetropoulos T (2001). Clinical phenotype in patients with alpha-synuclein Parkinson's disease living in Greece in comparison with patients with sporadic Parkinson's disease. *J Neurol Neurosurg Psychiatry* **70,** 662–665.

Parisiadou L, Xie C, Cho HJ, Lin X, Gu X-L, Long C-X, Lobbestael E, Baekelandt V, Taymans J-M, Sun L & Cai H (2009). Phosphorylation of ERM Proteins by LRRK2 Promotes the

Rearrangement of Actin Cytoskeleton in Neuronal Morphogenesis. *J Neurosci Off J Soc Neurosci* **29,** 13971–13980.

Park D, Xiang AP, Mao FF, Zhang L, Di C-G, Liu X-M, Shao Y, Ma B-F, Lee J-H, Ha K-S, Walton N & Lahn BT (2010). Nestin is required for the proper self-renewal of neural stem cells. *Stem Cells Dayt Ohio* **28,** 2162–2171.

Pearce RK, Hawkes CH & Daniel SE (1995). The anterior olfactory nucleus in Parkinson's disease. *Mov Disord Off J Mov Disord Soc* **10,** 283–287.

Pellegrini E, Mouriec K, Anglade I, Menuet A, Le Page Y, Gueguen M-M, Marmignon M-H, Brion F, Pakdel F & Kah O (2007). Identification of aromatase-positive radial glial cells as progenitor cells in the ventricular layer of the forebrain in zebrafish. *J Comp Neurol* **501,** 150–167.

Pencea V, Bingaman KD, Wiegand SJ & Luskin MB (2001). Infusion of brain-derived neurotrophic factor into the lateral ventricle of the adult rat leads to new neurons in the parenchyma of the striatum, septum, thalamus, and hypothalamus. *J Neurosci Off J Soc Neurosci* **21,** 6706–6717.

Perez FA & Palmiter RD (2005). Parkin-deficient mice are not a robust model of parkinsonism. *Proc Natl Acad Sci U S A* **102,** 2174–2179.

Pérez MR, Pellegrini E, Cano-Nicolau J, Gueguen M-M, Guillou DM-L, Merot Y, Vaillant C, Somoza GM & Kah O (2013). Relationships between radial glial progenitors and 5-HT neurons in the paraventricular organ of adult zebrafish – potential effects of serotonin on adult neurogenesis. *Eur J Neurosci* **38,** 3292–3301.

Pérez-Martín M, Cifuentes M, Grondona JM, López-Avalos MD, Gómez-Pinedo U, García-Verdugo JM & Fernández-Llebrez P (2010). IGF-I stimulates neurogenesis in the hypothalamus of adult rats. *Eur J Neurosci* **31,** 1533–1548.

Perier C, Tieu K, Guégan C, Caspersen C, Jackson-Lewis V, Carelli V, Martinuzzi A, Hirano M, Przedborski S & Vila M (2005). Complex I deficiency primes Bax-dependent neuronal apoptosis through mitochondrial oxidative damage. *Proc Natl Acad Sci* **102,** 19126–19131.

Petit A, Kawarai T, Paitel E, Sanjo N, Maj M, Scheid M, Chen F, Gu Y, Hasegawa H, Salehi-Rad S, Wang L, Rogaeva E, Fraser P, Robinson B, St George-Hyslop P & Tandon A (2005). Wild-type PINK1 prevents basal and induced neuronal apoptosis, a protective effect abrogated by Parkinson disease-related mutations. *J Biol Chem* **280,** 34025–34032.

Petreanu L & Alvarez-Buylla A (2002). Maturation and death of adult-born olfactory bulb granule neurons: role of olfaction. *J Neurosci Off J Soc Neurosci* **22,** 6106–6113.

Piccoli G, Condliffe SB, Bauer M, Giesert F, Boldt K, De Astis S, Meixner A, Sarioglu H, Vogt-Weisenhorn DM, Wurst W, Gloeckner CJ, Matteoli M, Sala C & Ueffing M (2011). LRRK2 controls synaptic vesicle storage and mobilization within the recycling pool. *J Neurosci Off J Soc Neurosci* **31,** 2225–2237.

Poewe W (2008). Non-motor symptoms in Parkinson's disease. *Eur J Neurol* **15,** 14–20.

Polymeropoulos MH et al. (1997). Mutation in the α-Synuclein Gene Identified in Families with Parkinson's Disease. *Science* **276,** 2045–2047.

Poole AC, Thomas RE, Andrews LA, McBride HM, Whitworth AJ & Pallanck LJ (2008). The PINK1/Parkin pathway regulates mitochondrial morphology. *Proc Natl Acad Sci* **105,** 1638–1643.

Porter AG & Jänicke RU (1999). Emerging roles of caspase-3 in apoptosis. *Cell Death Differ* **6,** 99–104.

Potashkin JA, Blume SR & Runkle NK (2011). Limitations of Animal Models of Parkinson's Disease. *Park Dis*; DOI: 10.4061/2011/658083. Available at: https://www.hindawi.com/journals/pd/2011/658083/ [Accessed March 17, 2018].

Poulopoulos M, Levy O & Alcalay R (2012). The Neuropathology of Genetic Parkinson's Disease. *Mov Disord* **27,** 831–842.

van Praag H, Kempermann G & Gage FH (1999). Running increases cell proliferation and neurogenesis in the adult mouse dentate gyrus. *Nat Neurosci* **2,** 266–270.

van Praag H, Schinder AF, Christie BR, Toni N, Palmer TD & Gage FH (2002). Functional neurogenesis in the adult hippocampus. *Nature* **415,** 1030–1034.

Pridgeon JW, Olzmann JA, Chin L-S & Li L (2007). PINK1 protects against oxidative stress by phosphorylating mitochondrial chaperone TRAP1. *PLoS Biol* **5,** e172.

Przedborski S, Jackson-Lewis V, Yokoyama R, Shibata T, Dawson VL & Dawson TM (1996). Role of neuronal nitric oxide in 1-methyl-4-phenyl-1,2,3,6-tetrahydropyridine (MPTP)-induced dopaminergic neurotoxicity. *Proc Natl Acad Sci U S A* **93,** 4565–4571.

Puschmann A (2013). Monogenic Parkinson's disease and parkinsonism: Clinical phenotypes and frequencies of known mutations. *Parkinsonism Relat Disord* **19,** 407–415.

Puschmann A, Ross OA, Vilariño-Güell C, Lincoln SJ, Kachergus JM, Cobb SA, Lindquist SG, Nielsen JE, Wszolek ZK, Farrer M, Widner H, van Westen D, Hägerström D, Markopoulou K, Chase BA, Nilsson K, Reimer J & Nilsson C (2009). A Swedish family with de novo alpha-synuclein A53T mutation: evidence for early cortical dysfunction. *Parkinsonism Relat Disord* **15,** 627–632.

Rakic P (2002). Progress: Neurogenesis in adult primate neocortex: an evaluation of the evidence. *Nat Rev Neurosci* **3,** 65–71.

Ramirez-Amaya V, Marrone DF, Gage FH, Worley PF & Barnes CA (2006). Integration of new neurons into functional neural networks. *J Neurosci Off J Soc Neurosci* **26,** 12237–12241.

Rao MS, Hattiangady B, Abdel-Rahman A, Stanley DP & Shetty AK (2005). Newly born cells in the ageing dentate gyrus display normal migration, survival and neuronal fate choice but endure retarded early maturation. *Eur J Neurosci* **21,** 464–476.

Recabal A, Caprile T & García-Robles M de LA (2017). Hypothalamic Neurogenesis as an Adaptive Metabolic Mechanism. *Front Neurosci* **11,** 190.

Ren G, Xin S, Li S, Zhong H & Lin S (2011). Disruption of LRRK2 Does Not Cause Specific Loss of Dopaminergic Neurons in Zebrafish. *PLoS ONE*; DOI: 10.1371/journal.pone.0020630.

Reynolds BA & Weiss S (1992). Generation of neurons and astrocytes from isolated cells of the adult mammalian central nervous system. *Science* **255,** 1707–1710.

Riddle DR & Lichtenwalner RJ (2007). Neurogenesis in the Adult and Aging Brain. In *Brain Aging: Models, Methods, and Mechanisms*, ed. Riddle DR, Frontiers in Neuroscience. CRC Press/Taylor & Francis, Boca Raton (FL). Available at: http://www.ncbi.nlm.nih.gov/books/NBK3874/ [Accessed March 5, 2018].

Rink E & Wullimann MF (2001*a*). The teleostean (zebrafish) dopaminergic system ascending to the subpallium (striatum) is located in the basal diencephalon (posterior tuberculum). *Brain Res* **889,** 316–330.

Rink E & Wullimann MF (2001*b*). The teleostean (zebrafish) dopaminergic system ascending to the subpallium (striatum) is located in the basal diencephalon (posterior tuberculum). *Brain Res* **889,** 316–330.

Rink E & Wullimann MF (2002*a*). Connections of the ventral telencephalon and tyrosine hydroxylase distribution in the zebrafish brain (Danio rerio) lead to identification of an ascending dopaminergic system in a teleost. *Brain Res Bull* **57,** 385–387.

Rink E & Wullimann MF (2002*b*). Development of the catecholaminergic system in the early zebrafish brain: an immunohistochemical study. *Dev Brain Res* **137,** 89–100.

Rink E & Wullimann MF (2004). Connections of the ventral telencephalon (subpallium) in the zebrafish (Danio rerio). *Brain Res* **1011,** 206–220.

Robins SC, Stewart I, McNay DE, Taylor V, Giachino C, Goetz M, Ninkovic J, Briancon N, Maratos-Flier E, Flier JS, Kokoeva MV & Placzek M (2013). α-Tanycytes of the adult hypothalamic third ventricle include distinct populations of FGF-responsive neural progenitors. *Nat Commun* **4,** 2049.

Ross GW, Petrovitch H, Abbott RD, Nelson J, Markesbery W, Davis D, Hardman J, Launer L, Masaki K, Tanner CM & White LR (2004). Parkinsonian signs and substantia nigra neuron density in decendents elders without PD. *Ann Neurol* **56,** 532–539.

Ross GW, Petrovitch H, Abbott RD, Tanner CM, Popper J, Masaki K, Launer L & White LR (2008). Association of olfactory dysfunction with risk for future Parkinson's disease. *Ann Neurol* **63,** 167–173.

Rothenaigner I, Krecsmarik M, Hayes JA, Bahn B, Lepier A, Fortin G, Götz M, Jagasia R & Bally-Cuif L (2011). Clonal analysis by distinct viral vectors identifies bona fide neural stem cells in the adult zebrafish telencephalon and characterizes their division properties and fate. *Dev Camb Engl* **138,** 1459–1469.

Ryu S, Holzschuh J, Mahler J & Driever W (2006). Genetic analysis of dopaminergic system development in zebrafish. *J Neural Transm Suppl*61–66.

Ryu S, Mahler J, Acampora D, Holzschuh J, Erhardt S, Omodei D, Simeone A & Driever W (2007*a*). Orthopedia homeodomain protein is essential for diencephalic dopaminergic neuron development. *Curr Biol CB* **17,** 873–880.

Ryu S, Mahler J, Acampora D, Holzschuh J, Erhardt S, Omodei D, Simeone A & Driever W (2007*b*). Orthopedia homeodomain protein is essential for diencephalic dopaminergic neuron development. *Curr Biol CB* **17,** 873–880.

Salic A & Mitchison TJ (2008). A chemical method for fast and sensitive detection of DNA synthesis in vivo. *Proc Natl Acad Sci* **105,** 2415–2420.

Sallinen V, Torkko V, Sundvik M, Reenilä I, Khrustalyov D, Kaslin J & Panula P (2009). MPTP and MPP+ target specific aminergic cell populations in larval zebrafish. *J Neurochem* **108,** 719–731.

Santangelo G, Barone P, Trojano L & Vitale C (2013). Pathological gambling in Parkinson's disease. A comprehensive review. *Parkinsonism Relat Disord* **19,** 645–653.

Satake W et al. (2009). Genome-wide association study identifies common variants at four loci as genetic risk factors for Parkinson's disease. *Nat Genet* **41,** 1303–1307.

Schapira AH, Cooper JM, Dexter D, Clark JB, Jenner P & Marsden CD (1990). Mitochondrial complex I deficiency in Parkinson's disease. *J Neurochem* **54,** 823–827.

Schmidt R, Strähle U & Scholpp S (2013). Neurogenesis in zebrafish – from embryo to adult. *Neural Develop* **8,** 3.

Schuurman AG, van den Akker M, Ensinck KTJL, Metsemakers JFM, Knottnerus JA, Leentjens AFG & Buntinx F (2002). Increased risk of Parkinson's disease after depression: a retrospective cohort study. *Neurology* **58,** 1501–1504.

Scott I & Youle RJ (2010). Mitochondrial fission and fusion. *Essays Biochem* **47,** 85–98.

Seidler A, Hellenbrand W, Robra BP, Vieregge P, Nischan P, Joerg J, Oertel WH, Ulm G & Schneider E (1996). Possible environmental, occupational, and other etiologic factors for Parkinson's disease: a case-control study in Germany. *Neurology* **46,** 1275–1284.

Seki T & Arai Y (1995). Age-related production of new granule cells in the adult dentate gyrus. *Neuroreport* **6,** 2479–2482.

Semchuk KM, Love EJ & Lee RG (1992). Parkinson's disease and exposure to agricultural work and pesticide chemicals. *Neurology* **42,** 1328–1335.

Seri B, García-Verdugo JM, McEwen BS & Alvarez-Buylla A (2001). Astrocytes give rise to new neurons in the adult mammalian hippocampus. *J Neurosci Off J Soc Neurosci* **21,** 7153–7160.

Shan X, Chi L, Bishop M, Luo C, Lien L, Zhang Z & Liu R (2006). Enhanced de novo neurogenesis and dopaminergic neurogenesis in the substantia nigra of 1-methyl-4-phenyl-1,2,3,6-tetrahydropyridine-induced Parkinson's disease-like mice. *Stem Cells Dayt Ohio* **24,** 1280–1287.

Sheng D, Qu D, Kwok KHH, Ng SS, Lim AYM, Aw SS, Lee CWH, Sung WK, Tan EK, Lufkin T, Jesuthasan S, Sinnakaruppan M & Liu J (2010). Deletion of the WD40 Domain of LRRK2 in Zebrafish Causes Parkinsonism-Like Loss of Neurons and Locomotive Defect. *PLOS Genet* **6,** e1000914.

Singleton AB et al. (2003). alpha-Synuclein locus triplication causes Parkinson's disease. *Science* **302,** 841.

Smeets WJ & González A (2000). Catecholamine systems in the brain of vertebrates: new perspectives through a comparative approach. *Brain Res Brain Res Rev* **33,** 308–379.

Smith LK, White CW & Villeda SA (2017). The systemic environment: at the interface of aging and adult neurogenesis. *Cell Tissue Res*; DOI: 10.1007/s00441-017-2715-8.

Smits SM, Ponnio T, Conneely OM, Burbach JPH & Smidt MP (2003). Involvement of Nurr1 in specifying the neurotransmitter identity of ventral midbrain dopaminergic neurons. *Eur J Neurosci* **18,** 1731–1738.

Sorrells SF, Paredes MF, Cebrian-Silla A, Sandoval K, Qi D, Kelley KW, James D, Mayer S, Chang J, Auguste KI, Chang EF, Gutierrez AJ, Kriegstein AR, Mathern GW, Oldham MC, Huang EJ, Garcia-Verdugo JM, Yang Z & Alvarez-Buylla A (2018). Human hippocampal neurogenesis drops sharply in children to undetectable levels in adults. *Nature* **555,** 377–381.

Spalding KL, Bergmann O, Alkass K, Bernard S, Salehpour M, Huttner HB, Boström E, Westerlund I, Vial C, Buchholz BA, Possnert G, Mash DC, Druid H & Frisén J (2013). Dynamics of Hippocampal Neurogenesis in Adult Humans. *Cell* **153,** 1219–1227.

Spanaki C, Latsoudis H & Plaitakis A (2006). LRRK2 mutations on Crete: R1441H associated with PD evolving to PSP. *Neurology* **67,** 1518–1519.

Stafa K, Tsika E, Moser R, Musso A, Glauser L, Jones A, Biskup S, Xiong Y, Bandopadhyay R, Dawson VL, Dawson TM & Moore DJ (2014). Functional interaction of Parkinson's disease-associated LRRK2 with members of the dynamin GTPase superfamily. *Hum Mol Genet* **23,** 2055–2077.

Stigloher C, Ninkovic J, Laplante M, Geling A, Tannhäuser B, Topp S, Kikuta H, Becker TS, Houart C & Bally-Cuif L (2006). Segregation of telencephalic and eye-field identities inside the zebrafish forebrain territory is controlled by Rx3. *Development* **133,** 2925–2935.

Suzzi S, Ahrendt R, Hans S, Semenova SA, Bilican S, Sayed S, Winkler S, Spiess S, Kaslin J, Panula P & Brand M (2017). Loss of lrrk2 impairs dopamine catabolism, cell proliferation, and neuronal regeneration in the zebrafish brain. *bioRxiv*140608.

Tan E-K, Yew K, Chua E, Puvan K, Shen H, Lee E, Puong K-Y, Zhao Y, Pavanni R, Wong M-C, Jamora D, de Silva D, Moe K-T, Woon F-P, Yuen Y & Tan L (2006). PINK1 mutations in sporadic early-onset Parkinson's disease. *Mov Disord Off J Mov Disord Soc* **21,** 789–793.

Taymans J-M, Van den Haute C & Baekelandt V (2006). Distribution of PINK1 and LRRK2 in rat and mouse brain. *J Neurochem* **98,** 951–961.

Than-Trong E & Bally-Cuif L (2015). Radial glia and neural progenitors in the adult zebrafish central nervous system. *Glia* **63,** 1406–1428.

Timmer M, Cesnulevicius K, Winkler C, Kolb J, Lipokatic-Takacs E, Jungnickel J & Grothe C (2007). Fibroblast growth factor (FGF)-2 and FGF receptor 3 are required for the development of the substantia nigra, and FGF-2 plays a crucial role for the rescue of dopaminergic neurons after 6-hydroxydopamine lesion. *J Neurosci Off J Soc Neurosci* **27,** 459–471.

Tipton KF & Singer TP (1993). Advances in our understanding of the mechanisms of the neurotoxicity of MPTP and related compounds. *J Neurochem* **61,** 1191–1206.

Tong Y, Pisani A, Martella G, Karouani M, Yamaguchi H, Pothos EN & Shen J (2009). R1441C mutation in LRRK2 impairs dopaminergic neurotransmission in mice. *Proc Natl Acad Sci U S A* **106,** 14622–14627.

Tong Y, Yamaguchi H, Giaime E, Boyle S, Kopan R, Kelleher RJ & Shen J (2010*a*). Loss of leucine-rich repeat kinase 2 causes impairment of protein degradation pathways, accumulation of alpha-synuclein, and apoptotic cell death in aged mice. *Proc Natl Acad Sci U S A* **107,** 9879–9884.

Tong Y, Yamaguchi H, Giaime E, Boyle S, Kopan R, Kelleher RJ & Shen J (2010*b*). Loss of leucine-rich repeat kinase 2 causes impairment of protein degradation pathways, accumulation of alpha-synuclein, and apoptotic cell death in aged mice. *Proc Natl Acad Sci U S A* **107,** 9879–9884.

Valente EM et al. (2004). Hereditary early-onset Parkinson's disease caused by mutations in PINK1. *Science* **304,** 1158–1160.

Van Den Eeden SK, Tanner CM, Bernstein AL, Fross RD, Leimpeter A, Bloch DA & Nelson LM (2003). Incidence of Parkinson's disease: variation by age, gender, and race/ethnicity. *Am J Epidemiol* **157,** 1015–1022.

Voon V, Mehta AR & Hallett M (2011). Impulse control disorders in Parkinson's disease: recent advances. *Curr Opin Neurol* **24,** 324–330.

Wakabayashi K, Tanji K, Mori F & Takahashi H (2007). The Lewy body in Parkinson's disease: molecules implicated in the formation and degradation of alpha-synuclein aggregates. *Neuropathol Off J Jpn Soc Neuropathol* **27,** 494–506.

Wang H, Russa ML & Qi LS (2016). CRISPR/Cas9 in Genome Editing and Beyond. *Annu Rev Biochem* **85,** 227–264.

Wang W & Lufkin T (2000). The murine Otp homeobox gene plays an essential role in the specification of neuronal cell lineages in the developing hypothalamus. *Dev Biol* **227,** 432–449.

Wang X, Yan MH, Fujioka H, Liu J, Wilson-Delfosse A, Chen SG, Perry G, Casadesus G & Zhu X (2012). LRRK2 regulates mitochondrial dynamics and function through direct interaction with DLP1. *Hum Mol Genet* **21,** 1931–1944.

Warner TT & Schapira AHV (2003). Genetic and environmental factors in the cause of Parkinson's disease. *Ann Neurol* **53,** S16–S25.

Weihofen A, Thomas KJ, Ostaszewski BL, Cookson MR & Selkoe DJ (2009). Pink1 forms a multiprotein complex with Miro and Milton, linking Pink1 function to mitochondrial trafficking. *Biochemistry (Mosc)* **48,** 2045–2052.

Winklhofer KF & Haass C (2010). Mitochondrial dysfunction in Parkinson's disease. *Biochim Biophys Acta BBA - Mol Basis Dis* **1802,** 29–44.

Winner B, Kohl Z & Gage FH (2011*a*). Neurodegenerative disease and adult neurogenesis. *Eur J Neurosci* **33,** 1139–1151.

Winner B, Lie DC, Rockenstein E, Aigner R, Aigner L, Masliah E, Kuhn HG & Winkler J (2004). Human Wild-Type α-Synuclein Impairs Neurogenesis. *J Neuropathol Exp Neurol* **63,** 1155–1166.

Winner B, Melrose HL, Zhao C, Hinkle KM, Yue M, Kent C, Braithwaite AT, Ogholikhan S, Aigner R, Winkler J, Farrer MJ & Gage FH (2011*b*). Adult neurogenesis and neurite outgrowth are impaired in LRRK2 G2019S mice. *Neurobiol Dis* **41,** 706–716.

Winner B, Regensburger M, Schreglmann S, Boyer L, Prots I, Rockenstein E, Mante M, Zhao C, Winkler J, Masliah E & Gage FH (2012). Role of α-synuclein in adult neurogenesis and neuronal maturation in the dentate gyrus. *J Neurosci Off J Soc Neurosci* **32,** 16906–16916.

Winner B, Rockenstein E, Lie DC, Aigner R, Mante M, Bogdahn U, Couillard-Despres S, Masliah E & Winkler J (2008). Mutant alpha-synuclein exacerbates age-related decrease of neurogenesis. *Neurobiol Aging* **29,** 913–925.

Xi Y, Noble S & Ekker M (2011). Modeling Neurodegeneration in Zebrafish. *Curr Neurol Neurosci Rep* **11,** 274–282.

Xi Y, Ryan J, Noble S, Yu M, Yilbas AE & Ekker M (2010). Impaired dopaminergic neuron development and locomotor function in zebrafish with loss of pink1 function. *Eur J Neurosci* **31,** 623–633.

Yamamura Y, Sobue I, Ando K, Iida M & Yanagi T (1973). Paralysis agitans of early onset with marked diurnal fluctuation of symptoms. *Neurology* **23,** 239–244.

Yoshimi K, Ren Y-R, Seki T, Yamada M, Ooizumi H, Onodera M, Saito Y, Murayama S, Okano H, Mizuno Y & Mochizuki H (2005). Possibility for neurogenesis in substantia nigra of parkinsonian brain. *Ann Neurol* **58,** 31–40.

Zabetian CP, Samii A, Mosley AD, Roberts JW, Leis BC, Yearout D, Raskind WH & Griffith A (2005). A clinic-based study of the LRRK2 gene in Parkinson disease yields new mutations. *Neurology* **65,** 741–744.

Zarranz JJ, Alegre J, Gómez-Esteban JC, Lezcano E, Ros R, Ampuero I, Vidal L, Hoenicka J, Rodriguez O, Atarés B, Llorens V, Gomez Tortosa E, del Ser T, Muñoz DG & de Yebenes JG (2004). The new mutation, E46K, of alpha-synuclein causes Parkinson and Lewy body dementia. *Ann Neurol* **55,** 164–173.

Zhang L, Mathers PH & Jamrich M (2000). Function of Rx, but not Pax6, is essential for the formation of retinal progenitor cells in mice. *Genes N Y N 2000* **28,** 135–142.

Zhang Y, Nguyen DT, Olzomer EM, Poon GP, Cole NJ, Puvanendran A, Phillips BR & Hesselson D (2017). Rescue of Pink1 Deficiency by Stress-Dependent Activation of Autophagy. *Cell Chem Biol* **24,** 471-480.e4.

Zhao C, Deng W & Gage FH (2008). Mechanisms and Functional Implications of Adult Neurogenesis. *Cell* **132,** 645–660.

Zhao C, Teng EM, Summers RG, Ming G-L & Gage FH (2006). Distinct morphological stages of dentate granule neuron maturation in the adult mouse hippocampus. *J Neurosci Off J Soc Neurosci* **26,** 3–11.

Zhao M, Momma S, Delfani K, Carlén M, Cassidy RM, Johansson CB, Brismar H, Shupliakov O, Frisén J & Janson AM (2003). Evidence for neurogenesis in the adult mammalian substantia nigra. *Proc Natl Acad Sci* **100,** 7925–7930.

Zhu X-R, Maskri L, Herold C, Bader V, Stichel CC, Güntürkün O & Lübbert H (2007). Non-motor behavioural impairments in parkin-deficient mice. *Eur J Neurosci* **26,** 1902–1911.

Zimprich A et al. (2004). Mutations in LRRK2 Cause Autosomal-Dominant Parkinsonism with Pleomorphic Pathology. *Neuron* **44,** 601–607.